Synaptic targeting and (re-)localization of gephyrin by thiol-modifications

Inaugural-Dissertation
zur
Erlangung des Doktorgrades
der Mathematisch-Naturwissenschaftlichen Fakultät
der Universität zu Köln

vorgelegt von:

Maria-Theresa Gehling (geb. Schneider)
aus Marsberg, Deutschland

Berichtersteller: Prof. Dr. Günter Schwarz
(Gutachter)

Tag der mündlichen Prüfung:

Dedicated to Titus and Mara

Content

List of Figures

Abbreviations

2ABA	2A 55 kDa regulatory subunit B alpha isoform
AD	Alzheimer's disease
ADP, AMP, ATP	adenosine diphosphate, - monophosphate, - triphosphate
AP	action potential
CamKII	calmodulin-dependent protein kinase II
Cat	catalase
Cb	collybistin
CDK5	cyclin-dependent kinase 5
CNS	central nervous system
cPMP	cyclic cyanopterin monophosphate
DAAO	D-amino acid oxidase
DH domain	diffuse B-cell lymphoma homology domain
DLC1/2	dynein light chain 1/2
E/I	ratio of excitation and inhibition
EPSP, IPSP	excitatory post-synaptic potential, inhibitory post-synaptic potential
ERK1	extracellular signal-regulated protein kinase1
GABA, $GABA_AR$	γ-amino butyric acid, GABA type A receptor, GABA type B receptor
GABARAP	GABA type A receptor-associated protein
GAPDH	glycerinaldehyd-3-phosphat-Dehydrogenase
GDP/GTP	guanosine diphosphate, - triphosphate
GEF	GDP/GTP-exchange factor
GlyR	glycine receptor
GPx	glutathione peroxidase
GSH	glutathione reduced
GSK3β	glycogen synthase kinase 3β
HD	Huntington's disease
ICD	intracellular domain
LLPS	liquid-liquid phase separation
MoCD	molybdenum co-factor deficiency
Moco	molybdenum co-factor
MPT	molybdopterin
NAPDH	nicotinamide adenine dinucleotide phosphate
NIMA	never in mitosis gene A
NL, NL2	neuroligin, neuroligin 2
nNOS	neuronal nitric oxide synthase
NMDA, NMDAR	*N*-methyl-D-aspartate, NMDA receptor
NO	nitric oxide

NOX, NOX2	NADPH oxidase, NADPH oxidase 2
PD	Parkinson's disease
PH domain	pleckstrin homology domain
PIN	protein inhibitor of neuronal nitric oxide synthase
Pin1	peptidyl-prolyl isomerase NIMA interacting protein 1
PKA	cAMP-dependent protein kinase
PKC	protein kinase C
PPT	palmitoyl protein thioesterase
Prx	peroxiredoxin
PSD	post-synaptic density
PSD95	post-synaptic density protein 95
PTM	post-translational modification
ROS, mROS	reactive oxygen species, mitochondria-derived ROS
S-H	free thiol
SH3 domain	SRC homology 3 domain
SNARE complex	soluble N-ethylmaleimide-sensitive-factor attachment receptor complex
S-NO	nitroso-thiol
S-palm	palmitoyl-thiol
SOD	superoxide dismutase
S-OH	sulfenic acid
$S\text{-}O_2H$	sulfinic acid
$S\text{-}O_2H$	sulfonic acid
SOX	sulfite oxidase
S-S	disulfide
SSC	S-sulfocysteine
S-SH	persulfide
SUMO	small ubiquitin-like modifier
vGAT	vesicular GABA transporter
vGLUT	vesicular glutamate transporter
XO	xanthine oxidase
zDHHC12	zinc finger DHHC domain-containing protein 12

Abstract

As a bifunctional protein, gephyrin is involved in molybdenum cofactor (Moco) biosynthesis as well as the clustering of receptors at the inhibitory synapse. Dysfunctions of gephyrin are linked to neurodegenerative diseases, such as encephalopathy, autism, epilepsy and Alzheimer's disease. Dynamic regulation of gephyrin is further important for the modulation of neurotransmission, known as synaptic plasticity. Thus, understanding of gephyrin function and its regulation is crucial.

Gephyrin is highly regulated by post-translational modifications (PTMs) targeting primarily its central C-domain that connects the N-terminal G- and the C-terminal E-domain. PTMs of gephyrin have been shown to regulate synaptic clustering, localization, stability and receptor interaction. However, the interplay of these PTMs and the underlying molecular mechanisms are not fully understood. Moreover, most PTMs were studied *in vitro* and *in cellulo*, leaving their biological relevance *in vivo* unclear.

This work aimed to understand the interplay of several PTMs regulating gephyrin by S-nitrosylation, S-palmitoylation as well as the interaction with dynein light chain (DLC) and to generate a mouse model for the investigation of these PTMs *in vivo*. In addition, this work aimed to identify the unknown roles of surface-exposed cysteines of gephyrin in a redox-dependent context.

Using several biochemical, cellular and animal experiments, this work revealed new insight into gephyrin regulation through PTMs and the role of the C-domain. A novel dynein-independent role of DLC was identified that regulates S-nitrosylation and S-palmityoaltion, competing for the same Cys212 and Cys284, in a reciprocal way. The underlying mechanism involves the formation of a ternary complex with gephyrin, neuronal nitric oxide synthase (nNOS) and DLC. DLC inhibits nNOS-mediated NO production and thus allows for S-palmitoylation. Gephyrin phosphorylation at Thr205 inhibits DLC binding permitting nNOS-mediated S-nitrosylation.

Furthermore, it was found that surface-exposed cysteines of gephyrin are redox-sensitive and important for redox-dependent synaptic clustering of gephyrin. The mechanism driving oxidation-mediated synaptic clustering involves oligomerization of gephyrin through disulfide bridges, which strengthens receptors clustering and increases resistance to proteolytic cleavage. A physiological source for gephyrin oxidation was identified as mitochondria-derived reactive oxygen species (mROS) linking neuronal and mitochondrial activities, important for aging and disease mechanisms.

Finally, a novel mouse model carrying a microdeletion of residue 199-233 (∆199-233) was generated, allowing for the investigation of the contribution of this C-domain area for gephyrin function *in vivo*. The phenotype of homozygous mice (∆/∆) was severe, causing high-mortality, epileptic-like seizures and weight loss before weaning age. The pathogenicity mechanism was narrowed down to disturbed synaptic targeting of gephyrin through loss of S-palmitoylation and PTM-independent structural modulation of the gephyrin-receptor interaction. These combined alterations caused a reduction in inhibitory transmission and adaptation at excitatory synapses, resulting in a disturbed excitation and inhibition interplay thus manifesting the hyperexcitation and epileptogenic phenotype in ∆/∆ mice.

In summary, this work sheds light on the importance and interplay of three thiol-based PTMs of gephyrin: S-nitrosylation, S-palmitoylation and Cys-reduction/oxidation. Furthermore, it extends the understanding of the C-domain beyond its role as a regulatory hub for the function of gephyrin through structural flexibility and PTMs, as a PTM-independent modulator of gephyrin-receptor interactions. The findings within this work extend our knowledge about gephyrin-dependent synaptic plasticity and offer potential for developing therapies for gephyrin-dependent neurodegenerative diseases and may be representative of other post-synaptic proteins.

Zusammenfassung

Gephyrin ist an der Biosynthese des Molybdän-Cofaktors (Moco) und der Clusterbildung von Rezeptoren an der inhibitorischen Synapse beteiligt. Funktionsstörungen von Gephyrin stehen im Zusammenhang mit neurodegenerativen Erkrankungen wie Enzephalopathie, Autismus, Epilepsie und Alzheimer. Die dynamische Regulation von Gephyrin ist wichtig für die Modulation der Neurotransmission, bekannt als synaptische Plastizität. Daher ist das Verständnis der Funktion von Gephyrin und seiner Regulation von großer Bedeutung.

Gephyrin wird durch verschiedene post-translationale Modifikationen (PTMs) innerhalb seiner zentralen C-Domäne reguliert, welche die N-terminale G-Domäne und die C-terminale E-Domäne verbindet. Diese PTMs kontrollieren die synaptische Clusterbildung, Lokalisation, Stabilität und Rezeptorinteraktion von Gephyrin. Allerdings sind die zugrunde liegenden molekularen Mechanismen noch nicht vollständig verstanden, und die biologische Relevanz der meisten PTMs *in vivo* bleibt unklar.

Das Ziel dieser Arbeit war es, das Zusammenspiel mehrerer PTMs, die Gephyrin regulieren, zu verstehen, einschließlich S-Nitrosylierung, S-Palmitoylierung sowie die Interaktion mit Dynein light chain (DLC). Darüber hinaus sollte ein Mausmodell erstellt werden, um diese PTMs *in vivo* zu untersuchen. Daneben sollte die unbekannte Rolle der oberflächenexponierten Cysteine von Gephyrin, die nicht mit S-Palmitoylierung und S-Nitrosylierung in Verbindung stehen, identifiziert werden. Verschiedene biochemische, zelluläre und tierexperimentelle Methoden führten zu neuen Erkenntnissen über die Regulation von Gephyrin durch PTMs und die Rolle der C-Domäne.

Eine neuartige Dynein-unabhängige Rolle von DLC wurde identifiziert, die S-Nitrosylierung und S-Palmitoylierung von Gephyrin, welche um die gleichen Cysteine 212 und 284 konkurrieren, reguliert. Der Mechanismus umfasst die Bildung eines ternären Komplexes aus Gephyrin, neuronaler Stickstoffmonoxidsynthase (nNOS) und DLC. DLC hemmt die nNOS-abhängige NO-Produktion und ermöglicht so Gephyrin-S-Palmitoylierung. Phosphorylierung von Gephyrin an Thr205 inhibiert die Bindung zu DLC und ermöglicht nNOS-abhängige S-Nitrosylierung von Gephyrin.

Es wurde festgestellt, dass die oberflächenexponierten Cysteine von Gephyrin redox-sensitiv sind und für die redox-abhängige synaptische Clusterbildung wichtig sind. Der Mechanismus umfasst die Verbindung von Gephyrin-Molekülen durch Disulfidbrücken, die die Rezeptorclusterung verstärken. Eine physiologische Quelle für die Oxidation von Gephyrin wurde als mitochondrial erzeugte reaktive Sauerstoffspezies (mROS) identifiziert, was neuronale und mitochondriale Aktivität verbindet und für alterungsbedingte sowie neurodegenerative Krankheitsmechanismen wichtig ist.

Schließlich wurde ein Mausmodell mit einer Mikrodeletion der Reste 199-233 (Δ199-233) erzeugt, das die Untersuchung des Beitrags dieses C-Domänenbereichs zur Funktion von Gephyrin *in vivo* ermöglicht. Der Phänotyp der homozygoten Mäuse (Δ/Δ) war schwerwiegend und verursachte hohe Sterblichkeit, epilepsieartige Anfälle und Gewichtsverlust vor dem Absetzalter. Der Pathomechanismus wurde auf eine gestörte, synaptische Rekrutierung von Gephyrin durch Verlust der S-Palmitoylierung und PTM-unabhängige strukturelle Modulation der Gephyrin-Rezeptor-Interaktion eingegrenzt. Diese Veränderungen führten zu einer Reduktion der inhibitorischen Transmission und Anpassungen an exzitatorische Synapsen, was zu einem gestörten Verhältnis zwischen Erregung und Hemmung führte und zum hyperexzitatorischen und epileptogenen Phänotyp in Δ/Δ-Mäusen beitrug.

Zusammenfassend beleuchtet diese Arbeit die Bedeutung und das Zusammenspiel dreier thiolbasierter PTMs von Gephyrin: S-Nitrosylierung, S-Palmitoylierung und Cystein-Reduktion/Oxidation. Des Weiteren erweitert sie das Verständnis der C-Domäne als PTM-unabhängigen Modulator der Gephyrin-Rezeptor-Interaktionen. Die gewonnenen Erkenntnisse erweitern unser Wissen über die Gephyrin-abhängige synaptische Plastizität und bieten Potenzial für die Entwicklung von Therapien für Gephyrin-abhängige neurodegenerative Erkrankungen und könnten repräsentativ für andere synaptische Proteine sein.

Chapter 1

General introduction

1.1. Neuronal signal transmission

The function of the central nervous system (CNS) relies on fast and complex communication among neurons. Neurons are highly polarized cells, consisting of a cell body (soma), a signal-input site (dendrites), a signal-conducting site (axon) and a signal-output site (terminal bouton) (Figure 1). Importantly, the human brain, as one part of the CNS, consists of over 80 billion neurons (Azevedo et al., 2009) each forming several thousand connections leading to the most complex biological structure in nature (Hawkins and Ahmad, 2016). The interplay of several neuronal contact/communication sites is the basis for the fascinating functions of our brain such as signal processing and memory storage.

Neuronal communication, known as neurotransmission, occurs primarily at synapses. At chemical synapses (Figure 1), neurotransmitters are released from the presynaptic neuron into the synaptic cleft, where they bind to receptors on the postsynaptic neuron (Manolov and Ovtscharoff, 1982). Activation of these receptors leads to various outcomes depending on the receptor type. For ligand-gated ion channels, receptor activation results in ion influx into the post-synaptic neuron, altering its membrane potential and initiating an electrochemical signal (daCosta and Baenziger, 2013).

Two fundamental types of changes in membrane potential occur in the post-synaptic neuron: Excitatory post-synaptic potentials (EPSPs), a depolarized membrane potential primarily caused by the influx of positively charged ions (e.g. Na^+, Ca^{2+}) and inhibitory post-synaptic potentials (IPSPs), hyperpolarized membrane potentials via the influx of negatively charged ions (Cl^-). EPSPs and IPSPs are integrated at the axon initial segment (AIS). If their sum reaches a depolarizing cell-specific threshold, an action potential (AP) is triggered and propagates along the axon leading to the activation of voltage-gated Ca^{2+} channels and Ca^{2+} influx into the axon terminal segment (bouton) (Bean, 2007). This Ca^{2+} signaling causes the interaction of synaptotagmin and the soluble *N*-ethylmaleimide-sensitive-factor attachment receptor (SNARE) complex, resulting in the fusion of neurotransmitter-packed vesicles with the pre-synaptic membrane and neurotransmitter release (Sudhof and Rothman, 2009; Sudhof, 2013).

In summary, the interplay of EPSPs and IPSPs determines whether an AP is generated and the signal is propagated. The generation of an AP is crucial for signal propagation throughout the brain. However, the process is complex and depends on the type of neurotransmitter released and the type of target cell. For example, inhibition of

an inhibitory neuron may increase the likelihood of excitation in a downstream neuron. This is why, it is of great interest to understand projection networks of excitatory and inhibitory neurons. Furthermore, the ratio and interplay of excitation and inhibition (E/I) is critical for healthy neurotransmission in the CNS (Froemke, 2015).

The molecular mechanisms responsible for AP generation and propagation, from incoming signals to neurotransmitter release, have been studied extensively. These mechanisms include processes that modify neurotransmission and neuronal network communication, known as synaptic plasticity. For example, during learning (such as while reading this text) synapses may form (synaptogenesis), be lost (retraction), or undergo fine-tuning of receptor activation/deactivation, all based on the interplay of EPSPs and IPSPs.

The nature of the membrane potential change depends on the receptor type and corresponding neurotransmitter. For example, excitatory synapses generating EPSPs involve glutamatergic synapses with *N*-methyl-D-aspartate receptors (NMDARs) or α-amino-3-hydroxy-5-methyl-4-isoxazolepropionic acid receptors (AMPARs), activated by the neurotransmitter glutamate, causing Ca^{2+} and Na^{+} influx, respectively. In contrast, inhibitory synapses generating IPSPs, involve glycine receptors (GlyRs) or γ-amino-butyric acid (GABA) type A receptors ($GABA_AR$s), activated by glycine or GABA respectively, causing Cl^{-} influx (Mihic and Harris, 1997; Lynch, 2009). Moreover, excitatory synapses appear on dendritic spines, while inhibitory synapses are mainly found on dendritic shafts and the soma, but some inhibitory synapses can also be near excitatory ones on dendritic spines (Chen et al., 2012).

Although excitatory and inhibitory synapses exhibit fundamentally different protein content (called protein density), structure and organization (Tao et al., 2018), their functional composition is comparable (Figure 1). The pre-synaptic density includes Ca^{2+} channels, membrane proteins (e.g. synaptophysin), SNARE proteins, transporters (e.g. vesicular GABA transporter (vGAT) and vesicular glutamate transporter (vGLUT)) and neurotransmitter-containing vesicles. The post-synaptic density (PSD) contains receptors (e.g. GlyRs and NMDARs) and various other components, including adhesion molecules (e.g. Neuroligins), scaffolding proteins, cytoskeletal proteins, and regulatory proteins, which influence PSD shape and function.

The dynamic adaptation of PSDs (besides pre-synaptic adaptation) is crucial for neuronal function, as well as synaptic plasticity (Conti and Weinberg, 1999). A key to organize and modulate PSDs and thus neurotransmission are scaffolding proteins (Tretter et al., 2012; Iasevoli et al., 2013): They link post-synaptic membrane-associated proteins to cytosolic proteins, efficiently cluster receptors for neuro-transmission and build a platform for various protein-protein interactions and involved signaling pathways.

At inhibitory synapses, gephyrin is the main scaffolding protein, while at excitatory synapses post-synaptic density protein 95 (PSD95) is predominant. In the following sections, gephyrin function and its importance in health and disease, as well as important regulation mechanisms will be presented.

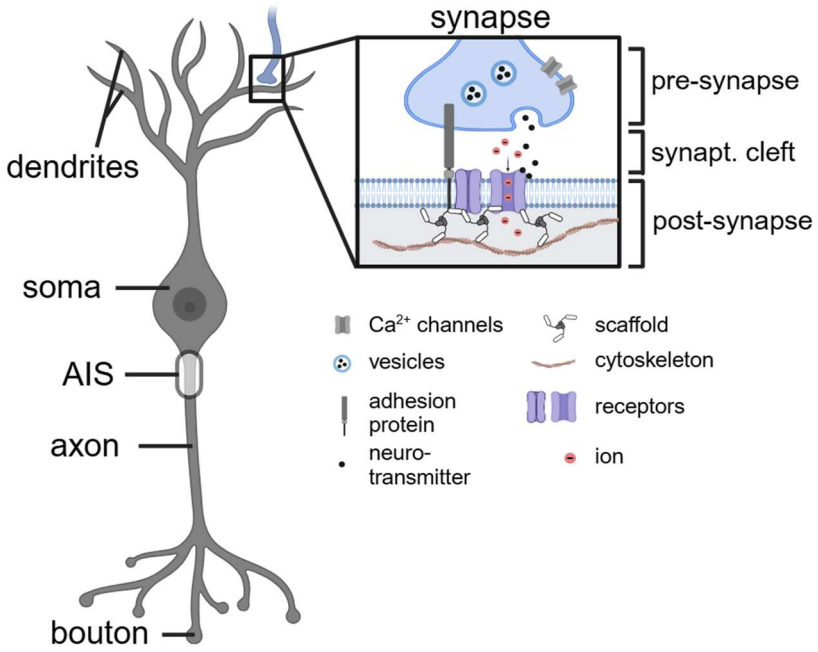

Figure 1: Architecture of neurons and synapses
Schematic illustration of the compartments of a neuron. Enlargement of a chemical synapse, which contains several components such as receptors, small molecules and channels.

1.2. Gephyrin – a bifunctional protein

Gephyrin is a cytosolic protein with two independent functions, which is why it belongs to the growing family of moonlighting proteins (Feng et al., 1998) (Figure 2). On the one hand, it catalyzes the final two steps of the synthesis of the molybdenum co-factor (Moco) (Figure 2A). This co-factor is important for redox-reactions in enzymes involved in nitrogen, carbon and sulfur metabolism (Schwarz, 2005). On the other hand, gephyrin acts as a scaffolding protein at inhibitory synapses, clustering GlyRs (Kirsch et al., 1993; Feng et al., 1998) and a subset of $GABA_ARs$ (Fritschy et al., 2008) at the post-synaptic membrane. Both functions are based on the molecular structure of gephyrin. A single gephyrin monomer consists of three domains: The N-terminal G-domain, the C-terminal E-domain and the C-domain that connects them (Figure 2A). The most recent evolutionary 'addition' to gephyrin is the C-domain, which allows for structural flexibility and connects G- and E-domains (Belaidi and Schwarz, 2013). The G-domain catalyzes the adenylation of molybdopterin (MPT) and forms trimers when isolated (Schwarz et al., 2001; Sola et al., 2001) (Figure 2B). The E-domain catalyzes the insertion of molybdenum into MPT-AMP and the cleavage of AMP, resulting in the formation of Moco,

and forms dimers when isolated (Kim et al., 2006) (Figure 2B). Notably, E-domain dimerization and G-domain trimerization are crucial for both of gephyrin's functions (Sola et al., 2004; Dejanovic et al., 2015; Grunewald et al., 2018). In addition, since G- and E-domain are involved in Moco biosynthesis, they are highly conserved with homologues present in all kingdoms of life. This coupling of both domains is believed to increase enzymatic productivity due product-substrate-channeling (Belaidi and Schwarz, 2013).

Full-length gephyrin forms trimers through the G-domain as the smallest building block, with trimers further assembling into more complex oligomers via additional E-domain interactions, facilitated/supported by the flexible C-domain (Saiyed et al., 2007) (Figure 2C). However, the exact molecular organization of gephyrin scaffolds *in vivo* is elusive, although a hexagonal lattice has been proposed (Kneussel and Betz, 2000), while other evidence suggests differently organized structures such as filaments (unpublished data from Schwarz-lab). Regardless of the exact organization, complex oligomerization is crucial for the synaptic function of gephyrin, resulting in a post-synaptic scaffold (Kim et al., 2021). These gephyrin scaffolds are necessary at post-synapses to cluster multiple receptors simultaneously and bridge the post-synaptic membrane with the cytoskeleton (Figure 2D). Clustering of gephyrin isolated from cells appears as - depending on the organism of origin - trimers, hexamers and high-order oligomers, also referred to as multimers (Herweg and Schwarz, 2012). Imaging of non-neuronal cells, such as HEK293 cells, shows overexpressed gephyrin as 'blobs' (Meyer et al., 1995). In cultivated neurons and brain tissue, both overexpressed and endogenous gephyrin form clusters, blobs or punctae (Feng et al., 1998; Waldvogel et al., 2003). Conversely, in liver, endogenous gephyrin exhibits a diffuse cytosolic distribution (Nawrotzki et al., 2012).

Gephyrin harbors 40 exons, which are spliced in various tissue- and organism-specific manners and further contribute to its functional diversity (Figure 2A) (Fritschy et al., 2008). Importantly, the nomenclature of splice cassettes and isoforms changed over time since more transcripts have been identified. Once, gephyrin isoforms were named by the affected domain (G1, G2, C3, C4a, C4b, C4c, C4d, E1 and E2) (Fritschy et al., 2008), later it was proposed to name them after their abundance and the affected exons, when over 277 gephyrin splice transcripts have been identified during brain development (Dos Reis et al., 2022). Importantly, after first nomenclature, the most abundant non-neuronal variant of gephyrin contains the C3 cassette (exon 15) (Rees et al., 2003; Fritschy et al., 2008). Following the newly suggested nomenclature, the most abundant neuronal isoform was determined as 'GPHN-1' (containing exons 1, 6, 8, 10, 12-14, 17, 25, 27-31 and 33-40) (Dos Reis et al., 2022), which was called 'P1' previously (Fritschy et al., 2008).

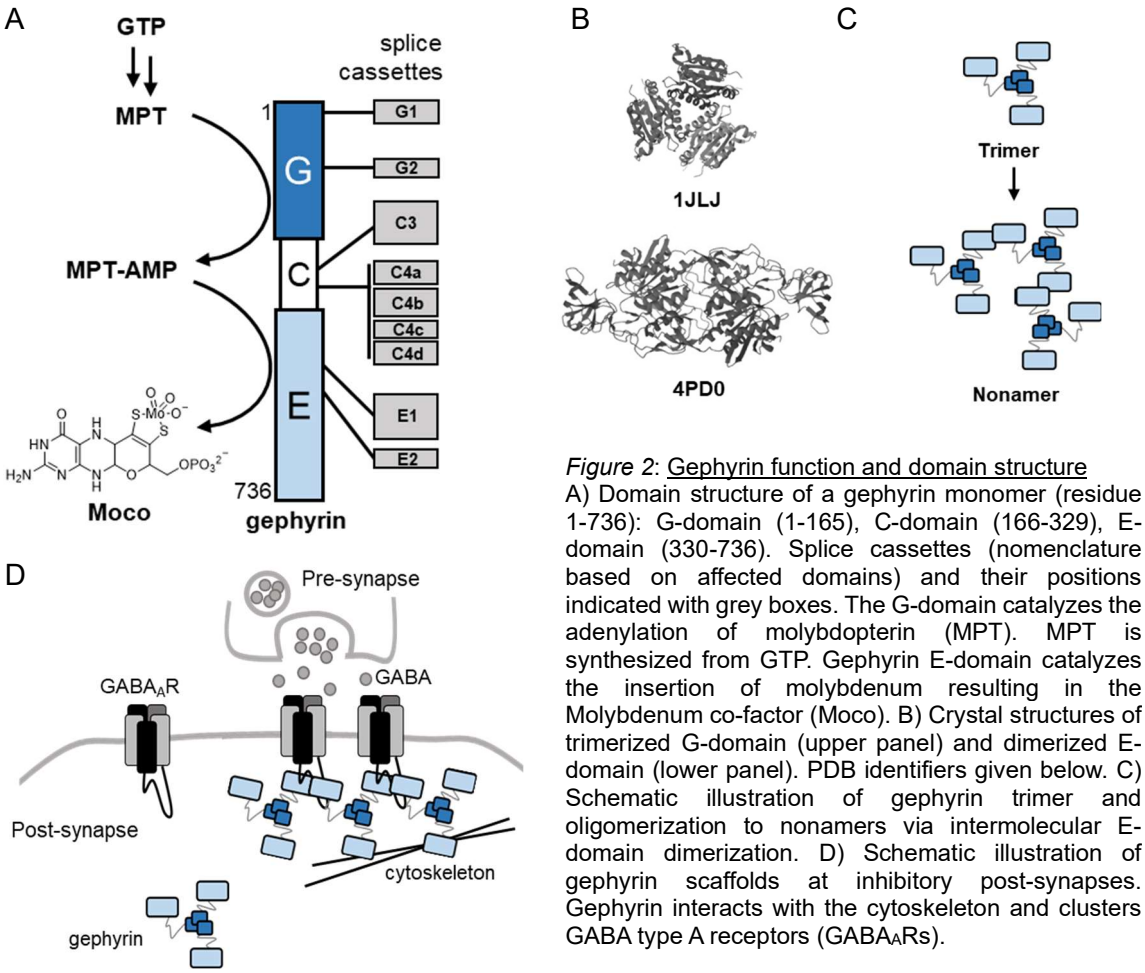

Figure 2: Gephyrin function and domain structure
A) Domain structure of a gephyrin monomer (residue 1-736): G-domain (1-165), C-domain (166-329), E-domain (330-736). Splice cassettes (nomenclature based on affected domains) and their positions indicated with grey boxes. The G-domain catalyzes the adenylation of molybdopterin (MPT). MPT is synthesized from GTP. Gephyrin E-domain catalyzes the insertion of molybdenum resulting in the Molybdenum co-factor (Moco). B) Crystal structures of trimerized G-domain (upper panel) and dimerized E-domain (lower panel). PDB identifiers given below. C) Schematic illustration of gephyrin trimer and oligomerization to nonamers via intermolecular E-domain dimerization. D) Schematic illustration of gephyrin scaffolds at inhibitory post-synapses. Gephyrin interacts with the cytoskeleton and clusters GABA type A receptors (GABA$_A$Rs).

The diffuse cytosolic distribution of gephyrin in liver (Nawrotzki et al., 2012), is maybe due to the insertion of the 'C3' splice cassette, which is an isoform known to destabilize receptor binding and high-order oligomerization to emphasize gephyrin's enzymatic activity (Herweg and Schwarz, 2012). Recent findings suggest that the insertion of the so called 'C4c' cassette (exon 21) leads to distal dendritic localization of gephyrin and modulates inhibitory signal transmission (Liebsch et al., 2023). However, the precise function of each exon splicing in gephyrin modulation is still under investigation.

1.3. Inhibitory receptors and receptor models

At inhibitory synapses, the PSD contains GlyRs and GABA$_A$Rs, which are ligand-gated pentameric ion (Cl^-) channels. Each subunit consists of four transmembrane helices, an N-terminal ligand-binding domain and an intracellular domain (Figure 3A). The type of subunit can vary. In case of GlyRs, each subunit can be made from five different genes (α1-4, β) (Lynch, 2004). The exact stoichiometry of GlyRs remains elusive, but besides homopentameric 5α (Legendre, 2001), compositions of 3α:2β (Burzomato et al., 2003), 2α:3β (Yang et al., 2012) and recently a 4α:1β (Zhu and Gouaux, 2021) stoichiometry

have been identified. GlyRs are found at inhibitory synapses in the brainstem and spinal cord, and are responsible for sensory and motoric computation (Legendre, 2001).

In contrast, the subunits of the $GABA_AR$s originate from 19 different genes (α1-6, β1-3, γ1-3, δ, ε, θ, π, ρ1-3) (Sieghart et al., 1999), and synaptic receptors are considered to consist of α1-3, β2-3 and γ2 subunits in a 2α/2β/1γ ratio (Baur et al., 2006). The γ2 subunit has been identified as most important for synaptic localization (Essrich et al., 1998), although some $GABA_AR$s containing a γ2 subunit are also found extra-synaptically (Luscher et al., 2011). $GABA_AR$s are the predominant receptor type among inhibition in the CNS and involved in many neuronal functions depending on the brain region (Young and Chu, 1990; Mihic and Harris, 1997). The distribution gets even more complex since subunits exhibit brain region specificity (Wagner et al., 2021). Importantly, $GABA_AR$s are the target of therapeutic drugs and involved in pathologies of neuronal disorders, such as epilepsy, autism, and anxiety (Griffin et al., 2013). Thus, GABAergic transmission is crucial in health and disease.

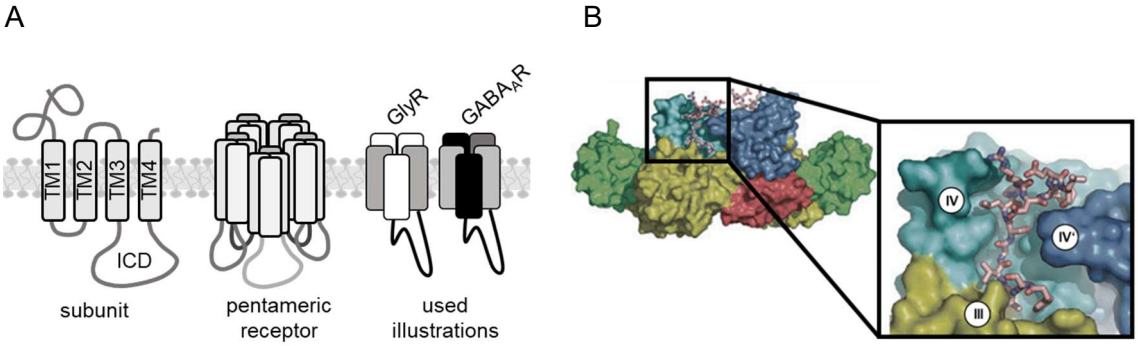

Figure 3: GlyRs and $GABA_AR$s and the interaction with gephyrin.
A) Schematic domain structure of pentameric ligand-gated ion channels. Each of the five subunits consists of an N-terminal ligand-binding domain, four transmembrane helices (TM1-4) and a cytosolic loop between TM3 and 4 representing the intracellular domain (ICD. GlyRs and $GABA_AR$s are ligand-gated ion channels made of five individual subunits. Certain types of ICDs of GlyRs and $GABA_AR$s interact with gephyrin. The simplified illustration is used in later images in this thesis. B) Crystal structure of a peptide derived from the ICD of the β subunit of the GlyR in the dimer interface of gephyrin E-domain (PDB: 2FTS). The binding pocket is built by the III and IV subdomains of one E-domain monomer, and the IV subdomain of the other monomer. Picture edited (Kim et al., 2006).

1.4. Receptor-gephyrin interaction and receptor models

Post-synaptic positioning of GlyRs and $GABA_AR$s is essential to ensure efficient synaptic clustering and is facilitated by gephyrin. The binding of both types of receptor is mediated through the ICD of a receptor subunit and the dimerized E-domain of gephyrin (Kim et al., 2006; Maric et al., 2011) (Figure 3B). The dimerization of the E-domain is required since the hydrophobic binding pocket is built by subdomains III and IV of one E-domain monomer and subdomain IV' of the second monomer (Sola et al., 2004; Kim et al., 2006). Importantly, the affinity of gephyrin for these ICDs depends on the receptor subunit type, but the ICD types share a few common required residues (Maric et al., 2011). For

instance, the core binding motif of the GlyR β-ICD was narrowed down to residue 420-432 (FSIVGSLPRDFEL) (Meyer et al., 1995), and that of $GABA_AR$ α3-ICD to 396-406 (FNIVGTTYPIN) (Maric et al., 2011). Through isothermal calorimetry (ITC) experiments, it was shown that gephyrin has a strong affinity (K_D in nM-range) for the ICD of the β-subunit of the GlyR (β-ICD) (Grunewald et al., 2018) but does not bind to GlyR α-subunits (Meyer et al., 1995). The gephyrin-GlyR interaction is so strong that gephyrin was considered a subunit of the receptor (Betz, 1991). The strongest affinity (K_D in lower μM-range) towards $GABA_ARs$ was measured with the α3 subunit (Maric et al., 2011). Interestingly, trimeric full-length gephyrin – in contrast to isolated dimerized E-domains – exhibits an altered binding profile towards the GlyR β-ICD resulting in a high- and a low-affinity binding site (Grunewald et al., 2018). As a result, it was hypothesized that the C-domain of gephyrin might influence/modulate gephyrin-GlyR interaction. However, to date, the exact importance of the low-affinity binding site and the direct structural influence of gephyrin C-domain for receptor binding remains elusive.

The investigation of the receptor-gephyrin interaction required the development of receptor models since native receptors are difficult to solubilize and purify with standard biochemical techniques. Thus, more and more receptor models have been invented over time, ranging from minimal peptides (Grunewald et al., 2018) to complex pentameric models (Macha et al., 2022a). Application advantages and the level of functional similarity to the *in vivo* situation differ among these models and each off represent their own strength and weakness in a given experimental setup.

The basic gephyrin-receptor interaction can be investigated *in vitro* (e.g. in ITC experiments) using established GlyR β-ICD peptides ranging from residue 378-426 (VGETRCKKVCTSKSDLRSND<u>FSIVGSLPRDFEL</u>SNYDCYGKPIEVNNGL, core motif underlined) (Grunewald et al., 2018). Other studies required multimeric models (Bai et al., 2021). Therefore, a dimeric model was generated with two GlyR β-ICD peptides from residue 349-474 (FSIVGSLPRDFEL) fused to the tail of a dimeric GCN4 coiled-coil domain for example (Bai et al., 2021). Recently, the 'Schwarz-lab' developed a soluble pentameric GlyR model consisting of five GlyR β-ICDs fused to the pentameric lumazine synthase (LS) (Macha et al., 2022a), which is comparable to the native GlyR, which was also utilized in this thesis besides the GlyR β-ICD peptide from residue 378-426. Additionally, more models resembling different subunit compositions, which may influence gephyrin-receptor interaction, are currently developed.

1.5. Gephyrin in diseases

Gephyrin is crucial protein in multiple ways for the survival of vertebrates. The dual function of gephyrin results in two possible impairment mechanisms, when gephyrin is absent or dysfunctional, a defect of Moco synthesis on the one hand and loss of synaptic clustering on the other hand. Depending on the combination of both and the severity, human patients often die within early childhood, in many cases most likely undiagnosed due to the severity of the resulting phenotype. Consistently, a full-body gephyrin knock-out in mice results in death within six hours after birth (Feng et al., 1998).

Although, both functions of gephyrin are very different from each other, both result in neuronal impairments independently, irrespectively, which of the two functions is altered. In case of a deficiency in the Moco synthesis (MoCD), early childhood death and severe neurological defects are triggered (Reiss and Johnson, 2003; Whitwell, 2023), mainly due to the deficiency of the Moco-dependent enzyme sulfite oxidase (SOX) (Schwarz and Belaidi, 2013). Reduction or loss of SOX activity results in the accumulation of toxic sulfite, forming *S*-sulfocysteine (SSC), a structural analogue to glutamate (Kumar et al., 2017). Glutamate acts as a neurotransmitter on NMDARs, thus excess of SSC leads to hyperexcitation and ultimately neurotoxicity. The influx of Ca^{2+} activates the protease calpain (1.6.4) as one of many Ca^{2+}-dependent downstream pathways (Brini et al., 2014; Metwally et al., 2023). Calpain-mediated cleavage of gephyrin at inhibitory synapses results in disruption of gephyrin/receptor clusters thus disturbs the interplay of E/I (Kumar et al., 2017).

Biomarkers of MoCD are sulfite (SO_3), SSC and thiosulfate (SSO_3) (Johannes et al., 2022), which allow for early disease identification. A few treatment options for MoCD have been developed previously, but only efficient if early steps of the co-factor synthesis are affected (Veldman et al., 2010). To date, MoCD caused by gephyrin dysfunction (MoCD type III) cannot be treated. The only option is the dietary restriction of sulfur (cysteine- and methionine-poor diet) to reduce cysteine catabolism and thus sulfite production (Abe et al., 2021), which may be still insufficient. Thus, research is still going on to find new treatment options tackling different angles, for instance the protection of SSC-mediated neurodegeneration, or inhibition of enzymes involved in cysteine-catabolism to reduce sulfite production.

If not the enzymatic, but the neuronal function of gephyrin is impaired, neuronal impairments are caused by a mechanism different from that of MoCD. Here, GABAergic and glycinergic impairments can be distinguished. Glycinergic synapses are predominantly found in the brain stem and spinal cord, CNS regions e.g. responsible for motion and sensation (Legendre, 2001). Impairments of gephyrin-GlyR interactions result in disturbed glycinergic inhibition leading to a lack of muscle inhibition and a

permanent tension and stiffness such as found in stiff-man syndrome (Butler et al., 2000) and hyperekplexia (Rees et al., 2003).

GABAergic impairments result in more and multiple disease facets. For instance, the gephyrin variant D422N was found in a patient with epileptic encephalopathy, which had no functional wt gephyrin allele (Macha et al., 2022b). The mutation led to an altered gephyrin structure resulting in reduced receptor clustering and inhibitory signal transmission, but interestingly enhanced Moco activity. The D422N variant had no dominant negative effect on wt gephyrin in heterozygous individuals. In contrast, the variant G375D found in a heterozygous patient with epileptic encephalopathy, had a dominant negative effect on the neuronal function of remaining wt gephyrin (Dejanovic et al., 2015). Here a spontaneous point mutation resulted in a single amino acid residue exchange disrupting the formation of synaptic gephyrin clusters resulting in reduced GABAergic signal transmission. The G375D variant showed abolished Moco activity, but in the heterozygous patient, this metabolic dysfunction could be rescued by the healthy gephyrin allele.

Besides missense mutations, several cases of gephyrin microdeletions have been found in patients suffering from autism, epilepsy and schizophrenia (Lionel et al., 2013; Dejanovic et al., 2014b). The microdeletions span different areas of the G-, C- and E-domain. One microdeletion, spanning exons 5-9, was functionally characterized (Dejanovic et al., 2014b). Again, synaptic clustering was disturbed leading to impairments in GABAergic neurotransmission due to reduction of gephyrin-dependent synaptic $GABA_ARs$ based on a dominant-negative effect of the variant on wt gephyrin. In some cases, the molecular role of gephyrin in diseases is not fully understood. Reasons could be the lack of knowledge about affected brain regions and neuronal circuits, as well as unknown downstream or upstream pathways. For instance, gephyrin expression was altered in cases of familiar AD and occurred in plaque-like accumulations, but the reason for this remains elusive (Hales et al., 2013). In another study, it was reported, that gephyrin expression and thus GABAergic neurotransmission is reduced in depression and social distress (Heshmati et al., 2020).

In summary, gephyrin-associated neuronal diseases targeting GABAergic signal transmission are more complex and not completely understood. Nevertheless, for some diseases, treatment options are available such as benzodiazepines as epileptic and anxiolytic drugs (Griffin et al., 2013). To develop more therapy options, it is worthy to investigate gephyrin functions in health and disease and get new molecular insight into up- and downstream effects related to gephyrin.

1.6. Regulation of gephyrin clustering

Gephyrin scaffolding properties are regulated by the interaction with and modification by many proteins (Figure 4). Crucial properties of gephyrin that are the target of regulation are oligomerization (gephyrin-gephyrin interaction), (re-)localization (synaptic trafficking), receptor binding (gephyrin-receptor interactions) and stability (turnover). Importantly, most PTM sites and binding motifs are located in the C-domain of gephyrin, likely due to the flexibility of this domain. A selection of important binding partners and PTMs of gephyrin are described in the following sections.

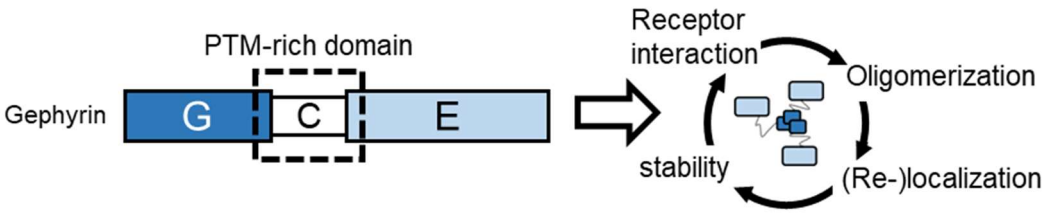

Figure 4: Gephyrin regulation.
The C-domain of gephyrin is the target of many PTMs and contains several motifs for the interaction with other proteins. The interaction/PTM influences four major properties of gephyrin: (Re-)localization, oligomerization, stability and receptor interaction. These properties are important for the synaptic function of gephyrin.

1.6.1. Phosphorylation - regulation of synaptic clustering

Over 18 residues (serines, tyrosines and threonines) - mainly in the C-domain of gephyrin - have been identified as phosphorylation sites (Tyagarajan et al., 2011; Herweg and Schwarz, 2012; Kuhse et al., 2012; Zacchi et al., 2014). Known kinases phosphorylating gephyrin are glycogen synthase kinase 3β (GSK3β) (Tyagarajan et al., 2011), cyclin-dependent kinase 5 (CDK5) (Kuhse et al., 2012), extracellular signal-regulated protein kinase1 (ERK1) (Tyagarajan et al., 2013), calmodulin-dependent protein kinase II (CamKII) (Flores et al., 2015) and cAMP-dependent protein kinase (PKA) (Battaglia et al., 2018). In functional synaptic clusters, gephyrin is expected to be constitutively phosphorylated at Ser270 and even a phospho-specific monoclonal antibody (mAb7a) is available (Kuhse et al., 2012). Interestingly, GSK3β and CDK5 compete for Ser270 (Tyagarajan et al., 2011; Kuhse et al., 2012), which highlights that gephyrin is involved in different signaling pathways and that the effects and interplays are complex. A phosphorylation-dependent induction of conformational changes leading to an interplay with other PTMs (1.6.5, 1.6.6) adds another level of complexity. Importantly, phosphorylation is a reversible PTM, which can be removed by phosphatases. One suggested gephyrin phosphatase is protein phosphatase 1 (PP1) (Bausen et al., 2010). Recently, additional phosphatases and kinases were identified in the gephyrin interactome, such as serine/threonine-protein phosphatase 2A 55 kDa

regulatory subunit B alpha isoform (2ABA) or mitogen-activated protein kinase 1 (MK01) (Campbell et al., 2022), but it is elusive whether gephyrin is a direct target. However, (de-)phosphorylation alters synaptic oligomerization and stability of gephyrin in a dynamic manner which is important for plasticity and inhibitory neurotransmission. The current picture of phosphorylation-dependent regulation of gephyrin is even incomplete, since for some phosphorylation sites the physiological relevance has not been investigated so far.

1.6.2. Collybistin – lipid and receptor adapter

The receptor-gephyrin interaction at GABAergic synapses is further facilitated by collybistin (Cb) (Kins et al., 2000), a GDP/GTP-exchange factor (GEF) that consists of three domains: The SRC homology 3 (SH3) domain, that interacts with neuroligin2 and $GABA_AR$ α2, the diffuse B-cell lymphoma homology (DH) domain that harbors the GEF activity and lastly, the pleckstrin homology (PH) domain, which interacts with lipids. Collybistin occurs in three splice variants, Cb I, II and III, which differ in the length of the C-terminal extension or the presence of the SH3 domain (Harvey et al., 2004). The SH3 domain showed autoinhibitory activity, that prevents GEF activity and lipid interaction. The interaction with binding partners or even ‘external’ SH3 domains was shown to activate Cb (Imam et al., 2022). The interaction of gephyrin and Cb is mediated through the E-domain and the DH domain respectively. Interestingly, it was recently shown that gephyrin E-domain dimerization is not crucial for Cb binding, but stabilizes the interaction (Imam et al., 2022). Gephyrin-collybistin interaction is necessary for $GABA_AR$ clustering in brain regions, where $GABA_AR$ subunits are composed of α1 and α2 subunits, while α3-containing receptors are clustered in a Cb-independent manner (Wagner et al., 2021). Consequently, loss of Cb leads to a brain region-specific loss of gephyrin and $GABA_AR$ clusters and thus neuronal impairments (Wagner et al., 2021).

1.6.3. Dynein light chain – Receptor transport

Dynein light chain 1 (DLC1) is also referred to as dynein LC8 or protein inhibitor of neuronal nitric oxide synthase (PIN) (Jaffrey and Snyder, 1996b) and has one homologue (DLC2). Gephyrin co-localizes with DLC1/2 at inhibitory synapses (Fuhrmann et al., 2002a). Here, two binding sites within the gephyrin C-domain have been identified, one high-affinity site spanning residue 203-212 (Fuhrmann et al., 2002b) and one low-affinity site spanning residue 246-258 (Bai et al., 2021). The interaction of DLC1/2 and gephyrin was initially thought to be required for the long retrograde transport of gephyrin-GlyRs via the dynein motor complex(Maas et al., 2006). So far it was revealed that disruption

of the DLC1/2-gephyrin interaction led to decreased synaptic GlyRs but had neglectable effects on GABAergic synapses indicating that the transport of $GABA_ARs$ is mediated by other mechanisms (Fuhrmann et al., 2002b; Maas et al., 2006). Additionally, the lack of the DLC-binding motif had no negative influence on synaptic clustering of gephyrin in cultured neurons, so it was assumed that DLC-binding is of minor importance for gephyrin function (Fuhrmann et al., 2002b). Recently, DLC1 binding of gephyrin was linked to the promotion of liquid-liquid phase separation (1.6.6) of gephyrin in the presence of a dimeric GlyR ICD model (Bai et al., 2021). Besides that, gephyrin interacts with both, nitric oxide synthase (nNOS) (1.7.2) and DLC1, which may act as an inhibitor of nNOS at synapses, thus the formation of a ternary complex controlling gephyrin function was supposed (Fuhrmann et al., 2002b; Dejanovic and Schwarz, 2014; Kress, 2016). Both new observations implicate that the importance of DLC-binding for gephyrin function is not yet completely understood and might be underestimated.

1.6.4. Calpain – irreversible cleavage

Calpain is a calcium-dependent protease, widely expressed in tissue-specific isoforms (Perrin and Huttenlocher, 2002). In contrast to most other proteases, which fully degrade their substrates upon activation, calpains cleave their substrates at specific and limited sites (duVerle and Mamitsuka, 2019; Fan et al., 2019). Accordingly, calpain targets only the C-domain of gephyrin (Gonzalez, 2019). Calcium-dependent activation of calpain is tightly regulated as it is involved in necrotic and apoptotic cell death pathways exceeding a critical role in cellular homeostasis (Metwally et al., 2023). Since calcium primarily emerges in neurons from excitatory synapses, calpain activation at inhibitory synapses may be the result of a cross-talk between the two synapse types. Irreversible calpain-mediated degradation is considered important for gephyrin homeostasis but is also associated with neurodegenerative onsets (Kumar et al., 2017). Consequently, calpain influences synaptic gephyrin pools and thus the clustering of inhibitory synapses important for neuronal health (Costa et al., 2016; Gonzalez, 2019).

1.6.5. Peptidyl-prolyl isomerase NIMA interacting protein 1 – *cis-trans*-isomerization

The proline-rich motif within gephyrin ranging from residue 88-201 (SPPPPLSPPPTTSP), recruits a peptidyl-prolyl isomerase called ‘Pin1’ in a phosphorylation-dependent manner (Zita et al., 2007). Pin1 stands for: Peptidyl-prolyl isomerase never in mitosis gene A (NIMA) interacting protein 1. Pin1 efficiently recognizes phosphorylated serines and threonines and induces *cis-trans*-isomerization

of neighboring prolines and thus induces conformational changes in the polypeptide chain of its target. In case of gephyrin, serines 188, 194 and 200 are crucial for the Pin1 interaction. Importantly, *cis-trans*-isomerization of gephyrin regulates the binding to the β-subunit of GlyRs. If Pin1-mediated prolyl-isomerization of gephyrin is disturbed, less GlyRs reach the post-synaptic site and inhibitory signal transmission is reduced. One molecular explanation is the influence of conformational changes on gephyrin binding to motor complexes and thus the transport of GlyRs. Alternatively, isomerization maybe needed to convert low-affinity receptor binding sites to high-affinity ones increasing the stability of gephyrin-GlyR clusters (Zita et al., 2007).

Cis-trans-isomerization is also important at GABAergic synapses. Phosphorylation-dependent prolyl-isomerization of NL2 negatively affects its complex formation with gephyrin and thus the number of synaptic $GABA_A$Rs (Antonelli et al., 2014). The conformational change of NL2 likely leads to the release of gephyrin from the complex. However, it is elusive, weather Pin1-NL2 interaction also leads to prolyl-isomerization within gephyrin. In contrast to glycinergic synapses, Pin1 activity downregulates the number of synaptic $GABA_A$Rs.

1.6.6. Liquid-liquid phase separation - generation of microdomains

Liquid-liquid phase separation (LLPS) is the formation of still soluble, but separated phases of macromolecules visible as droplets. Usually, the driving force for LLPS is the energetically favorable formation of macromolecule-macromolecule interactions over macromolecule-water interactions (Alberti et al., 2019). This can be influenced by the concentration and nature of the surrounding environment such as charged ions and the presence of other macromolecules.

Recently, it was discovered that gephyrin undergoes LLPS *in vitro* (Bai et al., 2021), which required the presence of a multimeric interaction partner. *In cellulo*, gephyrin forms condensates in an expression-dependent manner (Lee et al., 2024) (Figure 5). Importantly, LLPS is mediated through the E-domain and an oligomerization-deficient gephyrin variant (“RER” variant, G483R/R523E/A532R) (Saiyed et al., 2007) could not undergo LLPS indicating that gephyrin oligomerization is required for LLPS (Bai et al., 2021). The role of the C-domain for LLPS is still discussed. On the one hand, the C-domain is required for LLPS, since gephyrin variants lacking the C-domain (‘GE’ variants) are unable to undergo LLPS (Bai et al., 2021; Lee et al., 2024). Besides the connection of G- and E-domain to allow for oligomerization, it was shown that the C-domain harbors important positive charges required for LLPS (Lee et al., 2024). On the other hand, the C-domain acts LLPS-autoinhibitory, which was removed by DLC-interaction (1.6.3) and

phosphorylation at Ser305 (Bai et al., 2021). In summary, it is assumed that the C-domain influences LLPS in gephyrin through charged residues and may be further modulated by PTMs and interaction partners.

The discovery of LLPS of gephyrin adds a new dimension to the current picture of gephyrin regulation. Membraneless microdomains can be formed through LLPS, which may further compartmentalize synaptic components in PSDs, thus allowing for differences in molecule concentrations and influencing protein function within different phases. In case of gephyrin, receptor-interaction and consequently neurotransmission might be strengthened and regulated through LLPS. Moreover, it was recently suggested that LLPS is an important sorting mechanism, separating excitatory and inhibitory microdomains (Zhu et al., 2024).

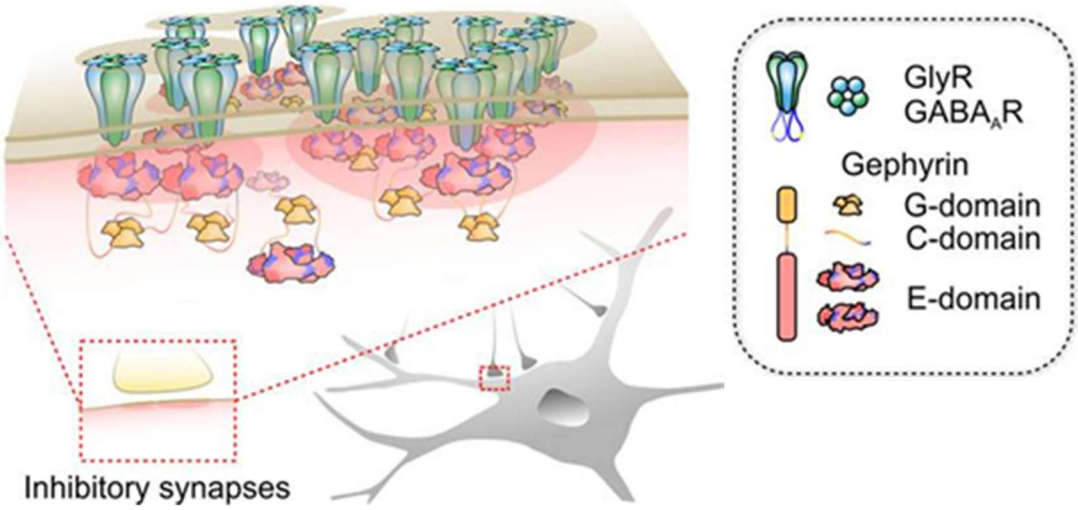

Figure 5: Liquid-liquid phase separation of gephyrin.
Edited picture (Bai et al., 2021). Schematic illustration of LLPS of gephyrin and receptors at inhibitory post-synapses.

1.7. Regulation on thiols and redox-signaling at synapses

1.7.1. Gephyrin S-palmitoylation

In this thesis, especially PTMs on cysteines were investigated. Previously, S-palmitoylation and S-nitrosylation were found to play crucial roles in localization of gephyrin (Dejanovic and Schwarz, 2014; Dejanovic et al., 2014a). Localization is a critical factor in regulating gephyrin function at synapses and consequently, inhibitory synaptic transmission. The current picture is, that gephyrin is S-palmitoylated at Cys212 and Cys284, with Cys212 being considered as the more relevant target of S-palmitoylation (Dejanovic et al., 2014a). This was demonstrated through overexpression of Cys-to-Ser variants in cultured hippocampal neurons: The absence of S-

palmitoylation, either by substitution of cysteines or by treatment with a palmitoyltransferase inhibitor, resulted in decreased cluster sizes and reduced synaptic ratios of gephyrin punctae. These effects were reflected in electrophysiological outcomes, as the lack of S-palmitoylation led to decreased inhibitory GABAergic signal transmission. The family of palmitoyltransferases comprises 23 known members (Fukata et al., 2004), with the enzyme responsible for attaching palmitoyl residues on gephyrin's cysteines identified as zinc finger DHHC domain-containing protein 12 (ZDHHC12) (Dejanovic et al., 2014a). In summary it was suggested that S-palmitoylation, which adds a fatty acid (C16) moiety on cysteines, increases the affinity of gephyrin for the post-synaptic membrane. Cleavage of these lipid anchors would result in re-localization of gephyrin to the cytosolic pool leading to dynamic, S-palmitoylation-dependent shuttling of gephyrin (Dejanovic et al., 2014a). However, a palmitoyl protein thioesterase (PPT), responsible for gephyrin S-depalmitoylation, has not been identified yet.

Initially, S-palmitoylation was predominantly investigated *in cellulo* and the physiological importance was elusive (Dejanovic et al., 2014a). Later, gephyrin S-palmitoylation was investigated for the first time *in vivo* using rats as a model system (Shen et al., 2019). The study provided new insight into the relation of anxiety and gephyrin S-palmitoylation. A reduction of gephyrin S-palmitoylation was identified in a cohort of rats with high-anxiety states. Additionally, the therapeutic effects of diazepam, an anxiolytic drug were examined (Shen et al., 2019). In the basal amygdala, the brain region responsible for anxiety response, diazepam enhances $GABA_AR$ activity leading to enhanced gephyrin S-palmitoylation recruiting more $GABA_ARs$, ultimately resulting in a feed-forward mechanism of synaptic pruning. GABAergic inhibition within this brain region leads to anxiolytic actions. With this, gephyrin S-palmitoylation could be linked to a specific behavioral outcome. Additional roles of gephyrin S-palmitoylation *in vivo*, for example in other brain regions or other organisms, remain to be discovered.

1.7.2. Gephyrin S-nitrosylation

Besides S-palmitoylation as a thiol-based reversible PTM, gephyrin undergoes NO-mediated S-nitrosylation and co-localizes with neuronal nitric oxide synthase (nNOS) (Dejanovic and Schwarz, 2014). The precise mechanism how nNOS mediates S-nitrosylation is still elusive. It was suggested that nNOS-produced NO either directly nitrosylates selected target proteins or S-nitrosylation occurs first on reduced glutathione and is further transferred through *trans*-S-nitrosylation (Stomberski et al., 2019). However, due to the reactivity of NO, close proximity to the NO source increases the chance for a protein to be S-nitrosylation (Nakamura and Lipton, 2016). Thus, S-nitrosylation of gephyrin is emphasized via co-localization with nNOS.

Importantly, in contrast to S-palmitoylation, S-nitrosylation led to a decrease in cluster sizes of synaptic gephyrin and thus causes opposite effects to S-palmitoylation (Dejanovic and Schwarz, 2014; Dejanovic et al., 2014a). Interestingly, preliminary data of the Schwarz Lab suggested that S-nitrosylation appears on Cys212 and 284 similar to S-palmitoylation (Kress, 2016). Thus, the competition and regulation of both thiol modifications remains one open question in the field (Figure 6). Moreover, nNOS is a calcium-dependent enzyme (Marletta, 1994) and calcium can originate as one source from excitatory glutamatergic synapses which indicates a signaling between excitatory and inhibitory synapses. Interestingly, nNOS can be inhibited by interaction with DLC (originally named protein inhibitor of neuronal nitric oxide synthase (PIN)) (Jaffrey and Snyder, 1996a). Since both, DLC and nNOS interact with gephyrin, a possible formation of a ternary complex would be feasible for the regulation of gephyrin S-nitrosylation.

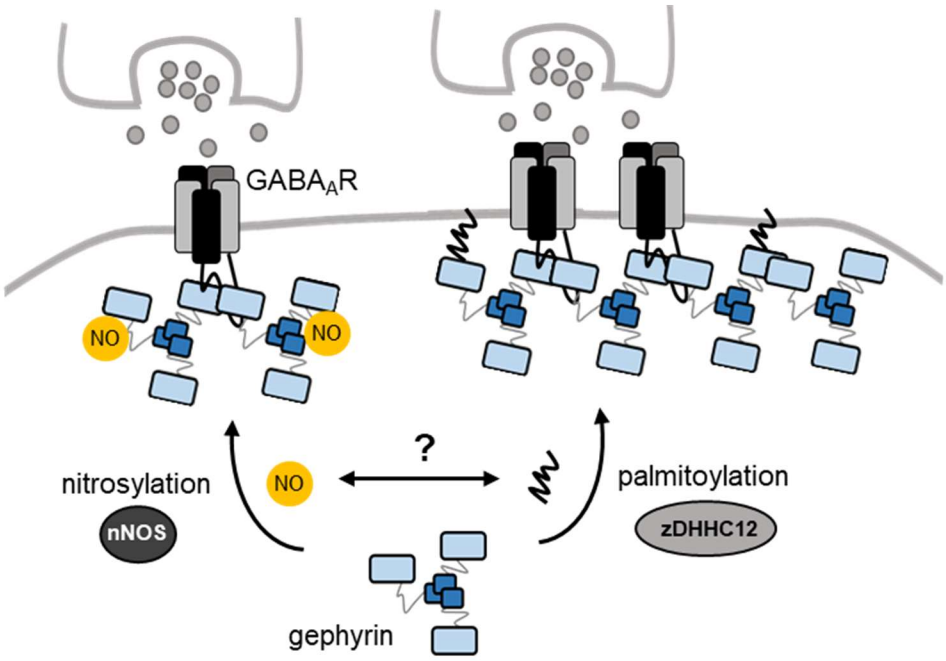

Figure 6: S-nitrosylation and S-palmitoylation of gephyrin
Gephyrin is S-nitrosylated possibly through interaction with neuronal nitric oxide synthase (nNOS) leading to smaller synaptic clusters. In contrast, gephyrin S-palmitoylation mediated by zinc finger DHHC domain-containing protein 12 (ZDHHC12) leads to bigger synaptic clusters. The regulation whether gephyrin is S-nitrosylated or S-palmitoylated is elusive (?).

1.7.3. Role of additional surface-exposed cysteines

Notably, gephyrin harbors in total 12 cysteines, four of which are internal ones, and eight of which are presumably surface-exposed. For the most abundant of gephyrin variant 'P1' or 'GPHN-1', Cys26, 154, 212, 284, 293, 419, 469 and 633 are potentially surface-exposed. Cys26 and 154 and 419, 469 and 633 in G- and E-domain, the respective crystal structures demonstrate their surface exposed nature in their trimeric and dimeric

state (Schwarz et al., 2001; Sola et al., 2001; Kim et al., 2006) (Figure 7). For Cys212, 284 and 293 in gephyrin C-domain surface-exposure may be suggested due to the domain flexibility and the identification of S-palmitoylation on Cys212 and 284 (Dejanovic et al., 2014a). Due to the lack of any structural data on full-length gephyrin or the C-domain, it remains open where those cysteines are localized.

Cysteine is a 'special' amino acid with the only free thiol group in the class of amino acids. This thiol group gives unique chemical features and is important for many processes in nature, such as regulation of enzymatic activity (e.g. 'redox switches' as in glycerinaldehyd-3-phosphat-Dehydrogenase (GAPDH) (Talwar et al., 2023)), catalysis of nucleophilic and redox reactions in active centers of enzymes (e.g. cysteine proteases such as calpain (Ohno et al., 1984), thiol oxidoreductases such as thioredoxin (Zhong et al., 2000)), metal binding (e.g. FeS clusters (Shi et al., 2021)), structural and localization aspects (di-sulfides (Trivedi et al., 2009), S-palmitoylation (Aicart-Ramos et al., 2011)) and more (Pace and Weerapana, 2013). Moreover, thiols are sensitive to reactive oxygen species impacting their redox-state and thus their function. Examples for different redox states are: Free thiol (S-H), persulfide (S-SH), di-sulfide (S-S), nitroso-thiol (S-NO), palmitoyl-thiol (S-palm), sulfenic acid (S-OH), sulfinic acid ($S-O_2H$) and sulfonic acid ($S-O_3H$). Importantly, proteins harboring accessible, surface-exposed cysteines are prone to redox-changes and cysteine-exposure is linked to its conservation and function (Marino and Gladyshev, 2010). This indicates that surface exposure of the eight cysteines of gephyrin may be linked to a certain function and a potential role for redox-regulation would be likely. For Cys212 and 284 one function has been shown, but the role of the other cysteines is unknown so far, which might be a redox-dependent function.

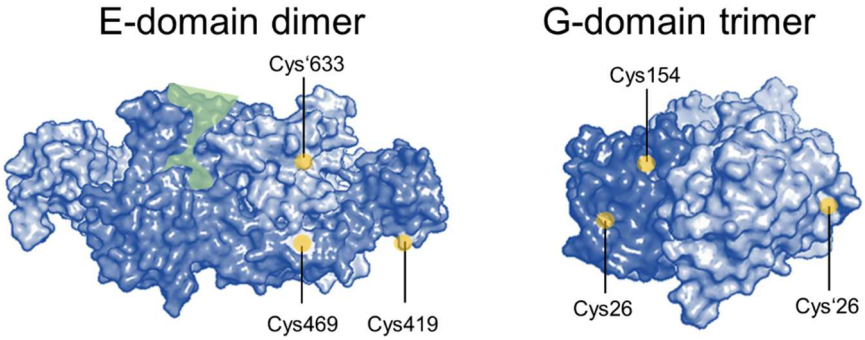

Figure 7: Surface-exposed cysteines in multimerized domains of gephyrin.
Crystal structures reveal surface-exposure of Cys26, 154, 419, 469 and 633 in gephyrin trimerized G-domain (1IHC (Sola et al., 2001)) and dimerized E-domain (2FU3 (Kim et al., 2006)), respectively. Cys indicated in yellow, binding pocket for receptor ICDs within the E-domain dimer indicated in green.

1.7.4. Insights into redox-regulation

The term redox-regulation describes the interplay of reduction (red) and oxidation (ox) reactions in biological processes. In a redox-reaction, at least one electron is intermolecularly removed from one atom and transferred to another leading to altered chemical properties of both biomolecules. The driving force and reactivity for electron donation or acceptance (redox potential) is given by the chemical properties of each reaction partner and both partners together are called a redox-couple.

One group of highly active electron acceptors are reactive oxygen species (ROS), which react with the next available target categorizing them as 'uncontrolled' thus limiting their radius of action (Collin, 2019). Primary ROS molecules are superoxide anion ($\cdot O_2^-$), hydroxyl radical ($HO^{\cdot}$) and hydrogen peroxide (H_2O_2). ROS quickly oxidize targets such as proteins (especially accessible protein thiols), lipids, DNA and small molecules, which is an important process in health and disease (Bardaweel et al., 2018). Thus, ROS levels are strictly controlled by production and clearance machineries (Figure 8).

ROS are mainly produced through oxidative phosphorylation during mitochondrial activity (Turrens, 2003) and NADPH oxidases (NOXs) (Vignais, 2002), but also several other enzymes such as xanthine oxidase (XO) (Schmidt et al., 2019) and *D*-amino acid oxidase (DAAO) (Pollegioni et al., 2007) contribute to ROS production under various physiological conditions. Due to the highly reactive and 'uncontrolled' nature, ROS require fast quenching systems. Inactivation of ROS is mediated for instance through small molecules such as reduced glutathione (GSH) and ascorbate (Steenvoorden and van Henegouwen, 1997), which need to be reduced enzymatically after their consumption (Khatami et al., 1986; Vogel et al., 1999). GSH is omnipresent in the cell, and GSH levels are maintained on high level in the cytosol making it a stable, reductive environment (Lopez-Mirabal and Winther, 2008). Since the reaction of GSH with ROS is considered slow, GSH is above all, co-substrate of ROS inactivating enzymes, such as glutathione peroxidase (GPx) (Mailloux et al., 2013). Alternatively, ROS can be removed by GSH-independent enzymes such as superoxide dismutase (SOD) (Fridovich, 1995) and catalase (Cat) (Deisseroth and Dounce, 1970). Other mechanisms involve enzymes, such as peroxiredoxin (Prx), which can also revert ROS-mediated reactions on lipids and proteins (Mailloux et al., 2013). Following the reaction between several redox-couples, the final electron donor of regeneration is NADPH.

Lastly, since ROS-producing machineries are compartmentalized in mitochondria for instance, it is assumed that ROS levels differ subcellularly resulting in redox-microenvironments (Buettner et al., 2013). Synapses are considered reductive compartments due to the connection to the reductive cytosol and the presence of

reductive machineries. However, measurements of precise redox-conditions are challenging since ROS-detection (e.g. through HyPer (Hernandez et al., 2018) and roGFP-fusion proteins (Schwarzlander et al., 2016)) is limited to display redox-changes but no absolute concentrations. Thus, specified resolution of redox-signaling at synapses is elusive so far. Furthermore, it is possible that LLPS (1.6.6) at synapses creates additional redox-microenvironments.

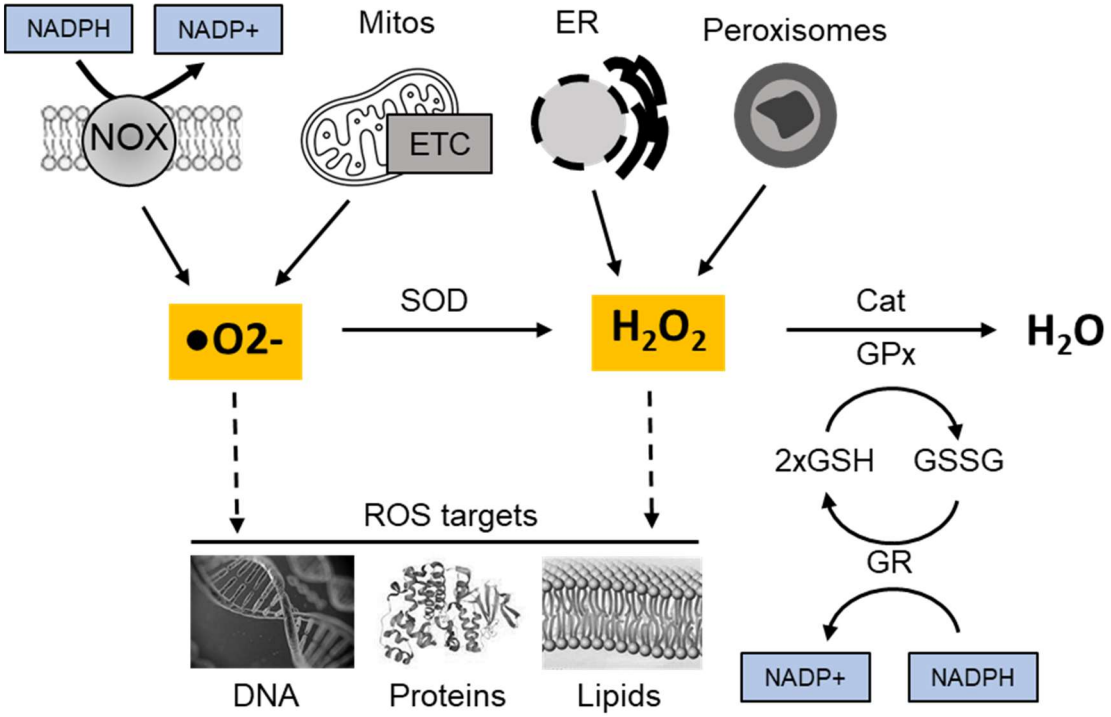

Figure 8: Examples of ROS sources and sinks
Superoxide ($\cdot O_2^-$) and hydrogen peroxide (H_2O_2) as examples of reactive oxygen species (ROS) and ROS targets. ROS originate e.g. from NADPH oxidase (NOX), mitochondria, the ER and peroxisomes. Clearance ma-chineries exist:$\cdot O_2^-$ is detoxified to H_2O_2 by superoxide dismutase (SOD). H_2O_2 is converted to water by catalase (Cat) or glutathione peroxidase (GPx), which oxidizes glutathione (2xGSH ->GSSG). GSSG is reduced by glutathione reductase (GR) using NADPH as final electron donor.

1.7.5. Redox-regulation at synapses - NOX2 and mROS

In the last decades, redox-regulation emerged as an innovative field in neuroscience. For a long time it was believed, that ROS mainly cause cellular damage and were associated with aging (Harman, 1956) and diseases such as Alzheimer's disease (AD) (Marcus et al., 2006) and Huntington's disease (HD) (Olanow, 1990). But the view on ROS has shifted and assigned ROS a new vital role as messengers in synaptic plasticity (Gahtan et al., 1998; Oswald et al., 2018). It is known that two main ROS-generating sources exist at synapses: First, mitochondria (Turrens, 2003) and second NADPH oxidases (Vignais, 2002).

Mitochondria as a ROS-source are comprehensive, since they exist at pre- and post-synapses in high density as neurotransmission demands high energy in form of ATP (Attwell and Laughlin, 2001), which is - with ROS as a byproduct – predominantly produced during oxidative phosphorylation (Turrens, 2003). On the other hand, NOX2, one isoform of the NOX family, was found in the post-synaptic plasma membrane (Tejada-Simon et al., 2005). NOX2 produces extracellular O_2^-, that is converted to H_2O_2 by SOD3, which can re-enter the cell through aquaporins (Bienert and Chaumont, 2014). Importantly, assembly and activity of the NOX2 complex requires Ca^{2+}-signaling, which in turn relies on excitatory signal transmission (Wang and Swanson, 2020). Thus, both ROS sources, mitochondria and NOX2, are linked to neuronal activity.

Although, redox-regulation has been well studied for excitatory synapses (Doser and Hoerndli, 2021; Villegas et al., 2021; Doser et al., 2024), less is known about inhibitory synapses. In one study, mROS were generated in neurons by antimycin A treatment (inhibitor of complex III of the respiratory chain) (Accardi et al., 2014). It was found that mitochondria-derived ROS (mROS) led to an increase in inhibitory signal transmission. Interestingly, this effect was dependent on $GABA_A$Rs containing the α3 subunit. The exact molecular reason for mROS-mediated strengthening of inhibitory transmission was elusive. In a second study, ROS were generated through the NOX2 pathway of glutamatergic synapses neighboring inhibitory sites (Larson et al., 2020). A signaling cascade between excitatory and inhibitory synapse was discovered, with the last step of NOX2-mediated ROS activation of protein kinase C (PKC). PKC in turn activated GABA type A receptor-associated protein (GABARAP) and recruited $GABA_A$Rs containing the α3 subunit.

The role of gephyrin in redox-regulation is elusive so far. Evidence that gephyrin might be involved in synaptic redox-regulation are that, a) it is the main organizer of inhibitory synapses and a key player in many processes, b) contains potential redox-sensitive surface-cysteines (1.7.3), and c) was found to interact with GPx4 (Campbell et al., 2022), which is an important enzyme in redox-control of membrane lipids (1.7.4). d) Furthermore, gephyrin has the strongest binding affinity towards the α3 subunit of $GABA_A$Rs (Maric et al., 2011), which was involved in the previously identified redox-regulation mechanisms (Larson et al., 2020) and e) undergoes LLPS which potentially offers an oxidative microenvironment in the reductive cytosol. Thus, significant potential remains for the identification of redox processes at inhibitory synapses, including those dependent on gephyrin.

1.8. Aims of this thesis

Although several regulation mechanisms of gephyrin clustering and synapse formation by PTMs have been reported, the picture remains still incomplete. The discovery of more PTMs raises the importance of understanding the interplay among diverse PTMs and their contribution to gephyrin function (Figure 9). This understanding is crucial for neuronal plasticity and signaling between excitatory and inhibitory synapses. Consequently, manipulating gephyrin regulation offers great potential for the treatment of neuronal diseases. To achieve this, it is necessary to understand regulation mechanisms (ideally) at spatial, temporal, and molecular levels. In this thesis, the primary aim was to shed more light on the importance and regulation mechanisms of thiol-based PTMs in gephyrin.

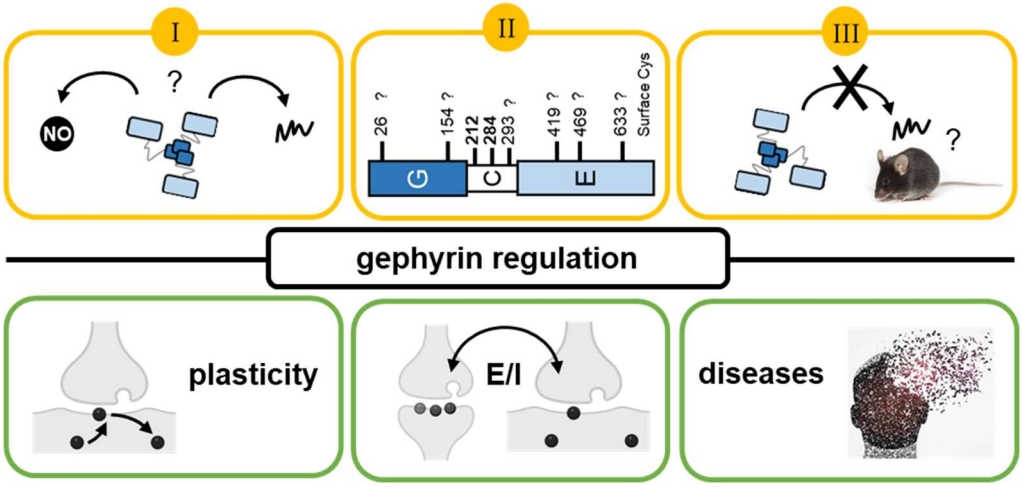

Figure 9: Importance of the understanding of gephyrin regulation.
Schematic illustration of the main goals (yellow boxes) of this thesis and the importance for understanding neuronal processes (green boxes). Main aims: Interplay of S-nitrosylation and S-palmitoylation (I), role of additional surface cysteines of gephyrin (II), relevance of PTMs *in vivo* by removal of PTMs (III). Global relevance: Role for synaptic plasticity, ratio of excitation and inhibition (E/I), role for pathology of diseases.

I. How are thiol-based PTMs of gephyrin regulated?

Both S-palmitoylation and S-nitrosylation of gephyrin occur on surface-exposed cysteines but lead to opposing effects (1.7.1, 1.7.2). This raises the question whether both modifications compete for the same cysteine residues of gephyrin, and if so, how this is regulated. Thus, one aim of this thesis was to further investigate the interplay of S-nitrosylation and S-palmitoylation and verify Cys212 and 284 as S-nitrosylation targets (chapter 2). The hypothesis was that gephyrin forms a ternary phosphorylation-dependent complex with nNOS and DLC. When this complex is formed, DLC inhibits nNOS and S-palmitoylation is favored. If DLC is not present, S-nitrosylation is favored instead. The expression of recombinant gephyrin variants in cultured hippocampal neurons of conditional gephyrin knock out mice was used to verify the postulated S-nitrosylation targets Cys212 and 284 and the formation of the gephyrin-DLC-nNOS complexes (chapter 2).

II. What are the functions of the surface-exposed cysteines of gephyrin?

S-palmitoylation is a well characterized PTM of gephyrin occurring at residues Cys212 and 284, but gephyrin also contains additional surface-exposed cysteines with unknown functions (1.7.3). Notably, the surface exposure of cysteines likely emphasizes their redox-sensitivity, and previous reports have indicated redox-dependent regulation mechanisms for excitatory and inhibitory synapses (1.7.5). Moreover, mitochondria, which are highly abundant in neurons, produce ROS, suggesting a potential ROS/redox signaling between mitochondrial and neuronal activity. This raises the question of which players (gephyrin?) are involved in such signaling mechanisms. Consequently, one aim of this thesis was to investigate the potential role of gephyrin's surface cysteines in redox regulation at synapses (chapter 3). A key experiment involved the generation of gephyrin cysteine-to-serine variants and studying their biochemical, structural and cellular function using a combination of various *in vitro* and *in cellulo* systems of synaptic clustering in a redox-dependent manner.

III. What is the physiological relevance of gephyrin thiol-based (and other) PTMs?

One common challenge in studying regulatory mechanisms such as PTMs is the limitation to simplified biological systems through *in vitro* and *in cellulo* experiments. This also applies to the identification of many PTMs of gephyrin (1.6). S-palmitoylation at Cys212 and Cys284 are examples for such a limitation. However, a recent study demonstrated that gephyrin-S-palmitoylation-deficient rats suffered from high-anxiety *in vivo* (1.7.1), but the behavioral examination was limited to the amygdala as a specific brain region. In this thesis, the aim was to create a new mouse line with the full-body gephyrin substitution of Cys212 to Ser212 to enable additional investigation of the importance of gephyrin S-palmitoylation *in vivo*. Although this mouse line could not be generated, a mouse line with the microdeletion ∆199-233 was established instead. The microdeletion mouse model was used to investigate the importance of the C-domain, with a focus on the DLC binding motif, as well as Cys212 (chapter 4). Given that human patients with microdeletions of gephyrin have been reported to cause various types of neurodegeneration, the new ∆199-233 mouse model has the potential to provide new insight into the contribution of different domains to gephyrin function and related pathological mechanisms of human cases.

References

Abe Y, Aihara Y, Endo W, Hasegawa H, Ichida K, Uematsu M, Kure S (2021) The effect of dietary protein restriction in a case of molybdenum cofactor deficiency with MOCS1 mutation. Mol Genet Metab Rep 26:100716.

Accardi MV, Daniels BA, Brown PM, Fritschy JM, Tyagarajan SK, Bowie D (2014) Mitochondrial reactive oxygen species regulate the strength of inhibitory GABA-mediated synaptic transmission. Nat Commun 5:3168.

Aicart-Ramos C, Valero RA, Rodriguez-Crespo I (2011) Protein palmitoylation and subcellular trafficking. Bba-Biomembranes 1808:2981-2994.

Alberti S, Gladfelter A, Mittag T (2019) Considerations and Challenges in Studying Liquid-Liquid Phase Separation and Biomolecular Condensates. Cell 176:419-434.

Antonelli R, Pizzarelli R, Pedroni A, Fritschy JM, Del Sal G, Cherubini E, Zacchi P (2014) Pin1-dependent signalling negatively affects GABAergic transmission by modulating neuroligin2/gephyrin interaction. Nat Commun 5:5066.

Attwell D, Laughlin SB (2001) An energy budget for signaling in the grey matter of the brain. J Cereb Blood Flow Metab 21:1133-1145.

Azevedo FA, Carvalho LR, Grinberg LT, Farfel JM, Ferretti RE, Leite RE, Jacob Filho W, Lent R, Herculano-Houzel S (2009) Equal numbers of neuronal and nonneuronal cells make the human brain an isometrically scaled-up primate brain. J Comp Neurol 513:532-541.

Bai G, Wang Y, Zhang M (2021) Gephyrin-mediated formation of inhibitory postsynaptic density sheet via phase separation. Cell Res 31:312-325.

Bardaweel SK, Gul M, Alzweiri M, Ishaqat A, HA AL, Bashatwah RM (2018) Reactive Oxygen Species: the Dual Role in Physiological and Pathological Conditions of the Human Body. Eurasian J Med 50:193-201.

Battaglia S, Renner M, Russeau M, Come E, Tyagarajan SK, Levi S (2018) Activity-Dependent Inhibitory Synapse Scaling Is Determined by Gephyrin Phosphorylation and Subsequent Regulation of GABA(A) Receptor Diffusion. eNeuro 5.

Baur R, Minier F, Sigel E (2006) A GABA(A) receptor of defined subunit composition and positioning: concatenation of five subunits. FEBS Lett 580:1616-1620.

Bausen M, Weltzien F, Betz H, O'Sullivan GA (2010) Regulation of postsynaptic gephyrin cluster size by protein phosphatase 1. Mol Cell Neurosci 44:201-209.

Bean BP (2007) The action potential in mammalian central neurons. Nat Rev Neurosci 8:451-465.

Belaidi AA, Schwarz G (2013) Metal insertion into the molybdenum cofactor: product-substrate channelling demonstrates the functional origin of domain fusion in gephyrin. Biochem J 450:149-157.

Betz H (1991) Glycine receptors: heterogeneous and widespread in the mammalian brain. Trends Neurosci 14:458-461.

Bienert GP, Chaumont F (2014) Aquaporin-facilitated transmembrane diffusion of hydrogen peroxide. Biochim Biophys Acta 1840:1596-1604.

Brini M, Cali T, Ottolini D, Carafoli E (2014) Neuronal calcium signaling: function and dysfunction. Cell Mol Life Sci 71:2787-2814.

Buettner GR, Wagner BA, Rodgers VG (2013) Quantitative redox biology: an approach to understand the role of reactive species in defining the cellular redox environment. Cell Biochem Biophys 67:477-483.

Burzomato V, Groot-Kormelink PJ, Sivilotti LG, Beato M (2003) Stoichiometry of recombinant heteromeric glycine receptors revealed by a pore-lining region point mutation. Recept Channels 9:353-361.

Butler MH, Hayashi A, Ohkoshi N, Villmann C, Becker CM, Feng G, De Camilli P, Solimena M (2000) Autoimmunity to gephyrin in Stiff-Man syndrome. Neuron 26:307-312.

Campbell BFN, Dittmann A, Dreier B, Pluckthun A, Tyagarajan SK (2022) A DARPin-based molecular toolset to probe gephyrin and inhibitory synapse biology. Elife 11.

Chen JL, Villa KL, Cha JW, So PT, Kubota Y, Nedivi E (2012) Clustered dynamics of inhibitory synapses and dendritic spines in the adult neocortex. Neuron 74:361-373.

Collin F (2019) Chemical Basis of Reactive Oxygen Species Reactivity and Involvement in Neurodegenerative Diseases. Int J Mol Sci 20.

Conti F, Weinberg RJ (1999) Shaping excitation at glutamatergic synapses. Trends Neurosci 22:451-458.

Costa JT, Mele M, Baptista MS, Gomes JR, Ruscher K, Nobre RJ, de Almeida LP, Wieloch T, Duarte CB (2016) Gephyrin Cleavage in In Vitro Brain Ischemia Decreases GABAA Receptor Clustering and Contributes to Neuronal Death. Mol Neurobiol 53:3513-3527.

daCosta CJ, Baenziger JE (2013) Gating of pentameric ligand-gated ion channels: structural insights and ambiguities. Structure 21:1271-1283.

Deisseroth A, Dounce AL (1970) Catalase: Physical and chemical properties, mechanism of catalysis, and physiological role. Physiol Rev 50:319-375.

Dejanovic B, Schwarz G (2014) Neuronal nitric oxide synthase-dependent S-nitrosylation of gephyrin regulates gephyrin clustering at GABAergic synapses. J Neurosci 34:7763-7768.

Dejanovic B, Semtner M, Ebert S, Lamkemeyer T, Neuser F, Luscher B, Meier JC, Schwarz G (2014a) Palmitoylation of gephyrin controls receptor clustering and plasticity of GABAergic synapses. PLoS Biol 12:e1001908.
Dejanovic B, Lal D, Catarino CB, Arjune S, Belaidi AA, Trucks H, Vollmar C, Surges R, Kunz WS, Motameny S, Altmuller J, Kohler A, Neubauer BA, Epicure C, Nurnberg P, Noachtar S, Schwarz G, Sander T (2014b) Exonic microdeletions of the gephyrin gene impair GABAergic synaptic inhibition in patients with idiopathic generalized epilepsy. Neurobiol Dis 67:88-96.
Dejanovic B, Djemie T, Grunewald N, Suls A, Kress V, Hetsch F, Craiu D, Zemel M, Gormley P, Lal D, Euro EDwg, Myers CT, Mefford HC, Palotie A, Helbig I, Meier JC, De Jonghe P, Weckhuysen S, Schwarz G (2015) Simultaneous impairment of neuronal and metabolic function of mutated gephyrin in a patient with epileptic encephalopathy. EMBO Mol Med 7:1580-1594.
Dos Reis R, Kornobis E, Pereira A, Tores F, Carrasco J, Gautier C, Jahannault-Talignani C, Nitschke P, Muchardt C, Schlosser A, Maric HM, Ango F, Allemand E (2022) Complex regulation of Gephyrin splicing is a determinant of inhibitory postsynaptic diversity. Nat Commun 13:3507.
Doser RL, Hoerndli FJ (2021) Regulation of neuronal excitability by reactive oxygen species and calcium signaling: Insights into brain aging. Curr Res Neurobiol 2:100012.
Doser RL, Knight KM, Deihl EW, Hoerndli FJ (2024) Activity-dependent mitochondrial ROS signaling regulates recruitment of glutamate receptors to synapses. Elife 13.
duVerle DA, Mamitsuka H (2019) CalCleaveMKL: a Tool for Calpain Cleavage Prediction. Methods Mol Biol 1915:121-147.
Essrich C, Lorez M, Benson JA, Fritschy JM, Luscher B (1998) Postsynaptic clustering of major GABAA receptor subtypes requires the gamma 2 subunit and gephyrin. Nat Neurosci 1:563-571.
Fan YX, Pan X, Zhang Y, Shen HB (2019) LabCaS for Ranking Potential Calpain Substrate Cleavage Sites from Amino Acid Sequence. Methods Mol Biol 1915:111-120.
Feng G, Tintrup H, Kirsch J, Nichol MC, Kuhse J, Betz H, Sanes JR (1998) Dual requirement for gephyrin in glycine receptor clustering and molybdoenzyme activity. Science 282:1321-1324.
Flores CE, Nikonenko I, Mendez P, Fritschy JM, Tyagarajan SK, Muller D (2015) Activity-dependent inhibitory synapse remodeling through gephyrin phosphorylation. Proc Natl Acad Sci U S A 112:E65-72.
Fridovich I (1995) Superoxide radical and superoxide dismutases. Annu Rev Biochem 64:97-112.
Fritschy JM, Harvey RJ, Schwarz G (2008) Gephyrin: where do we stand, where do we go? Trends Neurosci 31:257-264.
Froemke RC (2015) Plasticity of cortical excitatory-inhibitory balance. Annu Rev Neurosci 38:195-219.
Fuhrmann JC, Kins S, Rostaing P, El Far O, Kirsch J, Sheng M, Triller A, Betz H, Kneussel M (2002a) Gephyrin interacts with dynein light chains 1 and 2, components of motor protein complexes. Journal of Neuroscience 22:5393-5402.
Fukata M, Fukata Y, Adesnik H, Nicoll RA, Bredt DS (2004) Identification of PSD-95 palmitoylating enzymes. Neuron 44:987-996.
Gahtan E, Auerbach JM, Groner Y, Segal M (1998) Reversible impairment of long-term potentiation in transgenic Cu/Zn-SOD mice. Eur J Neurosci 10:538-544.
Gonzalez MI (2019) Calpain-dependent cleavage of GABAergic proteins during epileptogenesis. Epilepsy Res 157:106206.
Griffin CE, 3rd, Kaye AM, Bueno FR, Kaye AD (2013) Benzodiazepine pharmacology and central nervous system-mediated effects. Ochsner J 13:214-223.
Grunewald N, Jan A, Salvatico C, Kress V, Renner M, Triller A, Specht CG, Schwarz G (2018) Sequences Flanking the Gephyrin-Binding Site of GlyRbeta Tune Receptor Stabilization at Synapses. eNeuro 5.
Hales CM, Rees H, Seyfried NT, Dammer EB, Duong DM, Gearing M, Montine TJ, Troncoso JC, Thambisetty M, Levey AI, Lah JJ, Wingo TS (2013) Abnormal gephyrin immunoreactivity associated with Alzheimer disease pathologic changes. J Neuropathol Exp Neurol 72:1009-1015.
Harman D (1956) Aging: a theory based on free radical and radiation chemistry. J Gerontol 11:298-300.
Harvey K, Duguid IC, Alldred MJ, Beatty SE, Ward H, Keep NH, Lingenfelter SE, Pearce BR, Lundgren J, Owen MJ, Smart TG, Luscher B, Rees MI, Harvey RJ (2004) The GDP-GTP exchange factor collybistin: an essential determinant of neuronal gephyrin clustering. J Neurosci 24:5816-5826.
Hawkins J, Ahmad S (2016) Why Neurons Have Thousands of Synapses, a Theory of Sequence Memory in Neocortex. Front Neural Circuits 10:23.
Hernandez H, Parra A, Tobar N, Molina J, Kallens V, Hidalgo M, Varela D, Martinez J, Porras O (2018) Insights into the HyPer biosensor as molecular tool for monitoring cellular antioxidant capacity. Redox Biol 16:199-208.
Herweg J, Schwarz G (2012) Splice-specific Glycine Receptor Binding, Folding, and Phosphorylation of the Scaffolding Protein Gephyrin. Journal of Biological Chemistry 287:12645-12656.
Heshmati M, Christoffel DJ, LeClair K, Cathomas F, Golden SA, Aleyasin H, Turecki G, Friedman AK, Han MH, Menard C, Russo SJ (2020) Depression and Social Defeat Stress Are Associated with Inhibitory Synaptic Changes in the Nucleus Accumbens. J Neurosci 40:6228-6233.
Iasevoli F, Tomasetti C, de Bartolomeis A (2013) Scaffolding proteins of the post-synaptic density contribute to synaptic plasticity by regulating receptor localization and distribution: relevance for neuropsychiatric diseases. Neurochem Res 38:1-22.

Imam N, Choudhury S, Hemmen K, Heinze KG, Schindelin H (2022) Deciphering the conformational dynamics of gephyrin-mediated collybistin activation. Biophys Rep (N Y) 2:100079.
Jaffrey SR, Snyder SH (1996a) PIN: an associated protein inhibitor of neuronal nitric oxide synthase. Science 274:774-777.
Johannes L, Fu CY, Schwarz G (2022) Molybdenum Cofactor Deficiency in Humans. Molecules 27.
Khatami M, Roel LE, Li W, Rockey JH (1986) Ascorbate regeneration in bovine ocular tissues by NADH-dependent semidehydroascorbate reductase. Exp Eye Res 43:167-175.
Kim EY, Schrader N, Smolinsky B, Bedet C, Vannier C, Schwarz G, Schindelin H (2006) Deciphering the structural framework of glycine receptor anchoring by gephyrin. EMBO J 25:1385-1395.
Kim S, Kang M, Park D, Lee AR, Betz H, Ko J, Chang I, Um JW (2021) Impaired formation of high-order gephyrin oligomers underlies gephyrin dysfunction-associated pathologies. iScience 24:102037.
Kins S, Betz H, Kirsch J (2000) Collybistin, a newly identified brain-specific GEF, induces submembrane clustering of gephyrin. Nat Neurosci 3:22-29.
Kirsch J, Wolters I, Triller A, Betz H (1993) Gephyrin antisense oligonucleotides prevent glycine receptor clustering in spinal neurons. Nature 366:745-748.
Kneussel M, Betz H (2000) Clustering of inhibitory neurotransmitter receptors at developing postsynaptic sites: the membrane activation model. Trends Neurosci 23:429-435.
Kress V (2016) Collective Regulation of Synaptic Plasticity by Gephyrin, Dynein Light Chain and Neuronal Nitric Oxide Synthase In.
Kuhse J, Kalbouneh H, Schlicksupp A, Mukusch S, Nawrotzki R, Kirsch J (2012) Phosphorylation of gephyrin in hippocampal neurons by cyclin-dependent kinase CDK5 at Ser-270 is dependent on collybistin. J Biol Chem 287:30952-30966.
Kumar A, Dejanovic B, Hetsch F, Semtner M, Fusca D, Arjune S, Santamaria-Araujo JA, Winkelmann A, Ayton S, Bush AI, Kloppenburg P, Meier JC, Schwarz G, Belaidi AA (2017) S-sulfocysteine/NMDA receptor-dependent signaling underlies neurodegeneration in molybdenum cofactor deficiency. J Clin Invest 127:4365-4378.
Larson EA, Accardi MV, Wang Y, D'Antoni M, Karimi B, Siddiqui TJ, Bowie D (2020) Nitric Oxide Signaling Strengthens Inhibitory Synapses of Cerebellar Molecular Layer Interneurons through a GABARAP-Dependent Mechanism. J Neurosci 40:3348-3359.
Lee G, Kim S, Hwang DE, Eom YG, Jang G, Park HY, Choi JM, Ko J, Shin Y (2024) Thermodynamic modulation of gephyrin condensation by inhibitory synapse components. Proc Natl Acad Sci U S A 121:e2313236121.
Legendre P (2001) The glycinergic inhibitory synapse. Cell Mol Life Sci 58:760-793.
Liebsch F, Eggersmann FR, Merkler Y, Kloppenburg P, Schwarz G (2023) Automated Image Analysis Reveals Different Localization of Synaptic Gephyrin C4 Splice Variants. eNeuro 10.
Lionel AC et al. (2013) Rare exonic deletions implicate the synaptic organizer Gephyrin (GPHN) in risk for autism, schizophrenia and seizures. Hum Mol Genet 22:2055-2066.
Lopez-Mirabal HR, Winther JR (2008) Redox characteristics of the eukaryotic cytosol. Biochim Biophys Acta 1783:629-640.
Luscher B, Fuchs T, Kilpatrick CL (2011) GABAA receptor trafficking-mediated plasticity of inhibitory synapses. Neuron 70:385-409.
Lynch JW (2004) Molecular structure and function of the glycine receptor chloride channel. Physiol Rev 84:1051-1095.
Lynch JW (2009) Native glycine receptor subtypes and their physiological roles. Neuropharmacology 56:303-309.
Maas C, Tagnaouti N, Loebrich S, Behrend B, Lappe-Siefke C, Kneussel M (2006) Neuronal cotransport of glycine receptor and the scaffold protein gephyrin. J Cell Biol 172:441-451.
Macha A, Grünewald N, Havarushka N, Burdina N, Toelzer C, , Merkler Y, Cabrera-Orefice A, Brandt U, Pauly T, Nagle-Steger L, Niefind K, Schwarz G (2022a) Pentameric assembly of glycine receptor intracellular domains provides insights into gephyrin clustering. bioRxiv.
Macha A, Liebsch F, Fricke S, Hetsch F, Neuser F, Johannes L, Kress V, Djemie T, Santamaria-Araujo JA, Vilain C, Aeby A, Van Bogaert P, Dejanovic B, Weckhuysen S, Meier JC, Schwarz G (2022b) Biallelic gephyrin variants lead to impaired GABAergic inhibition in a patient with developmental and epileptic encephalopathy. Hum Mol Genet 31:901-913.
Mailloux RJ, McBride SL, Harper ME (2013) Unearthing the secrets of mitochondrial ROS and glutathione in bioenergetics. Trends Biochem Sci 38:592-602.
Manolov S, Ovtscharoff W (1982) Structure and cytochemistry of the chemical synapses. Int Rev Cytol 77:243-284.
Marcus DL, Strafaci JA, Freedman ML (2006) Differential neuronal expression of manganese superoxide dismutase in Alzheimer's disease. Med Sci Monit 12:BR8-14.
Maric HM, Mukherjee J, Tretter V, Moss SJ, Schindelin H (2011) Gephyrin-mediated gamma-aminobutyric acid type A and glycine receptor clustering relies on a common binding site. J Biol Chem 286:42105-42114.
Marino SM, Gladyshev VN (2010) Cysteine function governs its conservation and degeneration and restricts its utilization on protein surfaces. J Mol Biol 404:902-916.
Marletta MA (1994) Nitric oxide synthase: aspects concerning structure and catalysis. Cell 78:927-930.

Metwally E, Al-Abbadi HA, Hussain T, Murtaza G, Abdellatif AM, Ahmed MF (2023) Calpain signaling: from biology to therapeutic opportunities in neurodegenerative disorders. Front Vet Sci 10:1235163.
Meyer G, Kirsch J, Betz H, Langosch D (1995) Identification of a gephyrin binding motif on the glycine receptor beta subunit. Neuron 15:563-572.
Mihic SJ, Harris RA (1997) GABA and the GABAA receptor. Alcohol Health Res World 21:127-131.
Nakamura T, Lipton SA (2016) Protein S-Nitrosylation as a Therapeutic Target for Neurodegenerative Diseases. Trends Pharmacol Sci 37:73-84.
Nawrotzki R, Islinger M, Vogel I, Volkl A, Kirsch J (2012) Expression and subcellular distribution of gephyrin in non-neuronal tissues and cells. Histochem Cell Biol 137:471-482.
Ohno S, Emori Y, Imajoh S, Kawasaki H, Kisaragi M, Suzuki K (1984) Evolutionary Origin of a Calcium-Dependent Protease by Fusion of Genes for a Thiol Protease and a Calcium-Binding Protein. Nature 312:566-570.
Olanow CW (1990) Oxidation reactions in Parkinson's disease. Neurology 40:suppl 32-37; discussion 37-39.
Oswald MCW, Garnham N, Sweeney ST, Landgraf M (2018) Regulation of neuronal development and function by ROS. FEBS Lett 592:679-691.
Pace NJ, Weerapana E (2013) Diverse Functional Roles of Reactive Cysteines. Acs Chem Biol 8:283-296.
Perrin BJ, Huttenlocher A (2002) Calpain. Int J Biochem Cell Biol 34:722-725.
Pollegioni L, Piubelli L, Sacchi S, Pilone MS, Molla G (2007) Physiological functions of D-amino acid oxidases: from yeast to humans. Cell Mol Life Sci 64:1373-1394.
Rees MI, Harvey K, Ward H, White JH, Evans L, Duguid IC, Hsu CC, Coleman SL, Miller J, Baer K, Waldvogel HJ, Gibbon F, Smart TG, Owen MJ, Harvey RJ, Snell RG (2003) Isoform heterogeneity of the human gephyrin gene (GPHN), binding domains to the glycine receptor, and mutation analysis in hyperekplexia. J Biol Chem 278:24688-24696.
Reiss J, Johnson JL (2003) Mutations in the molybdenum cofactor biosynthetic genes MOCS1, MOCS2, and GEPH. Hum Mutat 21:569-576.
Saiyed T, Paarmann I, Schmitt B, Haeger S, Sola M, Schmalzing G, Weissenhorn W, Betz H (2007) Molecular basis of gephyrin clustering at inhibitory synapses: role of G- and E-domain interactions. J Biol Chem 282:5625-5632.
Schmidt HM, Kelley EE, Straub AC (2019) The impact of xanthine oxidase (XO) on hemolytic diseases. Redox Biol 21:101072.
Schwarz G (2005) Molybdenum cofactor biosynthesis and deficiency. Cell Mol Life Sci 62:2792-2810.
Schwarz G, Belaidi AA (2013) Molybdenum in human health and disease. Met Ions Life Sci 13:415-450.
Schwarz G, Schrader N, Mendel RR, Hecht HJ, Schindelin H (2001) Crystal structures of human gephyrin and plant Cnx1 G domains: comparative analysis and functional implications. J Mol Biol 312:405-418.
Schwarzlander M, Dick TP, Meyer AJ, Morgan B (2016) Dissecting Redox Biology Using Fluorescent Protein Sensors. Antioxid Redox Signal 24:680-712.
Shen ZC, Wu PF, Wang F, Xia ZX, Deng Q, Nie TL, Zhang SQ, Zheng HL, Liu WH, Lu JJ, Gao SQ, Yao XP, Long LH, Hu ZL, Chen JG (2019) Gephyrin Palmitoylation in Basolateral Amygdala Mediates the Anxiolytic Action of Benzodiazepine. Biol Psychiatry 85:202-213.
Shi RF, Hou WY, Wang ZQ, Xu XZ (2021) Biogenesis of Iron-Sulfur Clusters and Their Role in DNA Metabolism. Front Cell Dev Biol 9.
Sieghart W, Fuchs K, Tretter V, Ebert V, Jechlinger M, Hoger H, Adamiker D (1999) Structure and subunit composition of GABA(A) receptors. Neurochem Int 34:379-385.
Sola M, Kneussel M, Heck IS, Betz H, Weissenhorn W (2001) X-ray crystal structure of the trimeric N-terminal domain of gephyrin. J Biol Chem 276:25294-25301.
Sola M, Bavro VN, Timmins J, Franz T, Ricard-Blum S, Schoehn G, Ruigrok RW, Paarmann I, Saiyed T, O'Sullivan GA, Schmitt B, Betz H, Weissenhorn W (2004) Structural basis of dynamic glycine receptor clustering by gephyrin. EMBO J 23:2510-2519.
Steenvoorden DP, van Henegouwen GM (1997) The use of endogenous antioxidants to improve photoprotection. J Photochem Photobiol B 41:1-10.
Stomberski CT, Hess DT, Stamler JS (2019) Protein S-Nitrosylation: Determinants of Specificity and Enzymatic Regulation of S-Nitrosothiol-Based Signaling. Antioxid Redox Signal 30:1331-1351.
Sudhof TC (2013) Neurotransmitter release: the last millisecond in the life of a synaptic vesicle. Neuron 80:675-690.
Sudhof TC, Rothman JE (2009) Membrane fusion: grappling with SNARE and SM proteins. Science 323:474-477.
Talwar D, Miller CG, Grossmann J, Szyrwiel L, Schwecke T, Demichev V, Drazic AMM, Mayakonda A, Lutsik P, Veith C, Milsom MD, Müller-Decker K, Mülleder M, Ralser M, Dick TP (2023) The GAPDH redox switch safeguards reductive capacity and enables survival of stressed tumour cells. Nat Metab.
Tao CL, Liu YT, Sun R, Zhang B, Qi L, Shivakoti S, Tian CL, Zhang P, Lau PM, Zhou ZH, Bi GQ (2018) Differentiation and Characterization of Excitatory and Inhibitory Synapses by Cryo-electron Tomography and Correlative Microscopy. J Neurosci 38:1493-1510.
Tejada-Simon MV, Serrano F, Villasana LE, Kanterewicz BI, Wu GY, Quinn MT, Klann E (2005) Synaptic localization of a functional NADPH oxidase in the mouse hippocampus. Mol Cell Neurosci 29:97-106.

Tretter V, Mukherjee J, Maric HM, Schindelin H, Sieghart W, Moss SJ (2012) Gephyrin, the enigmatic organizer at GABAergic synapses. Front Cell Neurosci 6:23.
Trivedi MV, Laurence JS, Siahaan TJ (2009) The Role of Thiols and Disulfides on Protein Stability. Curr Protein Pept Sc 10:614-625.
Turrens JF (2003) Mitochondrial formation of reactive oxygen species. J Physiol 552:335-344.
Tyagarajan SK, Ghosh H, Yevenes GE, Imanishi SY, Zeilhofer HU, Gerrits B, Fritschy JM (2013) Extracellular signal-regulated kinase and glycogen synthase kinase 3beta regulate gephyrin postsynaptic aggregation and GABAergic synaptic function in a calpain-dependent mechanism. J Biol Chem 288:9634-9647.
Tyagarajan SK, Ghosh H, Yévenes GE, Nikonenko I, Ebeling C, Schwerdel C, Sidler C, Zeilhofer HU, Gerrits B, Muller D, Fritschy JM (2011) Regulation of GABAergic synapse formation and plasticity by GSK3β-dependent phosphorylation of gephyrin. P Natl Acad Sci USA 108:379-384.
Veldman A, Santamaria-Araujo JA, Sollazzo S, Pitt J, Gianello R, Yaplito-Lee J, Wong F, Ramsden CA, Reiss J, Cook I, Fairweather J, Schwarz G (2010) Successful treatment of molybdenum cofactor deficiency type A with cPMP. Pediatrics 125:e1249-1254.
Vignais PV (2002) The superoxide-generating NADPH oxidase: structural aspects and activation mechanism. Cell Mol Life Sci 59:1428-1459.
Villegas L, Norremolle A, Freude K, Vilhardt F (2021) Nicotinamide Adenine Dinucleotide Phosphate Oxidases Are Everywhere in Brain Disease, but Not in Huntington's Disease? Front Aging Neurosci 13:736734.
Vogel R, Wiesinger H, Hamprecht B, Dringen R (1999) The regeneration of reduced glutathione in rat forebrain mitochondria identifies metabolic pathways providing the NADPH required. Neurosci Lett 275:97-100.
Wagner S, Lee C, Rojas L, Specht CG, Rhee J, Brose N, Papadopoulos T (2021) The alpha3 subunit of GABA(A) receptors promotes formation of inhibitory synapses in the absence of collybistin. J Biol Chem 296:100709.
Waldvogel HJ, Baer K, Snell RG, During MJ, Faull RL, Rees MI (2003) Distribution of gephyrin in the human brain: an immunohistochemical analysis. Neuroscience 116:145-156.
Wang J, Swanson RA (2020) Superoxide and Non-ionotropic Signaling in Neuronal Excitotoxicity. Front Neurosci 4:861.
Whitwell JL (2023) Clinical and neuroimaging features of the progressive supranuclear palsy- corticobasal degeneration continuum. Curr Opin Neurol 36:283-290.
Yang Z, Taran E, Webb TI, Lynch JW (2012) Stoichiometry and subunit arrangement of alpha1beta glycine receptors as determined by atomic force microscopy. Biochemistry 51:5229-5231.
Young AB, Chu D (1990) Distribution of GABAA and GABAB receptors in mammalian brain: Potential targets for drug development. Drug Development Research 21:161-167.
Zacchi P, Antonelli R, Cherubini E (2014) Gephyrin phosphorylation in the functional organization and plasticity of GABAergic synapses. Front Cell Neurosci 8:103.
Zhong LW, Arnér ESJ, Holmgren A (2000) Structure and mechanism of mammalian thioredoxin reductase:: The active site is a redox-active selenolthiol/selenenylsulfide formed from the conserved cysteine-selenocysteine sequence. P Natl Acad Sci USA 97:5854-5859.
Zhu H, Gouaux E (2021) Architecture and assembly mechanism of native glycine receptors. Nature 599:513-517.
Zhu S, Shen Z, Wu X, Han W, Jia B, Lu W, Zhang M (2024) Demixing is a default process for biological condensates formed via phase separation. Science 384:920-928.
Zita MM, Marchionni I, Bottos E, Righi M, Del Sal G, Cherubini E, Zacchi P (2007) Post-phosphorylation prolyl isomerisation of gephyrin represents a mechanism to modulate glycine receptors function. EMBO J 26:1761-1771.

Chapter 2

Dynein light chain controls synaptic gephyrin via reciprocal S-nitrosylation and S-palmitoylation

Vanessa Kress[1], Maria-Theresa Gehling[1], Borislav Dejanovic[1], Joaquín Ortuño Gil[1], Filip Liebsch[1], Günter Schwarz[1,2,3,*]

[1]Institute of Biochemistry, Department of Chemistry, University of Cologne, 50674 Cologne, Germany
[2]Center for Molecular Medicine Cologne (CMMC), University of Cologne, Cologne, Germany
[3]Cologne Excellence Cluster on Cellular Stress Responses in Aging-Associated Diseases (CECAD), University of Cologne, Cologne, Germany
*corresponding author: Guenter Schwarz, e-mail: gschwarz@uni-koeln.de, phone: +49 221 4709 6440

Submitted to Journal of Neuroscience in June 2024.

2.1. Author contributions

Vanessa Kress, Borislav Dejanovic, Maria-Theresa Gehling and Guenter Schwarz designed the study. Maria-Theresa Gehling, Vanessa Kress, Borislav Dejanovic, Guenter Schwarz and Filip Liebsch wrote the manuscript. Vanessa Kress performed purification of recombinant proteins and ITC experiments, as well as COS7 cell experiments. Neuro cell culture experiments using cells from gephyrin wt mice were performed by Vanessa Kress and Borislav Dejanovic. Maria-Theresa Gehling performed neuro cell culture experiments using cells from gephyrin FLOX mice to obtain gephyrin knock out neurons. Borislav Dejanovic performed the detection of S-palmitoylation. Joaquín Ortuño Gil performed cloning of constructs. Filip Liebsch gave methodical input regarding the use of macros for the automated image analysis through Fiji/ImageJ.

2.2. Abstract

Gephyrin is the principal scaffolding protein at inhibitory post-synapses where it clusters glycine and GABA type A receptors ($GABA_ARs$). Gephyrin undergoes multiple post-translational modifications and protein interactions that collectively regulate inhibitory synapse formation. Synaptic gephyrin clustering is controlled by S-palmitoylation and S-nitrosylation, but how these reversible thiol modifications are regulated remained unclear. Here, we report that gephyrin forms a ternary complex with dynein light chain (DLC) and neuronal nitric oxide synthase (nNOS). Interaction with DLC, which is controlled by phosphorylation of gephyrin Thr205, enhances postsynaptic gephyrin clustering, whereas nNOS mediates gephyrin S-nitrosylation diminishing gephyrin clustering. Both, Cys212 and Cys284, which we previously identified as S-palmitoylation sites, were also found to be S-nitrosylated. Within the ternary complex, DLC inhibits nNOS activity thus reducing gephyrin S-nitrosylation, thereby augmenting gephyrin cluster formation. Our findings show that DLC and nNOS collectively modulate inhibitory synapses through a reciprocal regulation of gephyrin S-nitrosylation and S-palmitoylation.

2.3. Introduction

Gephyrin is the master regulator of inhibitory synapses and an essential modulator of synaptic plasticity (Tyagarajan and Fritschy, 2014). It directly binds and clusters inhibitory glycine receptors (GlyRs) and subtypes of GABA type A receptors ($GABA_ARs$) at the postsynaptic membrane (Fritschy et al., 2008). Additionally, gephyrin interacts with a number of signaling and cytoskeletal proteins and maintains the molecular architecture of inhibitory post-synapses (Tyagarajan and Fritschy, 2014). Genetic perturbations of gephyrin are implicated in epilepsy (Forstera et al., 2010; Dejanovic et al., 2015), autism and other neurodevelopmental disorders and intellectual disability (Lionel et al., 2013).

Gephyrin function and localization is extensively regulated by post-translational modifications (PTMs) (Zita et al., 2007; Herweg and Schwarz, 2012; Ghosh et al., 2016). Gephyrin consists of a highly conserved N-terminal G-domain and C-terminal GlyR- and $GABA_AR$-binding E-domain, both connected by an unstructured central C-domain (Fig. 1a), which is the main target for PTMs. Phosphorylation of gephyrin was shown to impact GABAergic transmission by enabling synapse formation and recruitment of $GABA_ARs$ to postsynaptic sites in an activity-dependent manner (Tyagarajan et al., 2013; Flores et al., 2015). Additionally, acetylation, SUMOylation and proteolytic cleavage by calpain regulate gephyrin scaffolding (Tyagarajan et al., 2011; Tyagarajan et al., 2013; Ghosh et al., 2016). Previously, we identified that S-palmitoylation and S-nitrosylation modulate plasticity and homeostatic assembly of GABAergic synapses (Dejanovic and Schwarz, 2014; Dejanovic et al., 2014a). S-palmitoylation-mediated membrane anchoring regulates postsynaptic gephyrin localization and synaptic strength (Dejanovic et al., 2014a). Gephyrin S-palmitoylation at Cys212 and Cys284 within its C-domain is reversibly and dynamically modulated by synaptic activity (Dejanovic et al., 2014a). On the other hand, neuronal nitric oxide synthase (nNOS) mediated S-nitrosylation of gephyrin negatively regulates postsynaptic gephyrin clustering and $GABA_AR$ surface expression (Dejanovic and Schwarz, 2014). Interestingly, gephyrin S-nitrosylation was identified in a proteome wide-study of a mouse model of Alzheimer's disease (Seneviratne et al., 2016).

Besides PTMs, interaction with synaptic proteins such as collybistin (Harvey et al., 2004) and neuroligin 2 regulates gephyrin function and postsynaptic membrane clustering (Poulopoulos et al., 2009; Papadopoulos and Soykan, 2011). Gephyrin also interacts with cytoplasmic dynein light chain (DLC) 1 and 2 (Fig. 1a) (Fuhrmann et al., 2002b; Navarro-Lerida et al., 2004; Bai et al., 2021), a central component of the large dynein motor complex, which serves long distance retrograde transport of proteins (Kapitein et al., 2010). DLC-binding takes place within the C-domain of gephyrin

(Fuhrmann et al., 2002b; Bai et al., 2021). While DLC was proposed to link gephyrin-GlyR to the dynein machinery, the mechanistic contribution of DLC to dynein function remains elusive as motor and cargo proteins compete for common DLC binding sites (Benison et al., 2007; Williams et al., 2007). For DLC, dynein-independent roles were reported that impact binding partner functions, e.g. by affecting oligomerization or activity of target proteins, which we aimed to identify for gephyrin. In addition, DLC was originally identified as a nNOS inhibitor and was therefore independently named as protein inhibitor of nNOS (PIN) (Jaffrey and Snyder, 1996a).

In this study we investigated the molecular significance of the gephyrin-DLC interaction at GABAergic synapses. We identified that the gephyrin-DLC interaction is regulated by gephyrin phosphorylation and tunes postsynaptic gephyrin clustering in neurons. Surprisingly, we found that synaptic gephyrin and DLC form a ternary complex with nNOS, where DLC inhibits nNOS and thereby regulates NO production and downstream gephyrin S-nitrosylation. We show that this gephyrin-DLC-nNOS-regulated S-nitrosylation reciprocally controls gephyrin S-palmitoylation and that both thiol-modifications compete for the same cysteine residues. Thus, we describe an entirely novel process that impacts the physiological clustering of gephyrin at inhibitory synapses.

2.4. Results

2.4.1. Gephyrin binding to DLC is regulated by phosphorylation of T205

Previous studies identified the DLC binding motif within the gephyrin C-domain spanning residues 203 and 212 (KQTEDKGVQC - Fig. 1a) (Navarro-Lerida et al., 2004). To characterize the gephyrin-DLC interaction further, we expressed and purified His-tagged gephyrin and DLC and analyzed their complex formation using analytical size-exclusion chromatography (SEC) and isothermal calorimetry (ITC) experiments (Figure 1). In SEC (Figure 1b), purified gephyrin eluted as a single peak at the corresponding molecular weight of the hydrodynamic radius of a trimer (approx. 360 kDa) (Saiyed et al., 2007), whereas purified DLC alone eluted mainly as a dimer (22 kDa) (Fan et al., 2001). Upon co-incubation of gephyrin with DLC, the resulting peak eluted at a molecular weight of approx. 390 kDa with a proportional increase in A280 absorption when compared to the gephyrin control, demonstrating gephyrin-DLC complex formation. The mass increase by 30 kDa suggests the binding of 1–2 DLC dimers to one gephyrin trimer.

Next, the binding affinity between DLC and gephyrin was determined using ITC (Figure 1c and d). Titration of the ligand DLC into gephyrin revealed an exothermic reaction and a binding affinity of KD = 2.14±0.01 µM . In line with the SEC results, the

binding stoichiometry of 0.58±0.04 (Fig. 1d) suggests that one DLC dimer binds to one gephyrin trimer (0.66 stoichiometry).

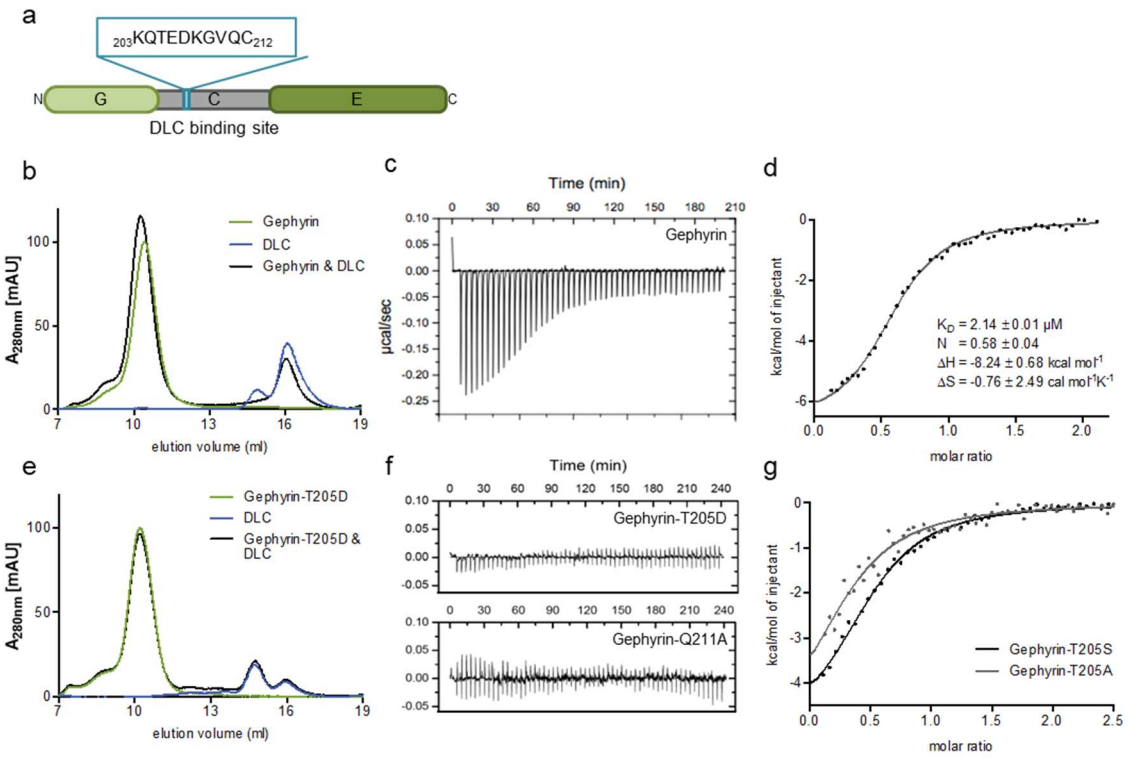

Fig. 1. DLC binds to non-phosphorylated gephyrin.
Size exclusion chromatography (SEC) and Isothermal titration calorimetry (ITC) experiments of recombinantly expressed gephyrin wt and variants and DLC derived from E. coli. (a) Schematic illustration or gephyrin domain structure. DLC binding site within the C-domain (K203-C212) highlighted. (b) SEC of gephyrin and DLC. Runs of single proteins indicated with green and blue lines, respectively. Interaction run of both proteins indicated with black lines. (c) ITC of DLC titration into gephyrin. Exemplary run of gephyrin wt. (d) Quantification of (c). One-site-fit used to calculate interaction parameters. (e) SEC of phospho-mimicking variants gephyrin-T205D and DLC. Runs of single proteins indicated with green and blue lines, respectively. Interaction run indicated with black line. (f) ITC titration of DLC into gephyrin-T205D (upper panel) and gephyrin-Q211A (lower panel). (g) One-site-fit of ITC runs using gephyrin-T205A (grey) and T205S (black) as non-phosphorylatable variants

Previously, we reported that PTMs impact gephyrin structure and function and identified T205 as a phospho-residue which resides within the DLC-binding motif (Herweg and Schwarz, 2012). We wondered whether phosphorylation of this residue might affect the gephyrin-DLC interaction and generated a phospho-mimetic gephyrin-T205D variant and analyzed the purified variant by SEC (Figure 1e). While gephyrin-T205D eluted as a trimer with a size similar to wt gephyrin, no complex formation with DLC was detectable. In line with the SEC results, no gephyrin-T205D/DLC interaction was measured by ITC (Fig. 1f), while the binding affinity of the control variants gephyrin-T205A and gephyrin-T205S were comparable to WT gephyrin (Fig. 1g). To further validate the specificity of the gephyrin-DLC interaction, we generated gephyrin-Q211A variant, which lacks the glutamine residue that is essential for various DLC-binding motifs

and DLC-Y65A, which is unable to bind known interaction partner (Liang et al., 1999). Indeed, ITC measurements with gephyrin-Q211A and DLC (Fig. 1f) or gephyrin and DLC-Y65A (Fig. 1-1) showed no detectable interaction between the proteins. Conclusively, SEC and ITC results collectively suggest that one gephyrin trimer and one DLC dimer bind to each other and that this interaction is abolished if gephyrin is phosphorylated within the DLC-binding motif at Thr205.

2.4.2. DLC is required for gephyrin cluster formation at inhibitory synapses

Given gephyrin's essential function as a regulator of inhibitory post-synapses (Tyagarajan and Fritschy, 2014) we wanted to probe whether the gephyrin-DLC interaction is important in neurons. Therefore, we expressed GFP-tagged gephyrin variants for 4 days in 9-days-old primary hippocampal neurons and analyzed postsynaptic clustering of gephyrin (Figure 2a-e).

First, we analyzed the phospho-mimicking variant gephyrin-T205D, two non-phosphorylatable variants, gephyrin-T205A and -T205S, and the DLC binding-deficient variant gephyrin-Q211A in neurons with a gephyrin wt background following transfection (Figure 2a-c). Compared to gephyrin wt (ctrl), the DLC binding-deficient variant gephyrin-Q211A formed significantly smaller (gephyrin-Q211A, 77.7±4.8% ctrl) and fewer (gephyrin-Q211A, 57.1±6.2% of ctrl) clusters. The phospho-mimetic gephyrin-T205D phenocopied gephyrin-T205D and formed significantly smaller (gephyrin-T205D, 79.8±4.9% of ctrl) and fewer clusters (gephyrin-T205D, 62.1±5.6 % of ctrl). In contrast, the non-phosphorylatable variants gephyrin-T205A and gephyrin-T205S were indistinguishable from gephyrin wt.

Next, we repeated the study using 8-days-old hippocampal neurons with a conditional gephyrin knock out background (Gephyrin-FLOX) and expressed gephyrin variants -T205D, -T205A and -Q211A for 6 days through viral transduction, which allows for a low and tunable expression and high transduction efficiency (Figure 2 d-e). The intensity of gephyrin-T205D and -Q211A were significantly and even further reduced compared to that of gephyrin wt (ctrl) (gephyrin-T205D, 31.4±3.7% of ctrl; gephyrin-Q211A, 64.4±4.0% of ctrl). In contrast, the intensity of gephyrin-T205A clusters was similar to that of gephyrin wt. The significant differences in cluster size of the individual gephyrin variants (gephyrin-T205D, 79.1±3.5% of ctrl; gephyrin-Q211A, 81.8±2.7% of ctrl) were also present upon depletion of endogenous Gephyrin (Figure 2d), suggesting that endogenous gephyrin had no apparent effect on the clustering of the chosen gephyrin variants.

Lastly, we analyzed whether expression of mCherry-DLC would influence synaptic clustering of endogenous gephyrin (Figure 2f). Indeed, expression of DLC significantly

increased the size of endogenous gephyrin clusters compared to the condition when only mCherry (ctrl) was overexpressed (mCherry-DLC, 125.0±6.7% of ctrl). Together, these results suggest that the interaction with DLC plays a vital role in postsynaptic clustering of gephyrin and that this interaction is tuned by phosphorylation of gephyrin Thr205.

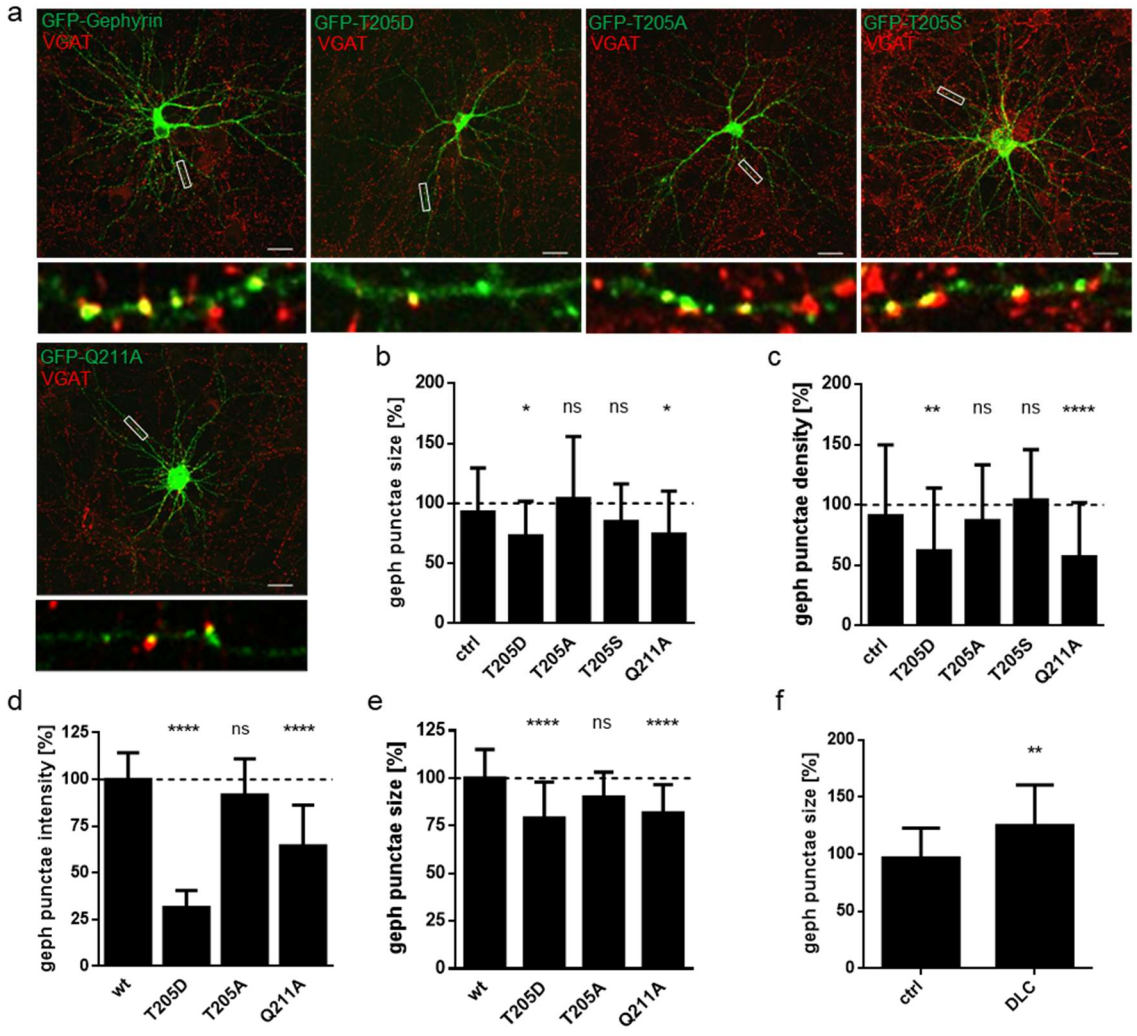

Fig. 2. DLC is critical for gephyrin cluster formation at inhibitory synapses.
(a-c) Expression of recombinant GFP-gephyrin variants through transfection in primary hippocampal neurons of wt mice. (d-e) Expression of recombinant mEGFP-gephyrin variants through transduction in primary hippocampal neurons of gephyrin-FLOX mice. Gephyrin knock-out induced by moxBFP-Cre transfection. (f) Expression of recombinant mCherry-DLC through transfection in primary hippocampal neurons of wt mice. (a-f) Co-localization with the pre-synaptic marker vGAT was used to identify synaptic gephyrin. (a) Exemplary images of transfected neurons with GFP-gephyrin wt, -T205D, -T205A, T205S and Q211A. Scale bar, 20 µm. Dendritic segments shown in enlargements. (b-e) Quantification of gephyrin punctae properties. Normalization to the average size of gephyrin wt (ctrl). Significance tested by 1-way ANOVA and *Bonferroni* post-hoc test of each variant vs ctrl. (b) Quantification of gephyrin punctae sizes. (c) Quantification of gephyrin punctae density (cluster number per area). (d) Quantification of gephyrin punctae intensities. (e) Quantification of gephyrin punctae sizes. (f) Quantification of endogenous gephyrin punctae sizes in mCherry-expressing control (ctrl) or mCherry-DLC expressing neurons. Normalization to average size of ctrl. Significance tested by *student's t-test*.

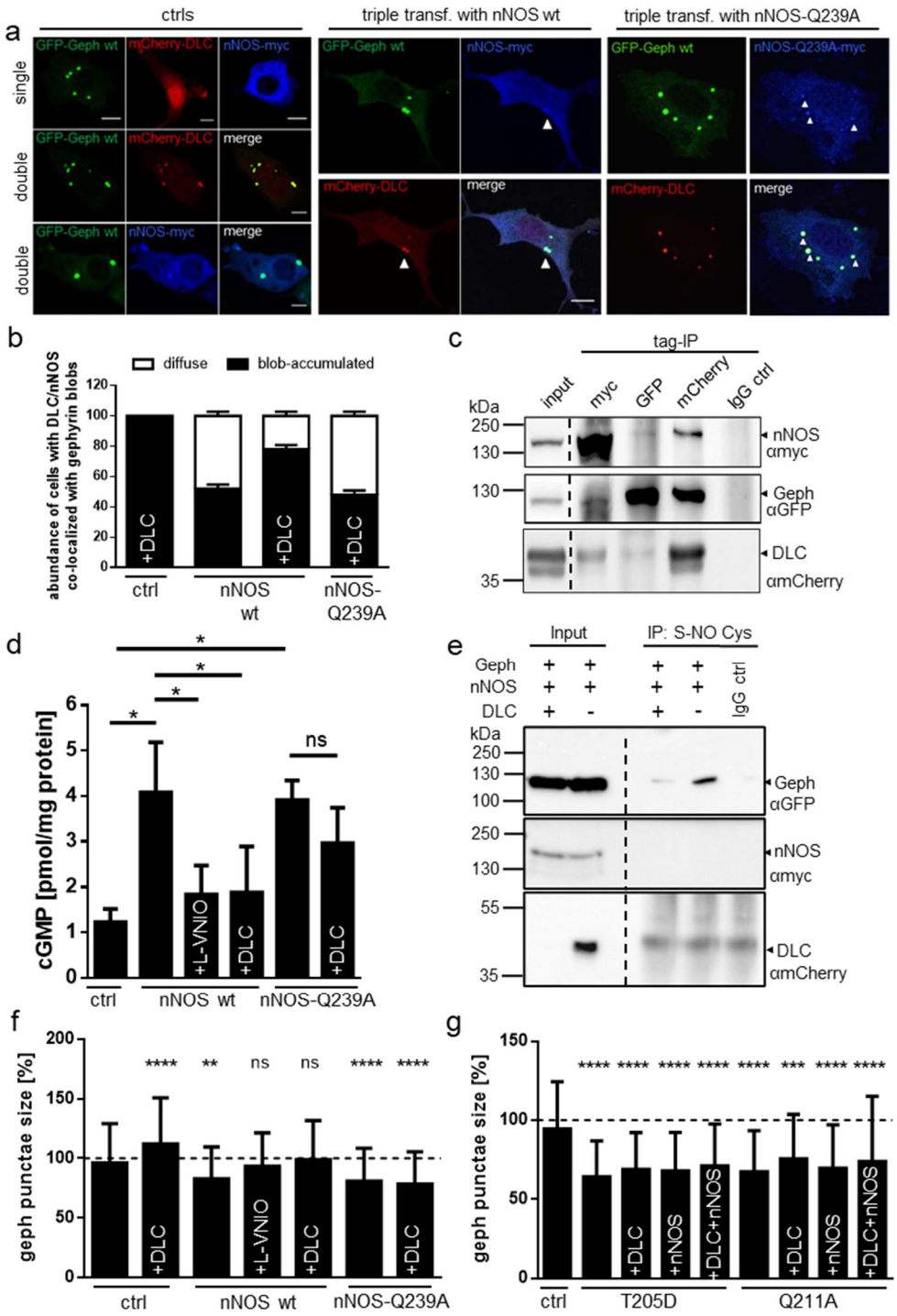

Fig. 3. Gephyrin, DLC and nNOS form a ternary complex.
Co-expression of GFP-gephyrin, mCherry-DLC and nNOS-myc or nNOS-Q239A-myc in COS7 cells (a, b), HEK293 cells (c-e) and hippocampal neurons of wt mice (f, g). (a) Representative images of transfected COS7 cells. Controls: Single transfection of each individual protein. Double transfection of gephyrin and DLC, or gephyrin and nNOS, respectively. Triple transfection: Arrows indicate accumulations of mCherry-DLC and nNOS-myc within GFP-gephyrin blobs. Scale bar 10 µm. (b) Relative abundance of cells with co-localization of DLC, nNOS wt or nNOS-Q239A with gephyrin. (c) Immunoprecipitation of gephyrin, DLC and nNOS with the corresponding tag specific antibody. Western blot analysis of the specific tags to identify co-precipitated interaction partners. (d) Determination of cGMP levels of cells expressing nNOS wt or nNOS-Q239A and DLC on top of gephyrin wt (ctrl) in different combinations. L-VNIO was used to inhibited nNOS. Significance tested by 1-way ANOVA and *Bonferroni* post-hoc test. (e) Immunoprecipitation of S-nitrosylated proteins (S-NO-Cys). Western blot analysis of protein content in input and immunoprecipitated samples. (f, g) Quantification of gephyrin punctae sizes in neurons. Normalization to the average of gephyrin wt (ctrl). Significance tested by 1-way ANOVA and *Bonferroni* post-hoc test of each individual condition vs ctrl. (f) Analysis of punctae sizes of gephyrin wt. (g) Analysis of punctae sizes of gephyrin variants.

2.4.3. Gephyrin, DLC and nNOS form a ternary complex

How does DLC regulate postsynaptic gephyrin clustering? We have previously identified that neuronal nitric oxide synthase (nNOS) forms a complex with gephyrin and S-nitrosylates gephyrin, which degreases postsynaptic gephyrin clustering (Dejanovic and Schwarz, 2014). Since nNOS is a known interactor of DLC (Jaffrey and Snyder, 1996b), we wondered whether DLC, gephyrin and nNOS form a ternary complex. Thus, we co-expressed GFP-gephyrin, mCherry-DLC and nNOS-myc in COS7 cells (Figure 3a). When expressed in non-neuronal cells, gephyrin forms large cytosolic aggregates so-called 'blobs' (Lardi-Studler et al., 2007). Upon co-expression of gephyrin and DLC, the vast majority of DLC was recruited into gephyrin blobs indicating a strong interaction (Figure 3b), confirming our previous *in vitro* interaction studies using SEC and ITC. In contrast, the interaction of nNOS and gephyrin was found to be more transient, since in cells co-expressing gephyrin and nNOS, only approx. 50% of the blobs were nNOS-enriched. Upon triple-transfection, in approx. 80% of all cells DLC and nNOS accumulated in gephyrin blobs, whereas in the remaining cells nNOS was diffusively distributed and was not enriched in gephyrin blobs. The increased percentage of blob-accumulated nNOS in DLC-co-expressing cells suggests that DLC stabilizes the gephyrin-nNOS complex. Indeed, the DLC-binding-deficient nNOS variant nNOS-Q239A showed reduced enrichment in gephyrin blobs when additionally co-expressed with DLC. In line with the co-localization results, following co-expression of tagged gephyrin, DLC and nNOS in HEK293 cells and co-immunoprecipitation (IP) using tag-specific antibodies, all three proteins co-immunoprecipitated with each other regardless of which tag was used for the IP (Figure 3c). In summary, our interaction studies in COS7 cells show the formation of a ternary complex between gephyrin, DLC and nNOS. Notably, DLC stabilizes the gephyrin-nNOS interaction.

2.4.4. Inhibition of nNOS by DLC increases gephyrin cluster size

Since DLC was originally identified as the inhibitor of nNOS (Jaffrey and Snyder, 1996a), we next asked whether DLC-mediated interacting with nNOS also inhibits nNOS activity in this ternary complex and thereby potentially regulates gephyrin S-nitrosylation. The initially reported inhibition of nNOS by DLC, however, seems controversial as some studies found DLC binding to nNOS in the absence of nNOS inhibition (Rodriguez-Crespo et al., 1998; Parhad et al., 2016). Thus, we first analyzed whether DLC inhibits nNOS in the ternary complex through measurement of the nitric oxide (NO)-dependent production of cyclic guanosine monophosphate (cGMP) (Denninger and Marletta, 1999) in HEK293 cells co-expressing gephyrin, nNOS and DLC. The expression of nNOS and

gephyrin solely increased NO production, as shown by significantly higher cGMP levels compared to cells only expressing gephyrin (ctrl) (nNOS wt: 4.1±0.6 pmol/mg, ctrl: 1.2±0.2 pmol/mg) (Figure 3d). This effect was abolished upon application of the nNOS-specific inhibitor N5-(1-imino-3-butenyl)-L-ornithine (L-VNIO) (nNOS wt+L-VNIO: 1.9±0.6 pmol/mg). Interestingly, co-expression of DLC with nNOS and gephyrin also significantly reduced cGMP levels (nNOS wt: 4.1±0.6 pmol/mg, nNOS wt+DLC: 1.9±0.6 pmol/mg). Although the expression of solely nNOS-Q239A, the DLC-binding-deficient nNOS variant, and gephyrin lead to a significant increase in cGMP production (nNOS-Q239A: 3.9±0.3 pmol/mg, ctrl: 1.2±0.2 pmol/mg), this effect was not significantly reversible by additionally co-expressed DLC (nNOS-Q239A+DLC: 3.0±0.6 pmol/mg). These results indicate that DLC inhibits nNOS even in the ternary complex and was equally effective as L-VNIO.

After establishing that DLC inhibits nNOS activity within the ternary complex, we wondered whether the presence of DLC affects gephyrin S-nitrosylation by nNOS. We expressed gephyrin and nNOS in HEK293 cells and used an S-nitroso cysteine (SNO-Cys) specific antibody to immunoprecipitate S-nitrosylated proteins (Dejanovic and Schwarz, 2014). While gephyrin was robustly S-nitrosylated in nNOS-expressing cells, gephyrin S-nitrosylation was greatly reduced in the presence of DLC, highlighting that the DLC-mediated inhibition of nNOS directly affects S-nitrosylation of gephyrin in cells (Figure 4e).

We next asked if DLC-mediated nNOS inhibition impacts postsynaptic clustering of gephyrin and co-expressed gephyrin with nNOS and DLC in 9-day-old hippocampal neurons and analyzed dendritic gephyrin clustering after 4 days of expression (Figure 4f). Consistent with previous findings (Dejanovic and Schwarz, 2014), expression of nNOS wt significantly reduced gephyrin cluster sizes compared to the condition only expressing gephyrin (ctrl) (nNOS wt, 82.8±2.7% of ctrl), which we also observed for the DLC-binding-deficient variant nNOS Q239A (nNOS-Q239A, 80.9±2.4% of ctrl). The nNOS-dependent effect on gephyrin clustering was reversible by L-VNIO treatment (nNOS wt+L-VNIO, 93.5±3.2% of ctrl) and DLC overexpression with nNOS wt (nNOS wt+DLC, 98.8±3.3% of ctrl). In contrast, DLC did not inhibit nNOS-Q239A (nNOS-Q239A+DLC, 78.4±2.6% of ctrl). On the other hand, expression of DLC led to a significant increase in gephyrin cluster size (DLC, 112.2±3.8%), as seen before with endogenous gephyrin (Figure 2f). This observation is compatible with the image that DLC inhibits endogenous nNOS and thus decreases S-nitrosylation-dependent reduction of gephyrin clustering.

Lastly, we wanted to investigate whether the phosphorylation site T205 and residue Q239, which we identified as crucial for gephyrin-DLC interaction (Figure 1f),

influence and regulate the DLC-gephyrin-nNOS complex. Thus, we co-expressed these T205D and Q239A variants with DLC and nNOS in hippocampal neurons at DIV8 and analyzed gephyrin cluster sizes after 6 days of expression (Figure 3g). Gephyrin-T205D and gephyrin-Q211A *per se* showed significantly reduced cluster sizes compared to gephyrin wt (ctrl) (gephyrin-T205D, 64.2±2.9% of ctrl; gephyrin-Q239A, 67.4±3.0% of ctrl) as previously seen (Figure 1b). But now, neither additional expression of DLC nor nNOS, were able to reverse variant-specific cluster size reduction. Together, the results suggest that DLC and nNOS act in concert via a ternary complex to regulate the postsynaptic clustering of gephyrin by S-nitrosylation.

2.4.5. Gephyrin is inversely regulated by S-nitrosylation and S-palmitoylation

Lastly, we wondered how S-nitrosylation affects neuronal gephyrin clustering. Interestingly, in two untargeted studies that profiled S-nitrosylated proteins in the brain, gephyrin was identified to be S-nitrosylated on Cys284 (Paige et al., 2008; Seneviratne et al., 2016), which we previously identified to be S-palmitoylated (together with Cys212) (Dejanovic et al., 2014a). Thus, we wondered whether S-nitrosylation as a negative regulator of gephyrin clustering and S-palmitoylation as a positive regulator compete for the same residues and are reciprocally regulated.

First, we expressed S-palmitoylation-deficient gephyrin variants gephyrin-C212S and gephyrin-C284S in hippocampal neurons with endogenous gephyrin wt background. The transfection was performed at DIV9 and expressed for 4 days. To test whether these residues are regulated by nNOS-mediated S-nitrosylation, we either pharmacologically inhibited or overexpressed nNOS and analyzed cluster sizes of wt, C212S and C284S gephyrin variants at DIV12 (Figure 4a). We found a significant reduction in cluster size of these variants when compared to GFP-gephyrin wt (ctrl) as we reported previously (Dejanovic et al., 2014a). Intriguingly, while L-VNIO increased and nNOS overexpression decreased gephyrin wt cluster size, respectively, gephyrin-C212S and gephyrin-C284S clusters were unaffected by both treatments, suggesting that gephyrin S-nitrosylation is again dependent on Cys212 and Cys284.

Next, we repeated nNOS inhibition by L-VNIO in hippocampal neurons derived from mice with a conditional gephyrin knockout. The transduction was performed at DIV8 and expressed for 6 days. The observed effects were similar to those found in neurons with endogenous gephyrin present. Again, gephyrin-C212S and -C284S showed significantly smaller clusters compared to gephyrin wt (ctrl) (gephyrin-C212S, 72.5±1.1% of ctrl; gephyrin-C284S, 71.0±1.8% of ctrl). On the other hand, L-VNIO treatment at DIV13 significantly increased cluster sizes of gephyrin wt (ctrl+L-VNIO; 113.6±3.0% of

ctrl), while gephyrin-C212S and -C284S were unaffected (gephyrin-C212S+L-VNIO, 70.2±1.3% of ctrl; gephyrin-C284S+L-VNIO, 76.8±2.0% of ctrl).

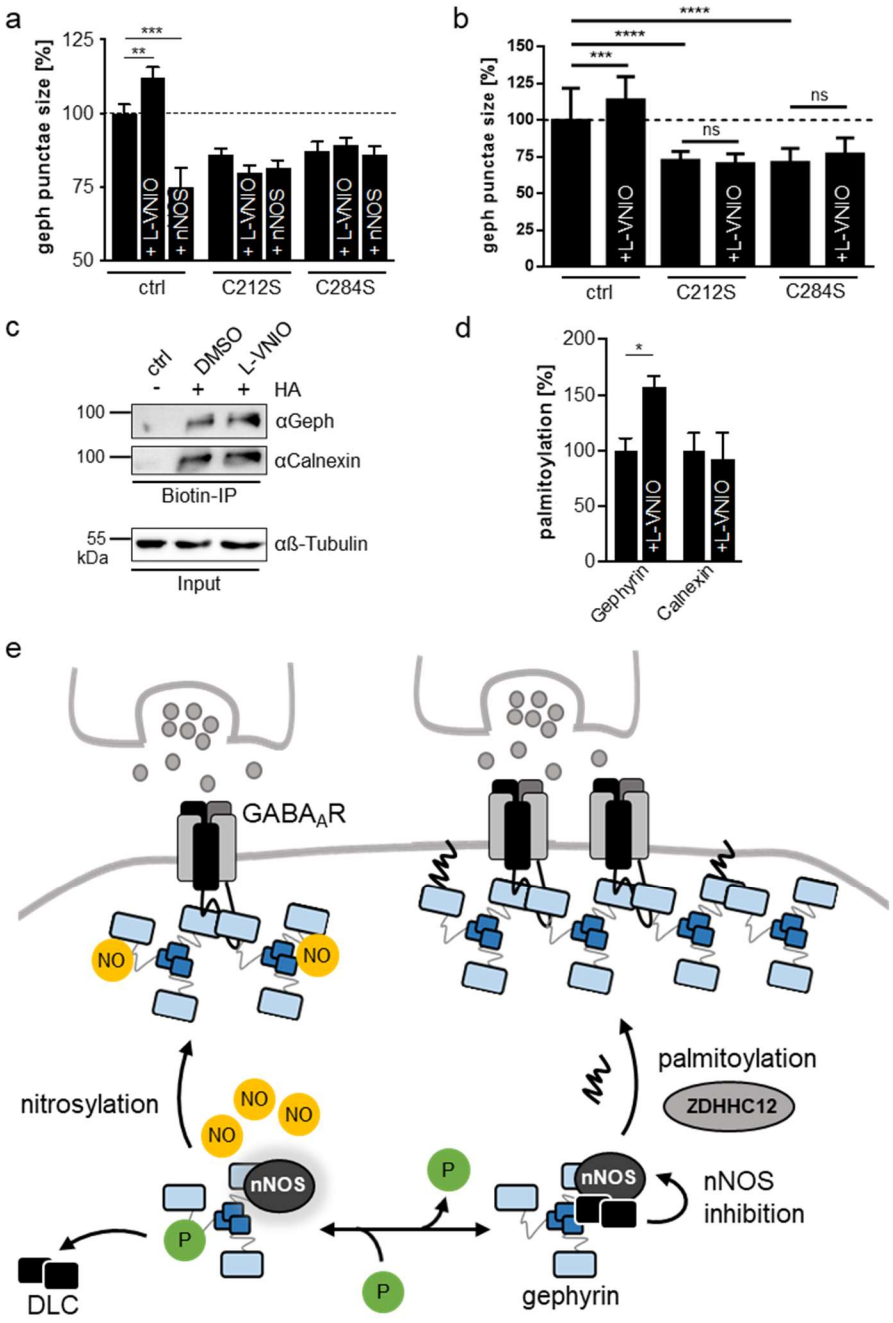

Fig. 4. Reciprocal regulation of gephyrin S-nitrosylation and S-palmitoylation.
(a) Expression of recombinant GFP-gephyrin variants through transfection in primary hippocampal neurons of wt mice. Quantification of gephyrin punctae sizes. Normalization to the average of gephyrin wt (ctrl). Significance tested by 1-way ANOVA and *Bonferroni* post-hoc test. (b) Expression of recombinant mEGFP-gephyrin variants through transduction in primary hippocampal neurons of gephyrin-FLOX mice. Gephyrin knock-out induced by moxBFP-Cre transfection. Normalization to the average of gephyrin wt (ctrl). Significance tested by 1-way ANOVA and *Bonferroni* post-hoc test. (c) Western blot analysis of S-palmitoylated proteins through Acyl-to-biotin exchange assays (ABE). HA=Hydroxylamine. Neurons were treated with L-VNIO or DMSO. β-Tubulin served as input control for the biotin immunoprecipitation. (d) Quantification of S-palmitoylation levels. Normalization to average band intensity of DMSO-treated neurons. (e) Graphical summary: gephyrin is found in a ternary complex with DLC and nNOS. In this complex, DLC inhibits nNOS, which allows the cysteines of gephyrin to be S-palmitoylated leading to bigger synaptic gephyrin clusters. Phosphorylation of gephyrin at T205 controls the disassembly of DLC from the ternary complex. With this, nNOS becomes active and gephyrin is S-nitrosylated leading to smaller synaptic clusters.

To biochemically evaluate whether S-nitrosylation and S-palmitoylation compete in cells, we measured S-palmitoylation of L-VNIO treated neurons using the acyl-to-biotin 258 exchange assay (ABE) (Figure 4c). We observed that gephyrin S-palmitoylation was increased in primary hippocampal neurons upon nNOS inhibition using L-VNIO (Fig. 4d). In contrast, S-palmitoylation of calnexin (Lakkaraju et al., 2012) was not altered upon L-VNIO treatment, suggesting that the regulation is restricted to a subset of S-palmitoylated proteins in neurons.

Together, these results reveal that gephyrin S-palmitoylation and S-nitrosylation compete for the same residues Cys212 and 284. Since S-nitrosylation negatively and S-palmitoylation positively regulate gephyrin clustering, we propose a reciprocal mechanism for gephyrin clustering thus collectively regulating neuronal plasticity.

2.5. Discussion

Using a combination of biochemical and cellular studies, we describe a novel molecular mechanism that modulates post-synaptic gephyrin clustering in neurons, a prerequisite for synaptic plasticity and synapse function. We propose a model wherein gephyrin forms a ternary complex with synaptic DLC and nNOS which is based on a crosstalk between gephyrin S-nitrosylation and S-palmitoylation thus regulating post-synaptic gephyrin clustering. Gephyrin-nNOS association and NO formation promotes S-nitrosylation of gephyrin, which competes with S-palmitoylation at residues C212 and C284. Within the ternary complex, activity of nNOS is controlled by DLC. In turn, DLC interaction with gephyrin, and hence complex assembly, is abolished by phosphorylation of gephyrin T205 (Figure 4e).

We suggest that the dynamic gephyrin S-palmitoylation/de-palmitoylation cycle is regulated, at least in part, by the competing action of S-nitrosylation. A similar signaling cascade has been reported for post-synaptic density protein 95 (PSD95), a scaffolding protein at glutamatergic excitatory synapses, where Cys3 and Cys5 of PSD95 are reciprocally regulated by S-palmitoylation and S-nitrosylation (Ho et al., 2011). NMDA receptor activity increases intracellular calcium levels, which stimulates nNOS-mediated NO production and decreases PSD95 S-palmitoylation and synaptic clustering. The observation that S-nitrosylation and S-palmitoylation compete for the same residues on gephyrin and PSD95 might reflect a general mechanism and could serve as an ‘on-off’ switch also in other proteins. Given that proteomic studies identified hundreds of S-palmitoylated and S-nitrosylated synaptic proteins (Kang et al., 2008; Paige et al., 2008; Seneviratne et al., 2016; Collins et al., 2017; Yang et al., 2022; Stykel and Ryan, 2024), we postulate that competitive interaction between S-nitrosylation and S-palmitoylation

could also regulate other neuronal proteins. Indeed, a competitive relationship between S-nitrosylation and S-palmitoylation has been shown for a number of neuronal proteins with decreased S-palmitoylation levels in the presence of NO donors (Hess et al., 1993; Ho et al., 2011). Notably, the interplay of S-palmitoylation, S-nitrosylation and phosphorylation of synaptic proteins becomes more and more disease relevant and was subject of several studies (Zareba-Koziol et al., 2019; Yan et al., 2022; Yucel et al., 2023). The identified phosphorylation-dependent interaction between gephyrin and DLC suggests that phosphorylation on gephyrin may regulate the strength of nNOS-mediated S-nitrosylation of gephyrin.

While our results suggest that DLC influences gephyrin clustering by inhibiting nNOS and NO release, it is possible that DLC binding also influences gephyrin structure and function. In line with that, it has been demonstrated recently, that DLC-interaction influences the ability of gephyrin to undergo liquid-liquid-phase separation (LLPS) in the presence of multimeric inhibitory GlyRs and $GABA_A$Rs, a mechanism that creates synaptic subdomains though the formation of liquid condensates (Bai et al., 2021). Importantly, it was stated that two DLC- binding sites exist within gephyrin C-domain, a high-affinity binding site (aa203-212) and a low-affinity binding site (aa246-258) (Bai et al., 2021). Only the removal of both binding-sites prohibited the formation of LLPS indicating, that solely one DLC-binding site is sufficient to maintain effects on LLPS. Since DLC binds to the intrinsically unstructured and highly flexible gephyrin C-domain, the interaction might induce conformational changes and folding within this domain affecting gephyrin function, as described for other interactors upon DLC-binding (Nyarko et al., 2004).

Strikingly, it has been previously described, that the lack of the high-affinity binding site for DLC within gephyrin C-domain (203-KQTEDKGVQC-212) did not affect synaptic gephyrin clustering (Fuhrmann et al., 2002a). Considering that this motif also includes cysteine 212, which is an important S-palmitoylation target in gephyrin (Dejanovic et al., 2014a), it is possible that reciprocal regulatory mechanisms were simultaneously removed. In our studies, we investigated the importance of the DLC-gephyrin interaction on synaptic clustering by manipulating only this interaction through the variants T205D and Q211A, which left the role of C212 untouched. Our data suggests that the DLC-gephyrin is *per se* important for synaptic clustering of gephyrin and is directly involved in the reciprocal regulation of S-nitrosylation and S-palmitoylation.

Besides the physiologically relevant regulation of synaptic function, the S-nitrosylation/S-palmitoylation signaling cascade could also be disease relevant. Increased gephyrin S-nitrosylation has been identified in mouse models of autism (Amal et al., 2020) and during early stages of neurodegeneration in an Alzheimer's disease

(AD) mouse model (Seneviratne et al., 2016). Following our hypothesis, increased S-nitrosylation would result in decreased S-palmitoylation and reduced postsynaptic gephyrin clustering. Indeed, gephyrin clusters were found to be decreased in the hippocampus of AD mouse models (Kiss et al., 2016), which might contribute to hyperexcitability and reduced synaptic integrity in AD. Moreover, disturbance of gephyrin S-palmitoylation was identified in rats with high-anxiety (Shen et al., 2019). Analogous to excitatory synapses, where small molecule inhibitors of the PSD-95/nNOS interaction have clinical potential (Doucet et al., 2012; Lee et al., 2015), modulation of gephyrin PTMs, e.g. by inhibiting the interaction with nNOS might be used to further decipher the significance of the here identified protein complex formation and dynamic PTMs. In conclusion, our data advances the understanding of the molecular features of gephyrin regulation, specifically the role and regulation of different thiol-modifications in GABAergic synapse function.

2.6. Material and methods

DNA/expression constructs

EGFP-tagged gephyrin and myc-tagged nNOS have been described previously (Dejanovic et al., 2014b; Dejanovic and Schwarz, 2014). 6His-tagged DLC was cloned into the pQE80 and mCherry-C3 vectors (Clontech). 6His-tagged gephyrin and expression vectors, as well as constructs for viral production have been introduced before (Schrader et al., 2004; Liebsch et al., 2023). Mutations have been generated by fusion-PCR and all constructs have subsequently been sequenced.

Cell cultures and transfections

Primary hippocampal neurons, HEK293 and COS7 cells were cultured as described previously (Dejanovic et al., 2014b). HEK293 and COS7 cells were transfected with polyethylenimine using standard protocols. Neurons were usually transfected after 9 days *in vitro* (DIV) using Lipofectamine 2000 according to the manufacturer's protocol and cultured for 4 consecutive days. In case of viral transduction, we used established protocols (Liebsch et al., 2023) and transduced cells at DIV8 and fixed after 6 days.

Expression and purification of recombinant proteins from E. coli cells

Recombinant 6His-tagged gephyrin and DLC were expressed in E. coli and affinity-purified using nickel-nitrilotriacetic acid resin (Ni-NTA, Quiagen) as suggested by the manufacturer. Cells were lysed in lysis buffer (50 mM potassium-phosphate buffer pH 8.0, 300 mM NaCl, 20 mM imidazole) and protease inhibitors (Roche) using an

EmulsiFlex C5 (Avestin) high-pressure homogenizer. After pelleting cell debris, supernatant was incubated with Ni-NTA beads. Unbound proteins were removed by using an increasing imidazole gradient eluted in PBS containing 250 mM imidazole. For further purification of affinity-purified proteins, Superdex 200 16/60 and 75 16/60 columns (120 ml column volume, GE Healthcare) were used.

Size exclusion chromatography

2 nmol purified gephyrin and/or 3 nmol purified DLC were loaded on a size-exclusion column (Superdex 200 10/300) connected to an ÄKTApurifier (GE Healthcare) and run at 0.5 ml/min with SEC buffer (20 mM Tris, pH 7.4, 250 mM NaCl). Elution was monitored by measuring absorbance at 280 nm. Molecular weights were calculated according to the elution profile of standard proteins.

Isothermal titration calorimetry

Isothermal titration calorimetry (ITC) measurements were performed with recombinant 6His-tagged gephyrin and purified 6His-tagged DLC. Ligand and binding partner were present in the identical ITC-buffer (10 mM Tris/HCl, 250 mM NaCl, 1 mM β-Mercaptoethanol). ITC experiments were performed at 37°C using a VP-ITC system with cell concentrations of 18-30 µM gephyrin and syringe concentrations of 270-350 µM purified DLC. The injection volume was set to 4-6 µl/8-12 s for each injection with 240 s spacing and an initial delay of 120 s. Reference power and stirring speed were set to 5 µCal/s and 310 rpm, respectively. Raw data were analyzed with Origin 7 software.

Acyl biotin exchange assay

The ABE assay has previously been described in detail (Dejanovic et al., 2014a). Cells were treated with 50 µM A23187 for 1 h (to activate nNOS) or 20 µM L-VNIO for 12 h.

Pharmacological treatment of hippocampal neurons

Where indicated, cells were treated with 50 µM L-VNIO (N5-(1-imino-3-butenyl)-L-ornithine) for 14 h. DMSO was added to the control neurons. For downstream Western blotting, neurons were dissolved directly in 2xSDS loading buffer.

Immunostaining and image analysis

Neurons were fixed after 11-14 DIV. Immunostaining and laser scanning microscopy of cultured cells have been described previously (Dejanovic and Schwarz, 2014; Liebsch et al., 2023). The following antibodies were used: rabbit anti-vesicular GABA transporter (VGAT) (1:500, Synaptic Systems, AB_887871), rabbit anti-DLC/LC8; (1:1 000, Abcam,

AB_51603), goat anti-rabbit Alexa Fluor 568 (1:500, Invitrogen) and goat anti-rabbit Alexa Fluor 647 (1:500, A11031, Thermo Fisher Scientific, A-21245). Images were taken with a Nikon AZ-C2+ confocal laser scanning microscope or with a Leica SP8 LIGHTNING upright confocal microscope. As objectives we either used a Plan Apo VC 60x/1.40/0.13 Oil PFS objective or an HC PL APO CS2 63x/1.30 glycerol objective, respectively. Images were acquired with a z-stack size of 0.5 or 0.33 µm with a resolution of 1024x1024 (212.16x212.16 µm) or 2048x2048 (144.77x144.77 µm). In case of transfected samples, gephyrin clusters were quantified within two 20x5 µm regions-of-interest (ROI) per neuron. Due to the high transduction efficiency, samples derived from viral transduction were analyzed in an automated fashion using adapted published protocols (Liebsch et al., 2023). Clusters with a size of >0.05 μm^2 were excluded. Cluster size was averaged per neuron and mean values were compared for significance tests.

Western blotting and statistical analysis

Proteins were separated by SDS-PAGE (10%-12% acrylamide) and immunoblotted using standard protocols. Horseradish peroxidase-signals were detected by chemiluminescence (Thermo Scientific) and an electrochemiluminescence- (ECL) system with a cooled CCD camera (Decon; Bio-Rad). Band intensities were quantified using ImageJ.

Co-immunoprecipitation

Transfected HEK293 cells were lysed in IP buffer (20 mM Tris, pH 7.4, 150 mM NaCl, 1 mM EDTA) containing protease inhibitor (Roche) by sonication. Cleared lysate was incubated with primary GFP- (Santa Cruz), mCherry- (Pierce), myc- (cell culture supernatant) or S-NO Cys-antibody (Abcam) for 1 h at room temperature (RT). Protein A/G Sepharose beads (Santa Cruz) were added for an additional hour at RT. Normal mouse IgG loaded beads were used as control. After washing three times, bound proteins were eluted from the beads by boiling in 2xSDS-loading buffer and analyzed via Western blotting.

cGMP assay

The Cayman cGMP EIA Kit was used to quantify cGMP levels. HEK293 cells were grown in 6-well plates and transfected with GFP-gephyrin, nNOS- myc and mCherry DLC. nNOS was inhibited by the application of 50 µM L-VNIO for 14 h. Cells were harvested after 24 h expression time and measurements were performed according to the manufacturer's protocol. Results were obtained from three independent transfections and triplicate measurements.

Quantification and statistical analysis

Number of samples and used cultures is described in the figure legends. Statistical analysis was performed using GraphPad Prism 8 and the used statistical tests are defined in the figure legend. In all instances, statistical significance was defined as follows: *$p < 0.05$, **$p < 0.01$, ***$p < 0.001$, ****$p < 0.0001$. Data throughout the paper is displayed as mean ± standard deviation (SD). Outlier analysis was performed using GraphPad Prism 8 using default settings. Sample size was chosen according to that used for similar experiments in previously published literature. Experimenters were blinded whenever possible to experimental condition during data acquisition or quantification.

Acknowledgements

Technical help from Joana Stegemann is greatly appreciated. We thank the imaging facility of the Cologne Biocentre of the University of Cologne. This work was supported by the German Science Foundation (SFB635 to GS) and the german research foundation (DFG) (RTG2550 reloc to JR).

Conflict of interest

The authors declare no conflict of interest.

Study approval

We complied with all ethical regulations for animal testing and research. Experiments were approved by the local research ethics committee (German, Landesamt für Natur, Umwelt und Verbraucherschutz (LANUV) Nordrhein-Westfalen, reference 2016.A466).

2.7. References

Amal H, Barak B, Bhat V, Gong G, Joughin BA, Wang X, Wishnok JS, Feng G, Tannenbaum SR (2020) Shank3 mutation in a mouse model of autism leads to changes in the S453 nitroso-proteome and affects key proteins involved in vesicle release and synaptic function. Mol Psychiatry 25:1835-1848.

Bai G, Wang Y, Zhang M (2021) Gephyrin-mediated formation of inhibitory postsynaptic density sheet via phase separation. Cell Res 31:312-325.

Benison G, Karplus PA, Barbar E (2007) Structure and dynamics of LC8 complexes with KXTQT-motif peptides: swallow and dynein intermediate chain compete for a common site. J Mol Biol 371:457-468.

Collins MO, Woodley KT, Choudhary JS (2017) Global, site-specific analysis of neuronal protein S-acylation. Sci Rep 7:4683.

Dejanovic B, Schwarz G (2014) Neuronal nitric oxide synthase-dependent S-nitrosylation of gephyrin regulates gephyrin clustering at GABAergic synapses. J Neurosci 34:7763-7768.

Dejanovic B, Semtner M, Ebert S, Lamkemeyer T, Neuser F, Luscher B, Meier JC, Schwarz G (2014a) Palmitoylation of gephyrin controls receptor clustering and plasticity of GABAergic synapses. PLoS Biol 12:e1001908.

Dejanovic B, Lal D, Catarino CB, Arjune S, Belaidi AA, Trucks H, Vollmar C, Surges R, Kunz WS, Motameny S, Altmuller J, Kohler A, Neubauer BA, Epicure C, Nurnberg P, Noachtar S, Schwarz G, Sander T (2014b) Exonic microdeletions of the gephyrin gene impair GABAergic synaptic inhibition in patients with idiopathic generalized epilepsy. Neurobiol Dis 67:88-96.

Dejanovic B, Djemie T, Grunewald N, Suls A, Kress V, Hetsch F, Craiu D, Zemel M, Gormley P, Lal D, Euro EDwg, Myers CT, Mefford HC, Palotie A, Helbig I, Meier JC, De Jonghe P, Weckhuysen S, Schwarz G (2015) Simultaneous impairment of neuronal and metabolic function of mutated gephyrin in a patient with epileptic encephalopathy. EMBO Mol Med 7:1580-1594.

Denninger JW, Marletta MA (1999) Guanylate cyclase and the .NO/cGMP signaling pathway. Biochim Biophys Acta 1411:334-350.

Doucet MV, Harkin A, Dev KK (2012) The PSD-95/nNOS complex: new drugs for depression? Pharmacol Ther 133:218-229.

Fan J, Zhang Q, Tochio H, Li M, Zhang M (2001) Structural basis of diverse sequence483 dependent target recognition by the 8 kDa dynein light chain. J Mol Biol 306:97-108. Flores CE, Nikonenko I, Mendez P, Fritschy JM, Tyagarajan SK, Muller D (2015) Activity485 dependent inhibitory synapse remodeling through gephyrin phosphorylation. Proc Natl Acad Sci U S A 112:E65-72.

Forstera B, Belaidi AA, Juttner R, Bernert C, Tsokos M, Lehmann TN, Horn P, Dehnicke C, Schwarz G, Meier JC (2010) Irregular RNA splicing curtails postsynaptic gephyrin in the cornu ammonis of patients with epilepsy. Brain 133:3778-3794.

Fritschy JM, Harvey RJ, Schwarz G (2008) Gephyrin: where do we stand, where do we go? Trends Neurosci 31:257-264.

Fuhrmann JC, Kins S, Rostaing P, El Far O, Kirsch J, Sheng M, Triller A, Betz H, Kneussel M (2002a) Gephyrin interacts with dynein light chains 1 and 2, components of motor protein complexes. Journal of Neuroscience 22:5393-5402.

Fuhrmann JC, Kins S, Rostaing P, El Far O, Kirsch J, Sheng M, Triller A, Betz H, Kneussel M (2002b) Gephyrin interacts with Dynein light chains 1 and 2, components of motor protein complexes. J Neurosci 22:5393-5402.

Ghosh H, Auguadri L, Battaglia S, Simone Thirouin Z, Zemoura K, Messner S, Acuna MA, Wildner H, Yevenes GE, Dieter A, Kawasaki H, M OH, Zeilhofer HU, Fritschy JM, Tyagarajan SK (2016) Several posttranslational modifications act in concert to regulate gephyrin scaffolding and GABAergic transmission. Nat Commun 7:13365.

Harvey K, Duguid IC, Alldred MJ, Beatty SE, Ward H, Keep NH, Lingenfelter SE, Pearce BR, Lundgren J, Owen MJ, Smart TG, Luscher B, Rees MI, Harvey RJ (2004) The GDP-GTP exchange factor collybistin: an essential determinant of neuronal gephyrin clustering. J Neurosci 24:5816-5826.

Herweg J, Schwarz G (2012) Splice-specific Glycine Receptor Binding, Folding, and Phosphorylation of the Scaffolding Protein Gephyrin. Journal of Biological Chemistry 287:12645-12656.

Hess DT, Patterson SI, Smith DS, Skene JH (1993) Neuronal growth cone collapse and inhibition of protein fatty acylation by nitric oxide. Nature 366:562-565.

Ho GP, Selvakumar B, Mukai J, Hester LD, Wang Y, Gogos JA, Snyder SH (2011) S512 nitrosylation and S-palmitoylation reciprocally regulate synaptic targeting of PSD-95. Neuron 71:131-141.

Jaffrey SR, Snyder SH (1996a) PIN: An associated protein inhibitor of neuronal nitric oxide synthase. Science 274:774-777.

Kang R, Wan J, Arstikaitis P, Takahashi H, Huang K, Bailey AO, Thompson JX, Roth AF, Drisdel RC, Mastro R, Green WN, Yates JR, 3rd, Davis NG, El-Husseini A (2008) Neural palmitoyl-proteomics reveals dynamic synaptic palmitoylation. Nature 456:904-909.

Kapitein LC, Schlager MA, Kuijpers M, Wulf PS, van Spronsen M, MacKintosh FC, Hoogenraad CC (2010) Mixed microtubules steer dynein-driven cargo transport into dendrites. Curr Biol 20:290-299.

Kiss E, Gorgas K, Schlicksupp A, Gross D, Kins S, Kirsch J, Kuhse J (2016) Biphasic Alteration of the Inhibitory Synapse Scaffold Protein Gephyrin in Early and Late Stages of an Alzheimer Disease Model. Am J Pathol 186:2279-2291.

Lakkaraju AK, Abrami L, Lemmin T, Blaskovic S, Kunz B, Kihara A, Dal Peraro M, van der Goot FG (2012) Palmitoylated calnexin is a key component of the ribosome-translocon complex. EMBO J 31:1823-1835.
Lardi-Studler B, Smolinsky B, Petitjean CM, Koenig F, Sidler C, Meier JC, Fritschy JM, Schwarz G (2007) Vertebrate-specific sequences in the gephyrin E-domain regulate cytosolic aggregation and postsynaptic clustering. J Cell Sci 120:1371-1382.
Lee WH, Xu Z, Ashpole NM, Hudmon A, Kulkarni PM, Thakur GA, Lai YY, Hohmann AG (2015) Small molecule inhibitors of PSD95-nNOS protein-protein interactions as novel analgesics. Neuropharmacology 97:464-475.
Liang J, Jaffrey SR, Guo W, Snyder SH, Clardy J (1999) Structure of the PIN/LC8 dimer with a bound peptide. Nat Struct Biol 6:735-740.
Liebsch F, Eggersmann FR, Merkler Y, Kloppenburg P, Schwarz G (2023) Automated Image Analysis Reveals Different Localization of Synaptic Gephyrin C4 Splice Variants. eNeuro 10.
Lionel AC et al. (2013) Rare exonic deletions implicate the synaptic organizer Gephyrin (GPHN) in risk for autism, schizophrenia and seizures. Hum Mol Genet 22:2055-2066.
Navarro-Lerida I, Martinez Moreno M, Roncal F, Gavilanes F, Albar JP, Rodriguez-Crespo I (2004) Proteomic identification of brain proteins that interact with dynein light chain LC8. Proteomics 4:339-346.
Nyarko A, Hare M, Hays TS, Barbar E (2004) The intermediate chain of cytoplasmic dynein is partially disordered and gains structure upon binding to light-chain LC8. Biochemistry 43:15595-15603.
Paige JS, Xu G, Stancevic B, Jaffrey SR (2008) Nitrosothiol reactivity profiling identifies S-nitrosylated proteins with unexpected stability. Chem Biol 15:1307-1316.
Papadopoulos T, Soykan T (2011) The role of collybistin in gephyrin clustering at inhibitory synapses: facts and open questions. Front Cell Neurosci 5:11.
Parhad SS, Jaiswal D, Ray K, Mazumdar S (2016) The protein inhibitor of nNOS (PIN/DLC1/LC8) binding does not inhibit the NADPH-dependent heme reduction in nNOS, a key step in NO synthesis. Biochem Biophys Res Commun 472:189-193.
Poulopoulos A, Aramuni G, Meyer G, Soykan T, Hoon M, Papadopoulos T, Zhang M, Paarmann I, Fuchs C, Harvey K, Jedlicka P, Schwarzacher SW, Betz H, Harvey RJ, Brose N, Zhang W, Varoqueaux F (2009) Neuroligin 2 drives postsynaptic assembly at perisomatic inhibitory synapses through gephyrin and collybistin. Neuron 63:628-642.
Rodriguez-Crespo I, Straub W, Gavilanes F, Ortiz de Montellano PR (1998) Binding of dynein light chain (PIN) to neuronal nitric oxide synthase in the absence of inhibition. Arch Biochem Biophys 359:297-304.
Saiyed T, Paarmann I, Schmitt B, Haeger S, Sola M, Schmalzing G, Weissenhorn W, Betz H (2007) Molecular basis of gephyrin clustering at inhibitory synapses: role of G- and E566 domain I nteractions. J Biol Chem 282:5625-5632.
Schrader N, Kim EY, Winking J, Paulukat J, Schindelin H, Schwarz G (2004) Biochemical characterization of the high affinity binding between the glycine receptor and gephyrin. J Biol Chem 279:18733-18741.
Seneviratne U, Nott A, Bhat VB, Ravindra KC, Wishnok JS, Tsai LH, Tannenbaum SR (2016) S-nitrosation of proteins relevant to Alzheimer's disease during early stages of neurodegeneration. Proc Natl Acad Sci U S A 113:4152-4157.
Shen ZC, Wu PF, Wang F, Xia ZX, Deng Q, Nie TL, Zhang SQ, Zheng HL, Liu WH, Lu JJ, Gao SQ, Yao XP, Long LH, Hu ZL, Chen JG (2019) Gephyrin Palmitoylation in Basolateral Amygdala Mediates the Anxiolytic Action of Benzodiazepine. Biol Psychiatry 85:202-213.
Stykel MG, Ryan SD (2024) Network analysis of S-nitrosylated synaptic proteins demonstrates unique roles in health and disease. Biochim Biophys Acta Mol Cell Res 1871:119720.
Tyagarajan SK, Fritschy JM (2014) Gephyrin: a master regulator of neuronal function? Nat Rev Neurosci 15:141-156.
Tyagarajan SK, Ghosh H, Yevenes GE, Imanishi SY, Zeilhofer HU, Gerrits B, Fritschy JM (2013) Extracellular signal-regulated kinase and glycogen synthase kinase 3beta regulate gephyrin postsynaptic aggregation and GABAergic synaptic function in a calpain-dependent mechanism. J Biol Chem 288:9634-9647.
Tyagarajan SK, Ghosh H, Yevenes GE, Nikonenko I, Ebeling C, Schwerdel C, Sidler C, Zeilhofer HU, Gerrits B, Muller D, Fritschy JM (2011) Regulation of GABAergic synapse formation and plasticity by GSK3beta-dependent phosphorylation of gephyrin. Proc Natl Acad Sci U S A 108:379-384.
Williams JC, Roulhac PL, Roy AG, Vallee RB, Fitzgerald MC, Hendrickson WA (2007) Structural and thermodynamic characterization of a cytoplasmic dynein light chain591 intermediate chain complex. Proc Natl Acad Sci U S A 104:10028-10033.
Yan P, Liu H, Zhou T, Sun P, Wang Y, Wang X, Zhang L, Wang T, Dong J, Zhu J, Lv L, Li W, Qi S, Liang Y, Kong E (2022) Crosstalk of Synapsin1 palmitoylation and phosphorylation controls the dynamicity of synaptic vesicles in neurons. Cell Death Dis 13:786.
Yang H, Oh CK, Amal H, Wishnok JS, Lewis S, Schahrer E, Trudler D, Nakamura T, Tannenbaum SR, Lipton SA (2022) Mechanistic insight into female predominance in Alzheimer's disease based on aberrant protein S-nitrosylation of C3. Sci Adv 8:eade0764.
Yucel BP, Momany EMA, Evans AJ, Seager R, Wilkinson KA, Henley JM (2023) Coordinated interplay between palmitoylation, phosphorylation and SUMOylation regulates kainate receptor surface expression. bioRxiv.

Zareba-Koziol M, Bartkowiak-Kaczmarek A, Figiel I, Krzystyniak A, Wojtowicz T, Bijata M, Wlodarczyk J (2019) Stress-induced Changes in the S-palmitoylation and S-nitrosylation of Synaptic Proteins. Mol Cell Proteomics 18:1916-1938.

Zita MM, Marchionni I, Bottos E, Righi M, Del Sal G, Cherubini E, Zacchi P (2007) Post-phosphorylation prolyl isomerisation of gephyrin represents a mechanism to modulate glycine receptors function. EMBO J 26:1761-1771

2.8. Supplementary figures

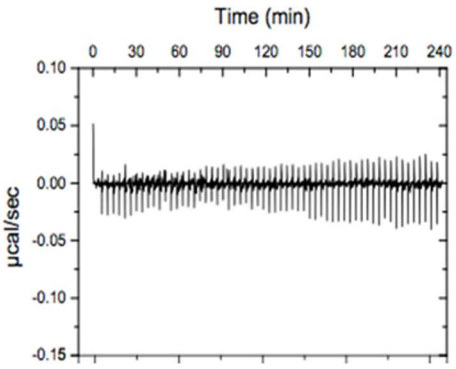

Fig. 1-1. DLC-Y65A does not interact with gephyrin.
Isothermal titration calorimetry of DLC-Y65A binding to gephyrin showed no significant heat changes except for the dilution heat.

Chapter 3

Redox-dependent synaptic clustering of gephyrin

Maria-Theresa Gehling[1], Filip Liebsch[1], Lianne Jacobs[1], Jan Riemer[1,2], Günter Schwarz[1,2,3]

[1]Institute of Biochemistry, Department of Chemistry, University of Cologne, 50674 Cologne, Germany

[2]Cologne Excellence Cluster on Cellular Stress Responses in Aging-Associated Diseases (CECAD), University of Cologne, Cologne, Germany

[3]Center for Molecular Medicine Cologne (CMMC), University of Cologne, Cologne, Germany

Available on BioRxiv (doi: https://doi.org/10.1101/2024.03.15.585209)

Submitted to Nature Communications on March 2024. Under revision since June 2024.

3.1. Author contributions

Maria-Theresa Gehling and Guenter Schwarz designed the study. Maria-Theresa Gehling, Guenter Schwarz and Filip Liebsch wrote the manuscript. All experiments were performed by Maria-Theresa Gehling. Methodical input was given from Lianne Jacobs and Jan Riemer regarding the manipulation of redox environments in neurons with the use of antimycin A and cytosolic D-amino acid oxidases. Filip Liebsch gave methodical input regarding the use of macros for the automated image analysis through Fiji/ImageJ.

3.2. Abstract

Reactive oxygen species (ROS) play a central role in enhancing inhibitory signal transmission, thus extending their role beyond oxidative stress in disease and aging. However, the underlying molecular mechanisms mediating these functions have remained elusive. At inhibitory synapses, the scaffolding protein gephyrin clusters glycine and GABA type A receptors. Since gephyrin harbors multiple surface-exposed cysteines, we investigated the regulatory influence of ROS on gephyrin. We show that H_2O_2-induced oxidation of gephyrin cysteines triggered reversible, synaptic multimerization through disulfide bridge formation, which provided more receptor binding sites, lead to proteolytic protection and enhanced liquid-liquid phase separation. We identified mitochondria-derived ROS as a physiological source and observed oxidized gephyrin multimers *in vivo,* indicating that gephyrin can be regulated by the redox environment. Collectively, our findings suggest that cysteines in gephyrin modulate synaptic localization and clustering as regulatory redox-switches thereby establishing a link between neuronal and mitochondrial activity.

3.3. Introduction

Neuronal activity is connected to oxygen consumption and the production of reactive oxygen species (ROS)[1], that were initially considered as neurotoxic[2]. However recently, redox signaling has emerged as an important pathway for modulating synaptic plasticity. For instance, mitochondria-derived ROS enhance neurotransmission at inhibitory synapses[3], which was attributed to the recruitment of GABA type A receptors ($GABA_AR$) to the synapse, but a molecular mechanism explaining this phenomenon remained elusive. Moreover, it is unclear, how synaptic ROS signaling would be facilitated or sustained in the reductive cytosol. Importantly, maintaining the proper relation of ROS production and clearance is crucial for healthy brain function, and disruptions in ROS homeostasis leading to oxidative stress have been linked to various neuronal diseases[4,5]. Consequently, unraveling the underlying molecular link between ROS production and

neuronal activity is of great interest for understanding synaptic plasticity and the onset of pathological processes.

One key component at inhibitory synapses is the bifunctional protein gephyrin. Gephyrin is crucial for the activity of molybdenum cofactor (Moco)-dependent enzymes involved in basic metabolism. The conserved N-terminal G-domain and C-terminal E-domain of gephyrin catalyze the last two steps of Moco biosynthesis[6]. In addition, in the CNS gephyrin serves as the main scaffolding protein at inhibitory synapses, where it clusters glycine receptors (GlyRs) and a subset of $GABA_A$Rs to facilitate efficient neurotransmission[7,8]. The synaptic clustering requires the self-assembly of gephyrin through E-domain dimerization and G-domain trimerization[9]. The interaction between receptors and gephyrin takes place between the intracellular domain (ICD) of one receptor subunit and the gephyrin E-domain[9]. The gephyrin C-domain links the catalytic G- and E-domain, providing flexibility as well as sites for post-translational modifications (PTMs) that regulate receptor binding and clustering[10,11]. One example is the proteolytic cleavage of gephyrin C-domain by the calcium-dependent protease calpain[12,13]. This irreversible modification is important for gephyrin homeostasis and links excitatory calcium signaling to the shaping of inhibitory gephyrin scaffolds[12]. Moreover, gephyrin participates in a complex network of protein interactions crucial for signal transmission and neuronal plasticity[14]. Thus, dysfunction of gephyrin has detrimental consequences for both metabolic and neuronal functions, ranging from delayed development to seizures and early childhood death[15-17].

Recent studies revealed that gephyrin regulation by PTMs, including those targeting cysteines, is essential for synaptic plasticity[18,19]. S-palmitoylation at Cys212 and Cys284 was identified to increase synaptic gephyrin clusters, while S-nitrosylation resulted in smaller synaptic clusters. However, not all of gephyrin's surface cysteines have been assigned a specific function. Given that in the absence of specific functions cysteines get lost during evolution[20], we investigated a potential link between redox-signaling and surface cysteines going beyond the previously reported S-nitrosylation and S-palmitoylation.

Redox modifications on cytosolic proteins are often regulated in space and time. Gephyrin is a cytosolic protein that reversibly associates with the postsynaptic membrane forming postsynaptic clusters/microdomains. Recently, liquid-liquid phase separation (LLPS) has emerged as a novel mechanism for creating subcellular microdomains important for many pre- and post-synaptic functions[21-23]. LLPS has been proposed as a possible mechanism for gephyrin multimerization[22]. In addition, the ability of gephyrin to undergo LLPS may be influenced by redox-changes or may impact gephyrin's accessibility to redox signals. Initially, it was found that interaction with an

artificial multimeric binding partner is necessary to enable gephyrin LLPS[22]. In the previous study, a dimeric model consisting of two ICDs of the GlyR β-subunit was utilized. In this study, we employed two different receptor models to study the binding and LLPS properties of gephyrin in relation to its redox state. One model is a newly developed pentameric and soluble fusion protein of yeast lumazine synthase (LS) and five ICDs of the GlyR β-subunit[24], while the other is the established monomeric peptide of the GlyR β-subunit ICD[25].

Our results demonstrate a dynamic redox-dependent regulatory mechanism for synaptic gephyrin clustering: Oxidation strengthened clustering, a process that was reversed by reduction. As result, the number of receptor binding sites increased, which was consistent with a previously reported redox-dependent enhancement of inhibitory neurotransmission[26]. We showed that LLPS forms the basis for creating oxidative microdomains, with H_2O_2 derived from mitochondria being a potential source for gephyrin oxidation. In conclusion, our study establishes a link between inhibitory neuronal and mitochondrial activity and offers a feedforward pathway through redox-dependent synaptic clustering of gephyrin.

3.4. Results

3.4.1. Surface cysteines of gephyrin are required for synaptic function

A crucial aspect of inhibitory synaptic transmission is the ability of gephyrin to build a scaffold by multimerization. To test whether the oligomeric state of gephyrin is dependent on cysteines and if those are redox-sensitive, we tested whether gephyrin presents redox-sensitive behavior in native tissue. Therefore, we perfused mice with N-ethyl-maleimide(NEM)-containing PBS to stabilize free thiols and avoid unspecific oxidation. In subsequent Western blot analysis, we either used the reductant dithiothreitol (DTT) or omitted it, allowing to compare the presence of redox-dependent gephyrin species (Figure 1A). In all tissues, the absence of a reductant resulted in bands corresponding to a molecular weight of approximately 300 kDa representing multimeric gephyrin species, whereas reduction of gephyrin led exclusively to monomeric gephyrin. The fractional abundance of multimeric gephyrin was approximately 20% (Figure 1B). Based on this finding, we hypothesized that gephyrin cysteines are redox-sensitive forming intermolecular disulfide bridges and thereby influence multimerization. Multimerization is a crucial parameter for the synaptic function of gephyrin[27]. Thus, we wondered which surface cysteines of gephyrin could be important for multimerization.

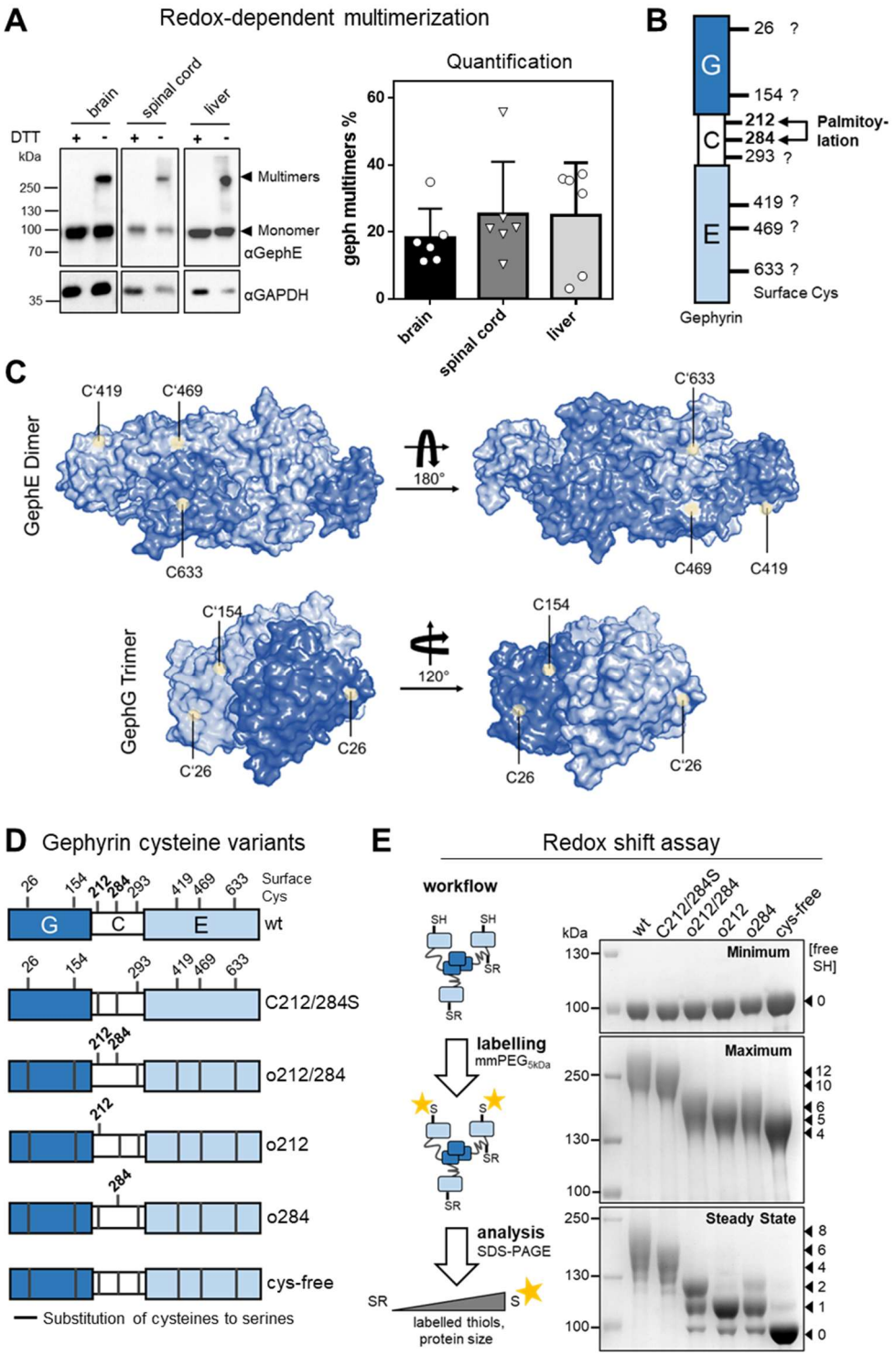

Figure 1: Role of Surface-exposed Cysteines of Gephyrin.
A) Western Blot analysis of tissue lysates generated from mice, that have been perfused with NEM. Samples of reduced (DTT) or non-reduced lysates (load of 45 µg). Monomeric and multimeric gephyrin marked with arrows. Quantification of gephyrin multimer bands from A, including six mice samples in total. Abundance in relation (%) to complete gephyrin amount loaded in one sample. B) Domain structure of gephyrin. G=G-domain; C=C-domain; E=E-domain. Positions of the eight potential surface-exposed cysteines highlighted. C) Crystal structures of trimeric G-domain (1IHC[28]) and dimeric E-domain (2FU3[25]). Surface cysteines highlighted in yellow. D) Genetically engineered cysteine variants used in this study. Cysteines were substituted with serines at indicated positions. E) Redox Shift Assay with the cysteine variants. Workflow: In this assay free thiols (-SH) are labelled with a maleimide-PEG-5kDa-tag (mmPEG) increasing the size in SDS-PAGE. Coomassie staining: Amount of labelled, free-thiols cysteines indicated with arrows. As controls mmPEG and SDS were left out (Minimum) and both were added to additionally label the 4 internal cys (Maximum). For the steady state redox-status mmPEG but no SDS was used.

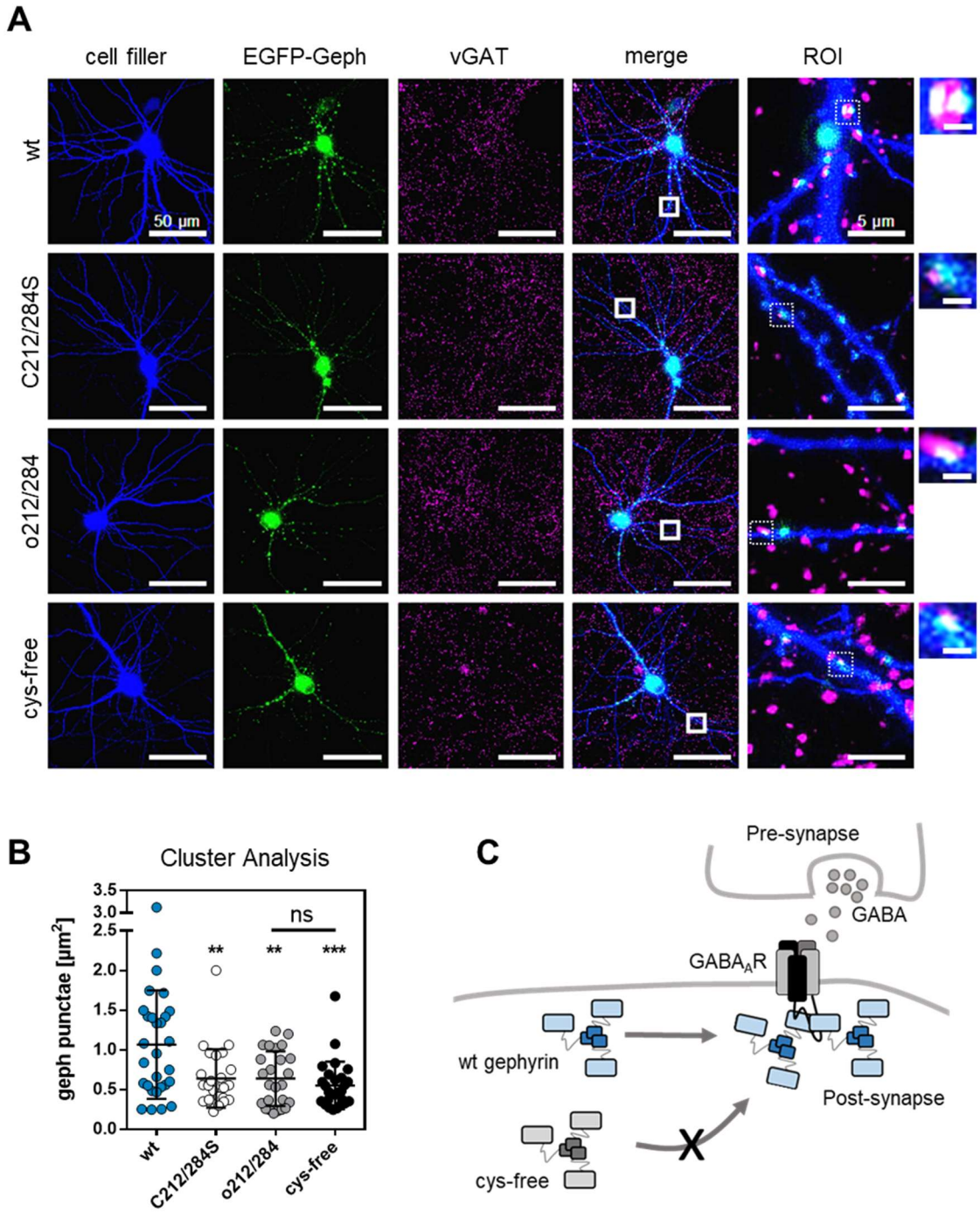

Figure 2: Role of the Surface-Exposed Cysteines for Gephyrin Function.
A) Primary, hippocampal neurons transfected with EGFP-gephyrin (green) and tdTomato (cell filler, blue) (scale bar 30 µm). Synaptic termini identified by vGAT staining. Dendrites enlarged (scalebar 5 µm) with increments of respective synaptic gephyrin clusters (scale bar 1 µm). B) Cluster analysis of synaptic gephyrin. Significance tested by 1way ANOVA $F(3,103)=7.240$, $p=0.0002$. *Bonferroni* post-hoc test in comparison to wt: C212/284S: $p=0.0033$ (**); o212/284: $p=0.0035$ (**), cys-free: $p=0.0002$ (***). *Bonferroni* post-hoc test of o212/284 and cys-free $p=0.9368$ (ns). C) Scheme of gephyrin clustering at GABAergic synapses. Cys-free gephyrin shows disturbed synaptic clustering

Crystal structures of G- and E-domain[25,28], as well as the identification of S-palmitoylation[19], assigned cysteines at position 26, 154, 212, 284, 419, 469 and 633 as surface-exposed (Figure 1 B and C). Interestingly, those cysteine residues are conserved in orthologues harboring a central nervous system (Figure S1), while other

proteins such as Cnx1 in plants or bacterial orthologues lack those cysteines. In addition, Cys293 within the C-domain is considered as surface-exposed in the absence of structural information and a prediction as an intrinsically unordered sequence within the protein[11]. To investigate the potential role of exposed surface cysteines in redox regulation of gephyrin function, we generated cysteine variants by the substitution to serine (Figure 1D). Previously, Cys212 and 284 were identified as targets of S-palmitoylation[19]. In this study, each of the other eight surface cysteines was individually substituted with serine. These variants were expressed in cultured primary hippocampal neurons, and the synaptic localization of gephyrin was analyzed. Except for the S-palmitoylated Cys212 and 284, none of the other substitutions resulted in any noticeable effect. This suggested that the other surface cysteines were individually dispensable. To test whether more than one cysteine outside the S-palmitoylation motif may have a functional role, we generated a gephyrin variant containing only Cys212 and 284 (o212/284) by replacing all other surface cysteines (Cys26, 154, 293, 419, 469, 663) with a serine. Additionally, we generated variants with remaining Cys212 (o212) and Cys284 (o284), respectively, and one variant without any surface-exposed cysteine, which we called “cys-free”. Importantly, in all variants the four internal cysteines (Cys74,133, 635, 676) were unchanged.

The respective gephyrin variants were expressed and purified to homogeneity (Figure S2A). All variants showed similar secondary structure distribution as judged by CD-spectroscopy (Figure S2B). Besides that, we observed similar expression in COS7 cells (Figure S3A and B) and functional enzymatic activity (Figure S3C).

With the purified variants we performed a redox-shift assay (Figure 1E) to determine free thiols by the attachment of a maleimide conjugate with a PEG-tag ($mmPEG_{5kDa}$), which requires an accessible, free thiol. Each labelled cysteine increased the size of gephyrin by approximal 10 kDa. Note that, internal Cys74, 133, 635 and 676 are accessible in the unfolded protein only (maximum shift). Thus, we confirmed that each individual cysteine among the eight predicted ones were indeed surface exposed, regardless of the presence of other cysteines (Figure 1E).

Based on the observed redox-dependent multimerization and redox-shift data, we anticipated a critical role for the eight surface-exposed cysteines in gephyrin. We focused on the scaffolding function of gephyrin in neurons. First, we performed Western blot and RT-PCR analysis demonstrating equal levels of expression for all variants (Figure S4). Afterwards, we expressed EGFP-tagged wt gephyrin, the variant lacking the S-palmitoylation sites (C212/284S), and our newly generated variants (o212/284 and cys-free) in hippocampal neurons (Figure 2A). Subsequently, we assessed synaptic gephyrin cluster size (Figure 2B). The o212/284 variant did not exhibit a wt-like phenotype. The

disturbance of synaptic clustering was similar to that observed in the C212/284S variant, as the synaptic cluster size was significantly reduced. This finding led us to conclude that the other surface cysteines serve an unidentified function, distinct from that of S-palmitoylation[19]. Furthermore, this unknown function appears to be dependent on multiple cysteines, as single substitutions that were studied before did not show any significant impact on synaptic function[19]. Moreover, the cysteine-free variant was in comparison to wt gephyrin significantly impaired, which was comparable to the o212/284 variant underlying the importance of all surface-exposed cysteines.

In summary, our data demonstrate that at least eight cysteines in gephyrin are surface exposed and play an important role in synaptic clustering (Figure 2C). Furthermore, the underlying mechanism, responsible for the multimerization of gephyrin at synapses relies on the cooperative action of multiple cysteines, which is in line with the identification of redox-dependent multimers found in native tissue.

3.4.2. Gephyrin undergoes reversible multimerization through disulfide bridge formations

Given that an unidentified mechanism involves the cooperation of cysteines and regulates the density of gephyrin at inhibitory synapses, we proposed the possibility of an oxidation-induced disulfide-bridge formation in gephyrin clusters. To test this hypothesis, we treated recombinantly expressed gephyrin derived from *E. coli* with either the oxidant diamide or the reductant Tris-2-carboxyethyl-phosphine (TCEP) and analyzed the multimeric state of gephyrin using size-exclusion chromatography (SEC). As a negative control, we used cysteine-free gephyrin. Upon oxidation, wt gephyrin displayed a significant increase in high-order multimers, which was not observed in the cysteine-free variant (Figure 3A and B). This led us to conclude that cysteines mediate a mechanism triggering multimerization. To confirm that disulfide bridges are responsible for gephyrin multimerization, we subjected the oxidation-induced multimers to treatment with DTT, which effectively reversed the formation of multimers back to their initial non-oligomeric state prior to oxidation. In addition, we collected samples of the different SEC peaks and prepared them for SDS-PAGE analysis under reducing or non-reducing conditions (Figure S4A and B). We found that reduction and denaturation of all samples including those of the oxidation-induced high-order multimers, resulted in monomeric gephyrin species at around 100 kDa. In contrast, without reductant prior to SDS-PAGE, monomeric gephyrin species disappeared. For the cysteine-free variant, no difference was observed before and after oxidation. In conclusion, we show that the mechanism behind redox-dependent multimerization of gephyrin is likely the induction of intermolecular disulfide bridges by oxidation, which can be reversed by reduction.

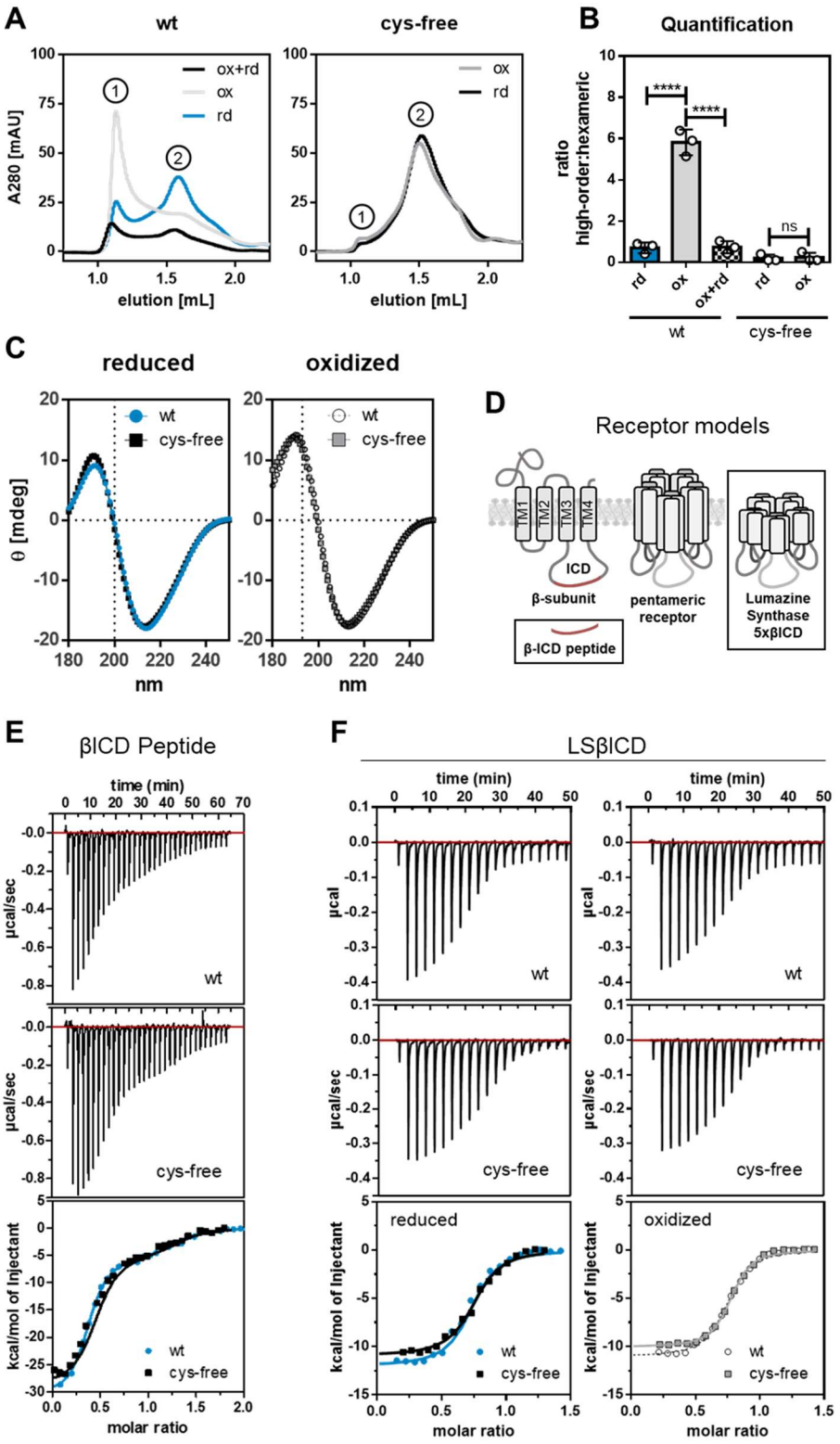

Figure 3: Reversible Redox-Dependent Oligomerization of Gephyrin *in vitro* and *in vivo*.
A-B) Size exclusion chromatography (SEC) with oxidized or reduced gephyrin wildtype (wt) or cysteine-free (cys-free) variant. A) Chromatograms with peaks of high-order multimers (1) or hexameric gephyrin (2). Reduced runs in blue (wt) or black (cys-free), oxidized in white (wt) or grey (cys-free) and oxidized peak collected and subsequently re-reduced in black (wt). B) Quantification of the ratio of the peak heights of three different runs. Significance tested by 1way ANOVA $F(4,10)=137.2$, $p<0.0001$, *Bonferroni* post-hoc test: $p<0.0001$ (****); $p>0.9999$ (ns). C) CD Spectroscopy. Spectra of oxidized or reduced gephyrin wt or cys-free variant. Vertical dotted line indicates HT threshold of 800 mV. D) Schematic illustration of receptor models used for binding studies. The glycine receptor (GlyR) is modelled by either a short peptide of the intracellular domains of the GlyRβ-subunit (βICD) or by the fusion of soluble, pentameric lumazine synthase (LS) with five βICDs. E) Isothermal colorimetry (ITC) experiment titrating βICD-peptide into gephyrin wt or cys-free variant. Experiment performed under reductive conditions. F) ITC titrating LSβICD into gephyrin wt or cys-free variant. Experiments were performed under non-reductive conditions with either pre-reduced or pre-oxidized gephyrin.

3.4.3. Gephyrin oxidation increases liquid-liquid phase separation

We identified that gephyrin multimerization was reversible and inducible by oxidation *in vitro* and we observed redox-dependent multimers *in vivo*. Next, we asked whether these oxidized, multimerized gephyrin species retain their functionality. Given that multimerization is a crucial feature of gephyrin, we sought to investigate the molecular consequences in respect to its biochemical properties, such as structure and receptor binding.

Firstly, we examined the secondary structure and binding capability of both wt gephyrin and the cysteine-free variant under oxidative and reductive conditions. Overall, we observed no alterations in the secondary structure, regardless of whether all cysteines were replaced with serines or if gephyrin underwent reduction or oxidation (Figure 3C). Similarly, we found no changes in the binding properties of gephyrin towards two glycine receptor models βICD and LS βICD[24,25] using isothermal titration calorimetry (ITC) experiments (Figure 3D-F). For both, wt and cys-free variant, the interaction with the βICD peptide occurred in a two-site binding mechanism (Figure S5C). The stoichiometry observed indicated approximately one gephyrin trimer interacting with one βICD peptide. The dissociation constant K_D was in the low micromolar range (wt = 0.041±0.010 μM; cys-free = 0.063±0.018 μM). The binding mechanism of gephyrin wt and cys-free variant with pentameric LS βICD followed a one-site binding model (Figure S5D) yielding a stoichiometry of one LS βICD pentamer to approximately two gephyrin trimers, which was observed for wt and cys-free variant independent of the redox-state. The K_D was in the low molecular range as well (wt^{rd} = 0.320±0.042 μM; wt^{ox} = 0.295±0.041 μM; $cys\text{-}free^{rd}$ = 0.373±0.041 μM; $cys\text{-}free^{ox}$ = 0.291±0.032 μM). Consequently, we concluded that the presence of disulfide bridges did not alter the secondary structure or binding properties of gephyrin, while it changed its oligomeric state.

It would be plausible that oxidation-induced multimerization could lead to tighter packing of gephyrin clusters. Importantly, the quantity of gephyrin present at synapses and the protein density of clusters are crucial factors determining the number of receptor binding sites. Consequently, clustering can impact synaptic plasticity and neuro-transmission. In line with this notion, we investigated in which manner oxidative processes would occur and be maintained, since gephyrin is a cytosolic protein and the cytosol represents a reductive environment. One possibility is the ability to form phase-separated droplets in the presence of a multimeric binding partner.

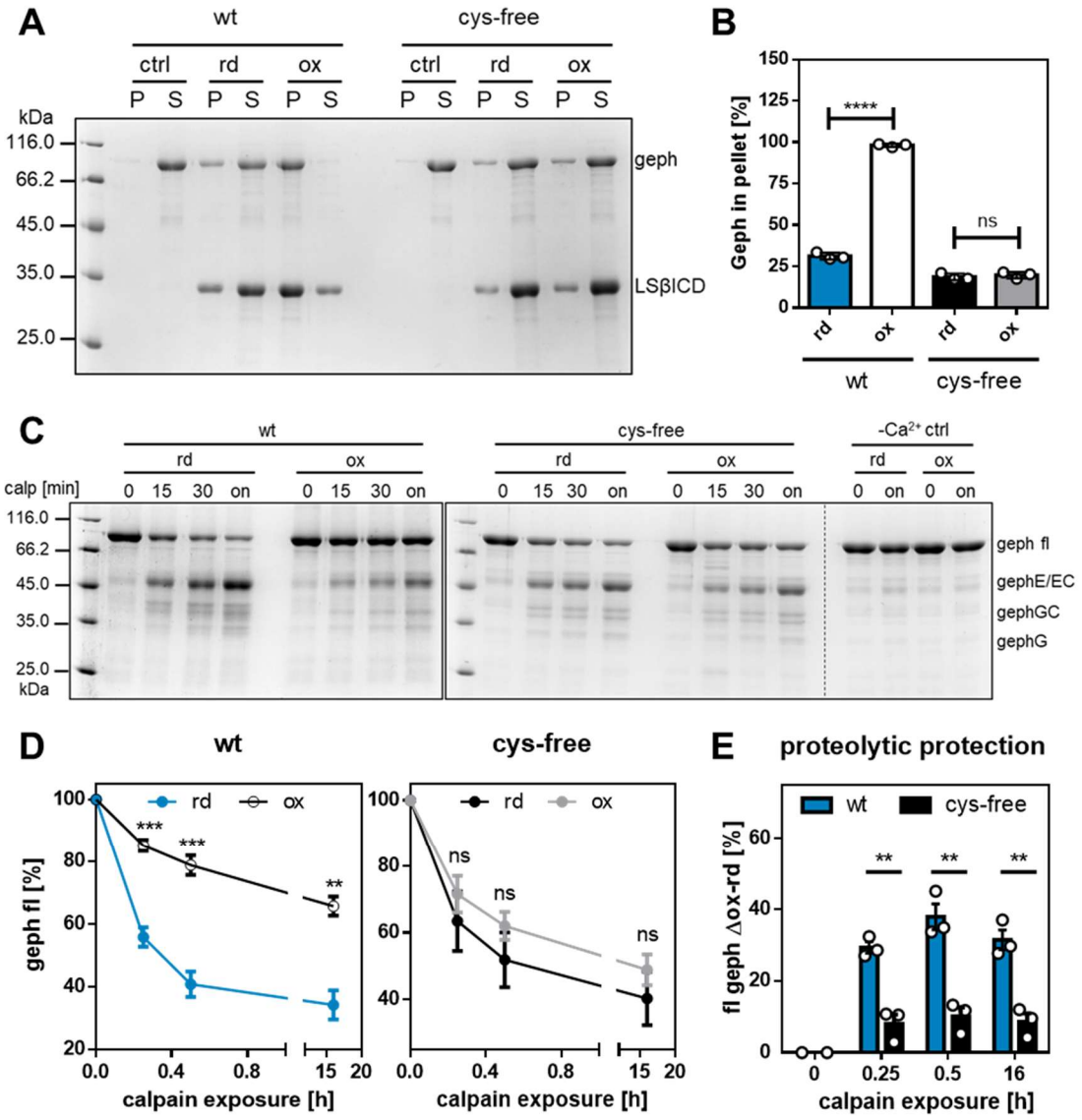

Figure 4: Sedimentation and Calpain Cleavage Assays of oxidized and reduced Gephyrin.
Oxidized (ox) or reduced (rd) gephyrin wt and cysteine-free were used for sedimentation (A-B) and calpain cleavage (C-E) assays. Sum of three replicates. Error bars determined by standard deviation. A-B) Successful interaction with LSβICD causes droplet formation (liquid-liquid phase separation), these droplets are sedimented by centrifugation. Sedimented protein is found in the pellet (P) fraction, non-phase separated protein stays in the supernatant (S). A) Coomassie Staining of fractions. B) Quantification of gephyrin band intensities. Relative abundance (%) normalized to sum of protein in pellet and supernatant of the corresponding fractions. Significance tested by 1way ANOVA $F_{3,8}$=1,328, p<0.0001. Bonferroni post-hoc test: wt: p<0.0001 (****); cys-free: p=0.9773 (ns). C-D) Exposure of gephyrin to the protease calpain for different times. C) Coomassie staining. Degradation products of gephyrin indicated at the different heights. fl=full-length; gephE=E-domain; gephEC=E-domain with C-domain fragments; gephG=G-domain, gephGC=G-domain with C-domain fragments. In the control, calcium was absent. D) Quantification of full-length (fl) gephyrin in each sample. Relative abundance (%) normalized to the start point 0. Significance between rd and ox determined by *t*-test and significance level alpha corrected by *Bonferroni* (/3): wt t1:p=0.0001 (***); t2:p=0.0002 *(***);* t3:p=0.006*;* cys-free*:* t1:p=0.2535 (ns); t2:p=0.1292 (ns); t3:p=0.1843 (ns). E) Comparison of proteolytic resistance. Relative abundance of fl geph in the reduced samples was subtracted from that of the oxidized ones (Δox-rd). Significance tested by t-test and significance level alpha *Bonferroni* corrected (/3)*:* t1:p=0.0022 (**); p=0.0031 (**); p=0.0033 (**).

To investigate LLPS of gephyrin in relation to its redox-state, we used the pentameric receptor model LSβICD[24] (Figure 4A). Following coincubation of a 2:1 molarity of LSβICD to oxidized gephyrin, we found a significantly stronger sedimentation with nearly 100% of all protein in the sedimented fraction, while the majority of reduced gephyrin stayed in the soluble supernatant. In comparison, oxidized and reduced cysteine-free variants remained in the soluble similar to reduced wt gephyrin (Figure 4B). This finding supports the idea that oxidized gephyrin forms high-order oligomeric networks in the presence of oligomeric ligands thus resulting in sedimentation.

Calpain-mediated cleavage is an important mechanism for the regulation of gephyrin clustering at synapses[12]. Besides calcium levels, the access to calpain cleavage sites determines the rate of proteolysis, which could be altered through redox-dependent multimerization. Therefore, the ability of calpain to cleave reduced or oxidized gephyrin was tested *in vitro* (Figure 4C-E). The sensitivity of oxidized gephyrin to calpain cleavage was significantly reduced by approximately two-fold, while there was no significant difference between reduced wt gephyrin and oxidized or reduced cysteine-free gephyrin (Figure 4D). Analyzing the difference in remaining full-length, undigested gephyrin between oxidized and reduced protein (Δox-rd), showed that wt gephyrin exhibited significant proteolytic resistance after oxidation even after short exposure towards calpain (Figure 4E). In contrast, the cysteine-free variant was equally digested as reduced wt gephyrin, regardless of whether it was in the reduced or oxidized state.

In summary, our results show that structural properties of gephyrin that are influenced by its oligomeric state, such phase separation as well as proteolytic sensitivity, were redox-dependent.

3.4.4. H_2O_2 mediates synaptic clustering of gephyrin *in cellulo*

To address the question of how gephyrin wt in comparison to the cys-free variant could be oxidized to multimerize via disulfide-bridge formation in neurons, we investigated H_2O_2, which is a commonly known oxidant emerging from different sources in the cell. Therefore, we expressed a cytosolic version of a D-amino acid oxidase (DAAO) with an mScarlet-tag in hippocampal neurons and tested the effect on endogenous gephyrin clusters (Figure 5A) and afterwards on recombinant cys-free and wt gephyrin (Figure 5B). DAAO enzyme produces H_2O_2 by the conversion of D-amino acids to the corresponding α-keto acids (Figure 5A), thus we treated our cells with D-Met. As a negative control we generated a less active variant of DAAO by substituting Arg285 to Lysin[29]. Following cell treatment, we stained for the presynaptic marker vGAT and

analyzed its co-localization with endogenous gephyrin to identify synaptic gephyrin species.

Firstly, the ubiquitous and cytosolic localization of DAAO could be demonstrated (Figure 5C, full images in Figure S6A). D-Met treatment caused a significant increase of synaptic cluster sizes by approximately 20% (from 0.1269 to 0.1521 μm^2) (Figure 5C and D). Additionally, the intensity of synaptic gephyrin was significantly increased by about 14% (from 1 364 to 1 559 a.u.) (Figure 5E). The expression of DAAO R285K variant in combination with D-Met treatment had a significant increase on gephyrin cluster size as well, but the effect size was smaller (Confidence Interval $[-0.011;-0.039]^{wt}$, $[-0.001;-0.030]^{R285K}$). The effect could be explained by the residual activity of the R285K mutant[29]. However, no effect of the treatment in combination with the R285K mutant on the intensity of gephyrin was observed. Based on this observation, we conclude that the effects on gephyrin resulted mainly from the enzymatic activity of DAAO, the production of H_2O_2. Since increase of cluster size and intensity are signs of gephyrin recruitment to the synapse, we concluded that H_2O_2 is able to trigger synaptic multimerization of gephyrin *in cellulo*.

Next, we verified that H_2O_2 has a direct effect on the cysteines of gephyrin to support the hypothesis of gephyrin oxidation-mediated multimerization via disulfide-bridges (Figure 5B). Thus, we combined the expression of DAAO and subsequent D-Met treatment with the overexpression of mEGFP-tagged gephyrin (Figure 5F, full images in Figure S6B). As expected, overexpressed wt gephyrin showed a significant increase of about 25% (from 0.1393 to 0.1750 μm^2) in cluster size following D-Met treatment, while cys-free gephyrin showed no effect (Figure 5F and G). Strikingly, the intensity of synaptic mEGFP-gephyrin wt upon DAAO-mediated H_2O_2 production was decreased by -15% (from 6 591 to 5 588 a.u.), but that of cys-free gephyrin was unchanged (Figure 5H). In this set up, oxidation extended existing gephyrin clusters in size but did not increase the density within clusters.

In conclusion, we could show that DAAO-mediated H_2O_2 promotes synaptic gephyrin cluster formation. The mechanism involves surface cysteines of gephyrin since cysteine-free gephyrin did not react to cellular H_2O_2 formation.

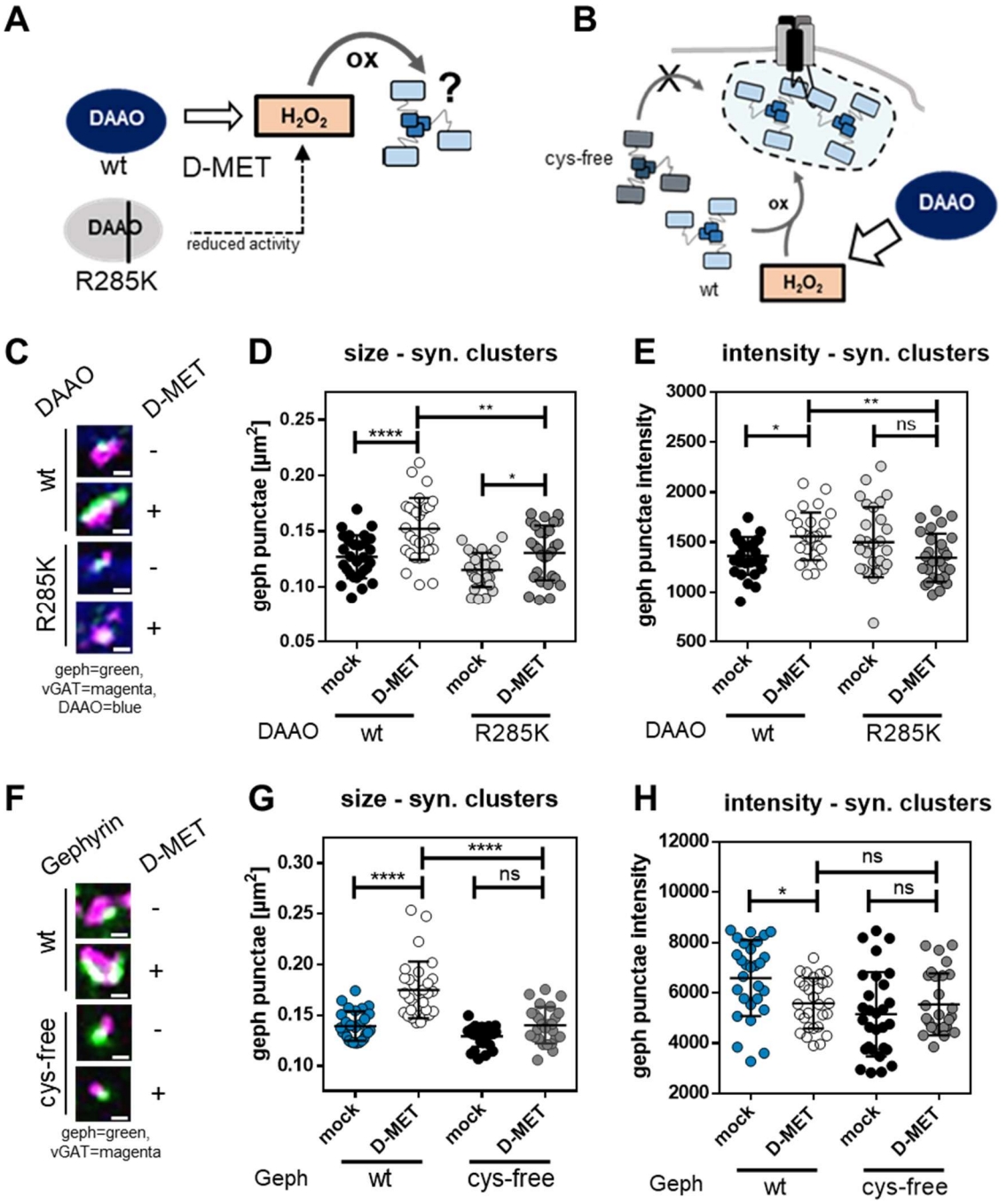

Figure 5: H_2O_2 drives Gephyrin Oligomerization at Synapses.

Expression of cytosolic mSclt-DAAO and mEGFP-Geph in primary, hippocampal neurons. Treatment at DIV14 with 5 mM D-MET. Analysis of cluster sizes [µm²], intensity [au] and co-localization with vGAT (=synaptic clusters) of gephyrin. A) Schematic description of H_2O_2 production of DAAO wt upon D-methionine acid treatment. DAAO mutant R285K is inactive. Can H_2O_2 oxidize gephyrin and influence its oligomerization? B) Schematic description of influence of DAAO-generated H_2O_2 on gephyrin clustering. Is cys-free gephyrin not influenced? C-D) mSclt-DAAO wt and R285K. Analysis of endogenous gephyrin clusters. C) Representative gephyrin clusters (Gephyrin: green, vGAT: magenta, DAAO: blue) (scale bar 0.5 µm). Synaptic termini identified by vGAT co-localization. D) Sizes of synaptic gephyrin. Significance tested by 1way ANOVA $F(3,113)=14.18$, $p<0.0001$. *Bonferroni* post-hoc test: wt vs. wt+D-MET: $p<0.0001$ (****); R285K vs R285K+D-MET: $p=0.0277$ (*), wt+D-MET vs R285K+D-MET: $p=0.0010$ (***). E) Intensity of synaptic gephyrin. Significance tested by 1way ANOVA $F(3,109)=4.431$, $p=0.0056$. *Bonferroni* post-hoc test: wt vs. wt+D-MET: $p=0.0204$ (*); R285K vs R285K+D-MET: $p=0.0808$ (ns), wt+D-MET vs R285K+D-MET: $p=0.0083$ (**). F-H) mSclt-DAAO wt and mEGFP-Geph wt and cys-free variants. Analysis of recombinant mEGFP-gephyrin clusters. F) Representative gephyrin clusters (Gephyrin: green, vGAT: magenta) (scale bar 0.5 µm). Synaptic termini identified by vGAT co-localization. G) Sizes of synaptic gephyrin. Significance tested by 1way ANOVA $F(3,107)=31.66$, $p<0.0001$. *Bonferroni* post-hoc test: wt vs. wt+D-MET: $p<0.0001$ (****); cys-free vs cys-free+D-MET: $p=0.1252$ (ns), wt+D-MET vs cys-free+D-MET: $p<0.0001$ (****). H) Intensity of synaptic gephyrin. Significance tested by 1way ANOVA $F(3,110)=5.608$, $p=0.0013$. *Bonferroni* post-hoc test: wt vs. wt+D-MET: $p=0.0212$ (*); cys-free vs cys-free+D-MET: $p=0.8567$ (ns), wt+D-MET vs cys-free+D-MET: $p>0.9999$ (ns).

3.4.5. Mitochondria-derived ROS are a source of gephyrin oxidation

Lastly, we were looking for a more natural source of oxidation since the expression of ubiquitous DAAO is an artificial approach. Such a natural source could be ROS generated by mitochondria (mROS). Although there are more pathways generating ROS, we chose mitochondria, since neurons are mitochondria-rich cells requiring ATP and thus active mitochondria[30-32]. In turn, mitochondria with oxidative phosphorylation activity, likely produce ROS such as superoxide radicals, that are quickly turned over to H_2O_2[33].

ROS production was triggered by the treatment of neurons with antimycin A. Antimycin A inhibits complex III of the respiratory chain in mitochondria leading to the accumulation of electrons[34]. These electrons react with oxygen to ROS[35]. Additionally, we introduced DTT treatment to reverse mROS-dependent oxidative stress (Figure 6A). Again, we monitored first endogenous gephyrin and the presynaptic marker vGAT (Figure 6C, full images in Figure S7A). Comparable to the results using DAAO as an oxidation source, mROS production led to a significant increase of gephyrin average cluster size by about 13% (from 0.1808 to 0.2051 μm^2) and significantly increased gephyrin intensity by about 25% (from 810.7 to 1 020 a.u.) at synapses (Figure 6D and E). This effect was reversible following DTT treatment (to 0.1851 μm^2 and 890.1 a.u.). Previously, it was reported that antimycin A treatment enhanced inhibitory neurotransmission by the recruitment of synaptically active $GABA_A$ R containing γ2 and α3 subunits to the synapse[26]. Oxidation-mediated multimerization of gephyrin potentially leads to more available receptor binding sites, which could be an explanation for the recruitment of $GABA_A$ Rs (Figure 6B). To test this functional link, we again treated hippocampal neurons with antimycin A to produce mROS and stained for synaptic $GABA_A$ R γ2 subunits (synaptic = co-localization with vGAT) (Figure 6F-H, full images in Figure S7B). Upon antimycin A treatment, the average sizes of synaptic $GABA_A$ R γ2 punctae significantly increased by about 11% (from 0.1421 to 0.1576 μm^2) (Figure 6G). This effect was again reversible following DTT treatment. The intensity of γ2 punctae was unchanged in all conditions (Figure 6H).

Taken together, mROS production enhanced synaptic gephyrin clustering, which was reversible by reduction. This finding indicates that the underlying mechanism of multimerization is redox-dependent and reversible. Since cysteine-free gephyrin did not respond to mROS, we propose that oxidation-driven multimerization is mediated via disulfide-bridge formation of gephyrin surface cysteines. The multimerization of gephyrin at the synapse is important for the supply of receptor binding sites. We could show that mROS-mediated oxidation of gephyrin strengthens the recruitment of synaptically active $GABA_A$ Rs containing γ2 subunits. This likely finally supports inhibitory

neurotransmission thus linking mitochondrial to neuronal activity through redox-dependent multimerization of gephyrin.

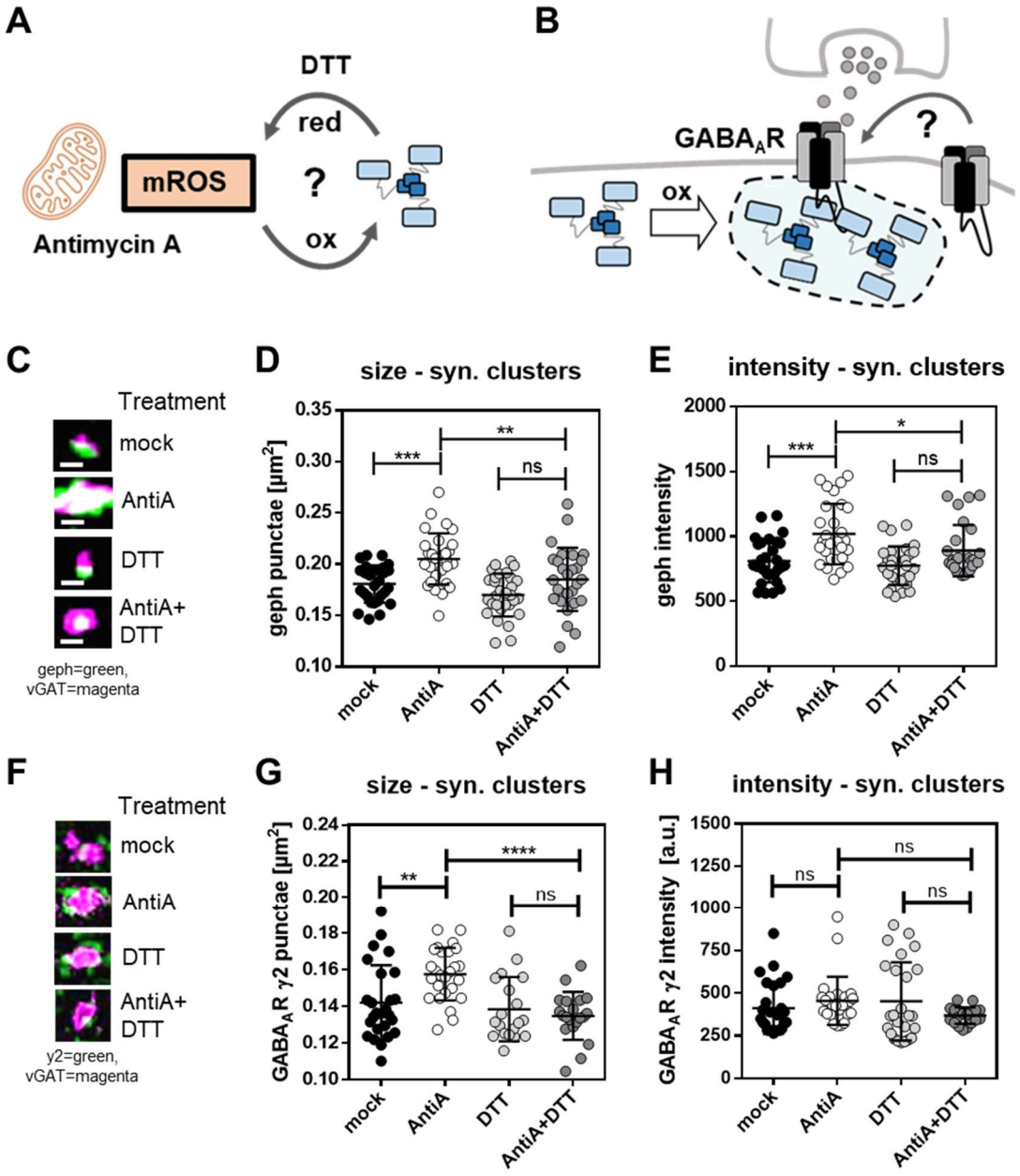

Figure 6: mROS reversibly drive Gephyrin Oligomerization and the Recruitment of GABA$_A$R γ2 Subunits
Treatment of primary hippocampal neurons at DIV14 with 1 µM Antimycin A (AntiA) and/or 5 µM DTT. Analysis of gephyrin or GABA$_A$R γ2 subunit cluster sizes [µm^2], intensity [au] and co-localization with vGAT (=synaptic clusters). A) Schematic description of mitochondrial ROS (mROS) production through Antimycin A treatment. Do mROS oxidize gephyrin and can DTT reverse this by reduction? B) Schematic description of influence of H_2O_2 on GABA$_A$R (containing γ2 subunits) clustering. Does gephyrin oxidation lead to more synaptic receptors? C-E) Analysis of endogenous gephyrin. C) Representative gephyrin clusters (Gephyrin: green, vGAT: magenta, DAAO: blue) (scale bar 0.5 µm). Synaptic termini identified by vGAT co-localization. D) Sizes of synaptic gephyrin. Significance tested by 1way ANOVA $F(3,112)=11.08$, $p<0.0001$. *Bonferroni* post-hoc test: mock vs. AntiA: $p=0.0006$ (***); DTT vs DTT+AntiA: $p=0.0540$ (ns), AntiA vs AntiA+DTT: $p=0.0065$ (**). E) Intensity of synaptic gephyrin. Significance tested by 1way ANOVA $F(3,111)=9.734$, $p<0.0001$. *Bonferroni* post-hoc test: mock vs. AntiA: $p=0.0001$ (***); DTT vs. DTT+AntiA: $p=0.0676$ (ns), AntiA vs. DTT+AntiA: $p=0.0341$ (*). F-H) Analysis of endogenous GABA$_A$R γ2 subunit clusters. F) Representative γ2 clusters (γ2 : green, vGAT: magenta) (scale bar 0.5 µm). Synaptic termini identified by vGAT co-localization. G) Sizes of synaptic γ2 clusters. Significance tested by 1way ANOVA $F(3,87)=8.567$, $p<0.0001$. *Bonferroni* post-hoc test: mock vs. AntiA: $p=0.0037$ (**); DTT vs. DTT+AntiA: $p>0.9999$ (ns), AntiA vs. DTT+AntiA: $p<0.0001$ (****). H) Intensity of synaptic γ2 clusters. Significance tested by 1way ANOVA $F(3,93)=1.432$, $p=0.2384$.

3.5. Discussion

Our study provides new insight into the mechanism of gephyrin-dependent inhibitory synapse formation. First, we identified surface exposed cysteines *in vitro* and demonstrated their sensitivity to redox changes. As a result, we found that the multimerization of gephyrin was regulated by oxidation and reduction. We identified redox-dependent multimers *in vivo* and induced synaptic multimerization *in cellulo* through DAAO-mediated H_2O_2 and antimycin A treatment targeting mitochondria. Oligomerization is a crucial aspect of gephyrin scaffolds, significantly impacting the plasticity of inhibitory synapses[27,36]. Consequently, the oligomeric state influences the number of available receptor binding sites and the sensitivity of gephyrin to proteolytic cleavage[37]. Changing the oligomeric state by oxidation enhanced clustering, while reduction reversed this process (Figure 7). In aggregate, this study provides a novel role of multiple surface-exposed cysteines in gephyrin, which were found to be conserved in orthologues with a central nervous system while other orthologs in plants, yeast, fungi and prokaryotes lack those residues (Figure S4).

Our data suggests that the molecular basis for redox-dependent multimerization of gephyrin is the formation of disulfide bridges. In comparison to PSD95, the excitatory pendant, multimerization by the formation of disulfide bridges was also detected *in cellulo* and *in vivo*[38]. Recently, the disruption of a cysteine linkage in PSD95 has been linked to an epileptic phenotype in rats[39] highlighting the importance of redox-regulation of neuronal scaffold proteins.

Cysteine oxidation in gephyrin could be reversed by reduction, which is essential for enabling dynamic changes and maintaining plasticity. Importantly, cysteine oxidation did not influence the secondary structure of gephyrin and its binding to the receptor, but it altered the density of gephyrin at the synapse, manipulating the availability of receptor binding sites. Since the y2 subunit is considered crucial for synaptic $GABA_ARs$[7], we provide an explanation for the increase in inhibitory neurotransmission caused by antimycin A in previous studies[26]: redox-dependent multimerization of gephyrin, which recruited $GABA_AR$-containing y2 subunits.

Although, redox-dependent regulation of synaptic proteins has previously been investigated, important questions remain open such as the source of oxidation. Given that neurons are rich in mitochondria and mitochondria are located in close proximity to the synapse[31], we propose that mitochondria-derived ROS could serve as a source for oxidation. In this sense, gephyrin could provide the functional link between mitochondrial and neuronal activity. Highly active neurons require ATP production mainly derived from mitochondrial respiration being accompanied by the formation of mROS, which is rapidly

converted to H_2O_2[40-42]. H_2O_2 can reach the synapse and trigger gephyrin recruitment and network expansion, thereby recruiting additional receptors to further increase neurotransmission. Mitochondria are located in both pre-synaptic and post-synaptic regions, so it is conceivable that mROS can regulate the post-synapse from various angles and in reverse it can impact both sites of the synapse.

Besides mitochondria, there are additional origins of H_2O_2, such as the NADPH-oxidase 2 (NOX2) pathway[43]. NOX2 is highly abundant in cells throughout the CNS[44] and produces superoxide radicals in the extracellular environment, which are subsequently converted to H_2O_2. This H_2O_2 can re-enter the cell through aquaporins. In a recent study, the effects of this pathway on inhibitory neurotransmission were investigated[45]. It was shown that communication of excitatory and inhibitory neurotransmission is mediated by ROS and nitric oxide, leading to the recruitment of $GABA_AR$-containing γ2 and α3 subunits at inhibitory synapses. In contrast to our study, they identified the $GABA_AR$-associated protein(GABARAP) as the primary mediator of receptor recruitment, a protein that has been found to interact with gephyrin[46]. Although, it is unclear, whether different ROS-mediated signaling mechanisms can co-exist, it highlights the importance of these mechanisms in regulating neuronal plasticity.

Another open question concerns the maintenance of oxidation processes in the reductive cytosol. In recent studies, LLPS has gained attention as a new principle of subcellular organization[21,47,48]. For gephyrin it was recently demonstrated that it forms liquid droplets in the presence of a multimeric receptor model[22]. Importantly, our data showed that oxidation of gephyrin strengthened LLPS. Assuming that gephyrin could form liquid droplets at synapses within the cell, these microdomains and their reactive cysteines may be shielded from the reductive cytosol allowing the maintenance of their disulfide bridges. Testing the hypothesis that gephyrin is shielded from the reducing cytosol to maintain its oxidized state is challenging *in cellulo* or *in vivo*. Moreover, it remains unclear whether oxidation leads to phase separation or *vice versa*. We showed that the multimerization of gephyrin can be controlled by oxidation and reduction, indicating a reversible and dynamic mechanism. Thus, it is possible that gephyrin could shuttle between phase-separated microdomains depending on its redox state. Additionally, these oxidizing microdomains are likely not a dead end, as reduction was able to reverse oxidation-mediated clustering of gephyrin *in cellulo*. This reversibility is essential to prevent harmful aggregation and facilitate dynamic plasticity.

More and more studies target a possible relation between redox state of cysteines and the ability to undergo LLPS. One example is synapsin 1, which harbors two cysteines directly affecting LLPS in a redox-dependent manner, which is also relevant in aging[23]. A study, that is mechanistically comparable to our work, was reported for oleosin, where

the disulfide-bridge formation of artificially added cysteine residues on the protein surface triggered LLPS, while reduction was able to reverse this effect[49]. In general, the concept of a reversible formation of phase-separated microdomains holds great potential and may be a key to understand redox-dependent processes in different cellular environments.

Oligomerization as a function of the redox state of cysteines (including S-nitrosylation, persulfidation, sulfenylation and disulfide-formation) has been investigated previously[23,40,50]. Such modifications may lead to functional multimers or harmful aggregates depending on the site and degree of oxidation thus reflecting the dose of ROS[51]. Imbalance in redox signaling is linked to aging and neurodegenerative diseases[52]. Our study identifies gephyrin as mediator between mitochondrial activity and inhibitory synapse formation using ROS as signaling mechanism.

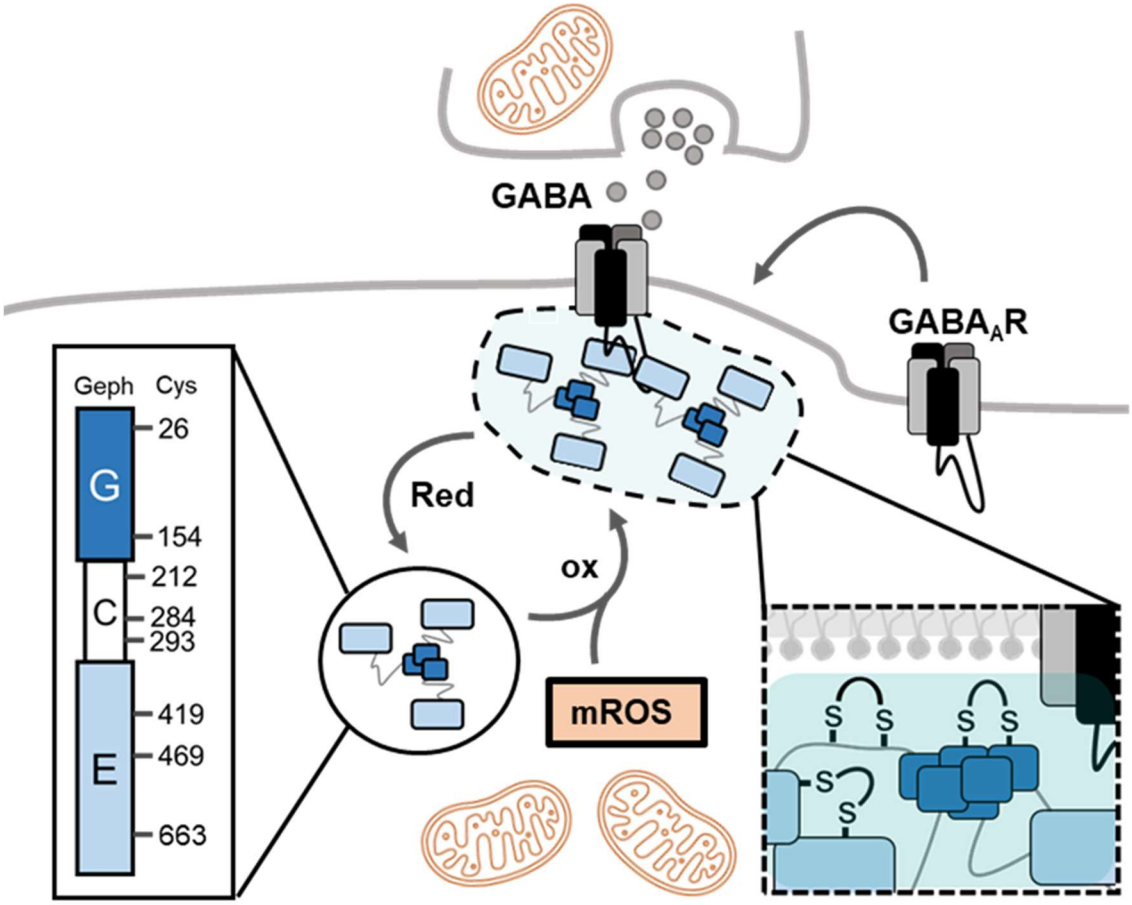

Figure 7: Redox-Regulation of Synaptic Gephyrin Clustering.
Hypothesized model of redox-dependent gephyrin oligomerization at inhibitory GABAergic post-synapses. Gephyrin harbors eight surface-exposed cysteines that are redox-sensitive. mROS-mediated oxidation leads to the formation of disulfide bridges (Enlargement highlighted with box surrounded by dotted lines) linking gephyrin molecules increasing gephyrin oligomerization. This oxidation is reversible by reduction and allows for dynamic shuttling of gephyrin localization. LLPS (highlighted in light-blue) might offer an oxidative microdomain facilitating disulfide bridge formation. Ultimately, gephyrin oligomerization at synapses offers binding sites for $GABA_A$Rs strengthening inhibitory signal transmission.

3.6. Material and methods

DNA/expression constructs

Gephyrin P1 and cysteine variants in pQE80L (Qiagen) were cloned by Gibson assembly using EcoRI into pAAV_hSyn_mScarlet (a gift from Karl Deisseroth, Addgene plasmid #131001) and using EcoRI into pAAV_hSyn_mEGFP (generated from moxBFP, a gift from Erik Snapp, Addgene plasmid #68064; http://n2t.net/addgene:68064; RRID: Addgene_68064). Gephyrin was cloned using PCR and XhoI and KpnI into pEGFP-C2 (Clonetech). The template for the generation of rat Gephyrin P1 constructs was in pQE80L[53]. The cysteine to serine substitutions were generated by site-directed mutagenesis. DAAO was cloned into pAAV_hSyn_mScarlet through PCR and Gibson Assembly using EcoRV and the R285K mutation was introduced by site-directed mutagenesis. The plasmids pAdDeltaF6 (a gift from James M. Wilson, Addgene plasmid #112867; http://n2t.net/addgene:112867; RRID: Addgene_112867) and pAAV2/1 (a gift from James M. Wilson, Addgene plasmid #112862; http://n2t.net/addgene:112862; RRID: Addgene_112862) were used for virus production. The expression constructs of LSβICD in pQE70 and GlyRβICD in ptYB were described previously[24,54].

Recombinant expression and purification of gephyrin

E. coli BL21 Rosetta star was used for the expression of His-gephyrin. Cultures were grown at 37°C at 110 rpm and the expression induced at an OD_{600} of 0.3 with 100 nM IPTG. After expression for 22 h at 18°C and 110 rpm, cells were harvested. To achieve reduced cysteines (free thiols), all solutions were supplemented with reductant until final storage of isolated proteins. The cell pellet was resuspended in lysis buffer (300 mM NaCl, 50 mM Tris/HCl, 5 mM beta-mercaptoethanol, 0.05% Tween20, 1 µg/mL lysozyme, 1x PI (*Roche*), pH 7.4) and stored at -80°C. Pellets were thawed in a water bath and all steps performed at 4°C. Cells were lysed through alternating ultrasound (3 min at 4°C, 30 s pulse, 30 s pulse, 40% amplitude) and pressure lysis (EmulsiFlex, 1 000-1 500 bar, 4°C) twice. The homogenate was centrifuged (45 min, 16 000 rpm, 4°C, JLA 16.250 rotor, Beckman-Coulter Centrifuge Avanti J25-01) and the supernatant subjected to Ni-NTA affinity purification (HIS-Select Nickel Affinity Gel (Sigma Aldrich)). All buffers for washing and elution were similar to the lysis buffer, contained no lysozyme, but contained 20 mM, 40 mM and 300 mM Imidazole, respectively. The eluate was further subjected to preparative size-exclusion chromatography (Superdex 200, 120 mL, *GE Healthcare*) using SEC buffer (300 mM NaCl, 50 mM Tris/HCl, 5 mM beta-mercapto ethanol, 0.05% Tween20, 5% glycerol, pH 7.4). The fractions of the peaks eluting around 60-70 mL (Trimers) and 45-60 mL (higher multimers) were collected and concentrated

by an *Amicon* filter with a Cut-off of 50 kDa. To remove reductants, the concentrated protein was buffer exchanged by gel filtration (PD10 column) to storage buffer (300 mM NaCl, 50 mM Tris/HCl, pH 7.4) and stored at -80°C.

Purification of receptor models LSβICD and βICD peptide from *E. coli*

E. coli BL21 Rosetta star was used for the expression of His-LSβICD. The expression was performed as previously described[24], but instead of preparative size exclusion chromatography, the buffer was exchanged by gel filtration using PD10 columns. The final storage buffer was 300 mM NaCl, 50 mM Tris/HCl, pH 7.4.

For the βICD peptide we used *E. coli* ER2566. Cultures grew at 37°C and 110 rpm until the OD600 reached 0.3. Induction was induced by 250 µM IPTG and expression performed for 20 h at 25°C and 110 rpm. Cells were harvested and stored at -80°C in ICD lysis buffer (300 mM NaCl, 50 mM Tris/HCl, 1 mM EDTA, 1x Protease Inhibitor (*Roche*), pH 7.4). Lysis of the thawed cells was performed by alternation of ultrasound (3 min at 4°C, 30 s pulse, 30 s pulse, 40% amplitude) and pressure lysis (*EmulsiFlex*, 1 000-1 500 bar, 4°C) twice. After centrifugation for 1 h at 16 000 x g (JLA 16.25 rotor) at 4°C, the supernatant was applied on a pre-equilibrated chitin matrix (*New England Biolabs*) and incubated 1.5 h at 4°C under shaking. The column was washed with 15 CV ICD buffer before 2.5 CV cleavage buffer (300 mM NaCl, 50 mM Tris/HCl, 1 mM EDTA, 50 mM DTT, pH 7.5) was applied an incubated for minimum 24 h at rt. The eluate was collected and another 2.5 CV cleavage buffer used for a second elution. The combined eluate was concentrated and filtered by *Amicon* filters with a cut-off of 10 kDa and 3 kDa. The buffer was exchanged to ITC buffer (300 mM NaCl, 50 mM Tris/HCl, pH 7.4) by dialysis over night at 4°C. The purified protein was stored at -80°C.

Redox shift assay

Typically, 10 µg protein were prepared in a total volume of 20 µL RSA buffer (50 mM Tris/HCl, 5 mM EDTA, pH 7.5) or denaturing RSA buffer (50 mM Tris/HCl, 5 mM EDTA, 2% SDS pH 7.5) and supplemented with 1 mM mmPEG5kDa or buffer as minimum controls. After incubation for 1 h in the dark at rt, samples were used for SDS PAGE. The expected shift size per labeled thiol is about 10 kDa. In denaturing conditions, internal cysteines are exposed to PEGylation additionally.

***In vitro* redox-modification**

Purified proteins were oxidized by incubation over night at 4°C with 1 mM Diamide. Reduction was performed with 1 mM TCEP or DTT. In case the reagent would disturb in further assays, the chemical was removed by gel filtration using PD10 columns.

Co-sedimentation assay

Recombinant protein was pre-cleared at 17 000 x g for 3 min at rt. We mixed gephyrin and LSβICD 5:10 µM in a final volume of 50 µL of assay buffer (150 mM NaCl and 25 mM Tris/HCl pH 7.5). After incubation of 10 min at rt, samples were centrifuged 10 min at 4°C and 17 000 x g. The supernatant was added in a new tube, supplemented with 15 µL 5x SDS sample buffer. The pellet was supplemented with 50 µL assay buffer and 15 µL 5x SDS sample buffer. Before performing SDS PAGE and Coomassie staining, samples were incubated 5 min at 95°C.

ITC

Isothermal titration Calorimetry (ITC) experiments were performed by using MicroCal Auto-ITC200 (*Malvern*) at 25 °C in ITC buffer (300 mM NaCl, 50 mM Tris/HCl, pH 7.4). We used an injection volume of 1-2 µL, a spacing of 150 sec between injections and an initial delay of 60 sec. The reference power was 5 µCal/sec and the stirring speed 1 000 rpm. The concentrations of LSβICD and GlyRβICD in the syringe were about 200-215 µM and 300-310 µM, respectively and the concentration of gephyrin in the sample cell was 31–35 µM. Parameters and curves were fitted and calculated by the software MicroCal Analysis and Origin7.

Size exclusion chromatography

Molecular masses of purified gephyrin and variants were detected by analytical size exclusion chromatography (SEC) using a Superose 6 increase 5/10 (*GE Healthcare*). Typically, 4 nmol pre-cleared protein in 50 µL total sample volume were applied. Proteins were separated at 4°C and a flow rate of 0.1 mL/min in SEC buffer (50 mM Tris/HCl, 300 mM NaCl pH 7.4). If desired, fractions of 100 µL were collected and those of corresponding peaks combined and concentrated using *Amicon* filters with a 50 kDa cut-off. The combined protein was then further subjected to redox-modifications, cleared by centrifugation and re-applied on the column.

Calpain cleavage assay

A mastermix of 50 µL contained 850 pmol redox-modified protein, 10 mM $Ca^{2+}Cl_2$, 1/2 U/mL calpain. The volume was adjusted using calpain buffer (300 mM NaCl, 50 mM Tris/HCl, pH 7.4). As a control, a calcium-free control was included because calpain is a calcium-dependent protease. At timepoints of 0, 5, 15, 30 min and overnight, 15 µL samples were taken out and the digestion stopped by addition of SDS sample buffer and incubation for 5 min at 96°C. Cleavage products were afterwards analyzed by SDS-PAGE.

Circular dichroism spectroscopy

Determination of the secondary structure was performed by circular dichroism spectroscopy (CD spec). Typically, 0.3 mg/mL pre-cleared protein in CD buffer (10 mM K_2HPO_4/KH_2PO_4, pH 7.5) was used and Far-UV spectra recorded with J-715 CD spectropolarimeter (*Jasco*) at 20°C in the range of 180-250 nm using quartz cuvette with 0.1 cm path length. The spectra were processed by the software Spectra Analysis version 1.53.07 of Spectra Manage version 1.54.0. We subtracted the buffer baseline and smoothed three-times by the Savitzky-Golay algorithm with a convolution width of 21.

Virus preparation

Recombinant virus particles (AAV2/1) were produced in HEK293 cells and isolated by PEG/NaCl precipitation followed by chloroform extraction according to the previously established protocol[55]. The titers were determined by a Gel green® (*Biotium*) protocol[56] and the fluorescence was detected (507 ± 5 nm excitation and 528 ± 5 nm emission) using a plate reader equipped with monochromators (Tecan Spark).

Culture of hippocampal neurons and expression of recombinant gephyrin

At E17.5, dissociated primary hippocampal cultures were prepared from C57BL/6NRj embryos. 90 000 cells were seeded on Poly-L-lysine coated 13-mm cover slips in 24-well plates. Neurons grew in neurobasal medium supplemented with B-27, N-2, and L-glutamine (*Thermo Fisher Scientific*). At 8 days *in vitro* (DIV), cells were transfected with 0.4 µg plasmid DNA per construct using lipofectamine 2000 (Life Technologies) according to the manufacturer's manual. Expression was performed for 5 days. Alternatively, at DIV10, cells were transduced with 2.5 x 10^8 viral genome copies (GC). The virus particles were directly added to each individual well. At DIV14 the cells were either fixed or subjected to treatment. Antimycin A treatments were performed over night at 37°C. Antimycin A (f.c. 1 µM) was directly added to each well, which contained 400 µL medium. D-Methionine (D-Met) treatment was performed 1 h at 37°C. The medium of neurons was removed and replaced by minimal NB medium, supplemented with 5 mM D-Met. Mock samples were treated with the same volume of solvent solution (PBS). After treatments neurons were fixed and used for ICC.

Immunocytochemistry (ICC)

Fixation was performed by replacing culture medium by 4% PFA in PBS. After incubation for 20 min at room temperature (rt), PFA was removed and cells washed twice with 50 mM NH_4Cl in PBS, each time 10 min at rt. Subsequently, cells were blocked for 1 h

at rt with blocking solution (10% goat serum, 1% BSA, 0.2% TritonX100, in PBS). After washing cells with PBS for 5 min at rt, antibody incubation was performed for 1 h at rt. Antibodies were diluted in PBS. Afterwards, three washing steps with PBS were performed, each 10 min at rt. Lastly, coverslips were mounted with Mowiol/Dabco and dried over night at rt. We used the following antibodies: anti-vesicular GABA transporter (vGAT) (1:1 000, #131003, *SYSY*); anti-$GABA_AR\gamma2$ (1:500, #224004, *SYSY*); anti-GephyrinE (3B11; 1:10, self-made); goat anti-mouse AlexaFluor 488 (1:500, #A-11029, *Invitrogen*), goat anti-rabbit AlexaFluor 647 (1:500, #A-21245, *Invitrogen*), goat anti-rabbit AlexaFluor 488 (1:500, #A-11075, *Invitrogen*).

Confocal microscopy and image analysis

Pictures were tacking using the *Leica* TCS SP8 LIGHNING upright confocal microscope with an HC PL APO CS2 63x/1.30 glycerol objective. The microscope was equipped with hybrid *Leica* HyD detectors and diode lasers with 405, 488, 522 and 638 nm. The LIGHTNING adaptive deconvolution of the mounting medium “Mowiol” was used, which is capable of theoretical resolutions down to 120 nm and 200 nm lateral and axial, respectively. Images were acquired with stacks of 3 µm z-step size, 2048 x 2048 (144.77 x 144.77 µm) and segmented and analyzed in an automated fashion using ImageJ/FIJI 1.53t. Therefore, the previously described macros[57] were used as a blueprint and adapted.

Perfusion of mice and sample preparation

Mice were anesthetized with Ketamine/Xylazine through intra-peritoneal injection. After surgical tolerance was achieved, the abdomen was opened and liver and heart uncovered. A canula was pricked into the bottom of the left heart chamber to inject PBS containing 50 mM NEM into the cardiovascular system. A drain was given by a cut above the liver. PBS was injected until the liver lost the red color and turned pale. After decapitation, liver, brain and spinal cord were removed and added to RIPA buffer (50 mM Tris/HCl pH 8.0, 150 mM NaCl, 0.1% SDS, 1% IGEPAL CA-630, 0.5% Na deoxycholate, 1 mM EDTA, freshly added protease inhibitor (*Roche*)) containing 50 mM NEM. The tissue was dounce homogenized with 1 200 rpm 20 times, sonicated 10 s at 4°C and 30% amplitude and subsequently centrifuged for 10 min at 4°C and 4 000 x g. The supernatant was transferred into a new tube and incubated for 1 h to let free thiols react with NEM. Afterwards, protein concentration was determined using BCA. Typically, 45 µg protein were used for SDS-PAGE for WB analysis.

SDS-PAGE, Coomassie and Western Blot

Samples were supplemented with 1x sample buffer (5x: 250 mM Tris/HCl pH 6.8, 30% glycerol, 0.1% Bromophenol blue, 10% SDS) and incubated for 5 min at 95-98°C. We used either 5 mM β-ME for recombinant protein samples or 5 mM DTT for tissue samples or omitted it. Separation was performed with 5-12% SDS acrylamide gels using running buffer (3.029 g/L Tris, 14.4 g/L glycine, 0.1% SDS). Afterwards gels were either stained with Coomassie (30% EtOH, 10% acetic acid, 0.25% Coomassie brilliant blue R250) or used for western blot. Therefore, the transfer was performed semi-dry using PVDF membranes and transfer buffer (3 g/L Tris, 24.15 g/L glycine pH 8.8, 10% MeOH). Blocking was performed for 1 h at rt under shaking in blocking solution (10% BSA in TBST). Primary and secondary antibodies (diluted in 1% BSA in TBST) were applied for 1 h at rt under shaking, with a wash step of 3 x 5 min with TBST (6.5 g/L Tris, 8.75 g/L NaCl pH 7.4, 0.05% Tween20) between primary and secondary antibody. After additional washing 3 x 5 min with TBST, detection was performed using ECL and the ChemiDocTM Imaging System (*BioRad*). The following antibodies were used: anti-GephyrinE (3B11; 1:10, self-made); anti-GAPDH (1:1 000, G9545, *Sigma*), anti-mouse HRP-coupled (1:10 000, AP181P, *Sigma*), anti-rabbit HRP-coupled (1:10 000, AP187P, *Sigma*)

Statistics

The visualization and statistical analysis were performed with GraphPad Prism6 and R vers. 4.2.1. Standard deviation, individual data points and used tests are shown in the individual graph and in the captions respectively. Data points were identified as outliers when a two-fold standard deviation was exceeded. If data was normalized, *student's* t-test was performed, and the significance level alpha corrected by the number of tests. Otherwise, we performed 1-way ANOVA and *Bonferroni* post-hoc tests. We analyzed: N = 6 individual mice for redox-dependent multimers; N = 3 technical replicates in the Moco activity assay, and N = 3 biological replicates; N = 3 biological replicates in SEC experiments; N = 3 biological replicates of gephyrin in ITC experiments; N = 3 biological replicates of gephyrin in co-sedimentation assays, N = 3 biological replicates of gephyrin in calpain cleavage assays; N = 10 cells per condition from 3 individual embryos of one neuron preparation in all experiments using hippocampal neurons.

Acknowledgements

Technical help from Julia Reich is greatly appreciated. Furthermore, we thank Franziska Neuser and the Center for Mouse Genetics (CMG) of the University of Cologne for the organization of mice experiments. This work was financed by the german research foundation (DFG) (RTG2550 reloc to JR).

Conflict of interest

The authors declare no conflict of interest

Study approval

We complied with all ethical regulations for animal testing and research. Experiments were approved by the local research ethics committee (German, Landesamt für Natur, Umwelt und Verbraucherschutz (LANUV) Nordrhein-Westfalen, reference 2016.A466).

3.7. References

1 Halliwell, B. Reactive Oxygen Species and the Central Nervous System. *Journal of Neurochemistry*, 1609-1623 (1992).

2 Mecocci, P. *et al.* Oxidative damage to mitochondrial DNA shows marked age-dependent increases in human brain. *Annals of Neurology*, 609-616 (1993).

3 Accardi, M. *et al.* Mitochondrial reactive oxygen species regulate the strength of inhibitory GABA-mediated synaptic transmission. *Nature Communications*, 3168 (2014).

4 Esposito, L. *et al.* Reduction in mitochondrial superoxide dismutase modulates Alzheimer's disease-like pathology and accelerates the onset of behavioral changes in human amyloid precursor protein transgenic mice. *Journal of Neuroscience*, 5167-5179 (2006).

5 Gutteridge, J. Free radicals in disease processes: a compilation of cause and consequence. *Free Radical Research Communication*, 141-158 (1993).

6 Feng, G. *et al.* Dual requirement for gephyrin in glycine receptor clustering and molybdoenzyme activity. *Science* **282**, 1321-1324 (1998). https://doi.org:10.1126/science.282.5392.1321

7 Alldred, M. J., Mulder-Rosi, J., Lingenfelter, S. E., Chen, G. & Luscher, B. Distinct gamma2 subunit domains mediate clustering and synaptic function of postsynaptic GABAA receptors and gephyrin. *J Neurosci* **25**, 594-603 (2005). https://doi.org:10.1523/JNEUROSCI.4011-04.2005

8 Bedet, C. *et al.* Regulation of gephyrin assembly and glycine receptor synaptic stability. *J Biol Chem* **281**, 30046-30056 (2006). https://doi.org:10.1074/jbc.M602155200

9 Saiyed, T. *et al.* Molecular basis of gephyrin clustering at inhibitory synapses: role of G- and E-domain interactions. *J Biol Chem* **282**, 5625-5632 (2007). https://doi.org:10.1074/jbc.M610290200

10 Fritschy, J. M., Harvey, R. J. & Schwarz, G. Gephyrin: where do we stand, where do we go? *Trends Neurosci* **31**, 257-264 (2008). https://doi.org:10.1016/j.tins.2008.02.006

11 Grunewald, N. *et al.* Sequences Flanking the Gephyrin-Binding Site of GlyRbeta Tune Receptor Stabilization at Synapses. *eNeuro* **5** (2018). https://doi.org:10.1523/ENEURO.0042-17.2018

12 Tyagarajan, S. K. *et al.* Regulation of GABAergic synapse formation and plasticity by GSK3β-dependent phosphorylation of gephyrin. *P Natl Acad Sci USA* **108**, 379-384 (2011). https://doi.org:10.1073/pnas.1011824108

13 Kawasaki, B. T., Hoffman, K. B., Yamamoto, R. S. & Bahr, B. A. Variants of the receptor/channel clustering molecule gephyrin in brain: distinct distribution patterns, developmental profiles, and proteolytic cleavage by calpain. *J Neurosci Res* **49**, 381-388 (1997). https://doi.org:10.1002/(sici)1097-4547(19970801)49:3<381::aid-jnr13>3.0.co;2-2

14 Tyagarajan, S. K. & Fritschy, J. M. Gephyrin: a master regulator of neuronal function? *Nat Rev Neurosci* **15**, 141-156 (2014). https://doi.org:10.1038/nrn3670

15 Dejanovic, B. *et al.* Simultaneous impairment of neuronal and metabolic function of mutated gephyrin in a patient with epileptic encephalopathy. *EMBO Mol Med* **7**, 1580-1594 (2015). https://doi.org:10.15252/emmm.201505323

16 Reiss, J. *et al.* A mutation in the gene for the neurotransmitter receptor-clustering protein gephyrin causes a novel form of molybdenum cofactor deficiency. *Am J Hum Genet* **68**, 208-213 (2001). https://doi.org:10.1086/316941

17 Lionel, A. C. *et al.* Rare exonic deletions implicate the synaptic organizer Gephyrin (GPHN) in risk for autism, schizophrenia and seizures. *Hum Mol Genet* **22**, 2055-2066 (2013). https://doi.org:10.1093/hmg/ddt056

18 Dejanovic, B. & Schwarz, G. Neuronal nitric oxide synthase-dependent S-nitrosylation of gephyrin regulates gephyrin clustering at GABAergic synapses. *J Neurosci* **34**, 7763-7768 (2014). https://doi.org:10.1523/JNEUROSCI.0531-14.2014

19 Dejanovic, B. *et al.* Palmitoylation of gephyrin controls receptor clustering and plasticity of GABAergic synapses. *PLoS Biol* **12**, e1001908 (2014). https://doi.org:10.1371/journal.pbio.1001908

20 Marino, S. M. & Gladyshev, V. N. Cysteine function governs its conservation and degeneration and restricts its utilization on protein surfaces. *J Mol Biol* **404**, 902-916 (2010). https://doi.org:10.1016/j.jmb.2010.09.027

21 Mehta, N., Mondal, S., Watson, E. T., Cui, Q. & Chapman, E. R. The juxtamembrane linker of synaptotagmin 1 regulates Ca(2+) binding via liquid-liquid phase separation. *Nat Commun* **15**, 262 (2024). https://doi.org:10.1038/s41467-023-44414-5

22 Bai, G., Wang, Y. & Zhang, M. Gephyrin-mediated formation of inhibitory postsynaptic density sheet via phase separation. *Cell Res* **31**, 312-325 (2021). https://doi.org:10.1038/s41422-020-00433-1

23 Thibaut Vignane, M. H., Christian Hoffmann, Antionia Katsouda, Jovan Petric, Han Wang, Marko Miler, Ferran Comas, Dunja Petrovic, Suyuan Chen, Jan Lj. Miljkovic, Jordan L Morris, Suvagata Roy Chowdhury, Julien Prudent, Natalija Polovic, Michael P. Murphy, Andreas Papapetropoulos, Dragomir Milovanovic, Milos R. Filipovic. Protein thiol alterations drive aberrant phase separation in aging. *bioRxiv* (2023). https://doi.org:https://doi.org/10.1101/2023.11.07.566021

24 Macha, A. *et al.* Pentameric assembly of glycine receptor intracellular domains provides insights into gephyrin clustering. *bioRxiv* (2022). https://doi.org:https://doi.org/10.1101/2022.11.10.512828

25 Kim, E. Y. *et al.* Deciphering the structural framework of glycine receptor anchoring by gephyrin. *EMBO J* **25**, 1385-1395 (2006). https://doi.org:10.1038/sj.emboj.7601029

26 Accardi, M. V. *et al.* Mitochondrial reactive oxygen species regulate the strength of inhibitory GABA-mediated synaptic transmission. *Nat Commun* **5**, 3168 (2014). https://doi.org:10.1038/ncomms4168

27 Calamai, M. *et al.* Gephyrin oligomerization controls GlyR mobility and synaptic clustering. *J Neurosci* **29**, 7639-7648 (2009). https://doi.org:10.1523/JNEUROSCI.5711-08.2009

28 Sola, M., Kneussel, M., Heck, I. S., Betz, H. & Weissenhorn, W. X-ray crystal structure of the trimeric N-terminal domain of gephyrin. *J Biol Chem* **276**, 25294-25301 (2001). https://doi.org:10.1074/jbc.M101923200

29 Molla, G. *et al.* Role of arginine 285 in the active site of Rhodotorula gracilis D-amino acid oxidase. A site-directed mutagenesis study. *J Biol Chem* **275**, 24715-24721 (2000). https://doi.org:10.1074/jbc.M908193199

30 Harris, J. J., Jolivet, R. & Attwell, D. Synaptic energy use and supply. *Neuron* **75**, 762-777 (2012). https://doi.org:10.1016/j.neuron.2012.08.019

31 Ly, C. V. & Verstreken, P. Mitochondria at the synapse. *Neuroscientist* **12**, 291-299 (2006). https://doi.org:10.1177/1073858406287661

32 Pauwels, P. J., Opperdoes, F. R. & Trouet, A. Effects of antimycin, glucose deprivation, and serum on cultures of neurons, astrocytes, and neuroblastoma cells. *J Neurochem* **44**, 143-148 (1985). https://doi.org:10.1111/j.1471-4159.1985.tb07123.x

33 Messner, K. R. & Imlay, J. A. Mechanism of superoxide and hydrogen peroxide formation

by fumarate reductase, succinate dehydrogenase, and aspartate oxidase. *J Biol Chem* **277**, 42563-42571 (2002). https://doi.org:10.1074/jbc.M204958200

34 Pham, N. A., Robinson, B. H. & Hedley, D. W. Simultaneous detection of mitochondrial respiratory chain activity and reactive oxygen in digitonin-permeabilized cells using flow cytometry. *Cytometry* **41**, 245-251 (2000). https://doi.org:10.1002/1097-0320(20001201)41:4<245::aid-cyto2>3.0.co;2-#

35 Bernardi, P., Veronese, P. & Petronilli, V. Modulation of the mitochondrial cyclosporin A-sensitive permeability transition pore. I. Evidence for two separate Me2+ binding sites with opposing effects on the pore open probability. *J Biol Chem* **268**, 1005-1010 (1993).

36 Kim, S. *et al.* Impaired formation of high-order gephyrin oligomers underlies gephyrin dysfunction-associated pathologies. *iScience* **24**, 102037 (2021). https://doi.org:10.1016/j.isci.2021.102037

37 Kumar, A. *et al.* S-sulfocysteine/NMDA receptor-dependent signaling underlies neurodegeneration in molybdenum cofactor deficiency. *J Clin Invest* **127**, 4365-4378 (2017). https://doi.org:10.1172/JCI89885

38 Hsueh, Y. P., Kim, E. & Sheng, M. Disulfide-linked head-to-head multimerization in the mechanism of ion channel clustering by PSD-95. *Neuron* **18**, 803-814 (1997). https://doi.org:10.1016/s0896-6273(00)80319-0

39 Lee, D. S. & Kim, J. E. PDI-Mediated Reduction of Disulfide Bond on PSD95 Increases Spontaneous Seizure Activity by Regulating NR2A-PSD95 Interaction in Epileptic Rats Independent of S-Nitrosylation. *Int J Mol Sci* **21** (2020). https://doi.org:10.3390/ijms21062094

40 Halliwell, B. Reactive oxygen species and the central nervous system. *J Neurochem* **59**, 1609-1623 (1992). https://doi.org:10.1111/j.1471-4159.1992.tb10990.x

41 Lopez-Mirabal, H. R. & Winther, J. R. Redox characteristics of the eukaryotic cytosol. *Biochim Biophys Acta* **1783**, 629-640 (2008). https://doi.org:10.1016/j.bbamcr.2007.10.013

42 Fridovich, I. Fundamental aspects of reactive oxygen species, or what's the matter with oxygen? *Ann N Y Acad Sci* **893**, 13-18 (1999). https://doi.org:10.1111/j.1749-6632.1999.tb07814.x

43 Olguin-Albuerne, M. & Moran, J. ROS produced by NOX2 control in vitro development of cerebellar granule neurons development. *ASN Neuro* **7** (2015). https://doi.org:10.1177/1759091415578712

44 Fan, L. M. *et al.* Nox2 contributes to age-related oxidative damage to neurons and the cerebral vasculature. *J Clin Invest* **129**, 3374-3386 (2019). https://doi.org:10.1172/JCI125173

45 Larson, E. A. *et al.* Nitric Oxide Signaling Strengthens Inhibitory Synapses of Cerebellar Molecular Layer Interneurons through a GABARAP-Dependent Mechanism. *J Neurosci* **40**, 3348-3359 (2020). https://doi.org:10.1523/JNEUROSCI.2211-19.2020

46 Kneussel, M. *et al.* The gamma-aminobutyric acid type A receptor (GABAAR)-associated protein GABARAP interacts with gephyrin but is not involved in receptor anchoring at the synapse. *Proc Natl Acad Sci U S A* **97**, 8594-8599 (2000). https://doi.org:10.1073/pnas.97.15.8594

47 Wang, B. *et al.* Liquid-liquid phase separation in human health and diseases. *Signal Transduct Target Ther* **6**, 290 (2021). https://doi.org:10.1038/s41392-021-00678-1

48 Zhang, Q. *et al.* Phase separation of BuGZ regulates gut regeneration and aging through interaction with m(6)A regulators. *Nat Commun* **14**, 6700 (2023). https://doi.org:10.1038/s41467-023-42474-1

49 Reed, E. H. & Hammer, D. A. Redox sensitive protein droplets from recombinant oleosin. *Soft Matter* **14**, 6506-6513 (2018). https://doi.org:10.1039/c8sm01047a

50 Ho, G. P. *et al.* S-nitrosylation and S-palmitoylation reciprocally regulate synaptic targeting of PSD-95. *Neuron* **71**, 131-141 (2011). https://doi.org:10.1016/j.neuron.2011.05.033

51 Gutteridge, J. M. Free radicals in disease processes: a compilation of cause and consequence. *Free Radic Res Commun* **19**, 141-158 (1993). https://doi.org:10.3109/10715769309111598

52 Esposito, L. *et al.* Reduction in mitochondrial superoxide dismutase modulates Alzheimer's disease-like pathology and accelerates the onset of behavioral changes in human amyloid precursor protein transgenic mice. *J Neurosci* **26**, 5167-5179 (2006). https://doi.org:10.1523/JNEUROSCI.0482-06.2006

53 Belaidi, A. A. & Schwarz, G. Metal insertion into the molybdenum cofactor: product-

substrate channelling demonstrates the functional origin of domain fusion in gephyrin. *Biochem J* **450**, 149-157 (2013). https://doi.org:10.1042/BJ20121078

54 Schrader, N. *et al.* Biochemical characterization of the high affinity binding between the glycine receptor and gephyrin. *J Biol Chem* **279**, 18733-18741 (2004). https://doi.org:10.1074/jbc.M311245200

55 Kimura, T. *et al.* Production of adeno-associated virus vectors for in vitro and in vivo applications. *Sci Rep* **9**, 13601 (2019). https://doi.org:10.1038/s41598-019-49624-w

56 Xu, J., DeVries, S. H. & Zhu, Y. Quantification of Adeno-Associated Virus with Safe Nucleic Acid Dyes. *Hum Gene Ther* **31**, 1086-1099 (2020). https://doi.org:10.1089/hum.2020.063

57 Liebsch, F., Eggersmann, F. R., Merkler, Y., Kloppenburg, P. & Schwarz, G. Automated Image Analysis Reveals Different Localization of Synaptic Gephyrin C4 Splice Variants. *eNeuro* **10** (2023). https://doi.org:10.1523/ENEURO.0102-22.2022

3.8. Supplementary figures

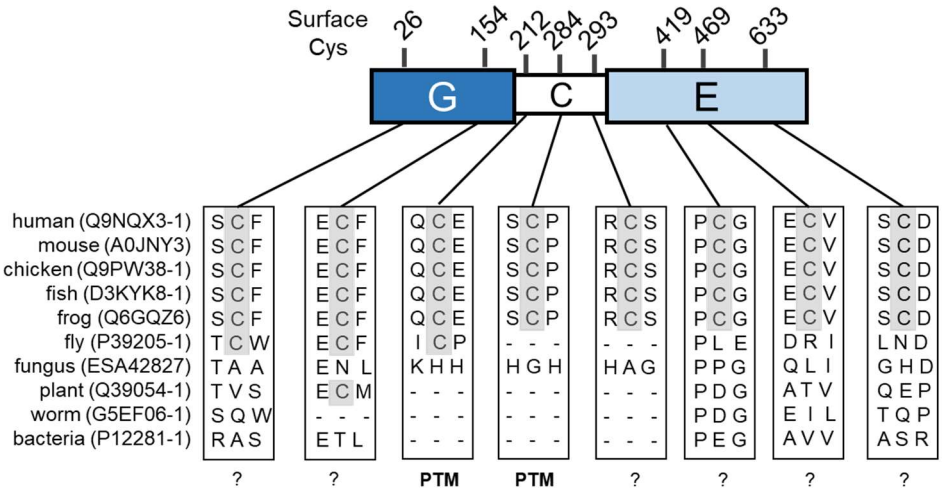

Figure S1: Alignment of Gephyrin and Homologues.
Alignment of protein sequence of different species. Areas around the chosen cysteines of gephyrin depicted with boxes. Cys 212 and 284 have assigned functions (targets of S-palmitoylation), while the function of the others is unknown (?).

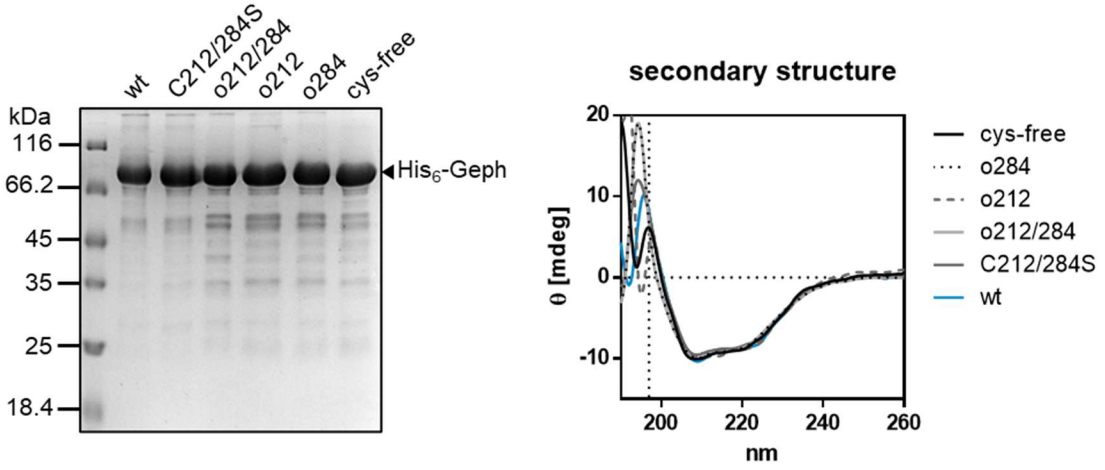

Figure S2: His_6-Gephyrin derived from *E. coli*.
His_6-Gephyrin variants recombinantly expressed and purified from *E. coli*. A) Coomassie gel of purified proteins. B) Analysis of secondary structure by CD Spec. Vertical, dotted line indicates data points with HT values above 800 mV (machine threshold).

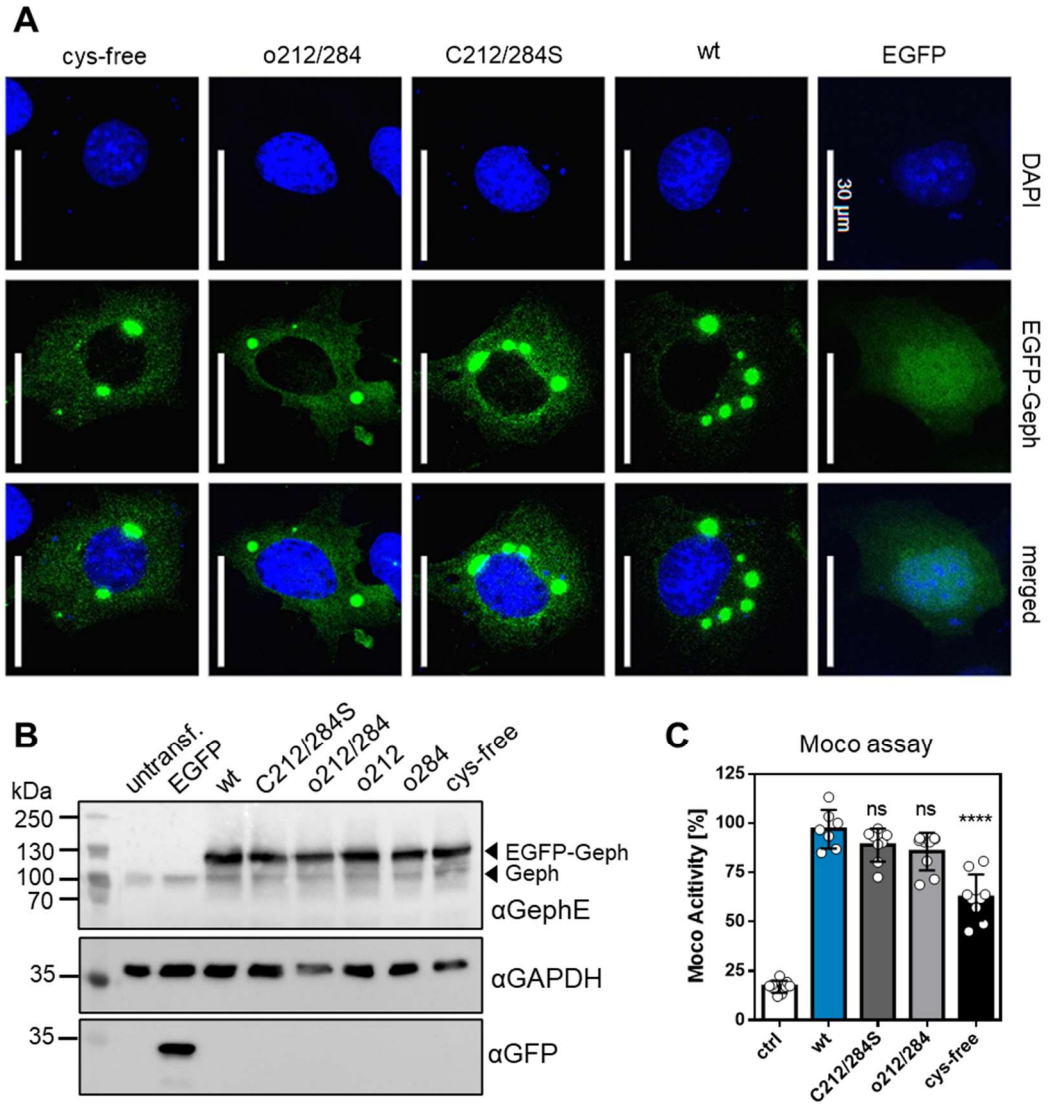

Figure S3: Expression of EGFP-Geph in COS7 and HEK293 Cells.
EGFP-Gephyrin variants were recombinantly expressed in COS7 and HEK293 cells for 48 h. A) Images of COS7 cells. Blue: DAPI, green: EGFP-Geph, scale bar of 30 µm. B) Expression in HEK293 cells. Protein amounts analyzed by Western blot. EGFP-Geph and endogenous gephyrin marked with arrows. C) Moco assay with cysteine variants. Moco activity normalized to wt. Significance towards wt tested by student's t-test, alpha level corrected by three. C212/284S: p=0.3288 (ns); o212/284: p=0.1026 (ns); cys-free: p<0.0001 (****).

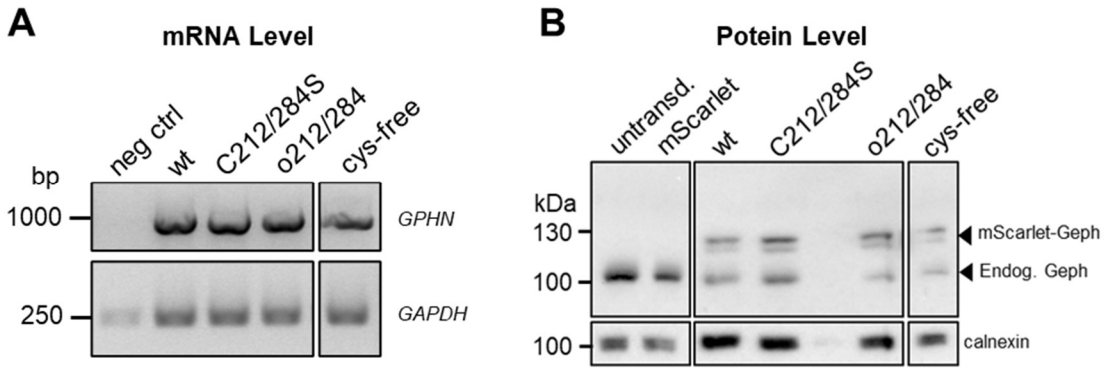

Figure S4: Expression of recombinant Gephyrin in Hippocampal Neurons.
Expression of mScarlet-gephyrin via transduction in primary hippocampal neurons. A) mRNA level determination. Isolated mRNA of mSclt-Geph was used for PCR. Primers were designed to exclusively bind to recombinant gephyrin. GAPDH used as a ctrl. B) Western Blot of neuronal lysates. Endogenous and recombinant gephyrin species indicated by arrows.

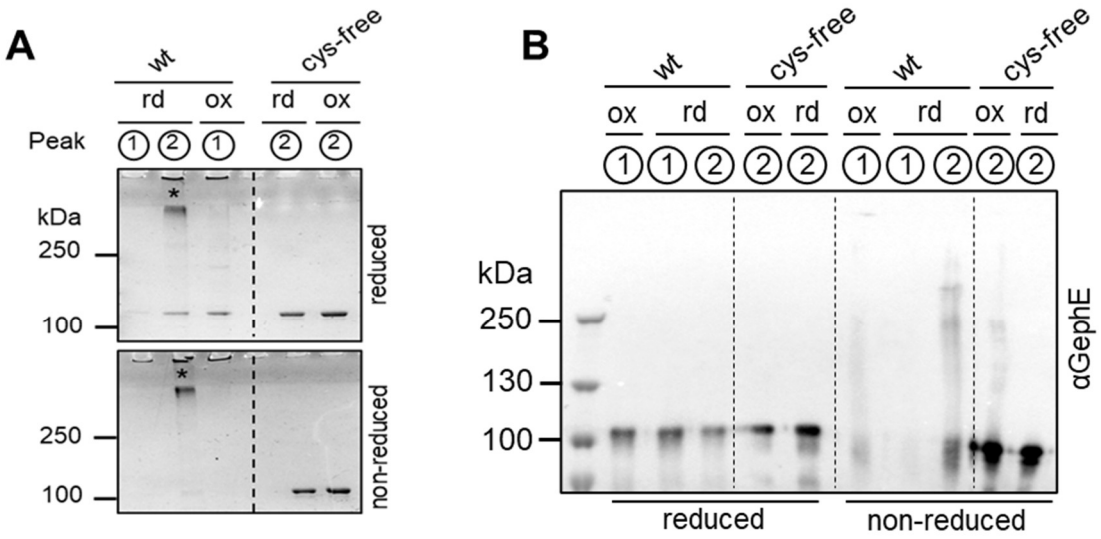

C

Variant	N^{high}	±	K_D^{high} [µM]	±	H^{high} [kcal/mol]	±	S^{high} [cal/mol/deg]
wt_1	0.302	0.006	0.0123	0.0029	-28.47	0.00	-55.60
cysfree_1	0.438	0.016	0.0763	0.0238	-31.53	0.72	-69.10
wt_2	0.360	0.005	0.0249	0.0074	-31.01	0.54	-65.20
cysfree_2	0.443	0.011	0.0391	0.0203	-29.34	0.74	-60.70
wt_3	0.349	0.006	0.0870	0.0191	-63.31	1.58	-172.00
cysfree_3	0.342	0.006	0.0735	0.0017	-65.20	1.64	-178.00

Variant	N^{low}	±	K_D^{low}[µM]	±	H^{low} [cal/mol]	±	S^{low} [cal/mol/deg]
wt_1	0.492	0.012	0.877	0.1808	-11.82	0.65	-10.40
cysfree_1	0.516	0.036	1.366	0.3919	-8.10	2.01	0.71
wt_2	0.920	0.027	0.787	0.2530	-5.40	0.43	10.50
cysfree_2	0.880	0.049	0.971	0.5316	-4.76	0.83	12.20
wt_3	0.952	0.031	1.412	0.3471	-10.93	1.13	-8.48
cysfree_3	0.964	0.030	1.259	0.3283	-10.69	-0.01	-7.49

D

Variant	N^{high}	±	K_A^{high} [M^{-1}]	±	H^{high} [kcal/mol]	±	S^{high} [cal/mol/deg]
wt_rd_1	0.716	0.007	0.226	0.030	-12.01	0.19	-11.20
wt_ox_1	0.728	0.006	0.281	0.053	-11.05	0.16	-7.56
cys-free_rd_1	0.739	0.001	0.203	0.035	-10.94	0.23	-7.84
cys-free_ox_1	0.750	0.005	0.429	0.056	-10.06	0.13	-3.40
wt_rd_2	0.687	0.007	0.467	0.059	-12.44	0.19	-12.80
wt_ox_2	0.729	0.005	0.408	0.043	-11.02	0.13	-7.72
cys-free_rd_2	0.778	0.005	0.714	0.059	-12.74	0.13	-14.60
cys-free_ox_2	0.750	0.004	0.261	0.022	-9.88	0.08	-3.02
wt_rd_3	0.712	0.006	0.267	0.038	-8.41	0.12	1.86
wt_ox_3	0.798	0.006	0.195	0.028	-8.06	0.11	3.68
cys-free_rd_3	0.809	0.006	0.201	0.029	-7.61	0.09	5.13
cys-free_ox_3	0.769	0.012	0.183	0.019	-8.39	0.24	1.10

Figure S5: Analysis of SEC fractions and ITC Data

A and B: Fractions taken of Peak 1 (high-order multimers) and Peak 2 (hexamers) of the respective runs using reduced (rd) or oxidized gephyrin wt or cys-free variant. The samples have been prepared for SDS-PAGE with a reducing or a non-reducing buffer. A) Coomassie Gel. Unspecific band marked with a star (*). B) Western blot using antibody against Gephyrin E-domain. C and D: Interaction parameters of gephyrin wt or cys-free variant towards different ligands determined by mathematical fitting of ITC runs. A) ITC experiment titrating GlyRβICD peptide into gephyrin under reductive conditions. Data of two-site fit. B) ITC experiment titrating LSβICD into pre-reduced or -oxidized gephyrin. Data of one-site fit.

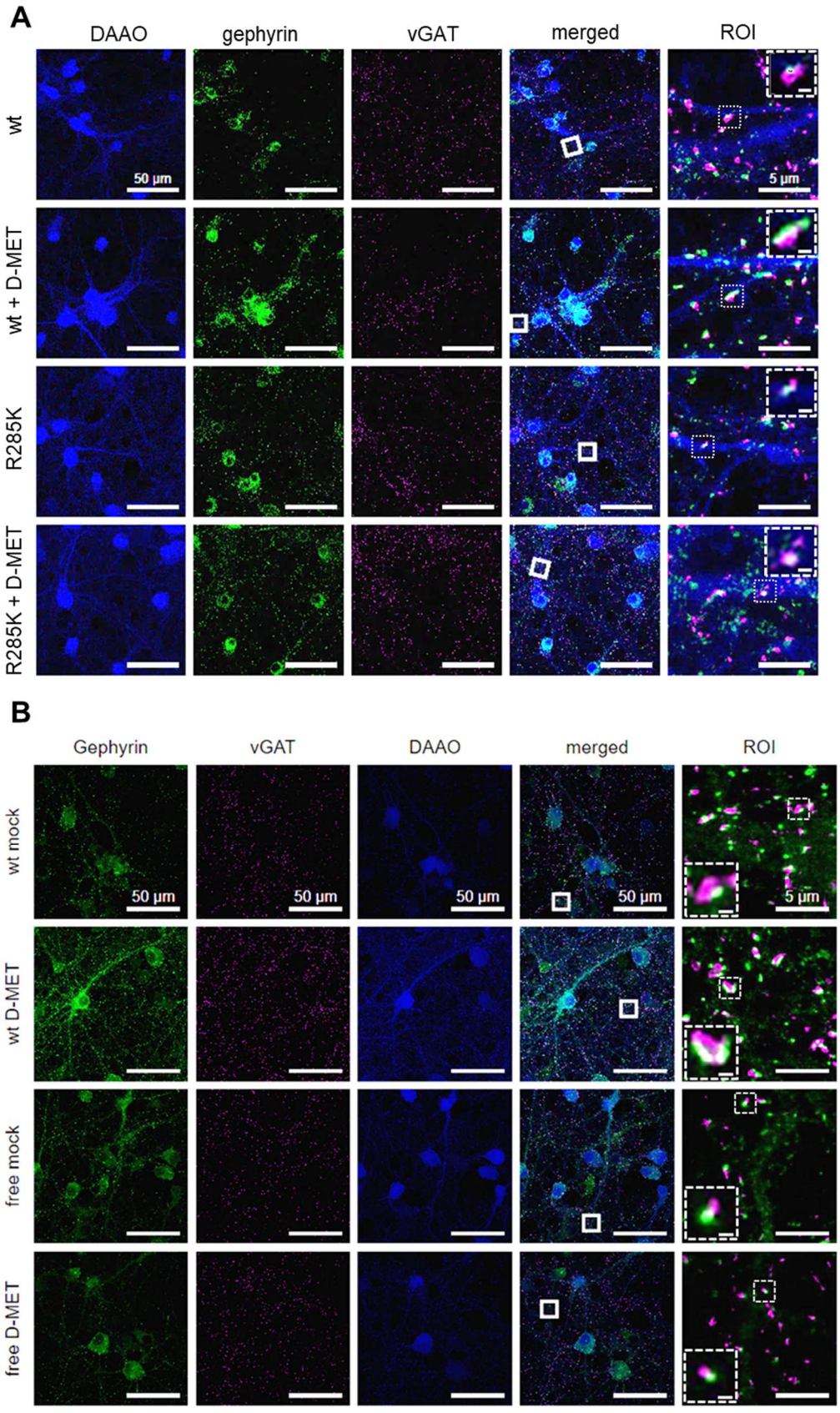

Figure S6:H_2O_2 drives Gephyrin Oligomerization at Synapses.
Expression of cytosolic mSclt-DAAO and mEGFP-Geph in primary, hippocampal neurons. Treatment at DIV14 with 5 mM D-MET. Analysis of cluster sizes [μm^2], intensity [au] and co-localization with vGAT (=synaptic clusters) of gephyrin. A) mSclt-DAAO wt and R285K. Analysis of endogenous gephyrin clusters. Gephyrin: green, vGAT: magenta, DAAO: blue; scale bar 30 and 0.5 µm. B) mSclt-DAAO wt and mEGFP-Geph wt and cys-free variants. Analysis of recombinant mEGFP-gephyrin clusters. Gephyrin: green, vGAT: magenta; scale bar 30 and 0.5 µm.

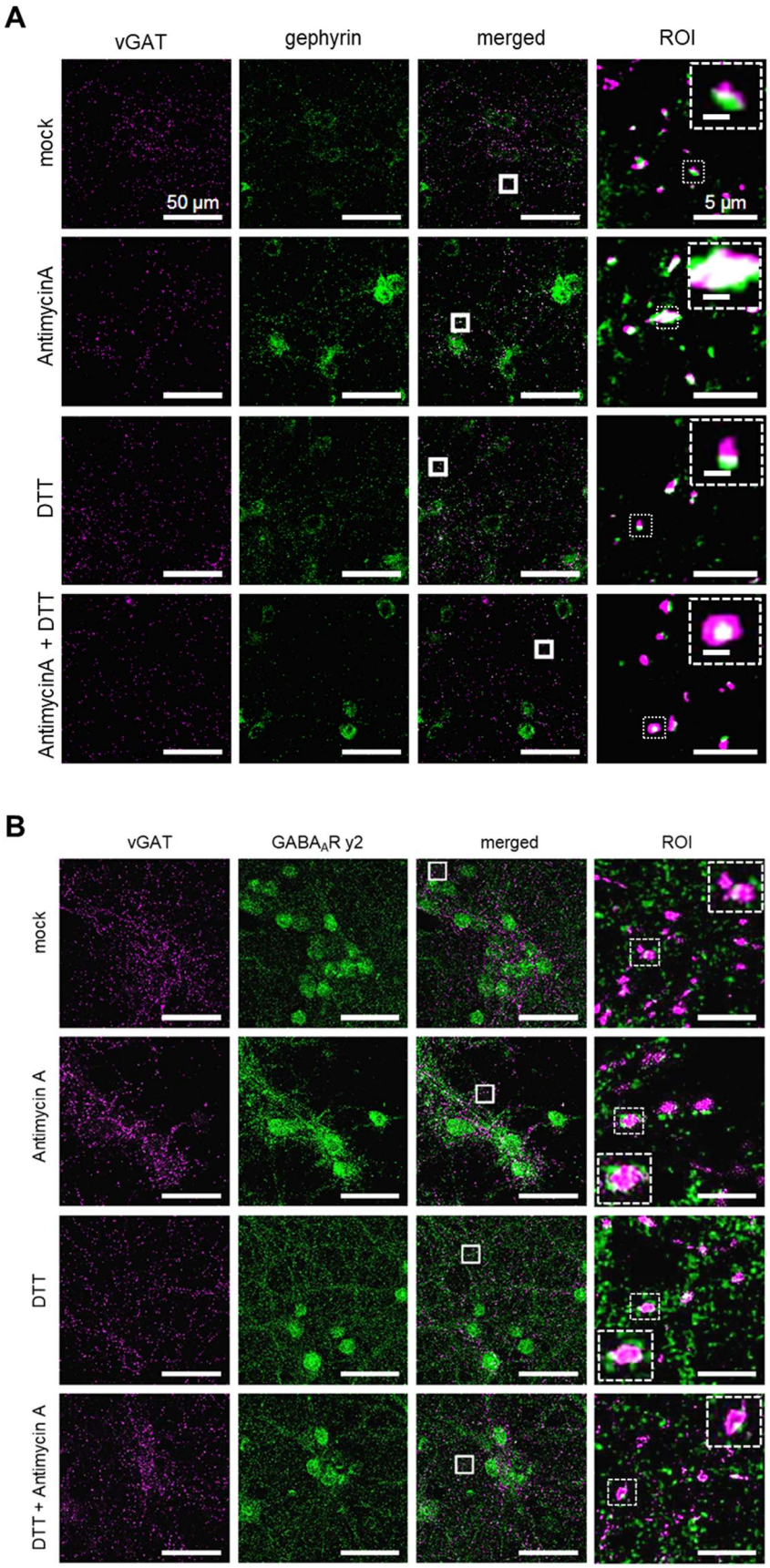

Figure S7: mROS reversibly drive Gephyrin Oligomerization and the Recruitment of $GABA_AR$ γ2 Subunits
Treatment of primary hippocampal neurons at DIV14 with 1 µM Antimycin A (AntiA) and/or 5 µM DTT. Analysis of gephyrin or $GABA_AR$ γ2 subunit cluster sizes [μm^2], intensity [au] and co-localization with vGAT (=synaptic clusters). A) Analysis of endogenous gephyrin. Gephyrin: green, vGAT: magenta, DAAO: blue; scale bar 50 and 0.5 µm. B) Analysis of endogenous $GABA_AR$ γ2 subunit clusters. γ2: green, vGAT: magenta; scale bar 50 and 0.5 µm.

Chapter 4

GephyrinΔ199-233 - an epileptogenic microdeletion

Maria-Theresa Gehling[1], Laura Buchwald[1], Fynn Eggersmann[2], Filip Liebsch[1], Peter[2,3,4] Kloppenburg, Günter Schwarz[1,3,4]

[1]Institute of Biochemistry, Department of Chemistry, University of Cologne, 50674 Cologne, Germany

[2]Biocenter, Institute for Zoology, University of Cologne, 50674 Cologne, Germany

[3]Center for Molecular Medicine Cologne (CMMC), University of Cologne, Cologne, Germany

[4]Cologne Excellence Cluster on Cellular Stress Responses in Aging-Associated Diseases (CECAD), University of Cologne, Cologne, Germany

4.1. Author contributions

Maria-Theresa Gehling and Guenter Schwarz designed the study. Maria-Theresa Gehling, Guenter Schwarz and Filip Liebsch wrote the manuscript. Experiments using mice and mice-derived samples, neuro cell culture experiments and COS7 cell experiments were performed by Maria-Theresa Gehling. Experiments using recombinantly expressed proteins (protein purification, SEC, ITC, sedimentation assay) were performed by Laura Buchwald. Electrophysiology experiments were performed by Fynn Eggersmann, with methodical input from Peter Kloppenburg. Filip Liebsch gave methodical input regarding the use of macros for the automated image analysis through Fiji/ImageJ.

4.2. Abstract

Gephyrin, as the main organizer of inhibitory synapses, is crucial for inhibitory signal transmission, and implicated in various neurological disorders. Various studies have identified gephyrin microdeletions in conditions of autism, schizophrenia, and epilepsy. Those deletions affected the N-terminal G-domain and/or the central C-domain of gephyrin while the receptor binding C-terminal E-domain was not affected. Here, we investigated the importance of a specific microdeletion (∆199-233) within the C-domain using a full-body knock-in mouse model. Homozygous mice displayed a severe phenotype characterized by reduced fertility, increased mortality, and neurological deficits at early developmental stages. Analyses in dissociated hippocampal neurons demonstrated disrupted synaptic targeting of gephyrin ∆199-233 that harbors the functionally important S-palmitoylation site at Cys212. Simultaneously, we found adaptations at the excitatory synapse, with smaller, but more numerous clusters of the excitatory scaffolding protein PSD95. Although, gephyrin ∆199-233 showed unexpectedly a facilitated receptor interaction, inhibitory signal transmission was reduced. We hypothesize, that the gephyrin ∆199-233-mediated reduction of inhibition triggers compensatory excitation, which possibly fails and/or disrupts the excitation/inhibition ratio in our mouse model. These findings highlight the critical role of the gephyrin C-domain and its post-translational modifications in synaptic function and neuronal health, offering a novel mouse model for the development of potential therapeutic targets addressing gephyrin-associated neurological disorders.

4.3. Introduction

Neuronal signal transmission depends on the precise localization of receptors at the post-synaptic site. Inhibitory glycine receptors (GlyRs) and a subset of GABA type A receptors ($GABA_ARs$) are clustered by the scaffolding protein gephyrin (geph, GPHN) at the post-synapse [1]. Gephyrin is a trimeric, cytosolic protein and consists of three domains, the E-, C- and G-domain. Dimerization of the E-domain and trimerization of the G-domain allow gephyrin to self-assemble in complex multimers [2, 3]. Moreover, the dimer interface of the E-domain builds the binding pocket for the intracellular domains (ICDs) of the receptors, which are both pentameric ion channels[4]. Although the composition of receptor types varies, the interaction with gephyrin appears via the β-subunit ICD in case of GlyRs [3], and the α1-3 and β1-2 subunit ICDs in case of $GABA_ARs$ [5-7]. Notably, the ICDs of both receptor types share essential structural elements required for gephyrin interaction [8, 9]. Moreover, the γ2 subunit of $GABA_ARs$ was identified as important for synaptically functional receptors and the interaction towards gephyrin even though indirectly [10, 11].

Dysfunctions of gephyrin are associated with different neuronal impairments, such as epilepsy [12, 13], anxiety [14], schizophrenia [15], autism [15] and hyperekplexia [16]. Besides its function at inhibitory post-synapses, gephyrin is also expressed in peripheral tissue where it catalyzes the final steps of molybdenum cofactor (Moco) biosynthesis [17]. Defects in Moco biosynthesis led to the loss of four different Moco-dependent enzymes of which the deficiency in sulfite oxidase is the primary contributor to a severe neurodegenerative phenotype. Due to the accumulation of toxic sulfite the amino acid derivative S-sulfocysteine (SSC) [18-20] is formed causing hyperexcitation and calcium-dependent calpain-mediated cleavage a various neuronal proteins including gephyrin [20].

Besides proteolytic cleavage, clustering, localization and receptor binding of gephyrin are regulated by a large variety of post-translational modifications (PTMs), which are mostly targeting gephyrin C-domain. Among the reversible PTMs are several phosphorylation sites, involved in complex signaling cascades [21-23]. S-palmitoylation of gephyrin at cysteine 212 and 284 was found to be crucial for synaptic targeting [24]. Additionally, *cis-trans*-isomerization of a proline-rich region is catalyzed by the interaction with peptidyl-prolyl *cis-trans* isomerase 1 (Pin1) and was shown to be important for GlyR clustering [25]. Furthermore, the nucleotide exchange factor collybistin and the dynein-light chain 1/2 (DLC1/2) [26] bind to the C-domain of gephyrin, the latter may influence the transport of gephyrin and GlyRs and thus glycinergic signal transmission [27], while the importance of this interaction for GABAergic synapses is less clear. Importantly, the

majority of gephyrin's PTMs have been investigated *in vitro* [28], and only a few were linked to physiological outcomes *in vivo* [29]. Besides that, studies of human cases focused on the G-and E-domain due to their importance for receptor binding and self-assembly [12, 15, 30] while the role of the regulatory C-domain remained largely unknown. Thus, our goal was to investigate the role of the C-domain *in vivo*.

We generated a full-body knock-in mouse model causing a truncation in gephyrin C-domain spanning residues 199-233 (Δ199-233). The deleted sequence included the proposed DLC1/2 binding motif, S-palmitoylation site Cys212 and the last three residues of the *cis-trans*-isomerization motif. Characterization of homozygous GPHNΔ199-233 mice revealed that the deleted region was important for murine neuronal development and survival. We found alterations of gephyrin-receptor binding towards a tighter interaction, but reduced synaptic targeting of gephyrin due to reduced S-palmitoylation, which lead to decreased inhibitory synaptic transmission. Assumably, to overcome altered inhibition, we found adaptions at excitatory synapses and hypothesize that an altered ratio of excitation and inhibition contributes to the neuronal impairments of our mouse model.

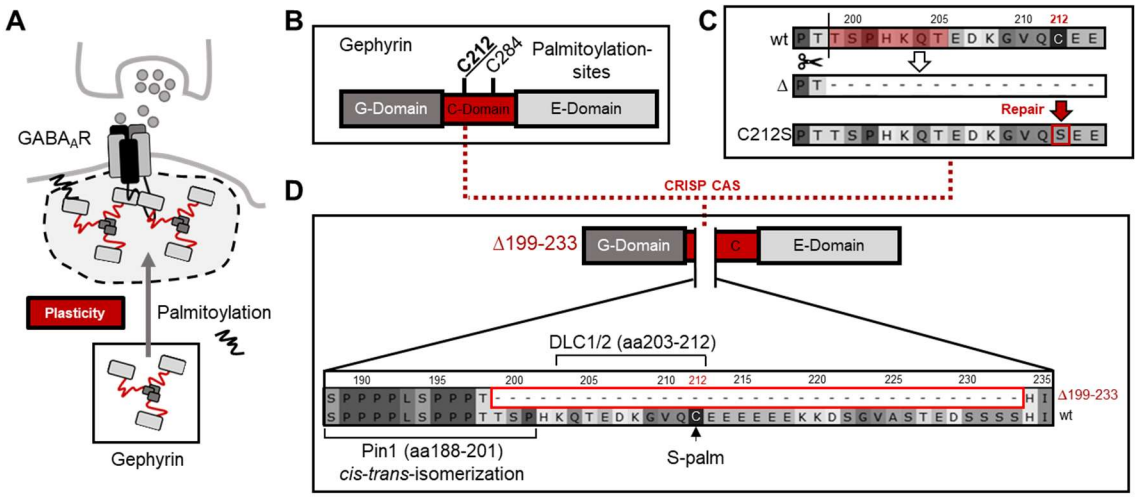

Figure 1: Generation of mice with microdeletion gephΔ199-233
A) Schematic description of S-palmitoylation of gephyrin influencing synaptic plasticity at GABAergic synapses. S-palmitoylation leads to gephyrin synaptic targeting and cluster size increase. B) Domain structure of a gephyrin monomer: S-palmitoylation targets are cysteines 212 and 284 in the C-domain. C212 (bold and underlined) was shown to be more relevant than C284. C) CRISPR/Cas9 strategy to obtain C212S KI mice visualized on the protein level. The potential cutting site of CAS is indicated by a scissor. Inefficient repair results in a truncated gephyrin species (Δ). Successful repair results in C212S substitution. D) Specific microdeletion of gephyrin Δ199-233 enlarged highlighting deleted PTM sites (e.g. S-palm=S-palmitoylation) and protein interaction motifs (Pin1=peptidyl-prolyl *cis-trans* isomerase 1; DLC1/2=dynein-light chain 1/2).

4.4. Results

4.4.1. Severe phenotype of homozygous gephyrin Δ199-233 mice

Previously, S-palmitoylation has been identified as one important PTM to regulate synaptic plasticity of gephyrin [24]. S-palmitoylation was assigned to cysteines 212 and 284, while Cys212 being the primary site [24] (Figure 1A and B). Originally, our aim was the introduction of single amino acid substitution (C212S) allowing us to investigate solely the physiological importance of S-palmitoylation on that Cys212 residue *in vivo*. Consequently, the CRISPR/Cas9 strategy was designed to achieve the Cys212 to Ser substitution (Figure 1C). Unexpectedly, using the designed guide RNA (gRNA) and repair template in CRISPR/Cas9 system resulted in a genetic variety. In the founder generation, we identified the desired substitution C212S, but also a set of INDELs (Figure S1A). The survival rate of the founder litter was low with 25% at P20 (Figure S1C), and one mouse had to be sacrificed at P20 due to a severe seizures. Considering the high mortality, we concluded that the area we aimed to modify is important for gephyrin function. However, no mouse with a single C212S variant survived and only one mouse with a larger deletion produced offsprings, which was sufficient to establish a new line. In the second heterozygous generation we verified that the gephyrin deletion was spanning residues 199-233 (Δ199-233) and off-targets could be excluded (Figure S1C). We decided to investigate the deletion (Δ199-233) further, since several microdeletions were observed in human patients causing neuronal disorders of different kind and severity [12, 15] (Figure S1D).

The truncated C-domain part is with 35 aa only a small part of the whole C-domain (residue 166-329) and includes a few PTM sites with assigned but also yet unassigned functions, which have been investigated mainly *in vitro* [24-26, 28, 31, 32]. Among the PTMs are the last three amino acids (residue 199-201) of the Pin1 interaction site, the interaction site of DLC (residue 203-212), and the S-palmitoylation site C212 (Figure 1D). Abolishing those PTMs could give new insights into their importance for synaptic plasticity *in vivo*. This would highlight the importance of regulation through gephyrin's C-domain beside oligomerization and receptor binding abilities of G- and E-domain, respectively. Thus, we started to characterize the phenotype of Δ199-233 mice.

We found a genotype distribution of 56.3% wt/wt, 27.3% wt/Δ, but only 16.4% Δ/Δ (Figure 2A). Considering mendelian rules of crossing wt/Δ mice, we expected 25% Δ/Δ mice, thus it might be that approx. half of Δ/Δ embryos were absorbed in the uterus . Moreover, Δ/Δ pups born had a lower survival rate and often died within the first 1-4 days (Figure 2B). Following those days, 50% of Δ/Δ reached an age of P16, while 75% wt/Δ and wt/wt litter mates reached P16. In addition, approximately every third litter with at least one

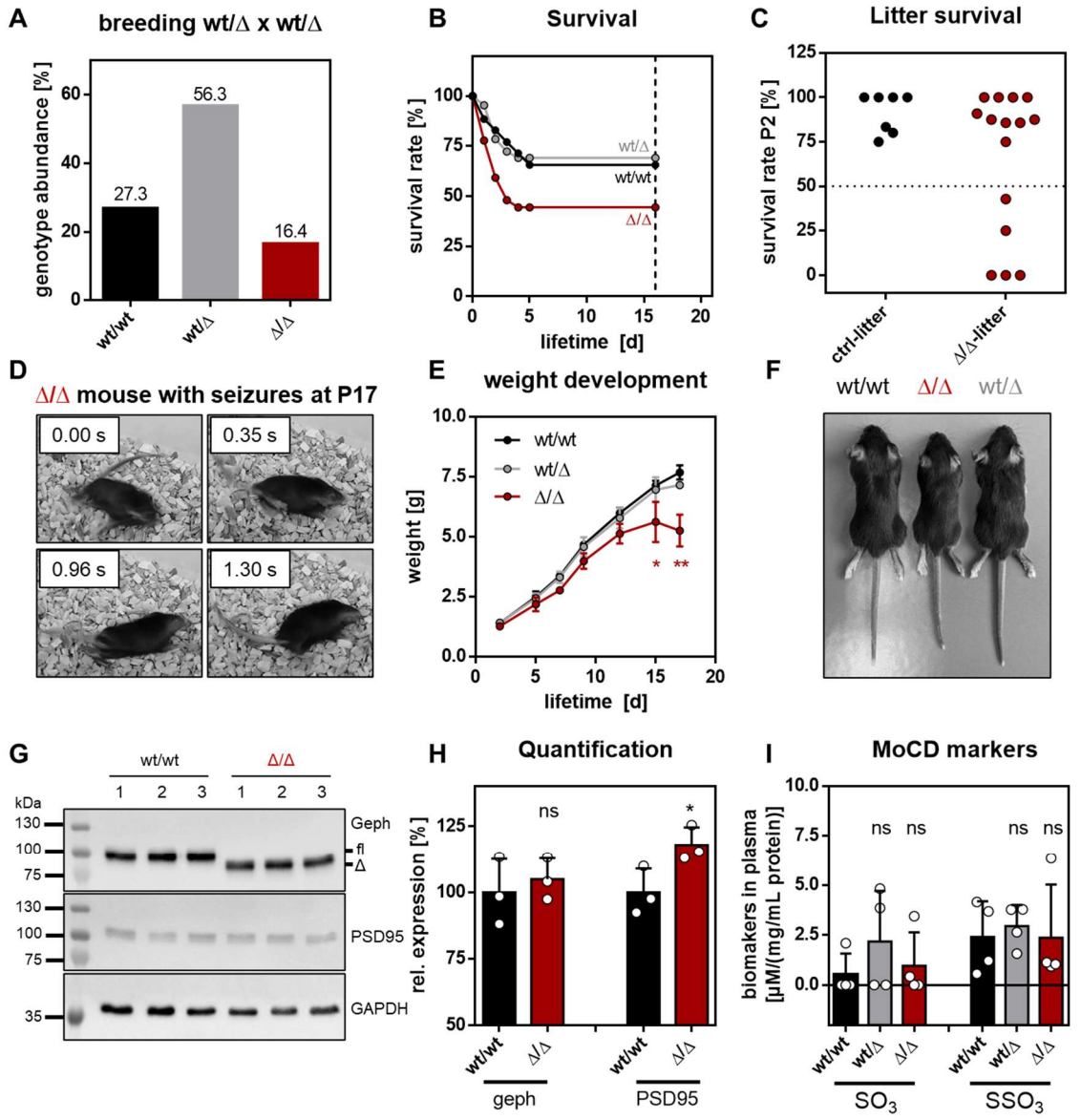

Figure 2: Phenotype of mice with microdeletion gephΔ199-233

A) Abundance of each genotype obtained from crossing wt/Δ x wt/Δ animals. Analysis of 164 animals. B) Survival rate of the different genotypes. Dashed line indicates analyzed animals with natural deaths and without intervention due to high stress levels (wt/wt n=35, wt/Δ n=65, Δ/Δ n=27). C) Survival rate at P2 of pups when the litter contained no Δ/Δ animal (ctrl litter, n=7) or at least one Δ/Δ animal (Δ/Δ litter, n=15). D) Images taken during a seizure episode of a homozygous GephΔ199-233 animal at P17: Rapid extension and contraction of limbs within a few milliseconds. E) Weight development of the different genotypes. Significance tested by 1way ANOVA $F(2,14)=8.118$; $p=0.0046$. *Bonferroni* post-hoc test: wt/wt vs. wt/Δ : $p>0.9999$ (ns, grey); wt/wt vs. Δ/Δ: $p=0.0077$ (**, red). Error bars determined by standard deviation. F) Litter mates of different genotypes at P17. G) Western Blot of brain lysates at P17 (n=3 per genotype). Upper panel: Gephyrin wt (fl) and truncated Δ199-233 species. Middel panel: PSD95. Lower panel: Loading ctrl GAPDH. H) Quantification of band intensities of G. Intensities of geph or PSD95 corrected by intensity of GAPDH and normalized to the average of wt/wt samples. Significance tested with *student's t-test*: geph $p=0.5984$ (ns); PSD95 $p=0.0492$ (*). Error bars determined by standard deviation. I) Analysis of Moco deficiency (MoCD) biomarkers (SO_3 and SSO_3) in plasma (n=4 mice per genotype). Values normalized to protein content in plasma. Error bars determined by standard deviation.

homozygous Δ199-233 mouse (Δ/Δ litter) completely died after P2 (Figure 2C). In comparison, in litters containing no Δ/Δ mouse (ctrl litter), approx. 90% of the pups survived P2 and no litter completely died before P2. This observation might be due to enhanced stress on maternal care induced by the sensation of impaired offspring. However, Δ/Δ mice surviving P2 did not reach weaning age P21 either. We observed that five individual mice suffered either from sudden death (P19) or had to be sacrificed in order to reduce stress levels given by their epileptic-like seizures (P17) (Figure 2D), impaired locomotion (P14-19), apathetic behavior (P18) or severe weight loss (P16). Thus, we decided to reduce animal harm and sacrificed Δ/Δ mice for experimental use before severe impairments manifested regularly. As a result, we could use only 12 Δ/Δ mice out of 164 born mice from wt/Δ x wt/Δ mating for organ harvest. In general, Δ/Δ mice were significantly lighter and thus smaller in comparison to heterozygous or wt litter mates (Figure 2E and F). Heterozygous mice were indistinguishable from wt littermates, a dominant negative effect of truncated Δ199-233 on wt gephyrin was rather unlikely and we determined heterozygous mice as wt-like.

Next, we checked protein levels of gephyrin in comparison to PSD95 in total brain lysates (Figure 2G). We found that in Δ/Δ mice the levels of gephyrin were unchanged in comparison to wt/wt mice, but the levels of PSD95 were slightly but significantly increased by approx. 20% (Figure 2H). Lastly, since weight loss, neuronal impairments and early mortality can be signs of MoCD, we tested whether Δ199-233 mice showed elevated levels of MoCD biomarkers sulfite (SO3) and thiosulfate (SSO3). The levels of these markers in blood plasma of animals at P16 (Figure 2I) were normal in all genotypes. Thus, we excluded a contribution of MoCD to this phenotype.

In summary, the phenotype of Δ/Δ mice was lethal and appeared at early developmental stages. Mostly, at an age of P16-P18 mice showed different signs of severe impairments (seizures, sudden death), most obvious a reduced body weight. The reason for sudden death and weight loss was not obvious, but we assumed that neuronal dysfunctions were the cause.

4.4.2. Altered post-synaptic scaffolds in gephyrin Δ199-233-expressing neurons

Breeding success to gain homozygous gephyrin Δ199-233 mice to analyze gephyrin clustering was limited, so we decided to overexpress recombinant mScarlet-tagged gephyrin wt and Δ199-233 in hippocampal cell cultures derived from conditional gephyrin knockout (GephyrinFlox) mice. We used adeno-associated viral transduction for efficient expression of the transgene. Identification of GABAergic synapses was performed by staining of vGAT and $GABA_AR$ γ2 (Figure 3A). For excitatory synapses we used PSD95

and vGLUT (Figure 4A). Via automated image analysis [33], scaffold cluster sizes, intensities and number of synaptic and non-synaptic punctae were determined (Figure 3B-G and Figure 4B-E).

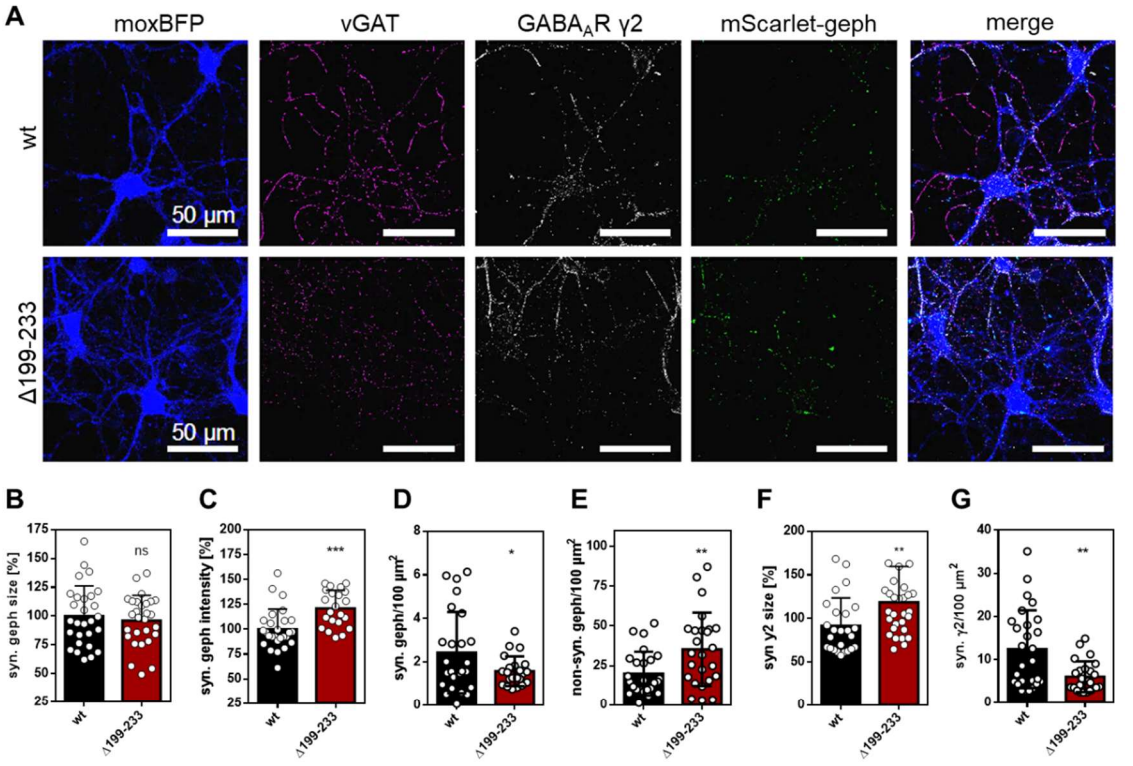

Figure 3: Inhibitory synapses in gephΔ199-233-expressing neurons. Expression of mScltGeph wt and Δ199-233 in primary hippocampal neurons of GephFlox mice. Endogenous Geph KO induced by moxBFP-P2A-Cre. Images were processed with equal brightness thresholds and DOGs in all channels except of moxBFP. Cluster analysis: Significance tested by *student's t-test*. Error bars determined by standard deviation. Analysis of inhibitory GABAergic synapses. Analysis of n=30 cells per condition. A) Images of representative neurons. Synaptic GABAergic gephyrin identified by co-localization with vGAT and $GABA_AR$ γ2. B) Sizes of synaptic gephyrin punctae normalized to average size of wt. p=0.3136 (ns). C) Intensity of synaptic gephyrin punctae normalized to average intensity of wt. p=0.0004 (***). D) Number of synaptic gephyrin punctae per 100 µm² cell area. p=0.0488 (*). E) Number of non-synaptic gephyrin punctae per 100 µm² cell area. p=0.0066 (**). F) Sizes of synaptic $GABA_AR$ γ2 punctae normalized to average size in wt condition. p=0.0099 (**). G) Number of synaptic $GABA_AR$ γ2 punctae per 100 µm² cell area. p=0.0022 (**). H) Schematic illustration of synaptic clustering Δ199-233 gephyrin in comparison to wt: Cluster sizes are maintained, but intensity increases, less synaptic clusters occur, while non-synaptic clusters accumulate.

At GABAergic synapses, we observed that the average fluorescence of gephyrin Δ199-233 punctae was significantly more intense in comparison to gephyrin wt (Figure 3C), but the sizes of punctae stayed comparable (Figure 3B)). The number of non-synaptic gephyrin Δ199-233 punctae increased significantly (Figure 3E), while the number of corresponding synaptic punctae significantly decreased (Figure 3D). This indicated that synaptic targeting of gephyrin Δ199-233 is likely disturbed, which fits to the lack of S-palmitoylation at C212 in gephyrin Δ199-233 [24]. Furthermore, we

observed that the sizes of $GABA_AR$ γ2 punctae at synapses increased significantly (Figure 3F), but significantly less synaptic $GABA_AR$ γ2 punctae could be found per area. This indicated that the interaction of receptor and gephyrin could be tighter, while synaptic targeting was disturbed, which could affect synaptic transmission in summary.

At excitatory synapses, we observed in gephyrin Δ199-233 expressing cells that PSD95 punctae were significantly smaller (Figure 4B) than those of gephyrin wt expressing cells. The average intensity stayed comparable (Figure 4C). Remarkably, the number of synaptic as well as of non-synaptic PSD95 punctae significantly increased (Figure 4D and E) in gephyrin Δ199-233 expressing neurons. These findings suggested that PSD95 scaffolds were split in smaller fractions, leading to overall more punctae (Figure 4F). Assumably, neurons aim to “balance” excitation and inhibition, which might be triggered though the observed changes at the inhibitory synapse.

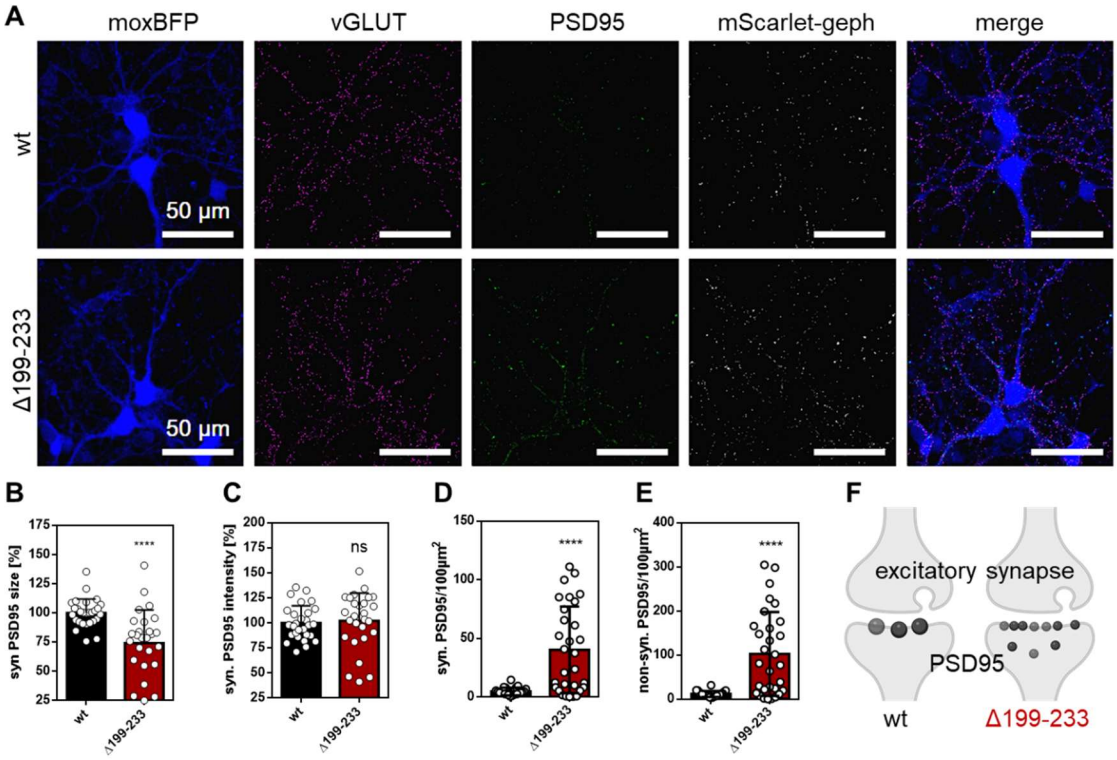

Figure 4: Excitatory synapses in gephΔ199-233-expressing neurons
Expression of mScItGeph wt and Δ199-233 in primary hippocampal neurons of GephFlox mice. Endogenous Geph KO induced by moxBFP-P2A-Cre. Images were processed with equal brightness thresholds and DOGs in all channels except of moxBFP. Cluster analysis: Significance tested by *student's t-test*. Error bars determined by standard deviation. Analysis of excitatory synapses. Analysis of n=30 cells per condition. A) Images of representative neurons. Synaptic PSD95 punctae identified by co-localization with vGLUT. B) Sizes of synaptic PSD95 punctae normalized to average size of wt. $p<0.0001$ (****). C) Intensity of synaptic PSD95 punctae normalized to average intensity of wt. $p=0.7221$ (ns). D) Number of synaptic PSD95 punctae per 100 µm² cell area. $p<0.0001$ (****). E) Number of non-synaptic PSD95 punctae per 100 µm² cell area. $p<0.0001$ (****). F) Schematic illustration of synaptic clustering of PSD95 in Δ199-233 gephyrin expressing neurons in comparison to wt expressing cells: Cluster intensities are maintained, but sizes decreased, more synaptic and non-synaptic clusters occur.

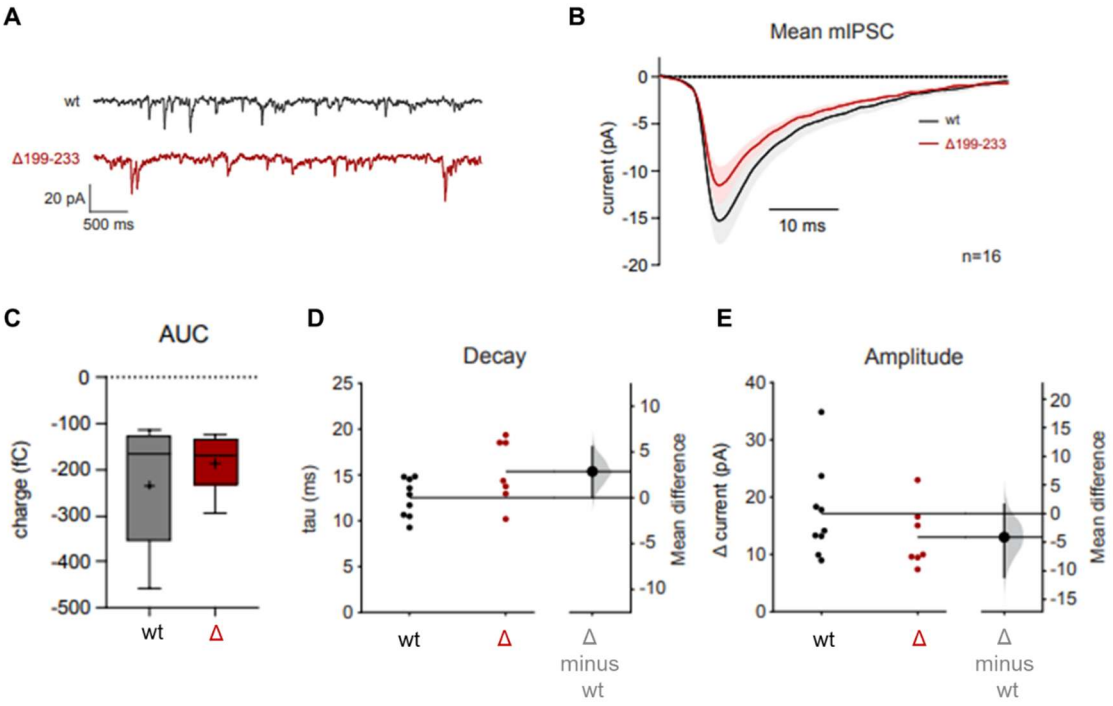

Figure 5: Inhibitory signaltransmission in gephΔ199-233-expressing neurons
Measurements and analysis of miniature inhibitory post-synaptic currents (mIPSCs) in in primary hippocampal neurons of GephFlox mice. Expression of mScltGeph wt and Δ199-233. Endogenous Geph KO induced by moxBFP-P2A-Cre. Analysis pf 16 cells per condition. Statistical analysis by mean difference of the confidence interval and *p*-value permutation test. Error bars determined by standard deviation. A) Representative mIPSCs of wt and Δ199-233 cells. B) Average mIPSCs. C) Quantification of the area under the mIPSC curve (AUC). D) Quantification of mIPSC decay time. E) Quantification of mIPSC amplitude.

To investigate the effects on inhibitory transmission, we performed electrophysiology experiments with the same experimental set up of neurons. We observed a tendency of alterations of miniature inhibitory post-synaptic currents (mIPSCs) (Figure 5). Surprisingly, the frequency of mIPSCs in gephyrinΔ199-233 expressing cells was comparable to gephyrin wt expressing neurons indicating an unchanged number of receptors present at the post-synapse. First, this seems contra-intuitive to the previous imaging analysis of reduced numbers of synaptic $GABA_AR$ γ2 punctae. But considering the increase of sizes of synaptic $GABA_AR$ γ2 punctae, it is possible, that still the same “amount” of $GABA_ARs$ was present to generate mIPSCs. Consequently, both parameters, number and size, are decisive for inhibitory signal transmission. Additionally, we observed a slight decrease of amplitude (Figure 5E), but surprisingly an increase of decay time (Figure 5D). The integration of mIPSCs displays the presence of negative charges at the post-synapse, which was decreased for gephyrinΔ199-233 expressing cells (Figure 5C). Assumably, the gephyrinΔ199-233-receptor-interaction might be changed as previously assumed resulting in decreased inhibitory neurotransmission.

In summary, both types of synapses were affected in gephyrin Δ199-233 expressing neurons. On the one hand, GABAergic synapses contained less synaptically localized but bigger gephyrin and $GABA_AR$ γ2 punctae combined resulting in reduced inhibitory signal transmission. On the other hand, excitatory synapses contained more synaptically localized, but smaller PSD95 punctae. These changes at both synapses might resemble a disturbance of E/I ratio in Δ/Δ mice, which is a possible explanation for a neuronal impaired phenotype.

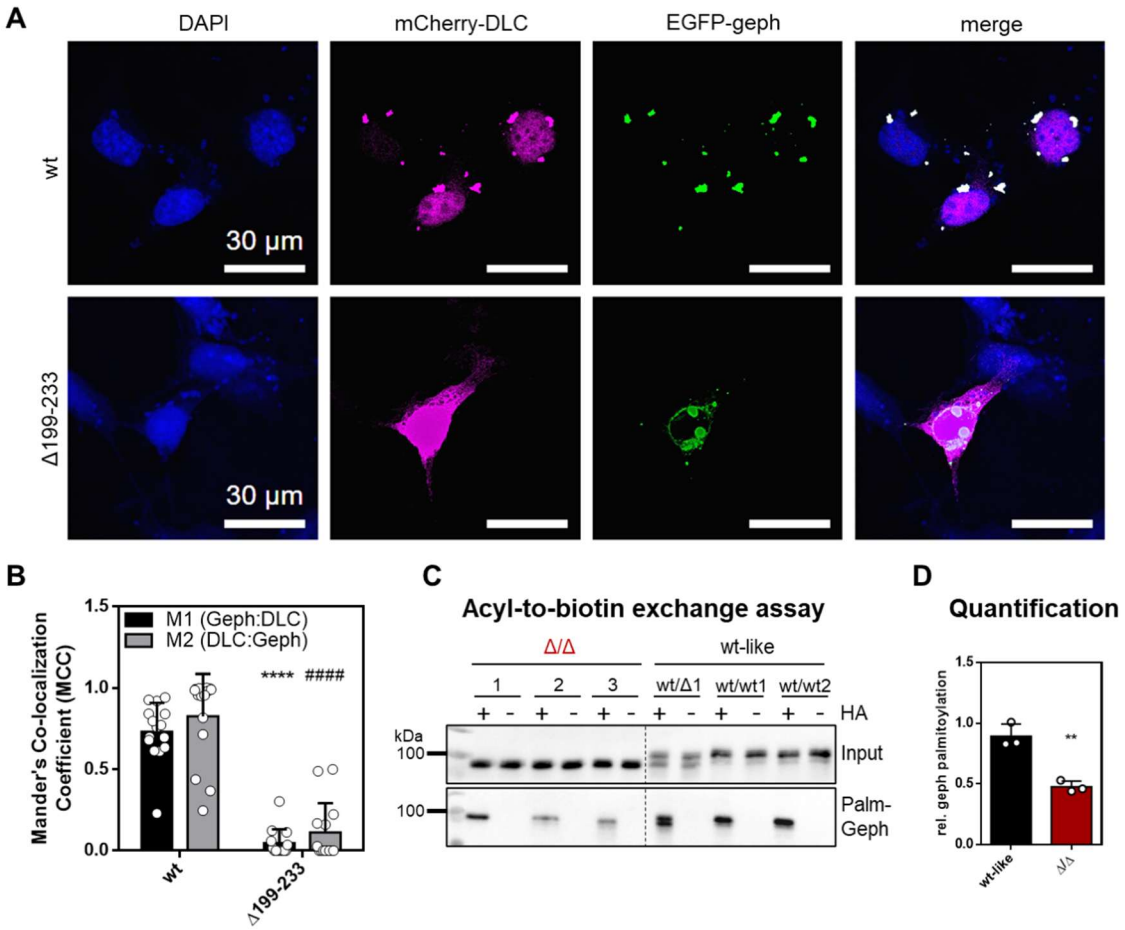

Figure 6: Characterization of selected PTMs and interaction partners of gephΔ199-233
A) Analysis of gephyrin S-palmitoylation via acyl-to-biotin exchange assay. S-palmitoylated gephyrin species (lower panel; Palm-Geph). Analysis of brain lysates (n=3 mice per condition). B) Quantification of band intensities of A. Palm-Geph normalized to input signal. Significance tested by *student's t-test* p=0.0030 (**). Error bars determined by standard deviation. C) Pull-down of endogenous gephyrin from brain lysates. Analysis of co-pulled binding partners. D) Representative images of COS7 cells expressing mCherry-DLC1 and EGFP-gephyrin wt and Δ199-233 respectively. Nuclei stained with DAPI. E) Quantification of co-localization of gephyrin and DLC using Mander's co-localization coefficient (MCC). M1: Gephyrin overlapping DLC; M2: DLC overlapping gephyrin. Significance tested by *student's t-test*, significance level alpha corrected by the number of tests (2). M1 wt vs M1 199-233: p<0.00005 (****); M2 wt vs M2 199-233: p<0.00005 (####). Analysis of n=15 cells per condition.

4.4.3. Disturbed S-palmitoylation and DLC interaction of gephyrin Δ199-233

Since several PTMs are affected by the microdeletion in gephyrin Δ199-233, we investigated the contribution of distinct PTMs. First, we co-expressed EGFP-gephyrin and mCherry-DLC1 in COS7 cells (Figure 6) according to the study, when the DLC

binding region of gephyrin was originally identified [26]. DLC is recruited into gephyrin clusters when gephyrin wt was expressed. In contrast co-expression with gephyrin Δ199-233 led to a diffusely distribution of DLC (Figure 6A). Quantification of the co-localization with Mander's co-localization coefficient (MCC) resulted in significantly less gephyrin Δ199-233 overlapping DLC (M1) and DLC overlapping gephyrin Δ199-233 (M2) in comparison to gephyrin wt (Figure 6B). The low affinity binding site of gephyrin for DLC is left in gephyrin Δ199-233, but this is not sufficient to enable an interaction. This is line with the first study of the gephyrin-DLC interaction, when only the high-affinity binding site was missing resulting in no interaction in several experiments [26]. Here, we verified that the binding of gephyrin Δ199-233 and DLC1 is disturbed due to the lack of the high affinity binding motif.

Furthermore, we analyzed the S-palmitoylation levels of gephyrin in full brain lysates of ∆/∆ mice in comparison to wt/wt and wt-like mice (Figure 6C and D). The biotin-to-acyl exchange assay revealed, that the S-palmitoylation level of gephyrin Δ199-233 was significantly reduced to half of that of gephyrin wt (Figure 6D). With this we verified our expectation that the impairment of synaptic trafficking observed in previous *in cellulo* experiments could be explained by the lack of S-palmitoylation [24].

4.4.4. Gephyrin ∆199-233 shows facilitated receptor interaction

Next, we characterized the microdeletion *in vitro* using recombinantly expressed gephyrin from E. coli. First, we examined secondary structure by circular dichroism spectroscopy (Figure 7A). We found the dominance of α-helices with minima around 210 and 220 nm for both geph∆199-233 and wt. Second, oligomerization was investigated by size exclusion chromatography (Figure 7B and C). As expected, Gephyrin ∆199-233 eluted later than gephyrin wt, due to the deletion of 34 aa per monomer. Since, gephyrin appears at minimum in a trimeric state (Figure 7B) when derived from E.coli [28], the deletion adds up to 102 aa, which mirrors a difference in the hydrodynamic radius of approx. 80 kDa. The more complex and higher the oligomeric state becomes, the bigger gets the apparent weight difference between gephyrin ∆199-233 and wt (Figure 7C). However, gephyrin ∆199-233 was still able to self-assemble and form networks.

Lastly, we tested the gephyrin-receptor interaction in binding studies and observed, that this interaction seems to be facilitated for gephyrin ∆199-233. This was revealed by two different approaches: a) ITC experiments using the established GlyR β-subunit peptide [3] (Figure 7E) and b) in a sedimentation assay (adapted after Bai et al [34]) in which we used a fusion protein of the lumazine synthase (LS) and five GlyR β-subunit ICDs (LSβ) as a pentameric GlyR model [35] (Figure 5D and F). In ITC experiments

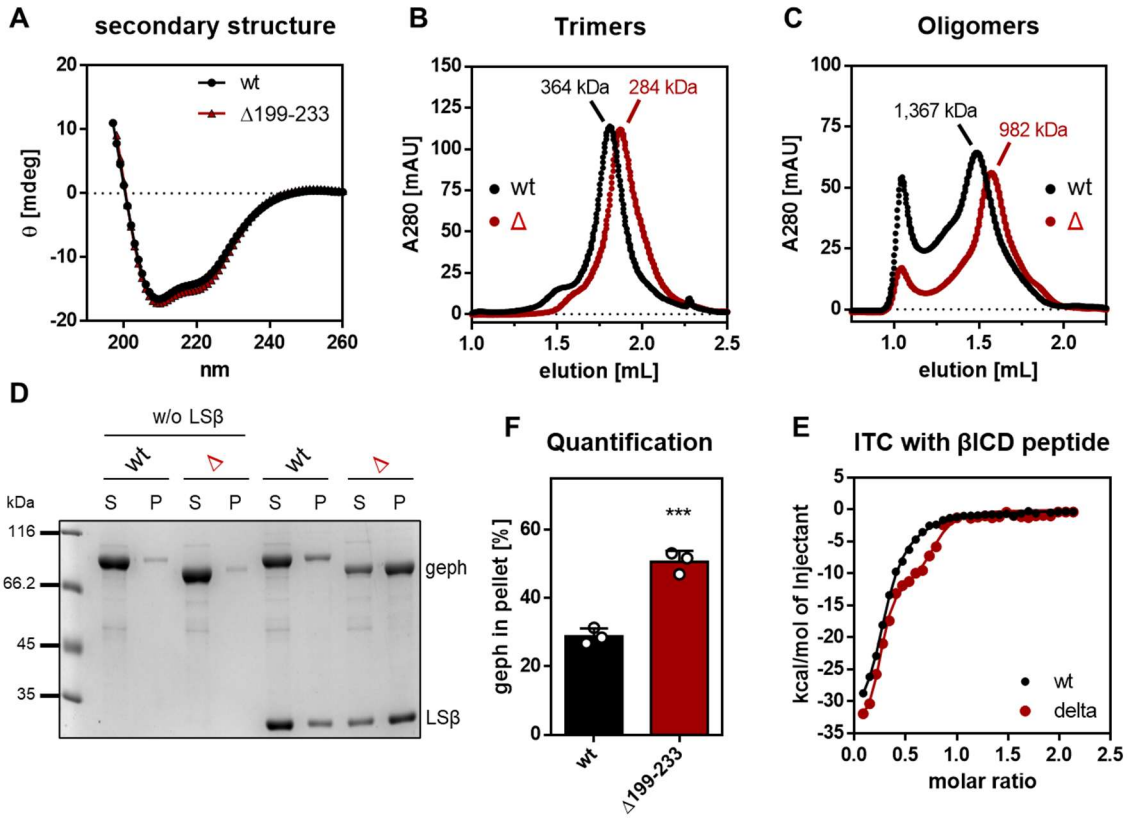

Figure 7*:* Characterization of GephΔ199-233 *in vitro*

Experiments performed with recombinantly expressed gephyrin wt and Δ199-233 from *E.coli*. Representative data from three individual experiments using proteins from three independent purifications (n=3). A) Secondary structure measured by circular dichroism spectroscopy. B-C) Oligomeric state detected by analytical size exclusion chromatography (SEC). B) Trimers of gephyrin eluted around 1.8 mL. Apparent weight determined to 364 kDa for wt gephyrin and 284 kDa for Δ199-233. C) Oligomers of gephyrin eluted around 1.6 mL and high-order oligomers at 1 mL. Apparent weight determined to 1 367 kDa for wt gephyrin and 982 kDa for Δ199-233. D) Sedimentation assay using LS βICD as a pentameric GlyR model. E) Quantification of F. Sedimented gephyrin in pellet determined and normalized to total protein. Significance tested by *student's* t-test: p=0.0007 (***). F) Isothermal calorimetry titration experiment using GlyRβICD peptide as a model for the GlyR. The peptide was titrated into gephyrin. Exemplary overlay of fitted curves of wt and Δ199-233 gephyrin. Find full plots in supplementary figure S2.

gephyrin shows a two-sided interaction with the peptide resulting in a low and a high affinity binding site [3]. The dissociation constants for wt and Δ199-233 gephyrin were comparable for both binding sites (K_D^{high} : wt=0.063±0.017 µm; Δ199-233=0.050±0.023 µm, K_D^{low} : wt=1.83±0.059 µm; Δ199 233=1.54±0.7 µm). But the shape of the ITC run reveals a more prominent low affinity binding site (Figure 5E, Figure S2). Interestingly, when exposing gephyrin to the pentameric GlyR model LSβ in the sedimentation assay (Figure 5D), we found twice as much gephΔ199-233 in the pelleted fraction compared to gephyrin wt (Figure 5E). The interaction towards the multimeric receptor is responsible for gephyrin sedimentation [34], which indicates that this interaction is facilitated for gephΔ199-233. Although, we used model systems for the GlyR, the required structural elements of both, gephyrin-GlyR β and gephyrin-$GABA_AR$ α3 interaction for instance, are comparable [8]. Additionally, gephyrin does not directly

bind to $GABA_AR$ γ2 subunits and requires additional α1-3 subunits. Thus, the results of the binding studies can be used as an explanation for the cluster analysis of expressed gephΔ199-233 at GABAergic synapses in neurons previously: Due to the facilitated gephyrin-receptor interaction, the intensity of gephΔ199-233 co-localizing with vGAT and $GABA_AR$ γ2 punctae was increased, while simultaneously the sizes of synaptic $GABA_AR$ γ2 punctae were increased.

4.5. Discussion

We identified gephyrin with the microdeletion ∆199-233 as a new pathogenic variant in mice. This pathogenicity is evident through reduced fertility and increased mortality, characterized by weight loss, sudden death, and epileptic-like seizures. The phenotype emerged in the early developmental stage (P16-P19) and was not related to MoCD. In comparison, human patients with larger exonic microdeletions in gephyrin suffer from complex neuronal disorders such as autism, schizophrenia, and seizures, which typically manifest in early childhood [12, 15]. Our mouse model thus appears suitable for investigating similar conditions in humans and might be valuable for developing treatment strategies. However, human cases often involve deletions in the G- and E-domains of gephyrin, [12, 15] which are critical for clustering and receptor binding [2]. These domains are believed to be major contributors to these disorders, whereas the C-domain has received less attention.

Our study highlights the crucial role of the C-domain of gephyrin, which includes several PTM sites [24, 28, 36], in the onset of neuronal diseases. We investigated these PTMs to understand their physiological relevance and their contribution to the phenotype in our mouse model. The absence of PTMs in gephyrin ∆199-233 could be attributed to the lack of S-palmitoylation and DLC interaction. The significance of missing phosphorylation (T199, T205, S222, S226, and T227) remains unclear as their roles in synaptic functions of gephyrin have not been fully defined [28]. However, phosphorylation site S200 is crucial for gephyrin-Pin1 interaction. A substitution significantly reduces this interaction, although some binding activity remains [25]. *Cis-trans* isomerization of gephyrin, facilitated by Pin1, is important for recruiting synaptic GlyRs [25], which mediate inhibition in the brain stem and spinal cord [37]. This impairment would typically manifest as stiffness [38, 39], contrary to the seizures observed in our model. Therefore, we hypothesize that a residual gephyrin-Pin1 interaction in gephyrin ∆199-233, is likely maintained and does not contribute to the phenotype.

In contrast, the interaction with DLC was completely abolished in Δ/Δ mice, as demonstrated *in cellulo*. This aligns with previous studies, where gephyrin variants lacking the high affinity DLC binding motif (residue 203-212) fail to interact with DLC [26]. Interestingly, it was previously stated that the 'DLC binding is not essential for synaptic localization of gephyrin' although the S-palmitoylation site Cys212 was also absent in those studies, possibly affecting the results. The absence of Cys212 alone reduces synaptic gephyrin due to lack of S-palmitoylation [24]. Thus, the combined absence of both PTMs may balance each other out through an unknown mechanism.

Furthermore, a new role of DLC-gephyrin binding was recently proposed with regard to liquid-liquid-phase separation (LLPS). LLPS might contribute to the complexity of synaptic structures by the formation of microdomains [34, 40]. It was shown, that gephyrin undergoes LLPS, proposed as a key mechanism for regulating synaptic clustering [34, 40, 41]. The interaction with DLC further strengthened LLPS formation of gephyrin [34]. Thus, while the synaptic function of gephyrin might not be heavily dependent on DLC-binding, the disrupted DLC-gephyrin interaction in Δ199-233 is likely not the primary cause of neuronal impairments observed in Δ/Δ mice.

The strongest contribution of PTMs was found for S-palmitoylation. S-palmitoylation levels of gephyrin Δ199-233 were significantly reduced to 50% *in vivo*, due to the missing residue Cys212. The second S-palmitoylation site Cys284 was unable to fully compensate, which is in line with previous reports [24]. Lack of S-palmitoylation resulted previously in reduced synaptic targeting and cluster sizes of gephyrin, impairing GABAergic neurotransmission [24]. Although gephyrin Δ199-233 showed reduced synaptic localization, cluster sizes were not reduced, suggesting an interplay of opposing PTM effects or another mechanism. *In vitro* binding studies indicated that the gephyrin-receptor interaction via the low affinity binding site was facilitated for gephyrin Δ199-233, possibly because the shorter C-domain no longer masked this site. This hypothesis is supported by previous studies, which suggested a direct modulation of the C-domain for gephyrin-receptor interaction independent on further PTMs [3, 42].

In conclusion, while gephyrin Δ199-233 was impaired in synaptic recruited likely due to reduced S-palmitoylation, a robust proportion still reached the synapse and interacted more strongly with receptors. Still, this proportion was not sufficient to maintain normal inhibition, since we observed reduced GABAergic transmission in electrophysiology experiments. This suggests that PTM-driven synaptic targeting, such as S-palmitoylation, may be crucial for gephyrin's function over mere receptor interaction.

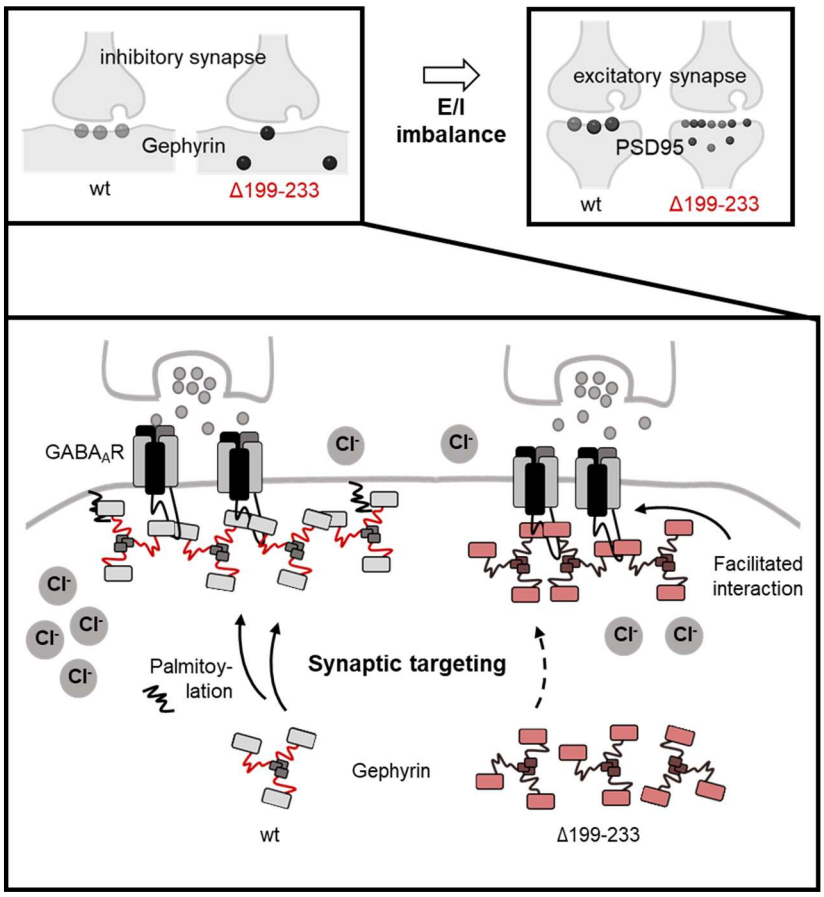

Figure 8: Hypothesized E/I imbalance in gephyrin Δ199-233 expressing neuronal networks
Schematic illustration of the phenotype of homozygous gephyrin Δ199-233 mice caused by an imbalance of excitation and inhibition (E/I): At GABAergic inhibitory synapses, gephyrin Δ199-233 leads to a reduced signal transmission (Cl^- influx). Although, the gephyrin-receptor interaction is facilitated, the recruitment by S-palmitoylation is disturbed for gephyrin Δ199-233 (indicated by a dashed arrow) leading to an accumulation of non-synaptic gephyrin. At the excitatory synapses, PSD95 shows smaller but more numerous clusters, likely an adaptation to the changes at the inhibitory synapse.

However, this hypothesis would lead to a reduction of the frequency of mIPSCs, which we did not observe. Instead, we observed a longer decay time. Consequently, we postulate that enough $GABA_A$Rs are clustered at the synapse, but their kinetics might be altered. Previous studies support this hypothesis, since it was suggested, that the receptor ICD contacts gephyrin C-domain [3]. Thus, it is possible, that the flexible C-domain not only masks the low-affinity receptor binding site, but also interferes with the chloride influx of $GABA_A$Rs. Regardless of the underlying molecular reason, a reduced GABAergic transmission alone is only one explanation for the observed phenotype in Δ/Δmice.

To further understand the phenotype of Δ/Δ mice, we considered the interplay of excitation and inhibition (E/I) and examined excitatory synapses. We observed equal expression of truncated and wt gephyrin *in vivo*, but slightly increased levels of the excitatory scaffolding protein PSD95 suggesting an alteration of E/I. Increased synaptic and non-synaptic PSD95 punctae with reduced sizes were also noted in cell culture experiments, supporting potential adaptations in E/I [43, 44]. As a result, complex neuronal impairments due to morphological changes of neuronal architectures could appear in Δ/Δ mice [45, 46], especially when the adaptions on one site cannot be mediated accordingly. Interestingly, the phenotype became visible after approx. 14 days,

which is the time window when mice develop full sensory receptivity and show increased sensitivity to extrinsic provocation [47]. In this period, the functional interplay of excitation and inhibition is even more challenged [48].

In summary, we propose that the phenotype observed in Δ/Δ was caused by a reduction of inhibition due to disturbed PTM-driven synaptic targeting, which leads to adaptations at excitatory synapses (Figure 8). This adaption might work till a certain point, until it became insufficient and caused hyperexcitation, visible as epileptic-like seizures for instance. However, the exact cellular changes in further neuronal networks *in vivo*, the disturbed E/I ratio and its adaption mechanisms in Δ/Δ mice are still under our research.

4.6. Material and Methods

CRISPR CAS

One step generation by electroporation in zygotes for C212S in the Gphn gene was used (DOI 10.3390/cells9051088; DOI 10.1038/s41598-017-08496-8). Used components: gRNA_1: TTATGTGGGCTAGTTGTAGG (AGG); gRNA2: TGCTGCAGTTATATGTGATG (AGG); ssODN repair template (Ultramer): A*A*GATTTACCTTCC CCACCACCTCCTCTCTCTCCACCTCCcACtACTAGCCCACATAAACAGACAGAAGA CAAAGGAGTTCAGTccGAgGAAGGGAAGAAGAAAAGAAAGACAGTGGTGTAGCTTC AACAGAAGATAGTTCaTCATCACATATAACTGCAGCAGCTCTTGCTGCAAAGGTAAG T*C*T (* = phosphorothioate bonds to increase nuclease resistance).

Genotyping and sequencing

DNA was isolated from ear punches or tail cuts using QuickExtractTM (Lucigen). The F0 generation was typed by using PCR (KAPA2G Fast Genotyping Mix (KAPA Biosystems)) (fw_TCAGTTCATACTGCCAGCTCTAC; rv_AGGCAATGACACATCATTAGTGC) followed by BsaJI digestion. The next generations were screened by PCR using fw_CCTCA TGCCATTGACCTTTTACG and rv_ATCATTAGTGCCTCAGAGCTCAA. Off-targets were screened by PCR using Chr1_fw_TGTCACGACAAAAGACAAAGATCA, Chr1_rv_CCCCACTTCTCTGGTCCCTA, Chr12_fw_CCAGATGGACCACACTAATG, Chr12_rv_TCTCCTAGGCCTACAAGACAA, Chr15_fw_AAGAAGCCTCCTTCCTCA CAAG and Chr15_rv_TGCTACATCAGACATGCCTTCTC. After agarose gel electrophoresis amplicons were extracted by the E.Z.N.A. Gel extraction Kit and sent for sanger sequencing (Eurofins).

Sacrifice of mice and sample preparation

Mice were anesthetized with Ketamine/Xylazine through intra-peritoneal injection until decapitation could be safely done. Blood samples were collected by a Pasteur pipette, flashed with 100 mM EDTA (pH 7.5) and centrifuged for 10 min at 17 000 x g and 4°C. The supernatant (blood serum) was collected, snap frozen with liquid nitrogen and stored at -80°C.

The brain was removed and used for lysates. Therefore, RIPA buffer (50 mM Tris/HCl pH 8.0, 150 mM NaCl, 0.1% SDS, 1% IGEPAL CA-630, 0.5% Na deoxycholate, 1 mM EDTA, freshly added protease inhibitor (Roche)) was added. The tissue was dounce homogenized with 1 200 rpm 20 times, sonicated 10 sec at 4°C and 30% amplitude and subsequently centrifuged for 10 min at 4°C and 4 000 x g. The supernatant was transferred into a new tube, snap frozen with liquid nitrogen and stored at -80°C. Protein concentration was determined using BCA. Typically, 100 µg protein were used for SDS-PAGE for WB analysis, 2 mg for acyl-to-biotin exchange assays and 2 mg for pull-down assays.

Ethics statement

We complied with all relevant ethical regulations for animal testing and research. Experiments were approved by the local research ethics committees (Germany, Landesamt für Natur, Umwelt und Verbraucherschutz Nordrhein-Westfalen, reference 2021.A089, 2019.A077 and 2021.A450).

Determination of MoCD markers in blood serum

Blood serum samples were thaw and cleared for 10 min at 17 000 x g and 4°C. 30 µL of the supernatant were supplemented with 30 µL 100% methanol and centrifuged at 17 000 x g for 15 min at 4°C. 15 µL of the supernatant were mixed with 15 µL reaction buffer (160 mM HEPES pH 8.0, 16 mM EDTA), 15 µL 100% acetonitrile, and 3 µL 46 mM mBBr in 10% acetonitrile. The reaction was incubated for 30 min at rt (room temperature) in the dark. 30 µL methanesulfonic acid were added and the sample diluted with 312 µL running buffer A (0.25% acetic acid, pH 4). The sample was centrifuged at 17 000 x g for 15 min at 4°C and 200 µL supernatant were used for HPCL analysis. Fluorescence was measured at 380 nm, emission at 480 nm. The run was performed following the protocol in the scheme below, using a 250 x 3 mm Nucleodur HTec C18 RP column, 5 µm particle size, buffer A and B (100% methanol), an injection volume of 10 µL and a column temperature of 40°C.

Acyl-to-biotin exchange assay

The previously described assay[23] was changed as followed: Acetone precipitation was used to remove chemicals; 2 mg brain lysate were used and the sample after blocking (reaction with methyl methanethiosulfonate) divided in two equal samples (-HA and + HA); 100 mM hydroxylamine (HA) were used.

cDNA Synthesis

100 mg mouse brain tissue were homogenized in 1 mL TRI Reagent (Sigma). After 5 min at rt, 100 µL 1-Brom-3-chlorpropane were added. The reaction was vortexed for 15 sec, incubated 10 min at rt, and centrifuged for 15 min at 12 000 x g and 4°C. 500 µL 2-Propanol were added to the aqueous top layer in a separate tube. The mixture was vortexed, incubated 5 min at rt and centrifuged for 10 min at 12 000 x g and 4°C. The RNA pellet was washed with 1 mL 75% ethanol and subsequently centrifuged at 7 500 x g for 5 min at 4°C. The pellet was dried at rt and resolved in 100 µL RNAse-free water. Typically, 5 µg RNA were used for cDNA synthesis and mixed with 1 µL 10 mM dNTPs, 1 µL of oligo(dT) primer, and filled up with water to 13 µL. The reaction was incubated at 65°C for 5 min and followed by 1 min on ice. 4 µL 5x First-Strand Buffer, 1 µL 0.1 M DTT and 1 µL SuperScriptTM III RT were added. After 60 min at 50°C, the reaction was inactivated for 15 min at 70°C. Isolated cDNA was stored at -20°C.

DNA/expression constructs

Gephyrin ∆199-233 was generated by overlap-extension PCR (OEP) using subcloned isolated cDNA from ∆/∆ mice and gephyrin P1 wt in pQE80L48 as templates. The PCR product (primers: 5' CCTCATGCCATTGACCTTTTACG 3' and 5' ATCATTAGTGCCTCAGAGCTCAA 3') from the cDNA was subcloned into pJET2.1 following the CloneJET PCR Cloning Kit (Thermo Fisher Scientific). For OEP, three fragments (aa1-162, aa153-243, aa234-736) generated and fused by PCR by combination of the following primer pairs: 5'CCAT CACGGATCCGCATGCGAGCTCGGTACCCCAATGGCGACCGAGGGAA3' and 5'GAA TTCTGCAGTCGACGGTACCGCGGGCCCATGGCGACCGAGGGAATGATCCTCA3'; 5'GAATGCTTTCAGTTCATACTGCCAGCTCTA3' and 5'TTTGCAGCAAGAGCTGCTG CAGTTATAT3'; 5'AGCTAATTAAGCTTGGCTGCAGGTCGACCCTCATAGC CGTCCGATGACCA3' and 5'ATGATCAGTTATCTAGATCCGGTGGATCCCTCATAGC CGTCCGATGACCATGACGT3'; 5'CCATCACGGATCCGCATGCGAGCTCGGTACCC CAATGGCGACCGAGGGAA3' and 5'ATGATCAGTTATCTAGATCCGGTGGA TCCCTCATAGCCGTCCGATGACCATGACGT3'. The final, fused fragment was cloned into pQE80L by Gibson assembly using SmaI. Gephyrin P1 wt and ∆199-233 from

pQE80L constructs were cloned by Gibson assembly into pAAV_hSyn_mScarlet (a gift from Karl Deisseroth, Addgene plasmid #131001) using EcoRI. Gephyrin was cloned using PCR and XhoI and KpnI into pEGFP-C2 (Clontech).

Furthermore, DLC1 was cloned into pmCherry-C3 (Clontech) by PCR and ligation using restriction sites XhoI and HindIII.

For virus production the plasmids pAdDeltaF6 (a gift from James M. Wilson, Addgene plasmid #112867; http://n2t.net/addgene:112867; RRID: Addgene_112867) and pAAV2/1 (a gift from James M. Wilson, Addgene plasmid #112862; http://n2t.net/addgene:112862; RRID: Addgene_112862) were used. The expression constructs of LSβ in pQE70 and GlyRβICD in ptYB were described previously[2,34].

Purification of recombinant gephyrin, LSβ and βICD peptide

Gephyrin P1 wt and ∆199-233 in pQE80L were transformed into *E. coli* BL21. Bacterial cultures grew o/n at 37°C under shaking at 110 rpm. At an OD600 of approx. 0.3., expression was induced by supplementation with 250 nM IPTG. Cells were harvested by centrifugation for 10 min at 5 000 rpm (JLA 8.1 rotor) at 4°C after incubation for 21 h at 18°C and 90 rpm. Cell pellets were resuspended in 100 mL ME lysis buffer (300 mM NaCl, 50 mM Tris/HCl, 5 mM β-Mercaptoethanol, 0.05% Tween20, pH 7.4) with the addition of 1 tablet of EDTA-free protease inhibitor (Roche) and a spatula of lysozyme and stored at -80°C until use. Thawed pellets were lysed by alternating twice sonification (3 min at 4°C with 40% amplitude, 30 sec pulse, and 30 sec pause) and pressure lysis (1 000 to 1 500 bar, EmulsiFlex). All subsequent steps were performed at 4°C. The homogenate was centrifuged for 1 h at 16 000 rpm (JLA 16.250 rotor). The supernatant was applied twice on 20 mL Ni-NTA beads (pre-equilibrated with ME lysis buffer). The column was washed three times each, with 5 column volumes (CV) ME lysis buffer, then with 5 CV ME wash buffer 1 (300 mM NaCl, 50 mM Tris/HCl, 5 mM β Mercaptoethanol, 0.05% Tween20, 20 mM Imidazole, pH 7.4), and lastly with 5 CV ME wash buffer 2 (300 mM NaCl, 50 mM Tris/HCl, 5 mM β Mercaptoethanol, 0.05% Tween20, 40 mM Imidazole, pH 7.4). Elution was performed with 2 CV ME elution buffer (300 mM NaCl, 50 mM Tris/HCl, 5 mM β-Mercaptoethanol, 0.05% Tween20, 300 mM Imidazole, pH 7.4). The eluate was concentrated with an Amicon filter (50 kDa cut off) at 3 220 x g and pre-cleared for gel filtration at 17 000 x g. Preparative gel filtration was performed with an ÄKTApurifier (SuperdexTM 200 or SuperdexTM 200 HiLoad 16/60 prep grade, GE Healthcare) using SEC buffer (300 mM NaCl, 50 mM Tris/HCl, 5 mM β Mercaptoethanol, 5% glycerol, pH 7.4). Fractions of gephyrin trimers and oligomers were collected and concentrated by Amicon filters (50 kDa cut off) at 3 220 x g. Final proteins were snap frozen with liquid nitrogen, and stored at -80°C.

E. coli BL21 Rosetta star was used for the expression of His-LSβICD. The expression was performed as previously described34. Proteins were stored in 300 mM NaCl, 50 mM Tris/HCl, pH 7.4.

For the βICD peptide *E. coli* ER2566 (New England Biolabs) was used. Cultures grew at 37°C and 110 rpm until the OD600 reached 0.3. Induction was induced by 250 µM IPTG and expression performed for 20 h at 25°C and 110 rpm. Cells were harvested and stored at -80°C in ICD lysis buffer (300 mM NaCl, 50 mM Tris/HCl, 1 mM EDTA, 1x Protease Inhibitor (Roche), pH 7.4). Lysis of the thawed cells was performed by alternation of ultrasound (3 min at 4°C, 30 sec pulse, 30 sec pulse, 40% amplitude) and pressure lysis (EmulsiFlex, 1 000-1 500 bar, 4°C) twice. After centrifugation for 1 h at 16 000 x g (JLA 16.25 rotor) at 4°C, the supernatant was applied on a pre-equilibrated chitin matrix (New England Biolabs) and incubated 1.5 h at 4°C under shaking. The column was washed with 15 CV ICD buffer before 2.5 CV cleavage buffer (300 mM NaCl, 50 mM Tris/HCl, 1 mM EDTA, 50 mM DTT, pH 7.5) was applied an incubated for minimum 24 h at rt. The eluate was collected and another 2.5 CV cleavage buffer used for a second elution. The combined eluate was concentrated and filtered by Amicon filters with a cut-off of 10 kDa and 3 kDa. The buffer was exchanged to ITC buffer (300 mM NaCl, 50 mM Tris/HCl, pH 7.4) by dialysis over night at 4°C. The purified protein was stored at -80°C.

Circular dichroism (CD) spectroscopy

Recombinant gephyrin was buffer exchanged to CD buffer (10 mM K_2HPO_4/KH_2PO_4, pH 7.5) and centrifuged for 10 min at 17 000 x g at 4°C. The concentration was adjusted to 0.2 mg/mL. Measurements were obtained using the JASCO J-715 CD Spectropolarimeter and data evaluated using Spectra Manager Version 2.

Co-sedimentation assay

The previously described sedimentation assay[33] was adapted as followed. Recombinant gephyrin and LSβ were pre-cleared by centrifugation at 17 000 x g for 3 min at rt. Gephyrin and LSβ were mixed 10:10 µM in a final volume of 50 µL of assay buffer (150 mM NaCl and 50 mM Tris/HCl, 5 mM TCEP, pH 7.5). After incubation of 10 min at rt, samples were centrifuged 10 min and 17 000 x g. The supernatant was added into a new tube and supplemented with 15 µL 5x SDS sample buffer. The pellet was supplemented with 50 µL assay buffer and 15 µL 5x SDS sample buffer.

Isothermal titration calorimetry (ITC)

Gephyrin wt and ∆199-233 were buffer exchanged to ITC buffer (250 mM NaCl, 20 mM Tris/HCl, 5 mM β-mercaptoethanol, 5% glycerol, pH 7.5). Samples were pre-cleared by centrifugation for 10 min at 17 000 x g and the concentrations adjusted to 300 µM (βICD) and 30 µM (gephyrin). The ITC runs were performed with the MicroCal Auto-iTC200 (Malvern Panalytical) at 37°C with 40 individual injections (first injection: 0.5 µL in 1 sec; following injections: 1.25 µL in 2.5 sec), spacing in between injections of 2 min, and stirring speed of 750 rpm. βICD was titrated into gephyrin. Thermodynamic parameters were determined using the software Microcal analysis Origin 7.

Analytical size exclusion chromatography (SEC)

Typically, 1 nmol of recombinant protein was supplemented with SEC buffer (300 mM NaCl, 50 mM Tris/HCl, 5 mM β-Mercaptoethanol, 5% glycerol, pH 7.4) in a final volume of 30 µL. Samples were centrifuged for 10 min at 17 000 x g and 4°C before injection. Runs were performed with Superose 6 Increase 5/150 GL in SEC buffer. The calibration curve was obtained using a protein standard containing thyroglobulin (669 kDa), ferritin (440 kDa), aldolose (158 kDa), conalbumin (75 kDa), and ovalbumin (44 kDa).

Expression of EGFP-gephyrin and mCherry-DLC1 in COS7 cells

Coverslips were placed into 12-well plates and coated with collagen (0.2 mg/mL in DPBS) for 4 h at 37°C and afterwards washed with PBS twice. 40 000 COS7 cells (cultured in DMEM (+/+; Panexin Mix/Gln)) were seeded per well. Cells grew o/n at 37°C and were subsequently transfected using PEI with EGFP-gephyrin (pEGFPC2) and mCherry-DLC1 (pmCherry-C3). On the next day, the medium was replaced with fresh medium and expression was performed for another day (in total 48 h). Afterwards, cells were used for ICC.

Culture of hippocampal neurons and expression of recombinant gephyrin

At E17.5, dissociated primary hippocampal cultures were prepared from C57BL/6NRj embryos. 90 000 cells were seeded on Poly-L-lysine coated 13 mm cover slips in 24-well plates. Neurons grew in neurobasal medium supplemented with B-27, N-2, and L-glutamine (Thermo Fisher Scientific). At 10 days *in vitro* (DIV), cells were transduced with 2.5 x 108 viral genome copies (GC) by exchanging a third of the medium to virus-containing medium. The virus was prepared and detected according to previous protocols [33]. At DIV14 the cells were either fixed or at DIV13-15 used for electrophysiology experiments. In case of electrophysiology measurements, 50 mM NaCl were added at DIV11 to maintain osmolarity. If cells should be used for Western

blot analysis, cells were seeded Poly-L-lysine 24-well plates without cover slips. At DIV14, the medium was exchanged to 100 µL RIPA buffer (50 mM Tris/HCl, pH 7.5, 150 mM NaCl, 0.1% SDS, 1% IGEPAL CA360, 0.5% Sodium deoxycholate, 5 mM EDTA, 1x protease inhibitor (Roche)) and incubated for 10 min at rt under mild shaking. The detached cells were lysed by sonification (10 sec, 30%, 4°C) and centrifuged for 10 min at 4 000 x g. Approx. 30 µg of protein in the supernatant was used for SDS-PAGE.

Immunocytochemistry (ICC)

Fixation was performed by replacing culture medium by 4% PFA in PBS. After incubation for 20 min at rt, PFA was removed and cells washed twice with 50 mM NH_4Cl in PBS, each time 10 min at rt. Subsequently, cells were blocked for 1 h at rt with blocking solution (10% goat serum, 1% BSA, 0.2% TritonX100, in PBS). After washing cells with PBS for 5 min at rt, antibody incubation was performed for 1 h at rt. Antibodies were diluted in PBS. Afterwards, three washing steps with PBS were performed, each 10 min at rt. Treatment with secondary antibody and subsequent washing was performed in the same manner. In case of COS7 cells, staining with 300 nM DAPI in PBS was performed for 5 min at rt and an additional washing step of 10 min with PBS. Lastly, coverslips were mounted with Mowiol/Dabco and dried over night at rt. We used the following antibodies: rabbit anti-vesicular GABA transporter (vGAT) (1:1 000, #131003, SYSY), guinea-pig anti-$GABA_A$Rγ2 (1:500, #224004, SYSY), rabbit anti-PSD95 (1:500; #ab18258; Abcam), guinea-pig anti-vesicular glutamate transporter (vGLUT) (1:1 000; #AB5905; Millipore), goat anti-rabbit AlexaFluor 647 (1:500, #A-21245, Invitrogen), goat anti-rabbit AlexaFluor 488 (1:500, #A-11075, Invitrogen), goat anti-guinea-pig AlexaFlour 647 (1:500; #ab150187; Abcam).

Confocal microscopy and image analysis

Image stacks [0.33 µm z-step size, 10 stacks (=3 µm), 2048 × 2048 (144.77 × 144.77 µm)] were acquired on a Leica TCS SP8 LIGHTNING upright confocal microscope with an HC PL APO CS2 63×/1.30 glycerol objective, equipped with hybrid detectors (Leica HyD) and the following diode lasers: 405, 488, 552, and 638 nm. LIGHTNING adaptive deconvolution using “Mowiol” setting was applied. This form of adaptive image reconstruction is capable of theoretical resolutions down to 120 nm (lateral) and 200 nm (axial). Images were segmented and analyzed in an automated fashion using ImageJ/FIJI 1.53t. Therefore, the macros described by Liebsch et al.[32] were used as a blueprint and adapted. Furthermore, we used the plugin JaCoP to determine Mander’s co-localization coefficients (MCCs).

Electrophysiology experiments

Whole-cell patch-clamp recordings under current clamp and voltage clamp were conducted on primary cultures of murine hippocampal mScarlet- and Cre-moxBFP-tagged neurons between DIV13 and DIV15 at 30°C. Neurons were visualized with a fixed-stage upright microscope (Axio Examiner.D1, Carl Zeiss GmbH) using a water-immersion objective (Plan-Apochromat, 40×, 1 numerical aperture, 2.5 mm working distance, Carl Zeiss GmbH). The microscope was equipped with fluorescence and infrared differential interference contrast optics [50]. Red fluorescing gephyrin-positive cells were visualized with an X-Cite 120 illumination system (EXFO Photonic Solutions). Recordings were performed with an EPC9 patch-clamp amplifier (HEKA) controlled by the program PatchMaster (version 2 × 90.5, HEKA running on Windows 10). Data were recorded using a Micro1401 data acquisition interface (Cambridge Electronic Design Limited) and Spike 2 (version 7.08, Cambridge Electronic Design Limited). Data were sampled at 20 kHz and low-pass filtered at 10 kHz with a four-pole Bessel filter. Offline, the signal was smoothed by averaging the values in a ±0.001 s interval around any given datapoint . Electrodes with tip resistances between 4 and 6 MΩ were made from borosilicate glass (0.86 mm inner diameter; 1.5 mm outer diameter; GB150-8P, Science Products) with a vertical pipette puller (PP-830, Narishige).

During the recording, neurons were continuously superfused at a flow rate of ~2.5 ml min−1 with a carbonated (95% O_2 and 5% CO_2) extracellular saline containing (in mM): 125 NaCl, 21 $NaHCO_3$, 2.5 KCl, 2 $MgCl_2$, 1.2 NaH_2PO_4, 10 HEPES, 5 glucose, adjusted to pH 7.2 with NaOH. For the voltage clamp recordings, glutamatergic input was blocked with 5 × 10−5 m DL-2-amino-5-phosphonopentanoic acid (DL-AP5; BN0086, Biotrend Chemikalien GmbH) and 10−5 M 6-cyano-7-nitroquinoxaline-2,3-dione (CNQX; C127, Sigma-Aldrich). Na^+ mediated action potentials were blocked by 10−7 M tetrodotoxin (TTX; T-550, Alomone, Jerusalem BioPark). Current-clamp recordings were performed with a pipette solution containing (in mM): 140 K-gluconate, 10 KCl, 2 $MgCl_2$, 10 HEPES, 0.1 EGTA, adjusted to pH 7.2 with KOH.

For voltage clamp recordings of miniature IPSCs (mIPSCs), the patch pipette solution contained (in mM): 133 CsCl, 2 $MgCl_2$, 1 $CaCl_2$, 10 HEPES, 10 EGTA, adjusted with CsOH to pH 7.2. The liquid junction potential between intracellular and extracellular solution for current-clamp (14.6 mV) and voltage-clamp (6.3 mV) recordings were calculated using the LJPcalc software (https://swharden.com/LJPcalc; arXiv:1403.3640v2; https://doi.org/10.48550/ arXiv.1403.3640) and compensated accordingly.

Neurons were voltage clamped at −70 mV. Because of the high intracellular chloride concentration, $GABA_A$ R-mediated currents were detected as inward currents.

Data were analyzed at 50 s intervals after the recording stabilized (~10 min after obtaining whole-cell configuration). Data analysis was performed with Spike 2 (version 7.08, Cambridge Electronic Design Limited), Igor Pro 6 (version 6.37, Wavemetrics), and GraphPad Prism (version 10.2.3, GraphPad Software Inc.). mIPSC frequency, amplitude, and decay were determined offline. Events in voltage clamp traces were automatically detected by Easy Electrophysiology (developer pre-release version: v2.7.0, Joseph J Ziminski, www.easyelectrophysiology.com), when the signal crossed a threshold that was set and adjusted manually depending on the noise level of the signal. Events were classified as mIPSCs by template matching (correlation cutoff: 0.80; decay search period: 50 ms; baseline search period: 5 ms). The recording-specific template was calculated by fitting the average of prior threshold-detected and visually reviewed events. Parameters including frequency, amplitude, rise, and decay were determined. Statistical analysis between the genotypes was performed using a two-sided permutation test.

SDS-PAGE, Coomassie and Western Blot

Samples were supplemented with 1-2.5x sample buffer (5 x: 250 mM Tris/HCl pH 6.8, 30% glycerol, 0.1% bromophenol-blue, 5% β-mercaptoethanol, 10% SDS) and incubated for 5 min at 95-98°C. SDS PAGE was performed with running buffer (25 mM Tris/HCl, 190 mM glycine, 0.1% SDS). As markers, the PageRulerTM Plus Prestained Protein Ladder or the unstained Protein Molecular Weight Marker were used.

For Coomassie staining, the SDS gel was stained with Coomassie stainer (30% EtOH, 10% acetic acid, 0.25% Coomassie brilliant blue R250) and destained first in destainer solution (30% EtOH, 10% acetic acid) and afterwards with water. Gel pictures were obtained using the ChemiDocTM MP Imaging System by BioRad.

For Western blot analysis, SDS gels were blotted semi-dry on PVDF membranes using transfer buffer (25 mM Tris/HCl, 320 mM glycine, 10% MeOH, pH 8.8) o/n at rt (25 mA). Blocking was performed for 1 h in blocking solution (10% milk powder in TBST buffer (50 mM Tris/HCl, 150 mM NaCl, 0.05% Tween20, pH 7.4)). Incubation in primary (antibody diluted in antibody solution (1% milk powder in TBST buffer)) was done for 1 h at rt. After washing three times for 5 min with TBST, incubation with the secondary antibody (diluted in antibody solution) was done for 1 h at rt. Afterwards blots were washed twice for 5 min with TBST, and once for 5 min with water. The membrane was developed using ECL and the ChemiDocTM MP Imaging System (BioRad).

When subsequent antibodies were used, membranes were incubated twice for 10 min each with stripping buffer (15 g/L glycine, 1 g/L SDS, 10 mL/L Tween20, pH 2.2),

PBS, and lastly TBST. Then, antibody staining was performed as described in the previous section.

The following antibodies were used: mouse anti-GephyrinE (3B11; 1:10, self-made); rabbit anti-GAPDH (1:1 000, #G9545, Sigma), rabbit anti-PSD95 (1:1 000, #ab18258, Abcam); goat anti-mouse HRP-coupled (1:10 000, #AP181P, Sigma), goat anti-rabbit HRP-coupled (1:10 000, #AP187P, Sigma).

Statistics

Statistical tests and methods used to determine significance and error bars are described in each figure legend. Data points exceeding two-fold standard deviation were determined as outliers. Numbers of replicates (N) are indicated in each figure legend. Note, that in case of neuro cell culture experiments, 10 cells per condition (technical N=10) from 3 individually prepared pups (biological N=3) were analyzed (total N=30). In case of COS7 cells, 5 cells per condition (technical N=5) from 3 individual seedings (biological N=3) were analyzed (total N=15). For electrophysiology experiments (voltage clamp recordings), we used cell cultures from 3 individual pups (biological N=3) and analyzed 7-9 individual cells (technical N = 9 for wt and N = 7 for gephΔ199-233).

Acknowledgements

Technical help from Julia Reich is greatly appreciated. We thank Simon Tröder and Branko Zevnik as well as the whole CECAD TCU for the generation of the mouse line. We also thank Franziska Neuser and the Center for Mouse Genetics (CMG) of the University of Cologne for the organization of mice experiments. Lastly, we thank the imaging facility of the Cologne Biocentre of the University of Cologne. This work was financed by the german research foundation (DFG) (RTG2550 reloc to JR).

Conflict of interest

The authors declare no conflict of interest.

Study approval

We complied with all ethical regulations for animal testing and research. Experiments were approved by the local research ethics committee (German, Landesamt für Natur, Umwelt und Verbraucherschutz (LANUV) Nordrhein-Westfalen, reference 2016.A466).

4.7. References

1. Stallmeyer, B., et al., The neurotransmitter receptor-anchoring protein gephyrin reconstitutes molybdenum cofactor biosynthesis in bacteria, plants, and mammalian cells. Proc Natl Acad Sci U S A, 1999. 96(4): p. 1333-8.

2. Saiyed, T., et al., Molecular basis of gephyrin clustering at inhibitory synapses: role of G- and E-domain interactions. J Biol Chem, 2007. 282(8): p. 5625-32.

3. Grunewald, N., et al., Sequences Flanking the Gephyrin-Binding Site of GlyRbeta Tune Receptor Stabilization at Synapses. eNeuro, 2018. 5(1).

4. Kim, E.Y., et al., Deciphering the structural framework of glycine receptor anchoring by gephyrin. Embo J, 2006. 25(6): p. 1385-95.

5. Tretter, V. and S.J. Moss, GABA(A) Receptor Dynamics and Constructing GABAergic Synapses. Front Mol Neurosci, 2008. 1: p. 7.

6. Tretter, V., et al., Molecular basis of the gamma-aminobutyric acid A receptor alpha3 subunit interaction with the clustering protein gephyrin. J Biol Chem, 2011. 286(43): p. 37702-11.

7. Mukherjee, J., et al., The residence time of GABA(A)Rs at inhibitory synapses is determined by direct binding of the receptor alpha1 subunit to gephyrin. J Neurosci, 2011. 31(41): p. 14677-87.

8. Kasaragod, V.B. and H. Schindelin, Structure-Function Relationships of Glycine and GABA(A) Receptors and Their Interplay With the Scaffolding Protein Gephyrin. Front Mol Neurosci, 2018. 11: p. 317.

9. Maric, H.M., et al., Gephyrin-mediated gamma-aminobutyric acid type A and glycine receptor clustering relies on a common binding site. J Biol Chem, 2011. 286(49): p. 42105-42114.

10. Sassoe-Pognetto, M., et al., Colocalization of multiple GABA(A) receptor subtypes with gephyrin at postsynaptic sites. J Comp Neurol, 2000. 420(4): p. 481-98.

11. Alldred, M.J., et al., Distinct gamma2 subunit domains mediate clustering and synaptic function of postsynaptic GABAA receptors and gephyrin. J Neurosci, 2005. 25(3): p. 594-603.

12. Dejanovic, B., et al., Exonic microdeletions of the gephyrin gene impair GABAergic synaptic inhibition in patients with idiopathic generalized epilepsy. Neurobiol Dis, 2014. 67: p. 88-96.

13. El-Tallawy, H.N., et al., Gephyrin and CYP2C9 Genetic Polymorphisms in Patients with Pharmacoresistant Epilepsy. Pharmgenomics Pers Med, 2021. 14: p. 1133-1140.

14. Silva, J., et al., Modulation of Hippocampal GABAergic Neurotransmission and Gephyrin Levels by Dihydromyricetin Improves Anxiety. Front Pharmacol, 2020. 11: p. 1008.

15. Lionel, A.C., et al., Rare exonic deletions implicate the synaptic organizer Gephyrin (GPHN) in risk for autism, schizophrenia and seizures. Hum Mol Genet, 2013. 22(10): p. 2055-66.

16. Rees, M.I., et al., Isoform heterogeneity of the human gephyrin gene (GPHN), binding domains to the glycine receptor, and mutation analysis in hyperekplexia. J Biol Chem, 2003. 278(27): p. 24688-96.

17. Feng, G., et al., Dual requirement for gephyrin in glycine receptor clustering and molybdoenzyme activity. Science, 1998. 282(5392): p. 1321-4.

18. Schwarz, G., Molybdenum cofactor biosynthesis and deficiency. Cell Mol Life Sci, 2005. 62(23): p. 2792-810.

19. Johannes, L., C.Y. Fu, and G. Schwarz, Molybdenum Cofactor Deficiency in Humans. Molecules, 2022. 27(20).

20. Kumar, A., et al., S-sulfocysteine/NMDA receptor-dependent signaling underlies neurodegeneration in molybdenum cofactor deficiency. J Clin Invest, 2017. 127(12): p. 4365-4378.

21. Battaglia, S., et al., Activity-Dependent Inhibitory Synapse Scaling Is Determined by Gephyrin Phosphorylation and Subsequent Regulation of GABA(A) Receptor Diffusion. eNeuro, 2018. 5(1).

22. Flores, C.E., et al., Activity-dependent inhibitory synapse remodeling through gephyrin phosphorylation. Proc Natl Acad Sci U S A, 2015. 112(1): p. E65-72.

23. Kuhse, J., et al., Phosphorylation of gephyrin in hippocampal neurons by cyclin-dependent kinase CDK5 at Ser-270 is dependent on collybistin. J Biol Chem, 2012. 287(37): p. 30952-66.

24. Dejanovic, B., et al., Palmitoylation of gephyrin controls receptor clustering and plasticity of GABAergic synapses. PLoS Biol, 2014. 12(7): p. e1001908.

25. Zita, M.M., et al., Post-phosphorylation prolyl isomerisation of gephyrin represents a mechanism to modulate glycine receptors function. EMBO J, 2007. 26(7): p. 1761-71.

26. Fuhrmann, J.C., et al., Gephyrin interacts with Dynein light chains 1 and 2, components of motor protein complexes. J Neurosci, 2002. 22(13): p. 5393-402.

27. Sola, M., et al., Structural basis of dynamic glycine receptor clustering by gephyrin. EMBO J, 2004. 23(13): p. 2510-9.

28. Herweg, J. and G. Schwarz, Splice-specific Glycine Receptor Binding, Folding, and Phosphorylation of the Scaffolding Protein Gephyrin. Journal of Biological Chemistry, 2012. 287(16): p. 12645-12656.

29. Shen, Z.C., et al., Gephyrin Palmitoylation in Basolateral Amygdala Mediates the Anxiolytic Action of Benzodiazepine. Biol Psychiatry, 2019. 85(3): p. 202-213.

30. Kim, S., et al., Impaired formation of high-order gephyrin oligomers underlies gephyrin dysfunction-associated pathologies. iScience, 2021. 24(2): p. 102037.

31. Zacchi, P., R. Antonelli, and E. Cherubini, Gephyrin phosphorylation in the functional organization and plasticity of GABAergic synapses. Front Cell Neurosci, 2014. 8: p. 103.

32. Dejanovic, B. and G. Schwarz, Neuronal nitric oxide synthase-dependent S-nitrosylation of gephyrin regulates gephyrin clustering at GABAergic synapses. J Neurosci, 2014. 34(23): p. 7763-8.

33. Liebsch, F., et al., Automated Image Analysis Reveals Different Localization of Synaptic Gephyrin C4 Splice Variants. eNeuro, 2023. 10(1).

34. Bai, G., Y. Wang, and M. Zhang, Gephyrin-mediated formation of inhibitory postsynaptic density sheet via phase separation. Cell Res, 2021. 31(3): p. 312-325.

35. Macha, A., et al., Pentameric assembly of glycine receptor intracellular domains provides insights into gephyrin clustering. bioRxiv, 2022.

36. Ghosh, H., et al., Several posttranslational modifications act in concert to regulate gephyrin scaffolding and GABAergic transmission. Nat Commun, 2016. 7: p. 13365.

37. Legendre, P., The glycinergic inhibitory synapse. Cell Mol Life Sci, 2001. 58(5-6): p. 760-93.

38. Shiang, R., et al., Mutations in the alpha 1 subunit of the inhibitory glycine receptor cause the dominant neurologic disorder, hyperekplexia. Nat Genet, 1993. 5(4): p. 351-8.

39. Butler, M.H., et al., Autoimmunity to gephyrin in Stiff-Man syndrome. Neuron, 2000. 26(2): p. 307-12.

40. Zhu, S., et al., Demixing is a default process for biological condensates formed via phase separation. Science, 2024. 384(6698): p. 920-928.

41. Lee, G., et al., Thermodynamic modulation of gephyrin condensation by inhibitory synapse components. Proc Natl Acad Sci U S A, 2024. 121(12): p. e2313236121.

42. Herweg, J. and G. Schwarz, Splice-specific glycine receptor binding, folding, and phosphorylation of the scaffolding protein gephyrin. J Biol Chem, 2012. 287(16): p. 12645-56.

43. He, H.Y., et al., Experience-Dependent Bimodal Plasticity of Inhibitory Neurons in Early Development. Neuron, 2016. 90(6): p. 1203-1214.

44. Anderson, J.S., M. Carandini, and D. Ferster, Orientation tuning of input conductance, excitation, and inhibition in cat primary visual cortex. J Neurophysiol, 2000. 84(2): p. 909-26.

45. Scharfman, H.E., The neurobiology of epilepsy. Curr Neurol Neurosci Rep, 2007. 7(4): p. 348-54.

46. Gao, R. and P. Penzes, Common mechanisms of excitatory and inhibitory imbalance in schizophrenia and autism spectrum disorders. Curr Mol Med, 2015. 15(2): p. 146-67.

47. Williams, E. and J.P. Scott, The Development of Social Behavior Patterns in the Mouse, in Relation to Natural Periods. Behaviour, 1953. 6(1): p. 35-65.

48. Brust, V., P.M. Schindler, and L. Lewejohann, Lifetime development of behavioural phenotype in the house mouse (Mus musculus). Front Zool, 2015. 12 Suppl 1(Suppl 1): p. S17.

49. Belaidi, A.A. and G. Schwarz, Metal insertion into the molybdenum cofactor: product-substrate channelling demonstrates the functional origin of domain fusion in gephyrin. Biochem J, 2013. 450(1): p. 149-57.

50. Dodt, H.U. and W. Zieglgansberger, Infrared videomicroscopy: a new look at neuronal structure and function. Trends Neurosci, 1994. 17(11): p. 453-8.

4.8. Supplementary figures

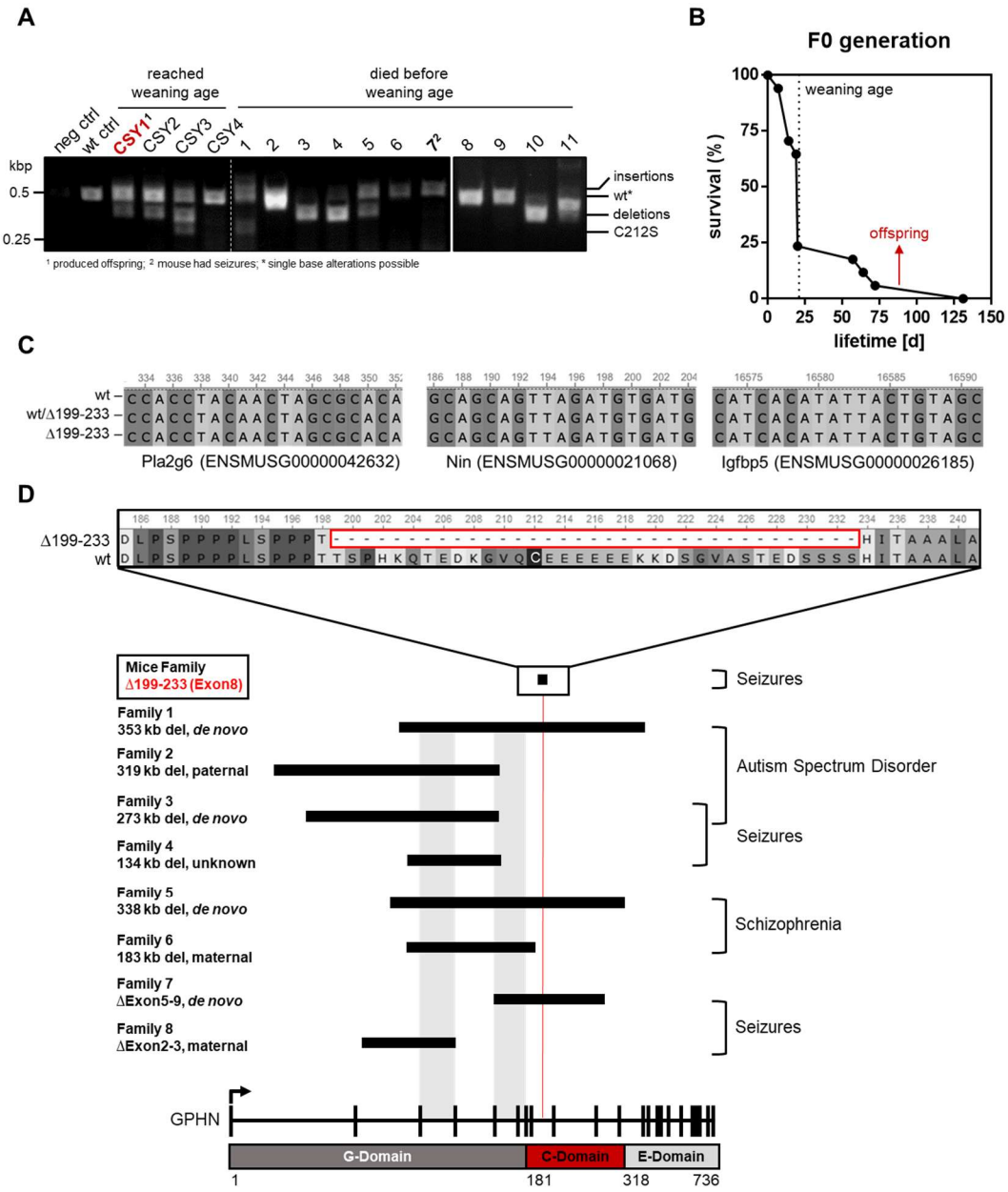

Figure S1: Generation of gephyrin C212S and gephyrin Δ199-233 KI mice
A) Genotyping of founder mice. PCR was designed to obtain amplicons around the area of the gRNA binding site. C212S point mutation identified, but several mice showed also insertions and deletions. Amplicons of expected wt-size can still carry single base alterations. Only mouse CSY1 was able to produce offspring. Mouse 7 had to be sacrificed after seizures. B) Survival rate [%] of the founder generation (F0). 25% mice reached weaning age. C) Alignment of off-target regions of the CRISPR/Cas guide RNA. Homozygous wt and Δ199-233 and heterozygous mice in comparison. D) Comparison of gephyrin deletion Δ199-233 in the new mice line with human patient deletions showing corresponding neuronal impairments. Deletions assigned to the different exons of the GPHN gene structure. Common exons shadowed in light grey. Specific region of gephyrin Δ199-233 enlarged.

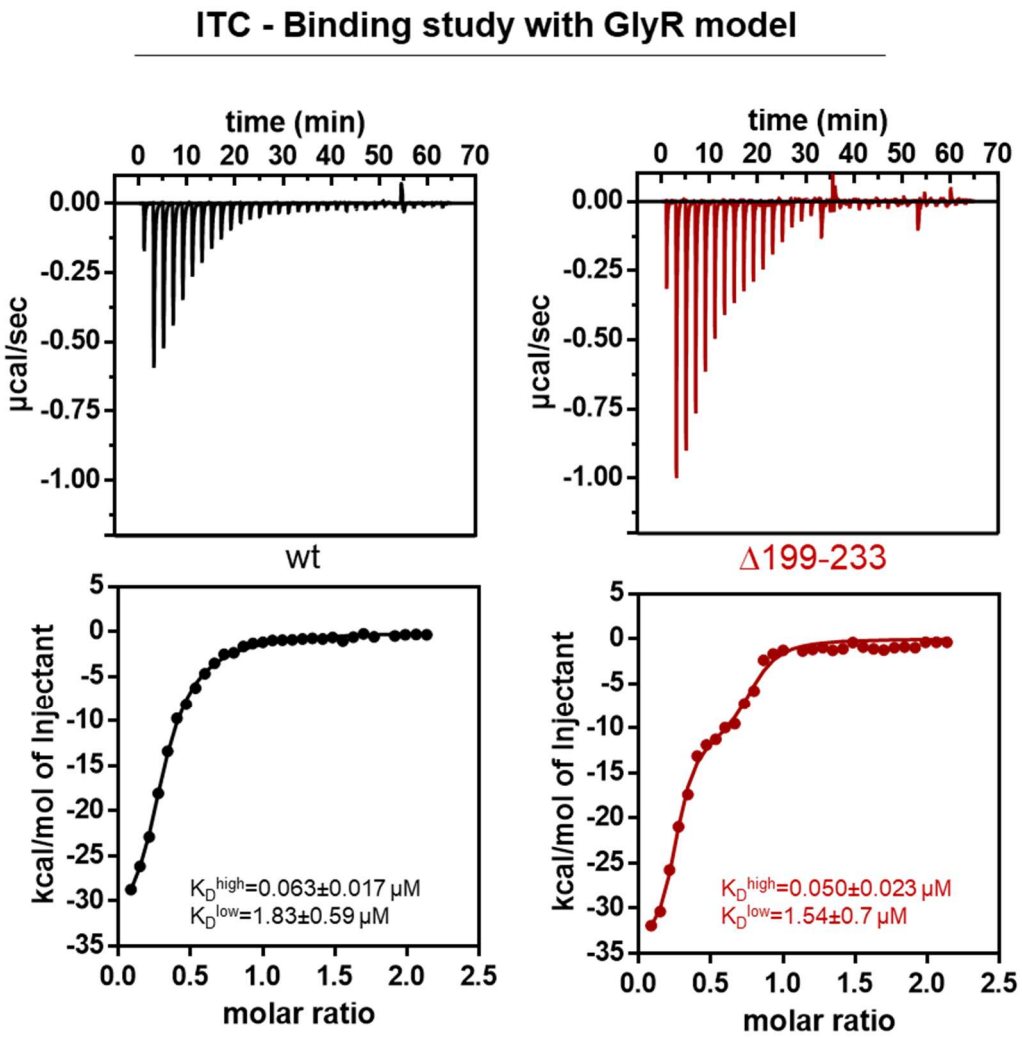

Figure S2: Receptor interaction study of gephyrin Δ199-233
A) Isothermal calorimetry titration experiment using GlyRβICD peptide as a model for the GlyR. The peptide was titrated into gephyrin. Data has been fitted with a two-binding site model giving a high and a low affinity dissociation constant (K_D^{high}; K_D^{low}).

Chapter 5

General Discussion

Gephyrin, as the central scaffolding protein at inhibitory GABA- and glycinergic post-synapses, determines the presence of synaptically clustered receptors and consequently inhibitory signal transmission (Kirsch et al., 1993; Fritschy et al., 2008). Clustering of gephyrin-receptor complexes is required for maintaining the interplay of excitation and inhibition (E/I) in the CNS, which is crucial for normal brain function and plasticity. Importantly, gephyrin function depends on three major biochemical properties: Localization (Dejanovic et al., 2014a), receptor interaction (Kim et al., 2006), and oligomerization (Kim et al., 2021). Understanding processes that control these features is of great interest, not only for understanding the onset of diseases and aging, but also for comprehending brain adaptation and plasticity in learning and memory. One type of mechanism controlling gephyrin function requires PTMs (Zita et al., 2007; Dejanovic et al., 2014a; Zacchi et al., 2014), of which thiol-based PTMs were the focus of this thesis.

This thesis sheds new light on the interplay of previously identified PTMs (S-palmitoylation, S-nitrosylation, phosphorylation and DLC-interaction) (chapter 2), presents a new redox-dependent regulation mechanism of gephyrin (chapter 3) and provides insight into the physiological importance of gephyrin C-domain and related specific PTM sites (chapter 4). The following sections will further discuss these key findings, their importance and interplay as well as their unexplored potential.

5.1 Reciprocal regulation of gephyrin S-nitrosylation and S-palmitoylation controls GABAergic synapses

5.1.1 Gephyrin regulation by the interplay of several PTMs

Gephyrin is crucial for controlling neurotransmission, making the investigation of its regulatory mechanisms essential for understanding processes influencing synaptic plasticity. One regulatory mechanism requires PTMs and gephyrin is subject to various PTMs such as phosphorylation (Zacchi et al., 2014), acetylation (Tyagarajan and Fritschy, 2014), SUMOylation (Ghosh et al., 2016) and cysteine modifications (Dejanovic and Schwarz, 2014; Dejanovic et al., 2014a). Importantly, the reversible nature of certain PTMs, such as phosphorylation, allows dynamic modulation of synaptic gephyrin function but also complicates spatial and temporal investigations.

Most PTMs occur in gephyrin's C-domain (Herweg and Schwarz, 2012; Dejanovic et al., 2014a; Ghosh et al., 2016). This may be due to the domain's accessibility to

modifying enzymes facilitated by its structural flexibility. However, the role of the C-domain may extend beyond structural connectivity to modulate gephyrin function. Various evidence suggests that the C-domain modulates receptor binding (Herweg and Schwarz, 2012; Grunewald et al., 2018). For instance, splice cassettes such as 'C3' alter the C-domain length and reduce gephyrin-receptor interaction (Herweg and Schwarz, 2012). Other findings indicate that the C-domain interacts with the low-affinity receptor binding site within the E-domain, influencing receptor binding (Grunewald et al., 2018; Macha, 2021). This might indicate that also PTM-independent influences of the C-domain on gephyrin function is possible. However, C-domain-mediated modulation of gephyrin function is not fully understood.

In non-neuronal tissue, gephyrin PTMs are less characterized and knowledge about its metabolic regulation is limited (Herweg and Schwarz, 2012). In contrast, at inhibitory synapses, gephyrin PTMs are well-studied and generally affect clustering, localization, stability, and receptor interaction. The large number of identified PTMs, sometimes with competitive (Tyagarajan et al., 2011; Kuhse et al., 2012) or reciprocal effects (Dejanovic and Schwarz, 2014; Dejanovic et al., 2014a), makes the understanding of a complex ‘PTM-interplayome’ challenging. Nonetheless, a few cross-talk mechanisms have been uncovered, such as the interplay of phosphorylation-dependent prolyl-isomerization (Zita et al., 2007) and the combined effects of phosphorylation, acetylation and SUMOylation (Ghosh et al., 2016).

This thesis explored the interplay of phosphorylation-dependent DLC interaction with S-nitrosylation and S-palmitoylation of gephyrin (chapter 2). Key findings include Thr205 in gephyrin C-domain as a phosphorylation site, potentially modified by Casein kinase I (CKI) (Kress, 2016) and Cys212 and Cys284 as S-nitrosylation targets, of which Cys284 was also confirmed by independent studies (Seneviratne et al., 2016). Additionally, a ternary complex involving nNOS, gephyrin, and DLC was identified, where gephyrin Thr205 phosphorylation inhibits DLC interaction. Since DLC is a known inhibitor of nNOS, Thr205 phosphorylation of gephyrin governs nNOS-mediated S-nitrosylation. Lack of S-nitrosylation enables S-palmitoylation at the same cysteines, indicating a competitive interplay between these modifications.

Evidence suggests that DLC has additional dynein-independent functions (Rayala et al., 2006; Morthorst and Olsen, 2013; He et al., 2018), supported by findings in this work. It was demonstrated recently that DLC interaction modulates the ability of gephyrin to undergo LLPS (1.6.6) (Bai et al., 2021). Since LLPS is suggested to be important for synaptic microdomain formation and contributes to diversity and complexity of PSDs (Bai et al., 2021; Lee et al., 2024; Zhu et al., 2024), the DLC-gephyrin interaction becomes important for the understanding of gephyrin LLPS regulation.

In summary, this work extends the role of DLC in synaptic transmission beyond acting as a transport adaptor. It highlights the role of DLC in regulating gephyrin S-palmitoylation and S-nitrosylation phosphorylation-dependent manner, with reciprocal effects on gephyrin synaptic clustering. With this an additional piece of the 'PTM-interplayome' of gephyrin was uncovered. But since another thiol-based PTM mechanism, a redox-dependent mechanism, has been discovered in this work (chapter 3), the interplay of S-palmitoylation, S-nitrosylation and redox-modifications on gephyrin's cysteines has to be investigated in future research.

5.1.2 Competition between S-palmitoylation and S-nitrosylation

S-palmitoylation and S-nitrosylation are reversible modifications on accessible cysteine residues with distinct mechanisms. S-palmitoylation is catalyzed by the family of palmitoyl-transferases (PATs) sharing a common catalytic zinc finger DHHC motive (ZDHHC) (Salaun et al., 2010). The specificity for targets and the subcellular distribution of each family member varies and the importance of this diversity is still under investigation (Cho and Park, 2016). Even more variety exists of de-palmitoylating enzymes, known as thioesterases, with the family of TE20 palmitoyl-protein thioesterases (PPT) (Swarbrick et al., 2020).

In contrast, the mechanism of S-nitrosylation is not fully understood. It is suggested that the likelihood of S-nitrosylation is a matter of exposure with local nitric oxide (NO), which is a ubiquitous signaling molecule and generated by nitric oxide synthases (NOS) or nitrate reductases (NR) (Tejada-Jimenez et al., 2019). Two mechanisms have been suggested: NO may either directly nitrosylate targets or S-nitrosylation occurs first on glutathione and is further transferred through *trans*-S-nitrosylation (Hess et al., 2005; Stomberski et al., 2019). Since the direction of *trans*-S-nitrosylation is determined by the redox-potential (Hess et al., 2005), it represents a dynamic mechanism to remove S-nitrosylation from cysteines. Additionally, enzymatic removal by Trx is one other possibilities (Chatterji and Sengupta, 2021b).

With regard to gephyrin, this study demonstrates a competitive relationship of S-nitrosylation and S-palmitoylation targeting the same Cys212 and 284 (chapter 2). The modifying enzymes were previously identified as DHHC12 (Dejanovic et al., 2014a) and nNOS (Dejanovic and Schwarz, 2014). In this work, a key element in the decision which thiol-PTM occurs, was the interaction of gephyrin and DLC, regulated by gephyrin phosphorylation. The interaction with DLC then determines the activity of nNOS and downstream NO production.

However, it is still unclear how S-nitrosylation prevents S-palmitoylation and *vice versa*. One aspect involves a concentration-dependent competition. For example, a certain NO level could prevent S-palmitoylation by blocking the same target thiol, since an already modified thiol cannot be further S-palmitoylated. Besides that, concentration-dependent S-nitrosylation could occur on the thiol residues of coenzyme A or DHHC enzymes, thus preventing S-palmitoylation (Hess and Stamler, 2012), but this requires the local proximity of both, the NO source and the S-palmitoylation machinery. Another aspect addresses the stability of each thiol-PTM. For instance, the question remains, whether S-palmitoylation is so stable, that it cannot be replaced by S-nitrosylation. With other words, it is unclear whether one type of thiol-PTM is a dead-end for other types of thiol-PTMs until removed. One fact supporting the stable nature of S-palmitoylation preventing further S-nitrosylation is the need of enzymatic removal (Swarbrick et al., 2020). In contrast, S-nitrosylation can be displaced through *trans*-S-nitrosylation by other thiols, such as omnipresent GSH (Hess et al., 2005). Moreover, NO is a better leaving group than palmitic acid. This indicates that the dose of bioavailable NO and nearby S-nitrosylated thiols is decisive for the occurrence and maintenance of S-nitrosylation of gephyrin and crucial for the competition with S-palmitoylation. Besides that, the substitution of Cys212 and Cys284, which means the absence of both thiol PTM types in gephyrin, resulted in S-palmitoylation-deficient-like reduction of cluster size, indicating that S-palmitoylation determines the growth of synaptic gephyrin clusters and is inhibited through S-nitrosylation. Thus, either removal of Cys or blockage through other PTMs prevents cluster growth inducing S-palmitoylation. In conclusion, nNOS-dependent NO concentration is a key step in inhibiting gephyrin synaptic clustering by S-palmitoylation (Figure 10).

However, since enzymatic and non-enzymatic mechanisms responsible for the removal of S-nitrosylation and S-palmitoylation of gephyrin have not been identified so far, the mechanistic decision whether gephyrin undergoes one or the other thiol-PTM cannot be precisely answered yet. The identification of additional regulatory steps, down- and upstream of S-palmitoylation and S-nitrosylation, offers potential to manipulate the competition between S-palmitoylation and S-nitrosylation, which might be disease relevant. This includes the identification of potential PPTs or kinases and phosphates regulating the phospho-dependent DLC interaction.

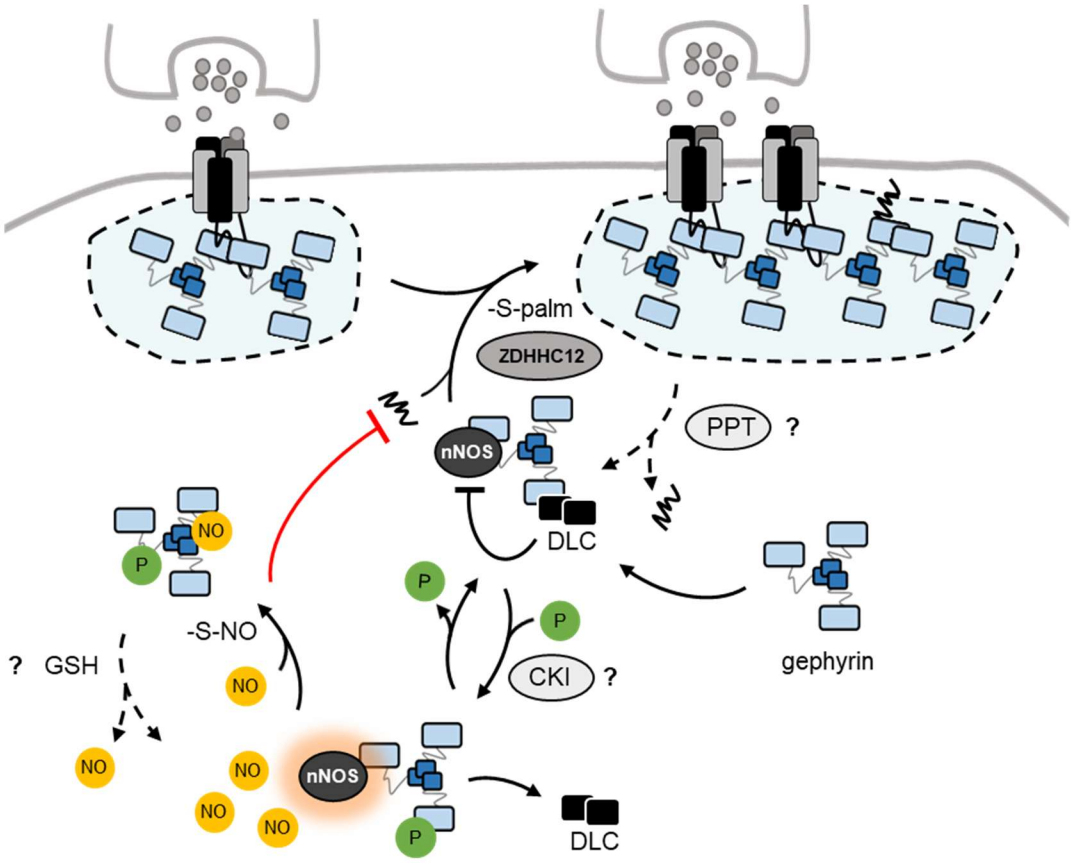

Figure 10: Postulated competition of S-nitrosylation and S-palmitoylation of gephyrin.
Gephyrin forms a ternary complex with dynein light chain (DLC) and neuronal nitric oxide synthase (nNOS). In this complex nNOS is inhibited by DLC. The inhibition of nNOS enables gephyrin S-palmitoylation through the protein palmitoyltransferase ZDHHC12 which triggers synaptic clustering of gephyrin. DLC-interaction of gephyrin can be prevented through gephyrin phosphorylation (green dot), possibly ('?') mediated by Casein kinase I (CKI). Leaving of DLC from the ternary complex activated nNOS-mediated NO production, which leads to S-nitrosylation of gephyrin. S-nitrosylation inhibits S-palmitoylation and thus synaptic clustering. Enzymes (protein palmitoyl thioesterase, PPT) and compounds (reduced glutathione, GSH) responsible for the removal of S-nitrosylation and S-palmitoylation of gephyrin have not been identified yet (indicated by '?').

5.1.3 Relevance of S-palmitoylation and S-nitrosylation

S-nitrosylation and S-palmitoylation are important PTMs influencing protein stability, localization and function (Stomberski et al., 2019; Yuan et al., 2024). Especially, S-nitrosylation and S-palmitoylation of synaptic proteins are involved in the regulation of neurotransmission (Dejanovic et al., 2014a; Nakamura and Lipton, 2016; Zareba-Koziol et al., 2019). Dysfunctions of these PTMs are linked to neuronal impairments (Nakamura and Lipton, 2016; Shen et al., 2019; Stykel and Ryan, 2024). For instance, it was reported that chronic stress in a mouse model altered the pattern of S-nitrosylated and S-palmitoylated synaptic proteins (Zareba-Koziol et al., 2019). Besides that, an increase of S-nitrosylation on the one hand and a decrease of S-palmitoylation of synaptic proteins on the other hand, was found in Huntington's, Parkinson's and Alzheimer's diseases (Cho and Park, 2016; Stykel and Ryan, 2024).

Interestingly, both PTMs target surface-exposed cysteines and thus, can have a competitive character when addressing the same residues. Thus, more studies addressed the investigation of the interplay of S-palmitoylation and S-nitrosylation and developed methods to monitor their cross-talk (PANIMoni = Palmitoylation and Nitrosylation Interplay Monitoring) (Zareba-Koziol et al., 2019). An interplay of S-nitrosylation and S-palmitoylation was identified for 122 synaptic proteins including receptors, scaffolding proteins, cytoskeletal components and more (Zareba-Koziol et al., 2019). PSD95 represents an established example of a synaptic protein that is reciprocally regulated through S-nitrosylation and S-palmitoylation on the same cysteines (Ho et al., 2011), which was demonstrated now through this work for gephyrin as well representing the other major class of post-synaptic proteins at inhibitory synapses. In both cases, S-nitrosylation leads to reduced synaptic targeting, while S-palmitoylation causes the opposite.

The mechanism why S-nitrosylation is causing smaller but more frequent gephyrin clusters (Dejanovic and Schwarz, 2014) might be relevant for understanding disease and aging processes. In AD, a general increase of S-nitrosylated synaptic proteins (Stykel and Ryan, 2024) as well as a reduction of gephyrin cluster sizes was observed (Kiss et al., 2016), indicating that gephyrin might be more frequently S-nitrosylated in AD. Considering the postulated competition mechanism between S-nitrosylation and S-palmitoylation (Figure 10), it might be possible that constitutive and abnormal gephyrin S-nitrosylation prevents S-palmitoylation-mediated cluster fusion and growth resulting in reduced synaptic plasticity.

However, the precise molecular effects of S-nitrosylation and S-palmitoylation on protein structure and function are not fully understood. So far it is known, that S-palmitoylation increases hydrophobicity and affinity for membranes (Tortosa and Hoogenraad, 2018). But the investigation of S-palmitoylated proteins is challenging, since methods are limited to so called ‘switch methods’, in which the palmitoyl-residue is exchanged to a label, used for indirect detection.

The recent development of an intrabody specific for PSD95 S-palmitoylation enabled deeper insight into the S-palmitoylation-driven molecular changes. With this, it was demonstrated that S-palmitoylation caused a conformational change in PSD95 (Fukata et al., 2013). Likely, more specific and direct S-palmitoylation detection systems will be invented. For gephyrin, the further characterization of S-palmitoylated species is limited to its low abundance with approximately 4% (Dejanovic et al., 2014a). Preliminary data based on circular dichroism (CD) analysis suggested that the secondary structure was unchanged for S-palmitoylated gephyrin (Dejanović, 2012). But in this experiment, protein with a low proportion of S-palmitoylated gephyrin species derived from insect

cells was used. Moreover, S-palmitoylation might affect the structural organization of the C-domain, which is often not visible in CD experiments due to the dominance of structured G- and E-domain.

Compared to S-palmitoylation, the investigation of S-nitrosylation is difficult due to another challenge. Although, S-nitrosylation is also a covalent attachment of a nitric oxide group on a cysteine, *trans*-S-nitrosylation represents one challenge to catch temporary targets, while also the stability was controversy discussed. Recently, evidence is given, that S-nitrosylation is more stable than initially believed (Chatterji and Sengupta, 2021a). In contrast to S-palmitoylation, antibodies against S-nitrosylated proteins as well as other kinds of detection methods exist (Chen et al., 2013).

To investigate the effects of S-palmitoylation and S-nitrosylation of gephyrin in more detail, one strategy performed in this work was the development of a non-enzymatic modification method for specific cysteine residues *in vitro* (supplementary data, 6.2). This included the substitution of specific residues to serines and the exposure to modifying reagents, such as S-nitroso glutathione (GSNO) and palmitoyl-Coenzyme A (palmCoA). Importantly, the secondary structure of gephyrin was unchanged upon substitution (chapter 3, S2). The success of gephyrin modification was optimized with pre-reduction and monitored through redox shift assays (supplementary data, 6.2). With this, it was possible to generate nearly 100% double-S-nitrosylated and to 50% single-S-palmitoylated gephyrin solely at Cys212 and Cys284 (supplementary data, 6.2).

The characterization of these S-nitrosylated and -palmitoylated species leaves great potential to understand the precise PTM-dependent molecular modulations on gephyrin in future research. For instance, the competitive character of both thiol-PTMs could be investigated by the additional trial to modify already modified gephyrin species. Besides that, the effects of modified gephyrin on receptor interaction, stability and lipid affinity can be investigated through diverse biochemical experiments such as isothermal titration calorimetry (ITC), CD spectroscopy and surface plasmon resonance (SPR) experiments. Uncovering the molecular changes induced by S-palmitoylation and S-nitrosylation holds great potential to understand the influence of these PTMs on neurotransmission and might also enable the development of antibodies targeting the modified species or the development of compounds inducing equal structural changes of the gephyrin backbone.

5.2 Redox-dependent synaptic clustering of gephyrin

5.2.1 Identification of redox-dependent synaptic regulation

Gephyrin contains eight surface-exposed cysteines (1.7.3), with Cys212 and Cys284 in the C-domain known to be targets of S-palmitoylation (Dejanovic et al., 2014a). In previous unpublished work, these cysteines were also suggested as targets for S-nitrosylation, a finding verified in this work (chapter 2). The roles of the other six surface-exposed cysteines 26, 154, 293, 419, 469 and 633 were previously unclear. Given the surface exposure of these cysteines and the identification of redox-signaling mechanisms at inhibitory synapses (Accardi et al., 2014), a redox-dependent regulation of gephyrin function was hypothesized (Marino and Gladyshev, 2010) (1.7.5).

Through various biochemical experiments, this work discovered that gephyrin's surface-exposed cysteines are redox-sensitive and can be oxidized *in vitro*, *in cellulo*, and *in vivo* (chapter 2). For example, manipulating the redox state of gephyrin, either chemically or enzymatically, revealed changes on gephyrin oligomerization and synaptic modulation. A key experiment involved isolation of gephyrin non-reductively from native murine brain tissue, showing clear multimers, that could be disrupted by chemical reduction. This demonstrated that gephyrin oxidation occurs through intermolecular disulfide bridges - a reversible process that covalently links gephyrin molecules within existing clusters. Consequently, upon oxidation, synaptic gephyrin clusters expand, become less sensitive towards proteolytic cleavage (1.6.4), and offer more $GABA_AR$ binding sites, thus enhancing inhibitory signal transmission.

Redox-dependent oligomerization through disulfide bridges has also been described for PSD95, chapsyn110 (PSD93) (Hsueh et al., 1997) and other synaptic proteins at excitatory synapses. Recent studies linked the reduction of disulfide bridges of PSD95 to chronic seizures in rats (Lee and Kim, 2020). Additionally, the interplay between PSD95 disulfide bridge formation and PSD95 S-nitrosylation was investigated, showing an independent relationship. However, the disease-association of gephyrin's redox-dependency and its interplay with S-nitrosylation (and S-palmitoylation and other PTMs) requires further investigation. It is possible, that other thiol-modifications must precede before oxidation occurs, likely on different cysteines. For example, S-palmitoylation could facilitate the recruitment of gephyrin to a sub-membranous synaptic localization (Dejanovic et al., 2014a), which might be rather oxidative than reductive (Lopez-Mirabal and Winther, 2008) to enable cysteine oxidation. In contrast, S-nitrosylation negatively regulates synaptic, sub-membranous localization of gephyrin (Dejanovic and Schwarz, 2014). Together, S-palmitoylation and S-nitrosylation may modulate gephyrin shuttling between different redox environments.

5.2.2 Relevance of redox-dependent synaptic regulation

Despite the unclear interplay of several thiol-PTMs, oxidation-mediated assembly and reduction-mediated disassembly of synaptic gephyrin clusters offer a dynamic mechanism for synaptic plasticity. Interestingly, around 20% of gephyrin in neuronal and non-neuronal murine tissue was found oxidized. Other modifications on gephyrin are also found only within a substoichiometric saturation of gephyrin, such as S-palmitoylation with 4% (Dejanovic et al., 2014a). This supports the hypothesis that gephyrin primarily exists in a cytosolic pool requiring specific signaling events such as PTMs for recruitment to the post-synapse. Identifying new regulatory principles, such as redox-dependent clustering, contributes to our understanding of the complexity and diversity of synapse formation and its plasticity, which also allows for therapeutic research. Redox-dependent clustering of gephyrin might offer an opportunity for therapies of imbalances of E/I (e.g. in aging and disease) (1.5) by the use of small molecule-driven manipulation of redox-states, for instance. The use of reductants could counteract hyper-inhibition, while oxidants could counteract hypo-inhibition.

To fully understand redox-signaling aspects and define therapeutic potentials, identifying the sources and precise targets of the underlying redox mechanisms is crucial. This thesis found that oxidation directly affected gephyrin's cysteines and is mediated by mitochondria as one possible ROS source, shedding light on the connection of mitochondria and synapses. But the hypothesized model of dynamic redox-dependent clustering of gephyrin requires, besides an oxidation source, also a reductive branch. In this work, chemical treatment with strong, non-physiological reductants such as DTT reversed oxidation-dependent oligomerization of gephyrin. More physiological reduction could be provided by the classic cytosolic reduction machineries, including enzymatic reduction by glutaredoxin (Grx) and thioredoxin (Trx) systems (Mailloux et al., 2013) (1.7.4). In case of PSD95, it was shown that the interaction with protein disulfide isomerase (PDI) was one possibility to reduce disulfide bridges of PSD95 (Lee and Kim, 2020). Although PDI becomes relevant for neurodegenerative diseases (Lee and Kim, 2020), it pre-dominantly localizes to the ER, thus a possible interaction with gephyrin might be unlikely (Matsusaki et al., 2020).

Interestingly, gephyrin co-localizes with GPx4 (Campbell et al., 2022), a GSH-dependent peroxidase enzyme, which converts lipids into their hydroxylated species. Importantly, lipid peroxidation is a key step in ferroptosis, an iron- and/or ROS-dependent form of regulated cell death being involved in neurodegeneration (Benarroch, 2023). GPx4 could use gephyrin as a substrate for its regeneration indicating that gephyrin might be part of an important redox system involved in neurodegeneration.

5.2.3 Synaptic ROS sources

For over a century, the relationship between mitochondrial and synaptic functions has fascinated scientists. Previous discoveries highlight the crucial role of mitochondria in maintaining neuronal health (Nicholls and Budd, 2000), particularly through their presence at synaptic sites. These synaptic mitochondria, distinct from their non-synaptic counterparts, are vital for calcium storage and buffering and essential for maintaining neuronal polarity, axon differentiation, and the rapid recovery required for effective neurotransmission (Faitg et al., 2021; Duarte et al., 2023). Additionally, ATP produced by these mitochondria is fundamental for numerous neuronal processes, including ion gradient and membrane potential maintenance, vesicle fusion, and neurotransmitter uptake (Nicholls and Budd, 2000).

A critical aspect of ATP production via OXPHOS is the inevitable generation of ROS as a byproduct (Turrens, 2003). This led to extensive research about the relationship between oxidative stress, neurodegeneration, and aging. Studies have shown that ROS-mediated hyperoxidation and mitochondrial dysfunction play significant roles in the onset of various diseases and aging processes (Moren et al., 2022). As a result, a wide range of antioxidants and ROS-preventing drugs, such as N-acetyl-cysteine (NAC) (Wu et al., 2019), melatonin (Sharif et al., 2017), and vitamins C and E (Wu et al., 2019), have been investigated for their potential in neuroprotection and treating conditions such as Alzheimer's, Parkinson's, and Huntington's diseases (Moren et al., 2022).

While some antioxidative treatments have shown promise, the role of ROS in neurotransmission is still being unraveled. The perception of ROS has shifted from being purely toxic to also being recognized as important signaling molecules modulating synaptic plasticity (Massaad and Klann, 2011). Understanding the delicate balance between beneficial and harmful ROS effects is crucial and requires further research to identify the molecular mechanisms involved. Most studies on redox manipulation in clinical contexts have so far mainly focused on the effects at excitatory synapses (Moren et al., 2022). This concentration is often due to the role of oxidative stress in neurodegenerative diseases and neurological injuries, where excessive activation of excitatory neurotransmitter systems and the associated cellular damage are predominant concerns. However, there is also research that highlights the effects of redox manipulation on inhibitory synapses, particularly regarding the regulation of neuroplasticity (Dejanovic and Schwarz, 2014). The regulated interplay between excitatory and inhibitory neurotransmission systems is crucial for neuronal activity and maintaining healthy brain function.

This thesis presents a novel gephyrin-dependent mechanism where mROS oxidize gephyrin's cysteines, triggering synaptic gephyrin-receptor clustering. This discovery

provides valuable insight into the interplay between neuronal and mitochondrial activity through gephyrin-dependent mROS signaling. The proposed hypothesis suggests a feed-forward mechanism where neuronal activity enhances mROS-mediated oxidation of gephyrin, leading to synaptic receptor recruitment. Additionally, it is hypothesized that initial neuronal activity, boosting mitochondrial activity and ROS production, may originate from neighboring excitatory synapse activity, supported by studies on NOX2-related ROS production (Larson et al., 2020) (1.7.5).

Previous research has shown that NOX2-dependent ROS production through excitatory synapse activity initiates a signaling cascade activating kinases at inhibitory synapses rather than directly oxidizing final targets (Larson et al., 2020). This NOX2-mediated ROS signaling is gephyrin-independent, contrasting with the mitochondria-mediated ROS signaling directly affecting gephyrin identified in this study. These findings suggest that various ROS-signaling mechanisms exist which may interact in a spatially organized way, presenting exciting avenues for future research into the redox-dependent modulation of synaptic plasticity.

In conclusion, this work sheds light on the sophisticated mechanisms by which ROS influence neuronal activity and synaptic function. Understanding these processes is essential for developing new therapeutic strategies for neurodegenerative diseases, highlighting the significant potential of this field for future discoveries.

5.2.4 Redox microenvironments

So far, it has been established that redox-signaling has emerged as an important mechanism for modulating synaptic activity. An additional aspect that needs consideration, is the assumption of different redox microenvironments (or microdomains) which drive further complexity and plasticity in redox processes. The existence of diverse compartmentalized redox-sources, machineries and the radius of action of ROS contribute to the formation of different cellular redox environments (Sies et al., 2024). The specific redox microenvironments of pre- and post-synapse are still unclear. To date, it has been assumed that the synapse is a reductive environment due to the connection to the reductive cytosol. This means that while oxidative processes can occur, they are usually rapidly reversed. But the finding of stable, mROS-mediated oxidized gephyrin multimers in this study supports to the hypothesis that microdomains exist which allow for not only the occurrence of oxidation, but also its maintenance. This hypothesis is further supported by the discovery of LLPS formation at inhibitory post-synapses creating such restricted microenvironments (Bai et al., 2021; Lee et al., 2024; Zhu et al., 2024) (1.6.6).

Cellular gephyrin LLPS is driven by the interaction with receptors and is further facilitated upon specific PTMs (Bai et al., 2021; Lee et al., 2024). This work has shown that gephyrin oxidation strengthens LLPS *in vitro*. However, the question remains, whether phase-separated gephyrin would leave condensates upon reduction or whether these condensates are reduction-resistant. In cell culture experiments, it was demonstrated that gephyrin's synaptic oligomerization is reversible by reduction (chapter 3). Thus, it is likely that gephyrin reduction is still possible in oxidative condensates, which is an important mechanism to prevent the formation of hyperoxidized, harmful aggregates.

To investigate this issue, unveil redox-microenvironments and decipher spatial and temporal redox-signaling, measurements of synaptic redox potentials would be desirable. Although, several well-established redox-sensors exist, no specific synaptic redox-sensor has been generated so far. One reason might be that so far, no universal synapse-targeting-motif has been discovered and distinct targeting to different synapses (e.g. excitatory vs inhibitory post-synapses) is not fully explored. To overcome this issue, one possibility is the fusion of a redox-sensor to a specific synaptic protein such as gephyrin. Assuming normal gephyrin clustering is maintained following such a fusion (similar to GFP), changes in the synaptic redox-potential upon synaptic and mitochondrial activity might be detectable. This approach holds great potential to track the delicate balance between beneficial and harmful ROS effects important for neurodegenerative and aging processes. Moreover, it might enable the investigation of redox-dependent cross-talk between organelles, neighboring synapses and many other research questions.

In a preliminary study within this work (supplementary data, 6.3), the redox-sensor Hyper7 (Jacobs et al., 2022) was expressed in primary, hippocampal neurons. The sensor was expressed in two fashions: one fused to the translocase of the outer membrane 20 (TOM20) to achieve an outer mitochondrial membrane localization, and one with a nucleus-export-sequence (NES) to achieve a global, cytosolic localization. Both sensor types were successfully expressed in neurons and showed signals corresponding to strong hyperoxidation. Although this hyperoxidation was reversible by DTT treatment, it is unclear whether under standard growth conditions of neurons such an oxidative environment was detected, or whether this was due to the chosen experimental condition. However, further optimization using different expression conditions, redox-sensors and fusion to different synapse-targeting-proteins could lead to the development of a suitable redox sensor to investigate synaptic redox environments.

In conclusion, this work might open the door to understand the relevance of synaptic redox microenvironments, potentially changing our current view on synaptic redox processes. This adds a new level to the role of ROS-signaling and extends the potential for future research further.

5.2.5 Potential gephyrin redox-regulation in a non-neuronal context

In this study, the redox-sensitivity of gephyrin was examined, alongside its enzymatic activity under redox-dependent conditions. Notably, the enzymatic activity of gephyrin was maintained after oxidation (supplementary data, 6.2) and Cys-to-Ser substitution of all surface-exposed cysteines (chapter 3, S3), although it was significantly reduced. The specific surface cysteines oxidized by H_2O_2 were not identified, but the reduction in enzymatic activity might be linked to the G-domain of gephyrin.

The G-domain is crucial for the adenylylation of MPT to AMP-MPT (Schwarz et al., 2001) (1.2). Interestingly, in the binding pocket, two cysteines (Cys26 and Cys154) align perfectly with nitrogen atoms of the substrates, as shown by the crystal structure alignment of MPT-bound G-domain plant homolog (cnx1 G-domain, PDB: 1UUY (Kuper et al., 2004)) and rat gephyrin G-domain (PDB: 1IHC (Sola et al., 2001)). This suggests that these cysteines may facilitate substrate interaction and enhance enzymatic activity. Consequently, the substitution of these cysteines with serine, or their modification through oxidation, could disrupt this thiol-dependent coordination, although the latter would be expected to prohibit substrate binding.

In other organisms, such as E. coli, the corresponding positions within the gephyrin G-domain ortholog (MogA, identifier: P0AF03 (Stallmeyer et al., 1999)) lack cysteines (Ala at Cys26, Thr at Cys154). If the hypothesized cysteine-dependent coordination of substrates holds true, the enzymatic activity of isolated MogA compared to the gephyrin G-domain should be reduced, a hypothesis that future research can explore. Additionally, the influence of cysteines within the E-domain and C-domain on gephyrin Moco activity remains unknown.

The question arises whether redox-regulation of gephyrin's Moco activity is feasible and if any evidence supports this hypothesis. This study found approximately 20% of gephyrin as oxidized multimers *in vivo* - in murine liver tissue, a key organ for Moco synthesis. Since the co-factor is redox-sensitive (Mendel, 2013), it is reasonable to down-regulate its synthesis under redox stress. Moco synthesis occurs partly in mitochondria, with intermediates transported into the cytosol. Stress-induced mROS production could downregulate gephyrin-dependent Moco synthesis near mitochondria, reducing mitochondrial energy demands by down-regulating this ATP-dependent

process. Additionally, MPT accumulation might downregulate upstream Moco synthesis (MOCS) enzymes (Mayr et al., 2021) in a feedback loop, further reducing mitochondrial energy challenges under stress. However, gephyrin shows diffuse cytosolic distribution in non-neuronal, Moco-productive tissue (Nawrotzki et al., 2012), suggesting specific subcellular localization near mitochondria is unlikely. Thus, only a portion of gephyrin might undergo mROS-dependent redox-regulation, ensuring partial and reversible downregulation of Moco production.

Although speculative, the potential regulation of gephyrin's Moco activity is intriguing and unexplored. For gephyrin-dependent MoCD (MoCD type III), no therapeutic treatment exists. Understanding regulation mechanisms that enhance Moco activity could aid in developing treatment options. For instance, antioxidant treatment might prevent gephyrin oxidation, thereby increasing the activity of residual functional gephyrin species in MoCD type III patients.

5.3 GephyrinΔ199-233 - an epileptogenic microdeletion

5.3.1 Lethality of gephyrin ∆199-233

Several PTMs of gephyrin regulating its synaptic function have been previously investigated, primarily through *in vitro* and *in cellulo* experiments (Herweg and Schwarz, 2012; Kuhse et al., 2012; Dejanovic and Schwarz, 2014; Dejanovic et al., 2014a). This work adds new insight into the interplay of thiol-based PTMs such as S-palmitoylation and S-nitrosylation (chapter 2) and has discovered a new redox-dependent regulation mechanism (chapter 3) of gephyrin. However, the majority of experiments was performed *in vitro* and *in cellulo*. To further understand the importance of PTM-based gephyrin regulation, *in vivo* models addressing specific PTMs are desirable. This work aimed to substitute Cys212 of gephyrin to Ser in a mouse model to investigate the absence of S-nitrosylation and S-palmitoylation at this specific residue *in vivo* (chapter 4). CRISPR/Cas9 gene editing resulted in several microdeletions in addition to the intended Cys212-to-Ser substitution. Importantly, a high mortality was observed in the founder generation, with only one mouse producing offspring, indicating the crucial nature of the targeted region. The offspring carried the microdeletion ∆199-233, which was established and investigated further (chapter 4). Off-targets of gene editing could be excluded.

Compared to known microdeletions in human patients of epilepsy, schizophrenia and autism (Lionel et al., 2013; Dejanovic et al., 2014b), the microdeletion investigated in this work is smaller and targets only the C-domain of gephyrin. This new variant,

gephyrin ∆199-233, holds great potential for understanding the importance of the C-domain and its corresponding PTMs and binding motifs for gephyrin's synaptic function.

Crossing of heterozygous mice resulted in only half of the expected number of homozygous ∆199-233 mice (∆/∆), according to Mendelian rules, thus complicating the generation of enough animals for all experiments. Alternatives *in vitro* and *in cellulo* had to be considered still. The embryonic mortality might indicate prenatal absorbance in the uterus (Papaioannou and Behringer, 2012). This hypothesis is supported by the fact, that born litters were usually found immediately after birth due to tight control windows and even dead pups provided sufficient material for genotyping. To further test for prenatal mortality, it will be necessary to prepare and genotype embryos at key steps of gestation (Papaioannou and Behringer, 2012). For example, at E12.5, it can be distinguished whether embryonic implantation is disturbed (Papaioannou and Behringer, 2012). However, since this process results in the sacrifice of the mother and the whole litter, additional uses for the sacrificed animals, such as IHC or electrophysiology experiments, are justified. Importantly, dysfunctions of gephyrin are associated with postnatal lethality (Feng et al., 1998). The generation of a gephyrin knock-out resulted in the expected distribution of genotypes (Feng et al., 1998). Since the phenotype of gephyrin ∆199-233 is less severe than that of gephyrin knock out, a role of gephyrin for embryogenesis might be unlikely.

High-mortality was apparent within the first five days after birth, especially in litters containing at least one ∆/∆ pup. Possible explanations include either stillbirth, sudden death or maternal neglect. Previous studies suggest that laboratory mice do not actively kill their litters (Weber et al., 2013) but rather remove already dead ones. Thus, the observed high-mortality of pups was likely not initially caused by the mother. Stress caused by dead ∆/∆ pups might still impair maternal care, resulting in neglect of the litter.

The phenotype of homozygous ∆199-233 mice included epileptic-like seizures, sudden death and reduced body weight manifesting after 16-19 days of life. Reduced body weight is also present in mouse models of MoCD type I and II and sulfite oxidase deficiency (SOXD) (Lee et al., 2002; Jakubiczka-Smorag et al., 2016; Fu et al., 2024). Thus, MoCD type III caused by the gephyrin microdeletion 199-233 was considered (1.5). Investigation of MoCD biomarkers showed no indication of MoCD and gephyrin ∆199-233 exhibited normal Moco activity *in vitro*. Human patients with MoCD and SOXD suffer from neuronal impairments (Reiss and Johnson, 2003), but mice models do not develop these phenotypes, as they die earlier (Lee et al., 2002; Fu et al., 2024). Therefore, weight reduction and neuronal impairments in ∆/∆ mice are likely due to altered neuronal function of gephyrin.

In summary, the phenotype of homozygous gephyrin ∆199-233 mice appeared lethal likely due to impaired neuronal function of gephyrin. Notably, only 7% mice from wt/∆ x wt/∆ crossings resulted in ∆/∆ mice (equals 12 animals) usable for follow up experiments. This finding is surprising, since G- and E-domains of gephyrin are not directly affected, highlighting the so far less important function of gephyrin's C-domain. This work presents – to my knowledge – for the first time, that a small deletion of the C-domain causes a severe phenotype in an *in vivo* model.

5.3.2 Pathogenicity of gephyrin ∆199-233

To understand the lethality caused by gephyrin ∆199-233, it is necessary to define its pathogenicity on a molecular level. The microdeletion ∆199-233 targets Cys212 (the target of S-palmitoylation (Dejanovic et al., 2014a) and S-nitrosylation (chapter 2)), the high-affinity binding motif of DLC (residue 203-212) (Fuhrmann et al., 2002; Bai et al., 2021), the last three amino acid residues (residue 199-201) of the Pin1 interaction motif (residues 188-201) (Zita et al., 2007) and phosphorylation sites Thr199, Ser200, Thr205, Ser222, Ser226 and Thr227 (Zita et al., 2007; Herweg and Schwarz, 2012). Thus, a pathogenicity could potentially be caused by the absence of PTMs and/or loss of interaction with the respective binding partners.

Starting with well-characterized PTMs, S-palmitoylation of gephyrin ∆199-233 was explored. In brain tissue of ∆/∆ mice, a 50% reduction of S-palmitoylated gephyrin was observed, consistent with previous studies suggesting that Cys212 is the predominant S-palmitoylation site and Cys284 could not compensate (Dejanovic et al., 2014a). Accordingly, synaptic targeting of gephyrin ∆199-233 was reduced in cell culture experiments. Strikingly, lack of S-palmitoylation caused reduced sizes of synaptic gephyrin clusters previously (Dejanovic et al., 2014a), but was neither observed for gephyrin ∆199-233 in this work, nor in studies using gephyrin species (∆181-243) lacking more than Cys212 (Fuhrmann et al., 2002). This suggests that additional mechanisms influence synaptic function of gephyrin and might counteract the lack of S-palmitoylation in gephyrin ∆199-233.

One possible mechanism is the absence of the high-affinity binding site for DLC. Considering the here reported ternary complex of gephyrin, nNOS and DLC and the role of DLC for gephyrin S-palmitoylation and S-nitrosylation presented in this work (chapter 2), an even stronger reduction in cluster sizes would be expected. In the ternary complex with gephyrin ∆199-233, DLC is absent, allowing activation of nNOS and S-nitrosylation of gephyrin, inhibiting S-palmitoylation. This dual disturbance of S-palmitoylation, through the absence of the main target Cys212 and through nNOS-mediated S-

nitrosylation at Cys284, is expected to result in reduction of gephyrin cluster sizes. Thus, a DLC-dependent mechanism explaining sufficient clustering of gephyrin ∆199-233 can be excluded and other causes need to be considered.

Another mechanism of altered synaptic gephyrin clustering could involve phosphorylation sites within the ∆199-233 region. Most of these were detected *in vitro* and their physiological importance has not been fully defined yet (1.6.1) (Herweg and Schwarz, 2012). Thus, a comparative analysis of their effects was not addressed in this work and is left for future research. The only characterized phosphorylation site, Ser200, regulates the interaction of gephyrin with Pin1 (Zita et al., 2007) (1.6.5). Previous work demonstrated that the absence of Ser200 led to residual gephyrin-Pin1 interaction (Zita et al., 2007), suggesting that Pin1-mediated *cis-trans*-isomerization, required for synaptic GlyR recruitment, is likely maintained for gephyrin ∆199-233. This hypothesis is further supported by the observed type of neuronal impairment in ∆/∆ mice, which do not show the typical phenotype of impaired glycinergic transmission such as stiffness (Shiang et al., 1993; Butler et al., 2000).

In conclusion, no addressed PTM fully explains the observed synaptic clustering behavior of gephyrin ∆199-233. An alternative pathogenicity mechanism of gephyrin ∆199-233 could be an altered structure. Analysis of the secondary structure revealed no difference of wt and gephyrin ∆199-233, but it needs to be considered that the C-domain is flexible and structural changes might occur only in the presence of binding partners. Indeed, binding studies with receptor models (Grunewald et al., 2018; Macha et al., 2022) showed an unexpected, facilitated binding property for gephyrin ∆199-233 derived from E. coli. Considering that gephyrin's PTMs are absent when expressed in E. coli, it is likely that the effects on receptor binding are potentially induced by PTM-independent structural properties of the C-domain.

The full-length C-domain could interact with dimerized E-domains, masking parts of the low-affinity binding site for the receptor (1.4) (Figure 11). In gephyrin ∆199-233 this masking could be absent, facilitating receptor binding. This hypothesis is supported by previous studies, observing cross-linking between gephyrin C- and E-domains (Macha, 2021) (unpublished data). But the C-domain could also interact with receptor ICDs, modulating gephyrin-receptor interaction. Previously, it was shown that the C-domain indeed interacted with the peptide of the GlyR β-ICD (Grunewald et al., 2018). Thus, it is possible that the C-domain modulates ICD structures, either influencing gephyrin binding or - directly or through neighboring lipids - affecting the gating mechanism of receptors (Figure 11). Interestingly, the microdeletion ∆199-233 contains a negatively charged glutamate hexa-repeat sequence (residue 213-218), which could modulate the gephyrin-receptor interaction based on non-covalent interactions (Grunewald et al., 2018).

Charged residues can influence protein folding and stability, solubility and the ability to undergo LLPS (Zhou and Pang, 2018). Charged residues can also influence lipid interactions (Machin et al., 2023), which was not demonstrated for gephyrin in an S-palmitoylation-independent manner yet.

Due to the flexibility of the C-domain, the structure of full-length gephyrin and the structural arrangement caused by receptor interaction have not been solved yet. Solving the structure offers potential to uncover the precise influence of the C-domain, including the glutamate hexa-repeat motif and complete microdeletion ∆199-233, on gephyrin structure and function and could answer the question, whether and how the C-domain possibly influences the receptor.

To further decipher the importance and contribution of the different deleted PTMs for the synaptic function of gephyrin ∆199-233, additional gephyrin variants should be generated and characterized. Comparative analysis of S-palmitoylation-deficient gephyrin Cys212Ser, DLC-binding-deficient variants (T205E, ∆203-211; still allowing for S-palmitoylation), a variant lacking the glutamate motif (∆213-218) and lastly, a variant lacking the last residues of the Pin1-interaction motif (∆199-201) could help to understand the contribution of each PTM for the phenotype of gephyrin ∆199-233. Furthermore, each phosphorylation site could be characterized by the generation of phosphor-mimetic and phospho-deficient variants using glutamate/aspartate and alanine/glycine substitutions, respectively.

In summary, this work suggests an interplay of different mechanisms affecting synaptic targeting of gephyrin ∆199-233 through disturbed S-palmitoylation for instance on the one hand and potentially facilitated receptor interaction through structural changes on the other hand. The combined result is manifested as reduced inhibitory transmission which also caused adaptations on excitatory synapses, a possible sign of an E/I balancing/regulating mechanism (Froemke, 2015; He et al., 2016). Impaired interplay of E/I may result in hyperexcitation in ∆/∆ mice causing neuronal impairments such as epileptic-like seizures and sudden death (Smolarz et al., 2021; Vlachou, 2022). The observed changes at the excitatory synapse might represent a trial to balance increased inhibition in ∆/∆ mice, which might work until a certain time window in early development, until the system collapses. This hypothesis fits to the appearance of neuronal impairments after the first two weeks of life (P14), when mice develop complete sensory receptivity and experience more excitation (Williams and Scott, 1953).

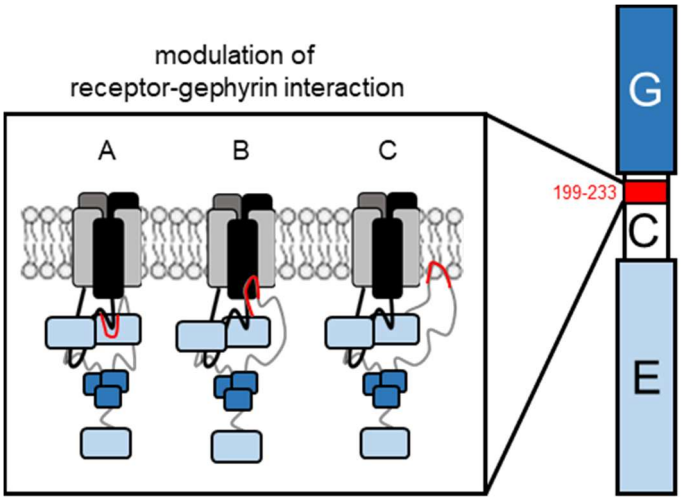

Figure 11: Postulated modes of loss of function in gephyrin Δ199-233 influencing receptor binding.
The region 199-233 (red) could modulate the gephyrin-receptor interaction through three mechanisms: A) the region masks the low-affinity binding site within the dimerized gephyrin E-domain (light blue), B) the region interacts with the receptor ICD, or C) the region interacts with neighboring lipids. Each mechanism could affect inhibitory neurotrans-mission.

5.3.3 Mouse with gephyrin Δ199-233 as disease model

Few mouse models exist that allow the investigation of gephyrin function *in vivo*. One early mouse model was a full-body knock out of gephyrin, which was lethal within the first day after birth (Feng et al., 1998), leading to the generation of conditional knock out mice (O'Sullivan et al., 2016). These conditional knock out models allow for preparation of neuronal cell culture and stereotactic injections to apply desired gephyrin variants in specific brain regions and drive knock out in chosen manners. Previously, gephyrin variants associated with diseases were typically investigated in cell culture experiments using neurons with an endogenous gephyrin background (Dejanovic et al., 2015).

To judge whether the mouse model generated in this work is a suitable disease model, the precise phenotype of Δ/Δ mice needs to be fully characterized in future research. One challenge is the diversity of individual neurological symptoms per mouse, a manifestation of disturbed GABAergic transmission in several manners. This diversity of symptoms could be further influenced by epigenetic factors, increasing biological diversity. Although off-target effects have been excluded, gephyrin-dependent (but MoCD unrelated) effects from the periphery may enhance the difficulty of clearly defining the neuronal phenotype of Δ/Δ mice. Generation of conditionally modifiable mice, for instance targeting specific brain regions, would be an alternative approach. However, since human patients also suffer from ‘full-body’ gephyrin impairments, the gephyrin Δ199-233 mouse model remains suitable and periphery-induced effects should not be excluded from the investigation of diseases.

A possible hypothesis explaining the phenotype, is that Δ/Δ mice suffer from epilepsy causing several symptoms (Batterman et al., 2019). Epilepsy could be monitored via brain activity in EEGs (Engel, 1984) or through specific detection of

epilepsy markers in IHC experiments (Pitkanen et al., 2019). The latter method might be more suitable with regard to Δ/Δ mice, since these mice develop the phenotype before weaning age and cannot be separated from their mother. Another challenge in IHC is the staining for gephyrin itself. Although different detection methods for gephyrin exist, staining in tissue is still in the process of optimization (Khayenko et al., 2022).

Under the premise that gephyrin Δ199-233 is indeed causing epilepsy, the mouse model generated in this work complements already existing epilepsy models (Kandratavicius et al., 2014). To my knowledge, it is the first *in vivo* model that allows for the specific investigation of gephyrin dependency in epileptogenesis. This opens the door for investigating the age-dependency and onset of epileptogenesis. Additionally, the gephyrin Δ199-233 mouse model could be used for the investigation of treatment options (Griffin et al., 2013), which could prolong the life-span of mice suffering from severe epilepsy and thus allow for methods that require adult mice such as behavioral studies.

It is still possible, that the pathogenic mechanism and the neuronal disease are different than expected in gephyrin Δ199-233 mice. Nevertheless, this mouse model holds great potential to further examine the role of gephyrin in epileptogenesis, other disease onsets or the development and characterization of treatment options.

5.3.4 Effects of gephyrin on the action potential

Preliminary examinations of APs in cell culture experiments suggested that the mouse model generated in this work holds great potential to uncover new gephyrin-dependent functions in neurotransmission. To my knowledge, this is the first time the effect of a gephyrin variant on the AP has been investigated, besides the classical measurements of mIPSCs.

Surprisingly, a significant alteration of the AP was observed in gephyrin Δ199-233 expressing neuronal cell cultures (chapter 6, 6.4). The AP shape was sharper, with higher depolarization and lower repolarization rates. This alteration is likely due to changes in ion influx through Na^+ and K^+ channels, respectively. An altered AP likely also affects the target pre-synapse (Bischofberger et al., 2006), influencing neurotransmitter release and thus neurotransmission. This finding indicates a novel role of gephyrin for AP generation, beyond its known and classical role at inhibitory sites. To which extend alterations in AP were the result of gephyrin-dependent changes in mIPSCs or there are gephyrin-dependent functions in the axons will be the subject of future studies.

In conclusion, it is possible that gephyrin either directly or indirectly influences Na^+ and K^+ channels which extends gephyrin's known neuronal function. Previous analysis of the gephyrin interactome indicates no direct interaction with Na^+ and K^+ channels

(Campbell et al., 2022), suggesting an indirect influence is more likely. Nevertheless, the question remains, whether this effect on the AP is limited to the gephyrin variant Δ199-233, or if it also applies for other gephyrin variants. Future studies should examine whether other disease-associated gephyrin variants, such as G375D (Dejanovic et al., 2015), could also affect APs.

Investigating this new role of gephyrin could enhance its importance and change the current view on its role in the pathogenesis of neuronal diseases, potentially extending therapeutic strategies.

5.4 Closing remarks

This work provided novel insight about the 'interplayome' (interplay of PTMs) by demonstrating the formation of a ternary complex involving gephyrin, DLC and nNOS, which regulates the competition between S-palmitoylation and S-nitrosylation. This competition is based on a postulated dose-dependency of nNOS-mediated NO production promoting S-nitrosylation and thus preventing S-palmitoylation-induced synaptic cluster growth. Initially, DLC acts as an inhibitor of nNOS activity within the ternary complex and its release upon gephyrin phosphorylation at Thr205, reveals a dynein-independent function.

Additionally, a novel redox-dependent mechanism involving eight surface exposed cysteines was identified. This mechanism involves mROS-mediated oxidation, leading to disulfide bridge formation among gephyrin molecules, which enhances receptor recruitment and strengthens inhibitory transmission. This finding underscores the critical link between mitochondrial function and neuronal activity, crucial in the context of disease and aging.

In summary, this work elucidated how three types of thiol-based PTMs (S-palmitoylation, S-nitrosylation, redox) dynamically influence synaptic function of gephyrin, crucial for synaptic plasticity (Figure 12, Figure 13). However, the interplay of S-palmitoylation/S-nitrosylation and redox-dependent Cys modifications and the pathways responsible for their removal remain unclear, presenting fertile ground for future research. Thiol-PTMs are also relevant for the regulation of other synaptic proteins and are related to neuronal diseases. Insight into molecular mechanisms affecting the modification status of Cys is necessary to develop therapy strategies. The presented, specific mechanisms of gephyrin thiol-based regulation might represent an important example for other synaptic proteins and could offer future therapy approaches.

Besides that, this work established a new mouse model expressing gephyrin with a microdeletion (Δ199-233). The phenotype was unexpectatly severe, marked by neuronal impairments. Beyond disrupted PTMs (predominantly S-palmitoylation) impairing synaptic targeting, this variant revealed PTM-independent structural influences on receptor binding (Figure 13). Different mechanisms are possible, ranging from direct to indirect influences on the receptor-gephyrin-interaction. Further studies are needed to elucidate the precise mechanisms involved, including the contribution of each PTM. Given its observed embryonic lethality, exploring gephyrin's role in embryogenesis is imperative for future research.

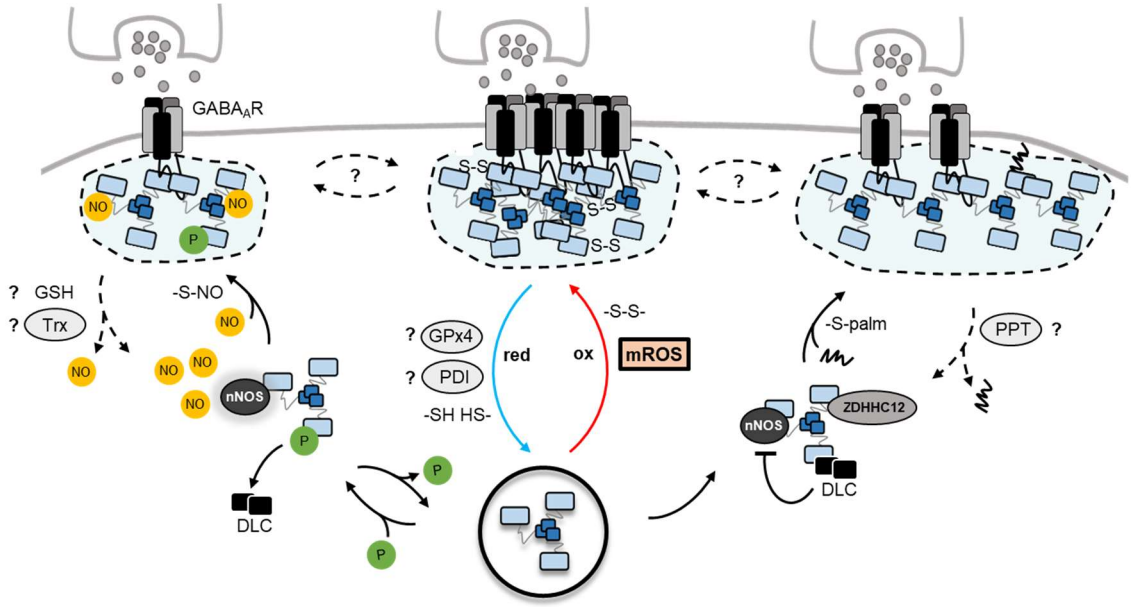

Figure 12: Thiol-based PTMs regulating gephyrin synaptic clustering.
Gephyrin undergoes S-palmitoylation (-S-palm), S-nitrosylation (-S-NO) and redox modifications (-S-S-/-SH HS-) on surface cysteines. S-nitrosylation and reduction reduce gephyrin cluster sizes, while S-palmitoylation and oxidation cause an increase. S-palmitoylation and S-nitrosylation are regulated through the ternary complex of gephyrin, nNOS and DLC. DLC inhibits nNOS and allows for ZDHHC12-mediated S-palmitoylation. Gephyrin phosphorylation releases DLC from the complex leading to nNOS activation and NO production leading to S-nitrosylation of gephyrin. Oxidation is mediated by mROS. Interplay of redox-modifications with either S-nitrosylation or S-palmitoylation are unknown, as well as pathways removing the respective modifications (indicated by '?'). Possible involved molecules and enzymes are marked with '?' and highlighted in grey.

However, the findings in this work strongly suggest an epileptogenic mechanisms of gephyrin Δ199-233 in homozygous mice due to reduced inhibitory neurotransmission. This *in vivo* model allows for further investigation of gephyrin's role in epilepsy to extend knowledge about disease onsets, mechanisms and mode of action of therapeutic compounds. Notably, analysis of the action potential revealed alterations caused by the gephyrin variant. A function of gephyrin relevant for the direct modulation of action potentials has not been demonstrated yet and would open a new door for the judgement of gephyrin-dependent neuronal impairments.

Overall, this study expands current understanding of synaptic gephyrin regulation, which is pivotal for comprehending associated diseases. It underscores the newfound importance of the gephyrin C-domain, traditionally viewed as a structural connector between G- and E-domains, now recognized as a crucial regulatory region through PTMs and interactions, as well as PTM-independent structural modulations (Figure 13). These findings are possibly important in epileptogenesis and other neurodegenerative diseases.

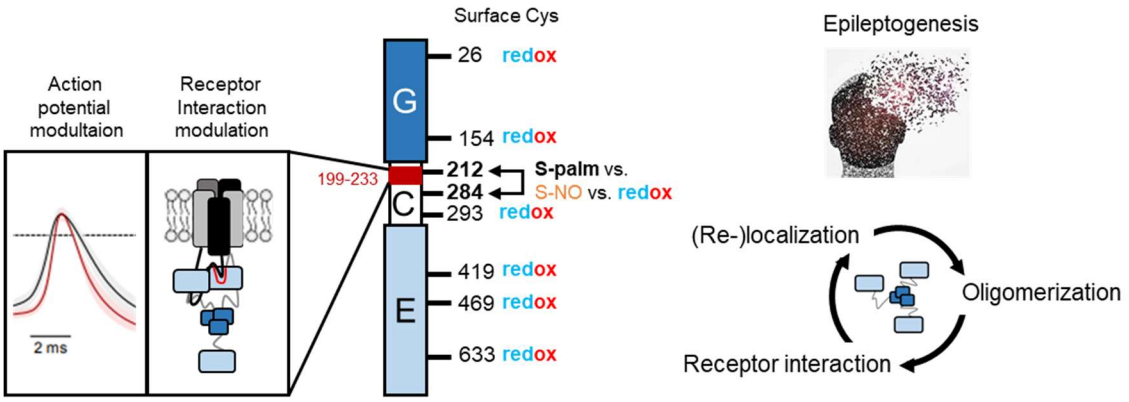

Figure 13: Role of the C-domain for the regulation of gephyrin at synapses.
Gephyrin harbors eight surface-exposed cysteines in G-, C- and E-domain. Three regulation mechanisms (redox, S-palm and S-NO) could be assigned to these Cys. Moreover, the region 199-233 (indicated in dark red) might be associated with the modulation of the gephyrin-receptor interaction and the generation of an action potential. The region and all modifications contribute to the regulation of receptor interaction, oligomerization and (re-)localization of synaptic gephyrin. These processes might be important in epileptogenesis.

References

Accardi MV, Daniels BA, Brown PM, Fritschy JM, Tyagarajan SK, Bowie D (2014) Mitochondrial reactive oxygen species regulate the strength of inhibitory GABA-mediated synaptic transmission. Nat Commun 5:3168.

Bai G, Wang Y, Zhang M (2021) Gephyrin-mediated formation of inhibitory postsynaptic density sheet via phase separation. Cell Res 31:312-325.

Batterman AI, DeChiara J, Islam A, Brenner MB, Fischer BD, Buono RJ, Keck TM, Ferraro TN (2019) Cognitive and behavioral effects of brief seizures in mice. Epilepsy Behav 98:249-257.

Benarroch E (2023) What Is the Role of Ferroptosis in Neurodegeneration? Neurology 101:312-319.

Bischofberger J, Engel D, Frotscher M, Jonas P (2006) Timing and efficacy of transmitter release at mossy fiber synapses in the hippocampal network. Pflugers Arch 453:361-372.

Butler MH, Hayashi A, Ohkoshi N, Villmann C, Becker CM, Feng G, De Camilli P, Solimena M (2000) Autoimmunity to gephyrin in Stiff-Man syndrome. Neuron 26:307-312.

Campbell BFN, Dittmann A, Dreier B, Pluckthun A, Tyagarajan SK (2022) A DARPin-based molecular toolset to probe gephyrin and inhibitory synapse biology. Elife 11.

Chatterji A, Sengupta R (2021a) Stability of S-nitrosothiols and S-nitrosylated proteins: A struggle for cellular existence! J Cell Biochem 122:1579-1593.

Chatterji A, Sengupta R (2021b) Cellular S-denitrosylases: Potential role and interplay of Thioredoxin, TRP14, and Glutaredoxin systems in thiol-dependent protein denitrosylation. Int J Biochem Cell Biol 131:105904.

Chen YJ, Ching WC, Lin YP, Chen YJ (2013) Methods for detection and characterization of protein S-nitrosylation. Methods 62:138-150.

Cho E, Park M (2016) Palmitoylation in Alzheimer's disease and other neurodegenerative diseases. Pharmacol Res 111:133-151.

Dejanovic B, Schwarz G (2014) Neuronal nitric oxide synthase-dependent S-nitrosylation of gephyrin regulates gephyrin clustering at GABAergic synapses. J Neurosci 34:7763-7768.

Dejanovic B, Semtner M, Ebert S, Lamkemeyer T, Neuser F, Luscher B, Meier JC, Schwarz G (2014a) Palmitoylation of gephyrin controls receptor clustering and plasticity of GABAergic synapses. PLoS Biol 12:e1001908.

Dejanovic B, Lal D, Catarino CB, Arjune S, Belaidi AA, Trucks H, Vollmar C, Surges R, Kunz WS, Motameny S, Altmuller J, Kohler A, Neubauer BA, Epicure C, Nurnberg P, Noachtar S, Schwarz G, Sander T (2014b) Exonic microdeletions of the gephyrin gene impair GABAergic synaptic inhibition in patients with idiopathic generalized epilepsy. Neurobiol Dis 67:88-96.

Dejanovic B, Djemie T, Grunewald N, Suls A, Kress V, Hetsch F, Craiu D, Zemel M, Gormley P, Lal D, Euro EDwg, Myers CT, Mefford HC, Palotie A, Helbig I, Meier JC, De Jonghe P, Weckhuysen S, Schwarz G (2015) Simultaneous impairment of neuronal and metabolic function of mutated gephyrin in a patient with epileptic encephalopathy. EMBO Mol Med 7:1580-1594.

Dejanović B (2012) Gephyrin palmitoylation and oligomerization in synaptic plasticity, membrane recruitment and proteostasis. In: Biochemistry: University of Cologne.

Duarte FV, Ciampi D, Duarte CB (2023) Mitochondria as central hubs in synaptic modulation. Cell Mol Life Sci 80:173.

Engel J, Jr. (1984) A practical guide for routine EEG studies in epilepsy. J Clin Neurophysiol 1:109-142.

Faitg J, Lacefield C, Davey T, White K, Laws R, Kosmidis S, Reeve AK, Kandel ER, Vincent AE, Picard M (2021) 3D neuronal mitochondrial morphology in axons, dendrites, and somata of the aging mouse hippocampus. Cell Rep 36:109509.

Feng G, Tintrup H, Kirsch J, Nichol MC, Kuhse J, Betz H, Sanes JR (1998) Dual requirement for gephyrin in glycine receptor clustering and molybdoenzyme activity. Science 282:1321-1324.

Fritschy JM, Harvey RJ, Schwarz G (2008) Gephyrin: where do we stand, where do we go? Trends Neurosci 31:257-264.

Froemke RC (2015) Plasticity of cortical excitatory-inhibitory balance. Annu Rev Neurosci 38:195-219.

Fu C-Y, Kohl JB, Liebsch F, D'Andrea D, Mai M, Mellis AT, Kouroussis E, Ditrói T, Santamaria-Araujo JA, Yeo SY, Endepols H, Křížková M, Kozich V, Barayeu U, Akaike T, Hennermann JB, Nagy P, Filipovic M, Schwarz G (2024) Sulfite oxidase deficiency causes persulfidation loss and H2S release. BioRxiv.

Fuhrmann JC, Kins S, Rostaing P, El Far O, Kirsch J, Sheng M, Triller A, Betz H, Kneussel M (2002) Gephyrin interacts with Dynein light chains 1 and 2, components of motor protein complexes. J Neurosci 22:5393-5402.

Fukata Y, Dimitrov A, Boncompain G, Vielemeyer O, Perez F, Fukata M (2013) Local palmitoylation cycles define activity-regulated postsynaptic subdomains. J Cell Biol 202:145-161.

Ghosh H, Auguadri L, Battaglia S, Simone Thirouin Z, Zemoura K, Messner S, Acuna MA, Wildner H, Yevenes GE, Dieter A, Kawasaki H, M OH, Zeilhofer HU, Fritschy JM, Tyagarajan SK (2016) Several posttranslational modifications act in concert to regulate gephyrin scaffolding and GABAergic transmission. Nat Commun 7:13365.

Griffin CE, 3rd, Kaye AM, Bueno FR, Kaye AD (2013) Benzodiazepine pharmacology and central nervous system-mediated effects. Ochsner J 13:214-223.

Grunewald N, Jan A, Salvatico C, Kress V, Renner M, Triller A, Specht CG, Schwarz G (2018) Sequences Flanking the Gephyrin-Binding Site of GlyRbeta Tune Receptor Stabilization at Synapses. eNeuro 5.

He HY, Shen W, Hiramoto M, Cline HT (2016) Experience-Dependent Bimodal Plasticity of Inhibitory Neurons in Early Development. Neuron 90:1203-1214.

He YJ, Meghani K, Caron MC, Yang C, Ronato DA, Bian J, Sharma A, Moore J, Niraj J, Detappe A, Doench JG, Legube G, Root DE, D'Andrea AD, Drane P, De S, Konstantinopoulos PA, Masson JY, Chowdhury D (2018) DYNLL1 binds to MRE11 to limit DNA end resection in BRCA1-deficient cells. Nature 563:522-526.

Herweg J, Schwarz G (2012) Splice-specific glycine receptor binding, folding, and phosphorylation of the scaffolding protein gephyrin. J Biol Chem 287:12645-12656.

Hess DT, Stamler JS (2012) Regulation by S-nitrosylation of protein post-translational modification. J Biol Chem 287:4411-4418.

Hess DT, Matsumoto A, Kim SO, Marshall HE, Stamler JS (2005) Protein S-nitrosylation: purview and parameters. Nat Rev Mol Cell Biol 6:150-166.

Ho GP, Selvakumar B, Mukai J, Hester LD, Wang Y, Gogos JA, Snyder SH (2011) S-nitrosylation and S-palmitoylation reciprocally regulate synaptic targeting of PSD-95. Neuron 71:131-141.

Hsueh YP, Kim E, Sheng M (1997) Disulfide-linked head-to-head multimerization in the mechanism of ion channel clustering by PSD-95. Neuron 18:803-814.

Jacobs L, Hoehne MN, Riemer J (2022) Measuring Intracellular H (2) O (2) in Intact Human Cells Using the Genetically Encoded Fluorescent Sensor HyPer7. Bio Protoc 12.

Jakubiczka-Smorag J, Santamaria-Araujo JA, Metz I, Kumar A, Hakroush S, Brueck W, Schwarz G, Burfeind P, Reiss J, Smorag L (2016) Mouse model for molybdenum cofactor deficiency type B recapitulates the phenotype observed in molybdenum cofactor deficient patients. Hum Genet 135:813-826.

Kandratavicius L, Balista PA, Lopes-Aguiar C, Ruggiero RN, Umeoka EH, Garcia-Cairasco N, Bueno-Junior LS, Leite JP (2014) Animal models of epilepsy: use and limitations. Neuropsychiatr Dis Treat 10:1693-1705.

Khayenko V, Schulte C, Reis SL, Avraham O, Schietroma C, Worschech R, Nordblom NF, Kachler S, Villmann C, Heinze KG, Schlosser A, Schueler-Furman O, Tovote P, Specht CG, Maric HM (2022) A Versatile Synthetic Affinity Probe Reveals Inhibitory Synapse Ultrastructure and Brain Connectivity. Angew Chem Int Ed Engl 61:e202202078.

Kim EY, Schrader N, Smolinsky B, Bedet C, Vannier C, Schwarz G, Schindelin H (2006) Deciphering the structural framework of glycine receptor anchoring by gephyrin. EMBO J 25:1385-1395.

Kim S, Kang M, Park D, Lee AR, Betz H, Ko J, Chang I, Um JW (2021) Impaired formation of high-order gephyrin oligomers underlies gephyrin dysfunction-associated pathologies. iScience 24:102037.

Kirsch J, Wolters I, Triller A, Betz H (1993) Gephyrin antisense oligonucleotides prevent glycine receptor clustering in spinal neurons. Nature 366:745-748.

Kiss E, Gorgas K, Schlicksupp A, Gross D, Kins S, Kirsch J, Kuhse J (2016) Biphasic Alteration of the Inhibitory Synapse Scaffold Protein Gephyrin in Early and Late Stages of an Alzheimer Disease Model. Am J Pathol 186:2279-2291.

Kress V (2016) Collective Regulation of Synaptic Plasticity by Gephyrin, Dynein Light Chain and Neuronal Nitric Oxide Synthase In.

Kuhse J, Kalbouneh H, Schlicksupp A, Mukusch S, Nawrotzki R, Kirsch J (2012) Phosphorylation of gephyrin in hippocampal neurons by cyclin-dependent kinase CDK5 at Ser-270 is dependent on collybistin. J Biol Chem 287:30952-30966.

Kuper J, Llamas A, Hecht HJ, Mendel RR, Schwarz G (2004) Structure of the molybdopterin-bound Cnx1G domain links molybdenum and copper metabolism. Nature 430:803-806.

Larson EA, Accardi MV, Wang Y, D'Antoni M, Karimi B, Siddiqui TJ, Bowie D (2020) Nitric Oxide Signaling Strengthens Inhibitory Synapses of Cerebellar Molecular Layer Interneurons through a GABARAP-Dependent Mechanism. J Neurosci 40:3348-3359.

Lee DS, Kim JE (2020) PDI-Mediated Reduction of Disulfide Bond on PSD95 Increases Spontaneous Seizure Activity by Regulating NR2A-PSD95 Interaction in Epileptic Rats Independent of S-Nitrosylation. Int J Mol Sci 21.

Lee G, Kim S, Hwang DE, Eom YG, Jang G, Park HY, Choi JM, Ko J, Shin Y (2024) Thermodynamic modulation of gephyrin condensation by inhibitory synapse components. Proc Natl Acad Sci U S A 121:e2313236121.

Lee HJ, Adham IM, Schwarz G, Kneussel M, Sass JO, Engel W, Reiss J (2002) Molybdenum cofactor-deficient mice resemble the phenotype of human patients. Hum Mol Genet 11:3309-3317.

Lionel AC et al. (2013) Rare exonic deletions implicate the synaptic organizer Gephyrin (GPHN) in risk for autism, schizophrenia and seizures. Hum Mol Genet 22:2055-2066.

Lopez-Mirabal HR, Winther JR (2008) Redox characteristics of the eukaryotic cytosol. Biochim Biophys Acta 1783:629-640.

Macha A (2021) Mechanism of gephyrin dependent inhibitory receptor clustering. In: Chemistry: University of Cologne.

Macha A, Grünewald N, Havarushka N, Burdina N, Toelzer C, , Merkler Y, Cabrera-Orefice A, Brandt U, Pauly T, Nagle-Steger L, Niefind K, Schwarz G (2022) Pentameric assembly of glycine receptor intracellular domains provides insights into gephyrin clustering. bioRxiv.

Machin JM, Kalli AC, Ranson NA, Radford SE (2023) Protein-lipid charge interactions control the folding of outer membrane proteins into asymmetric membranes. Nat Chem 15:1754-1764.

Mailloux RJ, McBride SL, Harper ME (2013) Unearthing the secrets of mitochondrial ROS and glutathione in bioenergetics. Trends Biochem Sci 38:592-602.

Marino SM, Gladyshev VN (2010) Cysteine Function Governs Its Conservation and Degeneration and Restricts Its Utilization on Protein Surfaces. Journal of Molecular Biology 404:902-916.

Massaad CA, Klann E (2011) Reactive oxygen species in the regulation of synaptic plasticity and memory. Antioxid Redox Signal 14:2013-2054.

Mayr SJ, Mendel RR, Schwarz G (2021) Molybdenum cofactor biology, evolution and deficiency. Biochim Biophys Acta Mol Cell Res 1868:118883.

Mendel RR (2013) The molybdenum cofactor. J Biol Chem 288:13165-13172.

Moren C, deSouza RM, Giraldo DM, Uff C (2022) Antioxidant Therapeutic Strategies in Neurodegenerative Diseases. Int J Mol Sci 23.

Morthorst TH, Olsen A (2013) Cell-nonautonomous inhibition of radiation-induced apoptosis by dynein light chain 1 in Caenorhabditis elegans. Cell Death Dis 4:e799.

Nakamura T, Lipton SA (2016) Protein S-Nitrosylation as a Therapeutic Target for Neurodegenerative Diseases. Trends Pharmacol Sci 37:73-84.

Nawrotzki R, Islinger M, Vogel I, Volkl A, Kirsch J (2012) Expression and subcellular distribution of gephyrin in non-neuronal tissues and cells. Histochem Cell Biol 137:471-482.

Nicholls DG, Budd SL (2000) Mitochondria and neuronal survival. Physiol Rev 80:315-360.

O'Sullivan GA, Jedlicka P, Chen HX, Kalbouneh H, Ippolito A, Deller T, Nawrotzki RA, Kuhse J, Kalaidzidis YL, Kirsch J, Schwarzacher SW, Betz H (2016) Forebrain-specific loss of synaptic GABAA receptors results in altered neuronal excitability and synaptic plasticity in mice. Mol Cell Neurosci 72:101-113.

Papaioannou VE, Behringer RR (2012) Early embryonic lethality in genetically engineered mice: diagnosis and phenotypic analysis. Vet Pathol 49:64-70.

Pitkanen A, Ekolle Ndode-Ekane X, Lapinlampi N, Puhakka N (2019) Epilepsy biomarkers - Toward etiology and pathology specificity. Neurobiol Dis 123:42-58.

Rayala SK, den Hollander P, Manavathi B, Talukder AH, Song C, Peng S, Barnekow A, Kremerskothen J, Kumar R (2006) Essential role of KIBRA in co-activator function of dynein light chain 1 in mammalian cells. J Biol Chem 281:19092-19099.

Reiss J, Johnson JL (2003) Mutations in the molybdenum cofactor biosynthetic genes MOCS1, MOCS2, and GEPH. Hum Mutat 21:569-576.

Salaun C, Greaves J, Chamberlain LH (2010) The intracellular dynamic of protein palmitoylation. J Cell Biol 191:1229-1238.

Schwarz G, Schrader N, Mendel RR, Hecht HJ, Schindelin H (2001) Crystal structures of human gephyrin and plant Cnx1 G domains: comparative analysis and functional implications. J Mol Biol 312:405-418.

Seneviratne U, Nott A, Bhat VB, Ravindra KC, Wishnok JS, Tsai LH, Tannenbaum SR (2016) S-nitrosation of proteins relevant to Alzheimer's disease during early stages of neurodegeneration. Proc Natl Acad Sci U S A 113:4152-4157.

Sharif R, Aghsami M, Gharghabi M, Sanati M, Khorshidahmad T, Vakilzadeh G, Mehdizadeh H, Gholizadeh S, Taghizadeh G, Sharifzadeh M (2017) Melatonin reverses H-89 induced spatial memory deficit: Involvement of oxidative stress and mitochondrial function. Behav Brain Res 316:115-124.

Shen ZC, Wu PF, Wang F, Xia ZX, Deng Q, Nie TL, Zhang SQ, Zheng HL, Liu WH, Lu JJ, Gao SQ, Yao XP, Long LH, Hu ZL, Chen JG (2019) Gephyrin Palmitoylation in Basolateral Amygdala Mediates the Anxiolytic Action of Benzodiazepine. Biol Psychiatry 85:202-213.

Shiang R, Ryan SG, Zhu YZ, Hahn AF, O'Connell P, Wasmuth JJ (1993) Mutations in the alpha 1 subunit of the inhibitory glycine receptor cause the dominant neurologic disorder, hyperekplexia. Nat Genet 5:351-358.

Sies H, Mailloux RJ, Jakob U (2024) Fundamentals of redox regulation in biology. Nat Rev Mol Cell Biol.

Smolarz B, Makowska M, Romanowicz H (2021) Pharmacogenetics of Drug-Resistant Epilepsy (Review of Literature). Int J Mol Sci 22.

Sola M, Kneussel M, Heck IS, Betz H, Weissenhorn W (2001) X-ray crystal structure of the trimeric N-terminal domain of gephyrin. J Biol Chem 276:25294-25301.

Stallmeyer B, Schwarz G, Schulze J, Nerlich A, Reiss J, Kirsch J, Mendel RR (1999) The neurotransmitter receptor-anchoring protein gephyrin reconstitutes molybdenum cofactor biosynthesis in bacteria, plants, and mammalian cells. Proc Natl Acad Sci U S A 96:1333-1338.

Steenvoorden DP, van Henegouwen GM (1997) The use of endogenous antioxidants to improve photoprotection. J Photochem Photobiol B 41:1-10.

Stomberski CT, Hess DT, Stamler JS (2019) Protein S-Nitrosylation: Determinants of Specificity and Enzymatic Regulation of S-Nitrosothiol-Based Signaling. Antioxid Redox Signal 30:1331-1351.

Stykel MG, Ryan SD (2024) Network analysis of S-nitrosylated synaptic proteins demonstrates unique roles in health and disease. Biochim Biophys Acta Mol Cell Res 1871:119720.

Swarbrick CMD, Nanson JD, Patterson EI, Forwood JK (2020) Structure, function, and regulation of thioesterases. Prog Lipid Res 79:101036.

Tejada-Jimenez M, Llamas A, Galvan A, Fernandez E (2019) Role of Nitrate Reductase in NO Production in Photosynthetic Eukaryotes. Plants (Basel) 8.

Tortosa E, Hoogenraad CC (2018) Polarized trafficking: the palmitoylation cycle distributes cytoplasmiccproteins to distinct neuronal compartments. Curr Opin Cell Biol 50:64-71.

Turrens JF (2003) Mitochondrial formation of reactive oxygen species. J Physiol 552:335-344.

Tyagarajan SK, Fritschy JM (2014) Gephyrin: a master regulator of neuronal function? Nat Rev Neurosci 15:141-156.

Tyagarajan SK, Ghosh H, Yevenes GE, Nikonenko I, Ebeling C, Schwerdel C, Sidler C, Zeilhofer HU, Gerrits B, Muller D, Fritschy JM (2011) Regulation of GABAergic synapse formation and plasticity by GSK3beta-dependent phosphorylation of gephyrin. Proc Natl Acad Sci U S A 108:379-384.

Vlachou S (2022) GABA(B) Receptors and Cognitive Processing in Health and Disease. Curr Top Behav Neurosci 52:291-329.

Weber EM, Algers B, Hultgren J, Olsson IA (2013) Pup mortality in laboratory mice--infanticide or not? Acta Vet Scand 55:83.

Williams E, Scott JP (1953) The Development of Social Behavior Patterns in the Mouse, in Relation to Natural Periods. Behaviour 6:35-65.

Wu Y, Chen M, Jiang J (2019) Mitochondrial dysfunction in neurodegenerative diseases and drug targets via apoptotic signaling. Mitochondrion 49:35-45.

Yuan Y, Li P, Li J, Zhao Q, Chang Y, He X (2024) Protein lipidation in health and disease: molecular basis, physiological function and pathological implication. Signal Transduct Target Ther 9:60.

Zacchi P, Antonelli R, Cherubini E (2014) Gephyrin phosphorylation in the functional organization and plasticity of GABAergic synapses. Front Cell Neurosci 8:103.

Zareba-Koziol M, Bartkowiak-Kaczmarek A, Figiel I, Krzystyniak A, Wojtowicz T, Bijata M, Wlodarczyk J (2019) Stress-induced Changes in the S-palmitoylation and S-nitrosylation of Synaptic Proteins. Mol Cell Proteomics 18:1916-1938.

Zhou HX, Pang X (2018) Electrostatic Interactions in Protein Structure, Folding, Binding, and Condensation. Chem Rev 118:1691-1741.

Zhu S, Shen Z, Wu X, Han W, Jia B, Lu W, Zhang M (2024) Demixing is a default process for biological condensates formed via phase separation. Science 384:920-928.

Zita MM, Marchionni I, Bottos E, Righi M, Del Sal G, Cherubini E, Zacchi P (2007) Post-phosphorylation prolyl isomerisation of gephyrin represents a mechanism to modulate glycine receptors function. EMBO J 26:1761-1771.

Chapter 6 (Supplementary Data)

6.1. Information to supplementary data

During this work, a few site projects have been investigated, which did not necessarily serve the complementation of the previously presented manuscripts. However, the preliminary findings will be provided in a comprehensive way, since they may hold potential for future research and inspiration.

6.2. *In vitro* modification of specific cysteines of gephyrin

Pre-reduction of gephyrin to obtain reduced cysteines

Note, that the generated Cys to Ser variants were introduced earlier (chapter 4, Figure 1D). The aim of this experiment was the generation of reduced, free-thiols prior to S-palmitoylation and S-nitrosylation attempts to ensure optimal reaction conditions and yields. The reduced status of cysteines was monitored by alkylation with size-increasing tags ($mmPEG_{5kDa}$ or $mmPEG_{10kDa}$) in a redox shift assay (RSA).

Importantly, reductants (such as TCEP, DTT and β-ME) interfere with alkylating reagents compounds and disturb correct monitoring of three thiols (Kantner et al., 2017). Thus, it was necessary to test for the best removal strategy. In this work, the removal of the reductant TCEP was tested by precipitation, gel-filtration or gel-filtration in combination with evaporation via SpeedVac (Figure 14). The quantification of free thiols via the RSA revealed, that the best pre-reduction condition is given by the use of 5-10 mM TCEP and subsequent removal through gel-filtration. Further concentration, e.g. through SpeedVac or concentrators (data not shown) is not recommended since the concentration of residual reductant again disturbs alkylation labeling.

Material and Method

10 µg protein was incubated in a 20 µL reaction in reaction buffer (50 mM Tris/HCl, 5 mM EDTA, pH 7.5) for 30 min at 45°C. The reaction contained either no TCEP or 1-50 mM TCEP. A positive control containing 2% SDS was included. Afterwards, samples were either acetone-precipitated or subjected to gel filtration using PD10 columns or subjected to gel filtration using PD10 columns with subsequent evaporation (SpeedVac, 40°C, 30°min) or directly used for the alkylation reaction. If precipitated or evaporated, the pellet was dissolved in 20 µL reaction buffer containing no or 1 mM $mmPEG_{5kDa}$. All other samples were supplemented with 1 mM $mmPEG_{5kDa}$. The alkylation reaction was performed for 1 h in the dark. Samples were prepared for SDS-PAGE followed by Coomassie staining. Quantification was done with ImageJ.

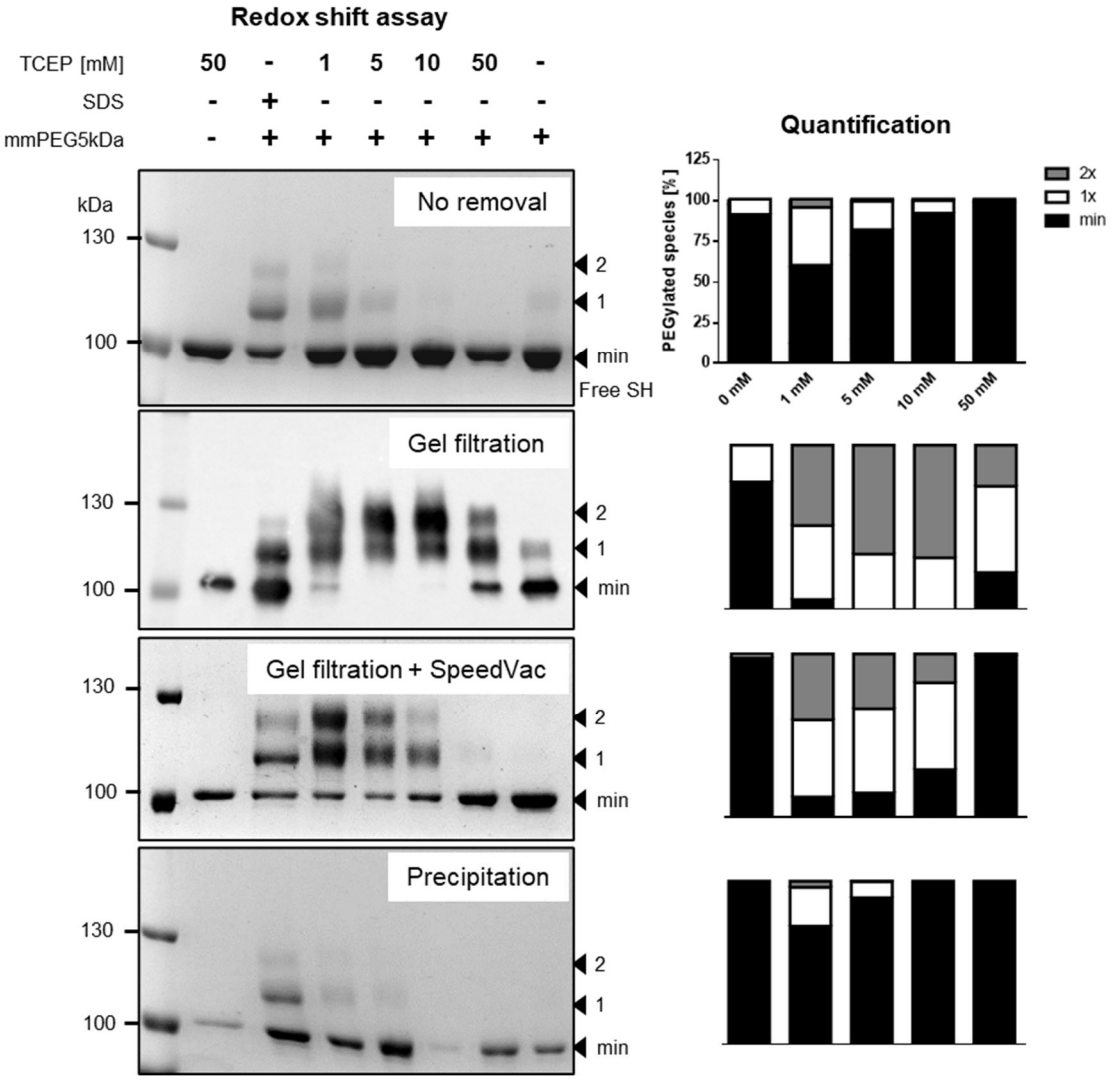

Figure 14: Pre-reduction tests to obtain reduced gephyrin cysteines.
The gephyrin variant 'o212/284' harboring two surface-exposed cysteines was used to establish optimal conditions for the reduction of gephyrin. Different amounts of TCEP and removal strategies were tested and the redox-state of cysteines analyzed through redox shift assay.

S-palmitoylation and S-nitrosylation of Cys212 and Cys284

Based on the previous experiment, best reduction of gephyrin cysteines was obtained by purifying gephyrin form *E. coli* in the presence of 5 mM TCEP and removal of TCEP by gel filtration right before storing the protein (chapter 3, Figure 1E). Importantly, with this it was verified that Cys212 and 284 in gephyrin C-domain were reduced and accessible for further modification.

The gephyrin variant o212/284 was exposed to S-nitroso glutathione (GSNO) and palmitoyl-Coenzyme A (palmCoA) to obtain S-palmitoylation and S-nitrosylation specifically at Cys212 and 284 (Figure 15). As a negative control the cys-free gephyrin variant was used. The RSA revealed that the untreated gephyrin was not fully reduced, instead approximately 75% of gephyrin contained two free thiols, and approximately 22% of gephyrin contained one reduced thiol. However, the treatment with palmCoA resulted

in gephyrin species with one or two free thiols in a ratio of 76% and 23% respectively. In conclusion, 50% of gephyrin was at least S-palmitoylated at one cysteines, but no double S-palmitoylated species was obtained. In contrast, the treatment with GSNO resulted in no remaining free thiol, indicating 100% S-nitrosylation of gephyrin, likely at both Cys.

Since, S-palmitoylation is performed by enzymes (Salaun et al., 2010), it is likely that a non-enzymatic reaction is slow and the here chosen reaction time was too short. In comparison, although the mechanism is not fully understood, S-nitrosylation is believed to appear rapidly and only depends on a NO-donor (Hess et al., 2005). Thus, full double-S-nitrosylation of gephyrin in this set-up is reasonable.

100% double-S-nitrosylation and 50% single-S-palmitoylation are good yields to start the characterization of the modified species in other experiments. In case of S-palmitoylation, it is elusive which Cys (212 or 284) is modified, which can be investigated in future work. Using additional generated gephyrin variants harboring only Cys212 OR Cys284 (chapter 3, Figure 1D) might reveal or exclude a special preferred residue for S-palmitoylation.

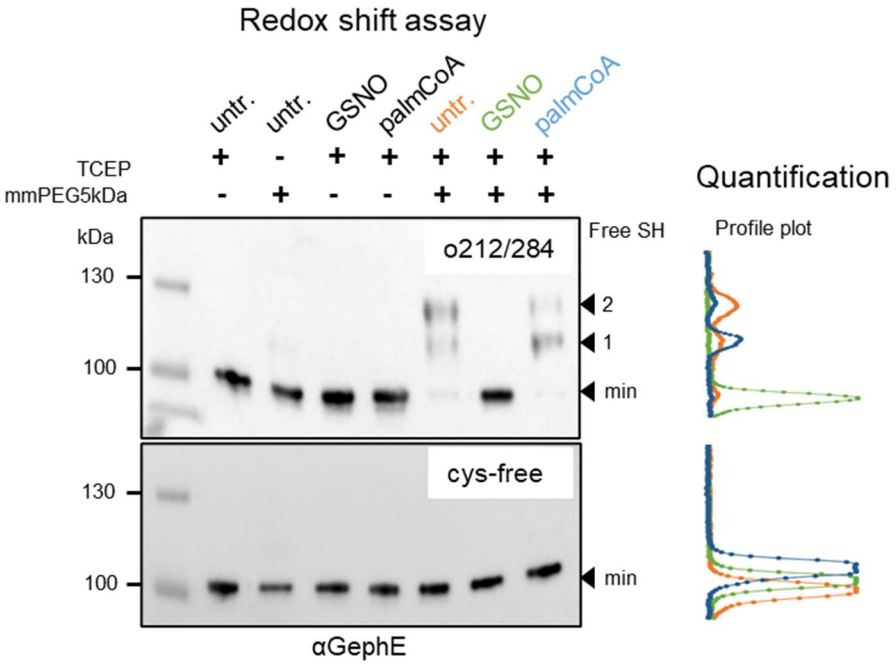

Figure 15: *In vitro* S-nitrosylation and S-palmitoylation of gephyrin at Cys212 and 284.
Redox shift assay after exposure of pre-reduced gephyrin with S-nitroso glutathione (GSNO) or palmitoyl-Coenzyme A (palmCoA). Quantification of free thiols through profile plot. Gephyrin variant o212/284 used for thiol modification, cys-free variant as negative control.

Material and Method

0.5 µg pre-reduced, buffer-exchanged gephyrin was prepared in a 30 µL reaction in MOD buffer (50 mM Tris/HCl, 5 mM EDTA, pH 7.5) containing no modifying reagent, or 10 mM GSNO, or 10 mM palmCoA. The reaction was performed for 1 h at 45°C. Afterwards, the volume was filled up with MOD buffer to 40 µL and supplemented with 1 mM $mmPEG_{5kDa}$. Alkylation was performed for 1 h in the dark and samples prepared with std SDS sample buffer for std western blot analysis. Gephyrin species were detected with anti-GephyrinE (3B11; 1:10, self-made) and anti-mouse HRP-coupled (1:10 000, AP181P, *Sigma*). Quantification of band intensities was done with ImageJ.

Moco activity after gephyrin oxidation

Redox-sensitivity of gephyrin for Moco activity was addressed in this experiment. Therefore, gephyrin was chemically oxidized via H_2O_2. As a control the cysteine-free variant was used. Afterwards, excess H_2O_2 was removed by catalase and a standard Moco activity assay performed (e.g. chapter 3). Interestingly, the enzymatic activity of oxidized gephyrin wt was reduced significantly to the level of cys-free gephyrin. The activity of cys-free gephyrin was unaltered regardless of the redox condition.

This finding suggests a redox-dependency of the enzymatic function of gephyrin and could be further investigated in the future.

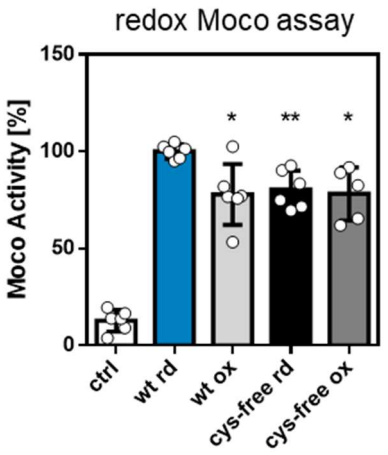

Figure 16: Moco activity using redox-modified gephyrin.
Moco assay using redox-modified gephyrin wt or the cys-free variant. Moco activity normalized to reduced wt (wt rd). Significance towards wt rd tested by student's t-test, alpha level corrected by three.

Material and Method

1.2 nmol gephyrin was prepared in 50 µL assay buffer (100 mM HEPES/NaOH, pH 7.5). Samples were either supplemented with assay buffer or assay buffer containing f.c. 5 µM H_2O_2 and incubated for 2 h at rt. Afterwards samples were incubated with 1.25 ng/mL catalase (f.c.) for 30 min at rt. Samples were then used for the standard Moco activity assay (e.g. chapter 4).

6.3. Generation of a redox-sensor for synapses

The ratiometric redox sensor Hyper7 was genetically modified by NES (nucleus export sequence) and Tom20 (Mitochondrial import receptor subunit TOM20 homolog) tags, leading to cytosolic localization or to the attachment to the outer mitochondrial membrane (Figure 13A). The redox-sensitive domain of the sensor (OxyRD) can be reduced or oxidized by H_2O_2 causing a change in two excitation peaks of cpYFP at 469 and 390 nm (Figure 13B) (Jacobs et al., 2022). Expression of both sensor types was successful in neuron cell cultures expressing a cytosolic GFP-tagged version of D-amino oxidase (DAAO) (Figure 13C). The redox status of the respective sensor was measured during sequential treatment with D-methionine (D-Met), antimycin A (AntiA), H_2O_2 and DTT. The ration of 469/390 nm revealed that the redox sensor is in a fully oxidized status, which could not be further oxidized through DAAO-mediated or mitochondrial ROS after D-Met or AntiA treatment, respectively. DTT treatment was able to reduce the sensor, displaying the integrity of the sensor. In summary, this experiment might point in the direction, that the redox environment could be more oxidative than expected considering reductive GSH as omnipresent in the cell.

To optimize the set-up, it is recommended to test different expression durations and avoid the co-expression with other construct to reduce cellular stress. Moreover, Hyper7 could be too sensitive, thus other types of redox-sensors might be tested as well. Lastly, the generation of a synaptically localized sensor requires an alternative tag, which could be gephyrin or the GlyR β-ICD peptide.

Material and Method

Primary, hippocampal neurons were prepared as earlier introduced (e.g. chapter 2 and 3) and 30,000 cells were seeded in coated 96-well plates. At DIV8 neurons were transduced with mScarlet-tagged DAAO as previously mentioned (chapter 4). At DIV9 neurons were transfected with pcDNA5_tom20-Hyper7 or pcS2_NES-Hyper7 according to previously introduced protocols (e.g. chapter 2 and 3). At DIV12 the media was exchanged to minimal medium (HBBS) and incubated for 10 min at 37°C and 5% CO_2. Afterwards excitation was recorded using the Cytation 3 (Agilent, BioTek). At different timepoints reagents were added prepared in minimal medium. The final concentration was D-Met=5 mM, Antimycin A=1 µM, DTT=5 mM, H_2O_2=20 µM.

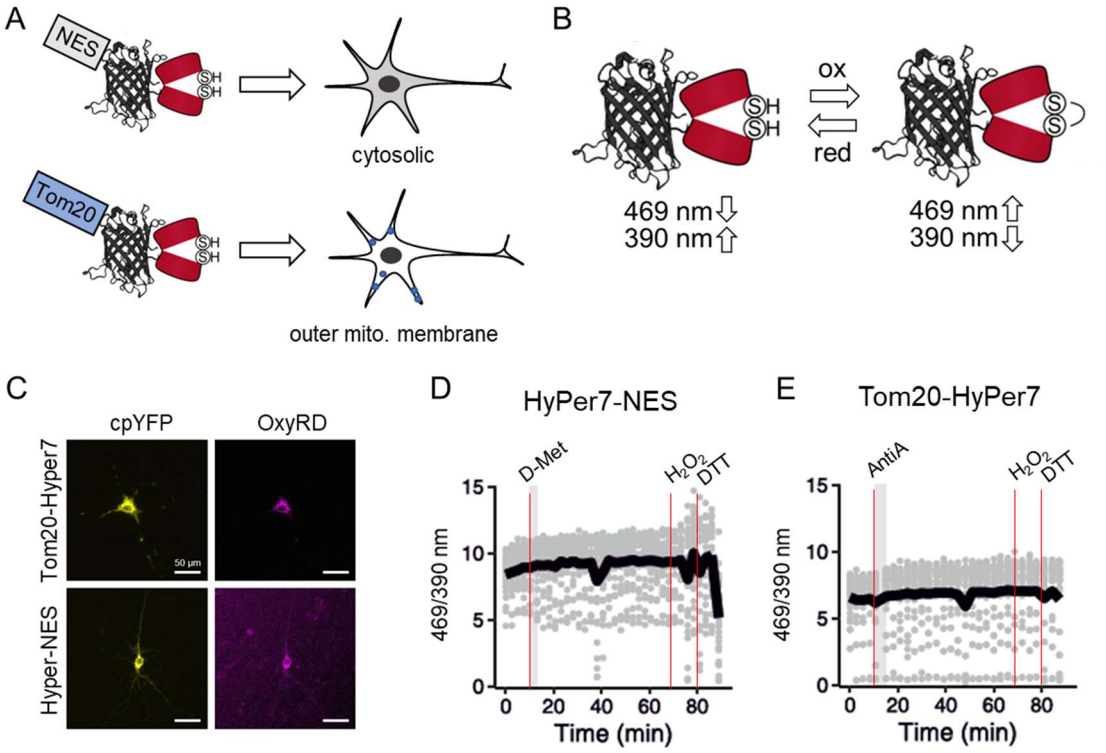

Figure 17: Redox sensors in hippocampal neurons.
Expression and analysis of redox-sensors HyPer7-NES and Tom20-Hyper7 in hippocampal neurons co-expressed with cytosolic GFP-D-amino oxidase (DAAO) after 3 days. A) Each redox sensor displays specific cellular localization due to the attached transport sequence. B) Excitation changes of the redox sensor at 469 ad 390 nm dependent on the redox state; cpYFP subunit in black, OxyRD subunit in red. C) Fluorescence images of each sensor subunit. Scalebar=50 µm. D) and E) Measurements of the ratio of 469 to 390 nm for 90 mins using the respective sensor. Treatment points indicated with red line. D-Met=5 mM, Antimycin A=1 µM, DTT=5 mM, H_2O_2=20 µM.

6.4. Electrophysiology studies of gephyrin Δ199-233

Electrophysiology measurements of mIPSCs were done with neuron cell cultures expressing gephyrin wt or the Δ199-233 variant (chapter 4). The investigation of the AP with regard to gephyrin variants has not been performed previously. Interestingly, the AP measurement revealed differences in shape of gephyrin Δ199-233 compared to wt gephyrin manifesting as a sharper AP with increased depolarization and decreased repolarization rate (Figure 13). So far, this data suggests a new role of gephyrin for the generation of Aps. This could either be through direct or indirect effects most likely targeting Na^+ and K^+ channels.

This data is promising to discover a novel synaptic function of gephyrin and it is highly recommended to repeat the experiment with several known gephyrin variants to answer the question whether this effect is only mediated by gephyrin Δ199-233 or also appeals for others.

Material and Method

Primary hippocampal cultures were prepared and seeded and grown according to standard protocols (e.g. chapter 4). At 10 days *in vitro* (DIV), cells were transduced with 2.5 x 108 viral genome copies (GC) by exchanging a third of the medium to virus-containing medium. At DIV11, 50 mM NaCl were added to maintain osmolarity. The cell were used at DIV13-15 for electrophysiology experiments. Electrophysiology measurement was performed by Fynn Eggersmann of the 'Kloppenburg lab'.

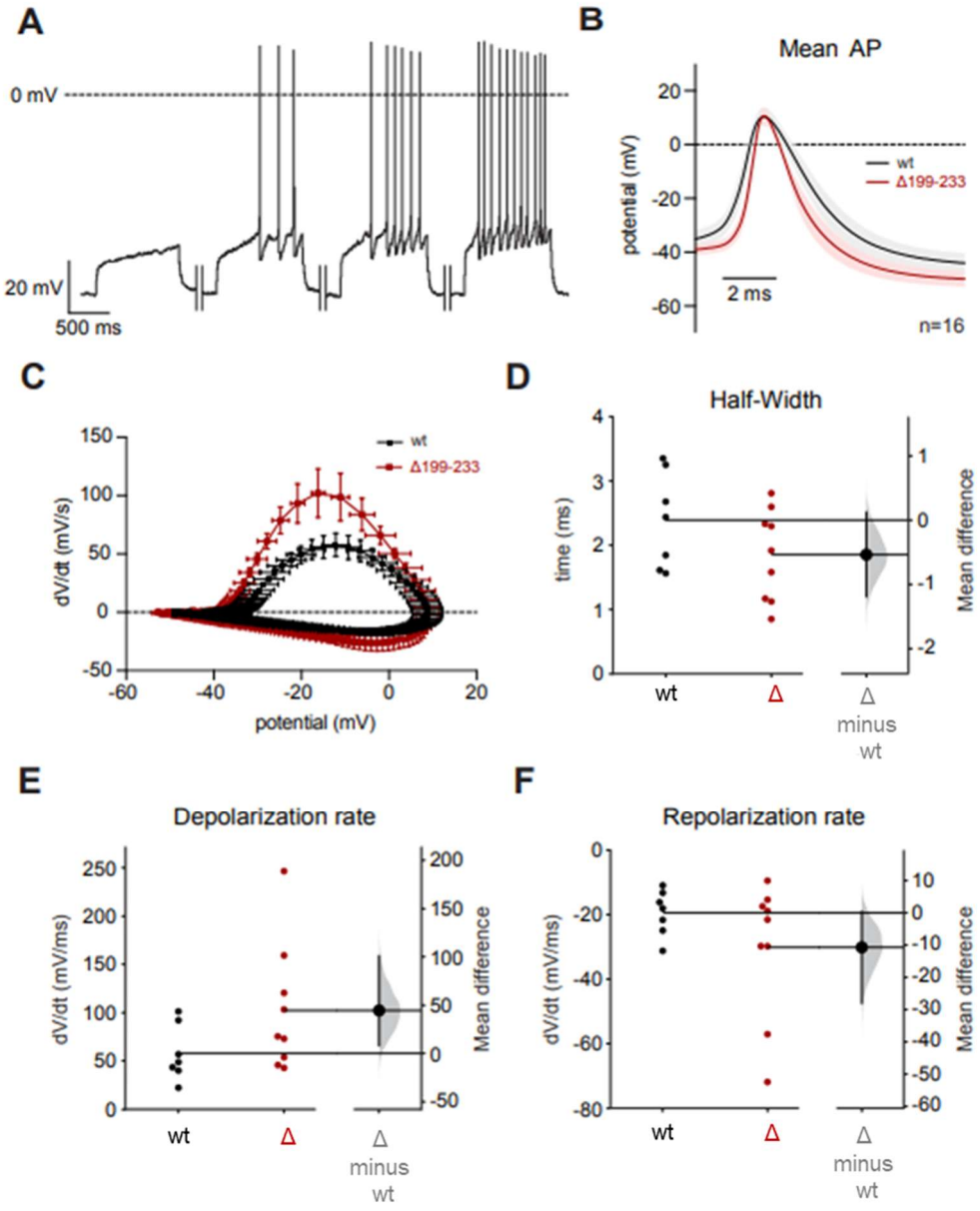

Figure 18: Measurement of the action potential in gephΔ199-233-expressing neurons.
Measurements and analysis of action potentials (APs) in in primary hippocampal neurons of GephFlox mice. Expression of mScltGeph wt and Δ199-233. Endogenous Geph KO induced by moxBFP-P2A-Cre. Analysis of 16 cells per condition. Statistical analysis by mean difference of the confidence interval and *p*-value permutation test. Error bars determined by standard deviation. A) Representative APs of wt and Δ199-233 cells. B) Average AP. C) Phase plot of APs. D) Quantification of AP Half-Width. E) Quantification of AP depolarization rate. F) Quantification of AP repolarization rate.

References

Hess DT, Matsumoto A, Kim SO, Marshall HE, Stamler JS (2005) Protein S-nitrosylation: purview and parameters. Nat Rev Mol Cell Biol 6:150-166.

Jacobs L, Hoehne MN, Riemer J (2022) Measuring Intracellular H (2) O (2) in Intact Human Cells Using the Genetically Encoded Fluorescent Sensor HyPer7. Bio Protoc 12.

Kantner T, Alkhawaja B, Watts AG (2017) In Situ Quenching of Trialkylphosphine Reducing Agents Using Water-Soluble PEG-Azides Improves Maleimide Conjugation to Proteins. ACS Omega 2:5785-5791.

Salaun C, Greaves J, Chamberlain LH (2010) The intracellular dynamic of protein palmitoylation. J Cell Biol 191:1229-1238.